

# NOTE TO USERS

This reproduction is the best copy available.

**UMI**<sup>®</sup>



**UNIVERSITY OF ALBERTA**

**ASSESSMENT OF HARMONIC DISTORTIONS FOR SYSTEMS  
WITH DISTRIBUTED HARMONIC SOURCES**

By



Emad Ezzat Ahmed

A thesis

submitted to the faculty of graduate studies and research  
in partial fulfillment of the requirements for the degree of  
Doctor of Philosophy

Department of Electrical and Computer Engineering

Edmonton, Alberta

Spring 2003

National Library  
of Canada

Acquisitions and  
Bibliographic Services

395 Wellington Street  
Ottawa ON K1A 0N4  
Canada

Bibliothèque nationale  
du Canada

Acquisitons et  
services bibliographiques

395, rue Wellington  
Ottawa ON K1A 0N4  
Canada

*Your file* *Votre référence*

*ISBN: 0-612-82075-0*

*Our file* *Notre référence*

*ISBN: 0-612-82075-0*

The author has granted a non-exclusive licence allowing the National Library of Canada to reproduce, loan, distribute or sell copies of this thesis in microform, paper or electronic formats.

The author retains ownership of the copyright in this thesis. Neither the thesis nor substantial extracts from it may be printed or otherwise reproduced without the author's permission.

L'auteur a accordé une licence non exclusive permettant à la Bibliothèque nationale du Canada de reproduire, prêter, distribuer ou vendre des copies de cette thèse sous la forme de microfiche/film, de reproduction sur papier ou sur format électronique.

L'auteur conserve la propriété du droit d'auteur qui protège cette thèse. Ni la thèse ni des extraits substantiels de celle-ci ne doivent être imprimés ou autrement reproduits sans son autorisation.

# Canada

**UNIVERSITY OF ALBERTA**

**LIBRARY RELEASE FORM**

**Name of Author:** Emad Ezzat Ahmed

**Title of Thesis:** Assessment of Harmonic Distortions for Systems with  
Distributed harmonic Sources

**Degree:** Doctor of Philosophy

**Year this Degree Granted:** 2003

Permission is hereby granted to the University of Alberta Library to reproduce single copies of this thesis and to lend or sell such copies for private, scholarly or scientific research purposes only.

The author reserves all other publication and other rights in association with the copyright in the thesis, and except as herein before provided, neither the thesis nor any substantial portion thereof may be printed or otherwise reproduced in any material form whatever without the author's prior written permission.

*Emad Ahmed*


Cairo University-Fayoum Campus,  
Department of Electrical Engineering, Fayoum, Egypt

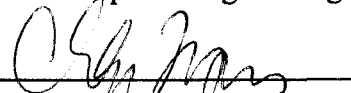
*April 23, 2003*


**UNIVERSITY OF ALBERTA**

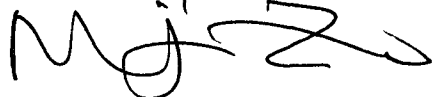
**FACULTY OF GRADUATE STUDIES AND RESEARCH**


The undersigned certify that they have read, and recommend to the Faculty of Graduate Studies and Research for acceptance, a thesis entitled "Assessment of Harmonic Distortions for Systems with Distributed Harmonic Sources" submitted by Emad Ezzat Ahmed in partial fulfillment of the requirements for the degree of Doctor of Philosophy.

  
Supervisor, Dr. Wilsun Xu  
Electrical and Computer Engineering

  
Dr. Tongwen Chen  
Electrical and Computer Engineering

  
Dr. Venkata Dinavahi  
Electrical and Computer Engineering

  
Dr. Ming J. Zuo  
Mechanical Engineering

  
External Examiner, Dr. Magdy Salama  
Electrical and Computer Engineering, University of Waterloo

April 23, 2003  
Date

## ABSTRACT

Harmonic analysis has been focused on systems with one or a few large harmonic-producing loads in the past. However, distributed harmonic sources with comparable sizes have recently become more common in commercial and industrial distribution systems. Two main issues should be addressed when conducting harmonic analysis for systems with distributed harmonic sources.

The first issue is the attenuation and diversity of harmonic currents. The distortion of the voltage supplied to each harmonic source can be considerable. This would reduce the injected harmonic current magnitudes (attenuation effect) and change the phase angles (diversity effect). Common harmonic analysis methods can not take into account these effects. They use typical harmonic current source model specified upon a supply voltage having little or no distortion. This thesis proposes an iterative harmonic analysis method to consider the attenuation and diversity of harmonic currents produced from distributed harmonic sources. This would provide more accurate assessment of the system distortion level. The developed method is verified by experimental measurements and simulation.

The second issue is the random harmonics generated from randomly varying loads. This behavior calls for probabilistic techniques for quantifying harmonic levels correctly avoiding the harmonic voltage and current overestimation that could be obtained using the traditional deterministic approach. A distribution system with harmonic sources of random loading level is considered. An analytical method utilizing the summation technique of random harmonic phasors is presented to get the probabilistic harmonic levels. The proposed method is verified by performing Monte Carlo simulation.

## **ACKNOWLEDGEMENT**

I would like to express my sincere gratitude and appreciation to Dr. Wilsun Xu for his encouragement, tireless help and patience in supervising this research work. It has been my honor and privilege to work under his supervision. I am deeply indebted for my current achievements to the invaluable guidance and advice I have been receiving from Dr. Xu. His professional supervision and critical discussions are the main factors that helped me to accomplish this work.

It has been a great opportunity to work with my colleagues in the power quality research group. I would like to thank all of them, especially Yuaning Wang and Thavatchai Tayjasanant, for their cooperation and fruitful discussions. The productive environment they created was helpful to conduct my research work.

I would like to thank my supervisors in my Master degree at Cairo University, Egypt, Dr. Mamdouh Abdel Aziz and Dr. Essam Abou El-Zahab, who put me on the first entrance to my post-graduate studies and helped me to build up my academic base to continue my research.

Finally, I would like to express due thanks to my parents for their encouragement during my period of study. I was blessed to have their support and care all these years. I got mainly from them the strength and inspiration that enabled me to finish this work and to them goes a great part of my gratitude.



# TABLE OF CONTENTS

	Page
<hr/> <b>Chapter 1</b> <hr/>	
<b>Introduction.....</b>	<b>1</b>
1.1 Power Quality.....	1
1.2 Harmonics and Harmonic Sources.....	3
1.3 Harmonics Effects.....	5
1.4 Objective and Scope.....	6
1.5 Outline of the Thesis.....	9
<hr/> <b>Chapter 2</b> <hr/>	
<b>Harmonics in Electric Power Systems.....</b>	<b>11</b>
2.1 Power Systems Harmonics.....	11
2.2 Modeling of Harmonic Sources.....	14
2.3 Power System Harmonic Analysis.....	15
2.3.1 Time Domain Analysis Methods.....	17
2.3.2 Frequency Domain Analysis Methods.....	17
2.4 Distributed Harmonic Sources.....	22
2.4.1 Main Concerns with the Operation of Distributed Harmonic Sources.....	22
2.4.2 Addition of Harmonics.....	24
2.4.3 Attenuation and Diversity of Harmonic Currents.....	25
2.4.4 Randomly Varying Harmonic-Producing Loads.....	29
2.5 Summary.....	36
<hr/> <b>Chapter 3</b> <hr/>	
<b>Harmonics Attenuation and Diversity for Single-Phase Power Electronic Loads ...</b>	<b>38</b>
3.1 Introduction.....	38
3.2 Single-Phase Capacitor-Filtered Diode Bridge Rectifier.....	40
3.3 Characterization of Single-Phase Harmonic Sources.....	42
3.3.1 Effect of Supply Impedance Variation.....	43
3.3.2 Effect of Background Voltage Distortion Variation.....	47
3.3.3 Comparison between the Results Obtained due to the Variation of Supply Impedance and Background Voltage Distortion.....	51
3.3.4 Results Justification.....	54

3.3.5 Investigating the Reliable Voltage Index on Characterizing the Harmonic Source Current Spectrum for Harmonic Analysis .....	58
3.3.6 Attenuation Factor for PC loads Based on the Supply Voltage Distortion .....	66
3.4 Summary and Conclusions .....	67

---

## Chapter 4

<b>An Iterative Method for Harmonic Distortion Assessment with Distributed PC Loads .....</b>	<b>69</b>
4.1 Introduction.....	69
4.2 Traditional Harmonic Analysis Method .....	71
4.3 Proposed Iterative Harmonic Analysis Method.....	73
4.4 Case Studies for Distributed PC Loads.....	80
4.4.1 Measurement and Calculation Results for PC system 1.....	81
4.4.2 Measurement and Calculation Results for PC system 2.....	85
4.4.3 Sensitivity Studies .....	87
4.5 Summary and Conclusions .....	95

---

## Chapter 5

<b>Harmonics Attenuation and Diversity for Three-Phase Power Electronic Loads....</b>	<b>96</b>
5.1 Introduction.....	96
5.2 Application of ASDs in Power Distribution Systems.....	97
5.2.1 Advantages of using ASDs.....	98
5.2.2 ASDs Structure and Classification .....	98
5.3 ASD Modeling and Harmonic Characteristics .....	100
5.3.1 An Equivalent Circuit Model for ASD.....	100
5.3.2 ASD Input Harmonic Current Characteristics.....	101
5.4 Characterization of Three-Phase Harmonic Sources .....	104
5.4.1 Effects of the Variation of Supply Impedance and Background Voltage Distortion .....	106
5.4.2 Results Justification.....	111
5.4.3 Justification of the Voltage Distortion Choice on Characterizing the Harmonic Source Current Spectrum for Harmonic Analysis .....	114
5.4.4 Attenuation Factor for ASD Loads Based on the Supply Voltage Distortion .....	118
5.5 Summary and Conclusions .....	118

---

## Chapter 6

---

<b>Application of the Iterative Harmonic Analysis Method with Distributed ASD Loads</b> .....	120
6.1 Introduction.....	120
6.2 Case Studies for Distributed ASD Loads.....	121
6.2.1 Goose River Oil Field System.....	122
6.2.2 Oil Field Systems F501 and F502 .....	135
6.3 Summary and Conclusions .....	143

---

## Chapter 7

---

<b>Probabilistic Evaluation of Harmonics with Randomly Varying Nonlinear Loads</b>	145
7.1 Introduction.....	145
7.2 Variation of ASD Input Harmonic Currents with Loading Level .....	147
7.3 Probabilistic ASD Model for Harmonics Assessment.....	149
7.3.1 Determination of Statistical Parameters of ASD Harmonic Currents.....	150
7.3.2 Probabilistic Bus Harmonic Voltages .....	155
7.3.3 Probabilistic Branch Harmonic Currents.....	161
7.4 Results of Probabilistic Harmonic Voltage and Current Levels.....	165
7.5 Comparison with Monte Carlo Simulation.....	170
7.6 Summary and Conclusions .....	180

---

## Chapter 8

---

<b>Conclusions</b> .....	181
8.1 Thesis Contributions.....	181
8.2 Suggestions for Future Work.....	183
<b>Bibliography</b> .....	185
<b>A. Experiment Set Up</b> .....	192
<b>B. Branch Current Statistical Parameters</b> .....	196
<b>C. Data for Study Systems</b> .....	200

## LIST OF TABLES

	<b>Page</b>
Table 6.1: Technical information of the oil field feeders .....	136
Table 7.1: Statistical parameters of harmonic voltage rectangular components .....	166
Table 7.2: Statistical parameters of harmonic current rectangular components .....	167
Table 7.3: Comparison of the 50% and 95% non-exceeding probability of the harmonic voltage magnitudes obtained by the Monte Carlo simulation and the improved analytical solution including the power flow analysis ..	178
Table 7.4: Comparison of the 50% and 95% non-exceeding probability of the harmonic current magnitudes obtained by the Monte Carlo simulation and the improved analytical solution including the power flow analysis ..	179

## LIST OF FIGURES

	<b>Page</b>
Figure 2.1: A typical distorted current waveform in electric power systems. ....	13
Figure 2.2: Harmonic source modeling. ....	15
Figure 2.3: A typical harmonic current spectrum magnitude of an ASD load. ....	15
Figure 2.4: A system with multiple harmonic sources. ....	24
Figure 2.5: Perpendicular components of random vectors. ....	30
Figure 3.1: Capacitor-filtered diode bridge rectifier Circuit.....	40
Figure 3.2: A typical measured input current waveform for a PC load with 135% current THD.....	41
Figure 3.3: Harmonic spectrum of the typical PC current waveform.....	41
Figure 3.4: Circuit connection to investigate the effect of supply impedance variation.....	43
Figure 3.5: Variation of PC current THD with voltage THD and CF due to supply impedance variation.....	44
Figure 3.6: Variation of PC individual harmonic current magnitudes with voltage THD and CF due to supply impedance variation. ....	45
Figure 3.7: Variation of PC individual harmonic current phase angles with voltage THD and CF due to supply impedance variation. ....	46
Figure 3.8: Circuit connection to investigate the effect of background voltage distortion variation.....	47
Figure 3.9: Variation of PC current THD with voltage THD and CF due to background voltage distortion variation. ....	48
Figure 3.10: Variation of PC individual harmonic current magnitudes with voltage THD and CF due to background voltage distortion variation. ....	49
Figure 3.11: Variation of PC individual harmonic current phase angles with voltage THD and CF due to background voltage distortion variation. ....	50
Figure 3.12: Variation of PC current THD with voltage THD and CF due to the change of supply impedance and background voltage distortion.....	51
Figure 3.13: Variation of PC individual harmonic current magnitudes with voltage THD and CF due to the change of supply impedance and background voltage distortion. ....	52
Figure 3.14: Variation of PC individual harmonic current phase angles with voltage THD and CF due to the change of supply impedance and background voltage distortion. ....	53
Figure 3.15: Variation of harmonic voltage components and accumulative waveforms with different supply impedance magnitudes. ....	55
Figure 3.16: Variation of harmonic voltage components and accumulative waveforms under different background voltage distortions. ....	56

Figure 3.17: Variation of harmonic voltage components and accumulative waveforms with different supply impedance $R/X$ ratios.....	57
Figure 3.18: Equivalent system to investigate the voltage response to the PC current distortion.....	60
Figure 3.19: A sample of PC current waveforms with different THD levels. ....	60
Figure 3.20: System voltage CF response to the PC current distortion. ....	62
Figure 3.21: System voltage THD response to the PC current distortion.....	63
Figure 3.22: Justification of system voltage response to the PC current distortion.....	65
Figure 3.23: Attenuation factor variation for PC harmonic current magnitudes with the supply voltage THD.....	67
Figure 4.1: Measured harmonic current spectra for a PC load under different supply voltage distortion levels.....	74
Figure 4.2: Variation of PC individual harmonic current magnitudes as a function of supply voltage distortion. ....	75
Figure 4.3: Variation of PC individual harmonic current phase angles as a function of supply voltage distortion. ....	76
Figure 4.4: Flow chart of the proposed iterative method for harmonic distortion assessment for systems with distributed harmonic sources.....	79
Figure 4.5: Single-line diagram of the two PC systems under study.....	80
Figure 4.6: Measurement and calculation results of the voltage and current THD for PC system 1. ....	82
Figure 4.7: Measurement and calculation results of the individual harmonic magnitudes and phase angles of system node voltages (PC system 1). ....	83
Figure 4.8: Measurement and calculation results of the individual harmonic magnitudes and phase angles of system harmonic source currents (PC system 1).....	84
Figure 4.9: Measurement and calculation results of the voltage and current THD for PC system 2. ....	85
Figure 4.10: Measurement and calculation results of the individual harmonic magnitudes and phase angles of the voltage and the harmonic current source at node 2 (PC system 2). ....	86
Figure 4.11: Iterative process with voltage THD and CF indices.....	88
Figure 4.12: Comparison of distortion results to show the impact of ignoring the harmonic currents diversity. ....	90
Figure 4.13: Convergence process of the voltage THD for different study cases of the supply impedance for PC system 1. ....	91
Figure 4.14: Variation of the number of iterations for convergence for different study cases of the supply impedance. ....	92
Figure 4.15: Multiplier factors for voltage and current THD. ....	94
Figure 5.1: Basic structure of an adjustable speed drive. ....	99
Figure 5.2: Generic converter circuit for ASD. ....	100
Figure 5.3: ASD high current distortion waveform and the harmonic spectrum.....	102

Figure 5.4: ASD normal current distortion waveform and the harmonic spectrum. ....	103
Figure 5.5: Harmonic current spectra for an ASD load under different supply voltage distortion levels. ....	105
Figure 5.6: Variation of ASD current THD with voltage THD and CF due to the change of supply impedance and background voltage distortion. ....	108
Figure 5.7: Variation of ASD individual harmonic current magnitudes with voltage THD due to the change of supply impedance and background voltage distortion. ....	109
Figure 5.8: Variation of ASD individual harmonic current phase angles with voltage THD due to the change of supply impedance and background voltage distortion. ....	110
Figure 5.9: Variation of different harmonic voltage components and accumulative waveforms with supply impedance. ....	112
Figure 5.10: Variation of different harmonic voltage components and accumulative waveforms with background voltage distortion. ....	113
Figure 5.11: Equivalent system to investigate the voltage response to the ASD current distortion. ....	114
Figure 5.12: System voltage response to the ASD current distortion. ....	115
Figure 5.13: Iterative process with voltage CF and THD indices. ....	116
Figure 5.14: Justification of system voltage response to the ASD current distortion. ....	117
Figure 5.15: Attenuation factor variation for ASD harmonic current spectrum magnitudes with the supply voltage THD. ....	118
Figure 6.1: Single-line diagram of Goose River oil field distribution system. ....	123
Figure 6.2: Convergence process of the voltage THD at different ASD locations. ....	125
Figure 6.3: System voltage and current THD using the traditional method and the iterative method. ....	125
Figure 6.4: Individual harmonic voltages and currents using the traditional method and the iterative method. ....	126
Figure 6.5: Comparison of individual harmonic current magnitudes. ....	127
Figure 6.6: Comparison of individual harmonic current phase angles. ....	128
Figure 6.7: Comparison of the ASD supply voltage and current distortion levels. ....	128
Figure 6.8: System voltage and current THD to show the impact of ignoring the harmonic currents diversity. ....	129
Figure 6.9: Summary of the individual harmonic voltage and current results. ....	130
Figure 6.10: Different multiplier factors for voltage and current THD (Goose River oil field system). ....	132
Figure 6.11: Individual harmonic current magnitudes (same spectrum case). ....	133
Figure 6.12: Individual harmonic current phase angles (same spectrum case). ....	134
Figure 6.13: Comparison of the ASD supply voltage and current distortion levels when applying the same harmonic current spectrum characteristic to all drives. ....	134
Figure 6.14: Single-line diagram of the oil field distribution systems F501 and F502. .	135
Figure 6.15: Iterative process with and without using the damping factor. ....	137

Figure 6.16: Results of voltage and current THD using the traditional method and the iterative method. ....	138
Figure 6.17: Results of voltage and current THD to show the impact of ignoring the harmonic currents diversity. ....	140
Figure 6.18: Different multiplier factors for voltage and current THD (systems F501 and F502). ....	141
Figure 6.19: Effect of damping factor on the speed of solution convergence. ....	142
Figure 6.20: Summary of the system bus voltage and branch current distortion results. ....	143
Figure 7.1: Variation of input current waveform with ASD loading level. ....	148
Figure 7.2: Variation of input current THD with ASD loading level. ....	148
Figure 7.3: Variation of input harmonic current magnitudes and phase angles with ASD loading level. ....	149
Figure 7.4: Variation of the real input harmonic current components with loading level for 150HP ASD. ....	152
Figure 7.5: Variation of the imaginary input harmonic current components with loading level for 150HP ASD. ....	153
Figure 7.6: Probability density function curves of the harmonic voltage magnitudes. ..	168
Figure 7.7: Probability density function curves of the harmonic current magnitudes. ....	169
Figure 7.8: The cdfs of harmonic magnitudes obtained from the analytical method and Monte Carlo simulation using the nodal equation with loading variation from 50-100%. ....	172
Figure 7.9: The cdfs of harmonic magnitudes obtained from the analytical method and Monte Carlo simulation using the nodal equation with loading variation from 80-100%. ....	173
Figure 7.10: The cdfs of harmonic magnitudes obtained from the analytical method using the nodal equation and from the Monte Carlo simulation including the power flow analysis with loading variation from 50-100%. ....	174
Figure 7.11: The cdfs of harmonic magnitudes obtained from the improved analytical method and Monte Carlo simulation including the power flow (loading 50-100%). ....	176
Figure 7.12: The cdfs of harmonic magnitudes obtained from the improved analytical method and Monte Carlo simulation including the power flow (loading 80-100%). ....	177



## LIST OF SYMBOLS

AF	: attenuation factor
ASD	: adjustable speed drive
BND	: bivariate normal distribution
C	: capacitance
CF	: crest factor
DF	: diversity factor
DM	: damping factor
f	: frequency in hertz
h	: order of harmonic
HP	: horsepower
$I_h$	: harmonic component of current of the order indicated by the subscript
IHD	: individual harmonic distortion
L	: inductance
MF	: multiplier factor
n	: higher harmonic order of interest
N	: number of harmonic sources
PC	: personal computer
PCC	: point of common coupling
pdf	: probability density function
PQ	: power quality
pu	: per unit quantities
R	: resistance
RMS	: root mean square or effective value of voltage or current
THD	: total harmonic distortion
$V_h$	: harmonic component of voltage of the order indicated by the subscript
Z	: impedance

# Chapter 1

## Introduction

Power system harmonics is an area that is receiving a great deal of attention with the advancement of power electronic technology. This is primarily due to the fact that nonlinear loads, which use solid state power electronic components, are comprising a larger and larger portion of the total connected load for a typical industrial plant [1]. Therefore, electric power distribution systems have been confronted with the fact that harmonic voltage and current distortion levels can be considerable. Harmonic distortion is one of the concerns of power quality. In this chapter, some insight into power quality is provided. Then, harmonics sources and effects are presented. The objective of the thesis is discussed, and the thesis outline is given at the end of the chapter.

### 1.1 Power Quality

In our modern world, we sometimes take for granted the vast number of electric processes that go on to support our daily life. These processes can be complex but have one thing in common, the need for high quality electric power. Power quality is the concept of powering and grounding electronic equipment in manner that is suitable to the operation of that equipment and compatible with the premise wiring system and other connected equipment [2]. Historically, most power system equipment has been able to operate successfully with relatively wide variation of these three parameters. However, within the last two decades a large amount of equipment has been added to the power system, which is not so tolerable to these variations. This has included equipment that is

controlled by power electronics. Much more precise control of different electric processes has been developed making the processes even more susceptible to the effects of power system disturbances [3].

Power quality has become a major issue for electric utilities and their customers, and indirectly to almost all of the manufacturers of equipment that depend on a supply of good quality electric power. It is a research area of exponentially increasing interest and an issue that needs continual attention. It has become of great importance due to the increase in the number of linear and nonlinear loads sensitive to power disturbances. In attempting to define power quality, the views of utilities, equipment manufacturers, and customers might be completely different.

Utilities regard power quality from the system reliability point of view. They are under increasing pressure to ensure providing adequate power quality to their customers. This has been an important task for them because of changes in user equipment and requirements. Equipment manufacturers consider power quality as being that level allowing for proper operation of their equipment so that their products' service life can be extended. For consumers, the problem of new equipment sensitivity to service quality is an essential issue to be considered. Therefore, they require that disturbance levels be limited in power systems. They are particularly interested in dependable power quality from their utility that ensures the continuous running of processes, operations, and businesses.

Generally, a power quality problem could be defined as being any power problem manifested in voltage, current, or frequency deviations that result in failure or misoperation of customer equipment. The growing concern with power quality is due to many reasons including the following [4]:

- The widespread use of sensitive microprocessor-based controls and power electronics devices.
- The complexity of industrial processes, which results in huge economic losses if equipment fails or malfunctions.

- The proliferation of large computer systems into many businesses and commercial facilities.
- The development of much sophisticated power electronics equipment used for improving system stability, operation, and efficiency. The presence of these devices degrades power quality and they are themselves vulnerable to such quality of power.
- Deregulation of power industry, which gives customers the right to demand higher quality of power.
- Growth in application of such devices as high efficiency adjustable speed drives and power factor improvement shunt capacitors. These devices have a negative impact on the system capability due to the increasing harmonic levels they cause.
- The complex interconnection of systems which can result in more severe consequences if any one component fails.

## 1.2 Harmonics and Harmonic Sources

In power systems, the alternating current (AC) electric networks are designed to operate with pure sinusoidal 50 Hz or 60 Hz alternating voltages and currents. Electric utilities strive to supply smooth sinusoidal voltage waveform of the fundamental frequency to their customers. The current flowing to the customer load can also be of pure sinusoidal waveform of the same frequency like the supplied voltage; in this case the load is linear. On the other hand, the flowing current for some load equipment can be distorted and deviated from the sinusoidal waveform; in this case the load is nonlinear and considered as a harmonic source.

The voltage and current waveforms in modern power systems are seldom sinusoidal because of the increased use of nonlinear electrical devices. The distorted waveforms contain sinusoidal components, which have frequencies of multiples of the fundamental frequency. These high frequency components are called harmonics. Typical nonlinear loads are adjustable speed drives (ASDs), electric arc furnaces (EAFs), personal

computers (PCs), light dimmers, battery chargers and all loads that use AC/DC converters [5,6].

Harmonics are one of the power quality concerns. The interest in harmonics on distribution systems is mainly due to the widespread use of power electronic devices and the increase in sensitivity of electronic loads with greater dependence upon their undisturbed operation. The proliferation of power electronic based loads has led to a significant increase in voltage distortion and harmonic currents [7,8].

The main sources of harmonics can be classified into the following three categories:

- 1) Power electronic devices.
- 2) Arcing devices.
- 3) Electromagnetic saturable devices.

For the first category, switching power electronic components which occurs within a single cycle of the power system fundamental frequency is responsible for the nonlinear characteristic and generation of harmonics [8]. This switching is necessary for the purpose of increasing the efficiency and controllability. As the cost of power electronics decreases, their application in customer loads will increase. This trend, while beneficial from a load efficiency point of view, is a cause of concern because the level of harmonic distortion in power systems will increase with the extensive use of power electronic devices [5]. The main harmonic sources under this category are: 1) three-phase static power converters, 2) switch mode power supplies, and 3) static VAR compensators used for maintaining constant voltage level. For the second category, the harmonics are generated as a result of the nonlinear relationship between the voltage and current due to the physical nature of the electric arc. The main harmonic sources under this category are electric arc furnaces and gas discharging lamps. For the third category, harmonics are generated due to the nonlinearity of the magnetic core caused by the electromagnetic saturation as found in electric power transformers [9].

### 1.3 Harmonics Effects

Harmonics in industrial systems are typically generated from variable frequency motor drives, electric arc furnaces, and static power converters. Reducing the amount of harmonics in power systems is one way to improve the system power quality. Increased level of harmonic distortion may cause one of the following effects:

- 1) Power system equipment are designed to operate under the fundamental power frequency, so the presence of harmonics can cause extra losses and heating to the power system equipment [10].
- 2) Harmonics can impose voltage and current stresses on power cables and can lead to dielectric failure [11].
- 3) Shortening capacitor life may be possible due to the presence of harmonics if the capacitor size is not carefully selected. Capacitors are usually used for power factor improvement, but they provide low shunt impedance path at higher frequencies. Therefore, they can be overloaded and eventually capacitor failure may occur [12]. A 10% increase in voltage stress caused by harmonic currents typically results in a 7% increase in the operating temperature of a capacitor bank and can reduce its life expectancy by 30% of normal [13].
- 4) Severe harmonic problems may happen when capacitor banks are added to an electrical system. The addition of capacitive reactance to the characteristic inductive nature of the system may cause parallel resonance. If the resonant frequency of the combined circuit is near to the frequency of harmonics produced by a harmonic source connected to the same system, this will result in high harmonic voltage magnitudes and magnified harmonic currents in the resonant circuit [9].
- 5) Communication interference is likely to occur when power lines run close to telephone lines [14,15].
- 6) Malfunctioning of power electronic loads can take place in harmonics environment. Some power electronic loads are sensitive to the AC supply voltage characteristics such as zero crossing time for the control purpose. Therefore, excessive harmonic distortion can make the power electronic load operate improperly [16].

- 7) Harmonics can cause errors in metering instruments [11]. This is because the relationship between different parameters in pure sinusoidal waveforms is no longer valid with distorted ones, for example, the ratio of the peak to the RMS value is not  $\sqrt{2}$ . This is prone to cause metering errors.

#### 1.4 Objective and Scope

Most of the past studies on distribution system harmonics have tended to focus on systems with only one or a few harmonic-producing loads. A noticeable trend in power systems nowadays is the emergence of distributed harmonic-producing loads. These loads typically have comparable sizes and are distributed all over an electric network. Traditional techniques for harmonic power flow analysis generally have difficulties in determining the collective impact of these loads. It is very often that harmonic distortion levels in distribution systems are substantially lower than what one would expect from a harmonic power flow study based on equipment inventory [10].

Determination of harmonic distortions for systems with distributed harmonic sources is a new and challenging research topic in the area of harmonic analysis. In this situation, the system distortion level is not only affected by the interaction between the harmonic source and the system but also by the interaction between each harmonic source and the others distributed across the system, which makes the situation more complicated. Some of the conducted work considered only the case of deterministic harmonic-producing loads and the sensitivity of the generated harmonic currents to the supply voltage distortion [17]. However, no research work has been conducted to perform harmonic power flow to assess system harmonic distortion levels considering the impact of the voltage distortion on the harmonic source current magnitudes (attenuation effect) and phase angles (diversity effect). On the other side, other research work considered the random variation of the harmonic sources and the subsequent effect on the harmonic currents without paying attention to the impact of the voltage distortion [18], i.e., the attenuation and diversity effects were ignored. Considering the two problems,

attenuation/diversity and random harmonics simultaneously would be complicated. In order to make the problem manageable, it has been sub-divided in this research work into two. This would provide the base to deal separately with each problem so that in the future a comprehensive harmonic power flow algorithm can be developed to solve for the combined two problems.

The first sub-problem can be described as the following: a distribution system has a number of harmonic-producing loads of comparable sizes. The loads operate at a constant load level. An office building with a lot of PCs and an industrial distribution system equipped with a large number of ASD loads are typical examples of such a case. It is required to determine the harmonic distortion level for this type of systems. Traditional method to solve this problem is to model each PC as a fixed harmonic current source. Harmonic power flow methods are then used to determine the distortion results. The main problem of this approach is that it can not take into account the attenuation and diversity effects of the harmonic sources. Consequently, the results can be quite conservative, since both effects help to reduce the overall harmonic distortion level in the system. Although several papers have been published on this subject [17,19], almost no method has been proposed to estimate the harmonic distortion levels for such systems.

The attenuation and diversity effects appear due to the considerable distortion of the system voltage associated with the operation of a considerable number of harmonic sources. The traditional harmonic analysis methods can provide reliable and accurate system harmonic levels when the system voltage distortion is not significant. However, the situation is different in the presence of distributed harmonic sources. The resultant harmonic current can be significant leading to severe voltage distortion across the system. The research work in this thesis is concerned with finding a way to take into account the impact of the voltage distortion on the harmonic currents produced by the harmonic sources and to consider the harmonics attenuation and diversity in the harmonic analysis for harmonic distortion evaluation.



The second sub-problem is to consider the random variation of the loads in addition to its distributed nature. A typical case can be described as the following: a distribution system has a number of harmonic-producing loads of comparable sizes. The loads vary randomly between minimum and maximum levels. With the variation of the loading level, the harmonic source currents are also varying. Therefore, using a deterministic method for harmonic analysis is not suitable because of the stochastic nature of the harmonics. How can one determine the mean value and the 95% probability value of the harmonic levels in the system? The 95% probability level is defined as the value that could be exceeded only for 5% probability. Hence, a probabilistic technique is needed for harmonics evaluation. The technique should consider the dependence of the harmonic source currents on the loading level.

The scope of this thesis can be summarized as follows:

- Determining the most appropriate index of the supply voltage waveform to characterize the harmonic current magnitudes and phase angles for typical single-phase and three-phase harmonic sources.
- Developing a harmonic analysis method based on the obtained harmonic current characteristics so that the harmonics attenuation and diversity can be included in the harmonic calculation.
- Verifying the proposed method through harmonic measurements and time domain simulation.
- Determining the dependence of the harmonic source currents on the loading level. Accordingly, an analytical method is proposed to calculate the probabilistic harmonic voltage and current levels for systems with distributed harmonic sources of randomly varying load.
- Verifying the proposed analytical probabilistic method by conducting Monte Carlo simulation of probabilistic harmonic power flow for a typical distribution system and comparing the results obtained by the two methods.

## 1.5 Outline of the Thesis

The contents of the thesis are organized as follows:

Chapter 2 provides an overview on harmonics in electric power systems. Harmonics representation of distorted waveforms is presented. The most common harmonic analysis techniques are reviewed. The concerns about harmonics in the presence of distributed harmonic sources are discussed. The attenuation and diversity of harmonic currents are defined. The summation technique of random harmonic phasors is presented showing how to get the probability density function of the summation magnitude.

Chapter 3 investigates the harmonic current characteristics of a PC load as one of the most commonly used single-phase power electronic loads. Extensive measurements are conducted under different distorted supply voltage waveforms and the corresponding variation of the harmonic current magnitudes and phase angles is addressed. In addition to the measurement results, further investigation is made to justify the choice of the total harmonic distortion of the supply voltage as the reliable index to determine the harmonic spectra of the currents injected from PC loads.

Chapter 4 proposes an iterative harmonic analysis method to account for harmonics attenuation and diversity based on the harmonic measurements conducted in Chapter 3. The method is verified by performing experimental measurements for distributed PC loads. Sensitivity studies are carried out to evaluate the performance of the proposed method and the extension possibility to other harmonic source loads.

Chapter 5 gives an overview about the three-phase ASD load, which is extensively used in industrial distribution systems. Then, it extends the work done in Chapter 3 by conducting extensive simulations on an ASD to investigate the relationship between the supply voltage waveform and the load harmonic current magnitudes and phase angles. The obtained results are examined to assert that the voltage total harmonic distortion can be adopted as an indicator of the harmonic source current spectrum. Therefore, the proposed harmonic analysis method can be applied with ASD loads.

Chapter 6 presents the implementation of the proposed harmonic analysis method on distribution systems with distributed ASD loads. The method utilizes the obtained relationships in Chapter 5 between the harmonic currents and the supply voltage distortion. Different distribution systems with different topologies are considered for such a study. Time domain simulation is performed to validate the application of the proposed method with ASD loads. Additionally, sensitivity studies are conducted to examine the performance of the method and its implementation with some approximations.

Chapter 7 considers the case with randomly varying harmonic source loads. A probabilistic ASD model is developed due to the random variation of the drive loading level. An analytical method utilizing the Central Limit theorem and summation technique of random harmonic phasors is applied to get the probabilistic harmonic voltage and current magnitudes. A comparison with the results obtained from Monte Carlo simulation of probabilistic harmonic power flow is performed to verify the implementation of the analytical method.

Chapter 8 provides the conclusions drawn from the work conducted in this thesis and gives suggestions for future research.

At the end of the thesis, a list of references regarding its scope is provided.

# Chapter 2

## Harmonics in Electric Power Systems

The proliferation of nonlinear loads deviates the voltage and current waveforms from their sinusoidal nature and harmonics are produced. This chapter presents many aspects related to power system harmonics such as representation, sources, and analysis. The main concerns about the operation of distributed harmonic sources are discussed. The attenuation and the diversity of harmonic currents associated with the operation of multiple harmonic sources of a constant load are explained. The summation of randomly varying harmonic vectors is presented showing how to obtain the probabilistic summation magnitude.

### 2.1 Power Systems Harmonics

The fundamental objective of electricity supply and distribution companies is to supply each electricity customer with energy at a single and constant frequency and at a specific voltage level of constant magnitudes. However, none of these conditions are fulfilled in practice since much of today's production equipment does not draw a sinusoidal current from the sinusoidal voltage source. This is known as nonlinear load where the relationship between voltage and current at every moment in time is not constant [9]. Nonlinear loads change the sinusoidal nature of the supply AC current and consequently the AC voltage drop across the power system impedance, thereby resulting in the flow of harmonic currents [10,11].

In an ideal electric power system, the voltage at any point is a constant sinusoid repeated at a fundamental frequency of 50 or 60 Hz. However, distorted current and voltage waveforms are frequently met in power systems. They contain sinusoidal components, which have frequencies of multiples of the fundamental frequency. These high frequency components are called harmonics and contribute to the distortion of the original fundamental frequency waveform.

Harmonics are a mathematical way of describing a steady-state nonsinusoidal voltage or current waveform [1]. Under periodic steady conditions, distorted voltage and current waveforms can be expressed in the form of Fourier Series. The Fourier Series for a periodic function  $f(t)$  with fundamental frequency  $\omega$  can be represented as [20]:

$$f(t) = C_0 + \sum_{h=1}^{\infty} C_h \cos(h\omega t + \theta_h) \quad (2.1)$$

The coefficient  $C_h$  and phase angles  $\theta_h$  for the  $h$ -th harmonic are given by:

$$C_h = \sqrt{A_h^2 + B_h^2}, \quad \theta_h = \tan^{-1}\left(-\frac{B_h}{A_h}\right) \quad (2.2)$$

where  $T=2\pi/\omega$  and  $C_0$  is the DC component of the function. The RMS value of  $f(t)$  is defined as:

$$A_h = \frac{2}{T} \int_0^T f(t) \cos(h\omega t) dt, \quad B_h = \frac{2}{T} \int_0^T f(t) \sin(h\omega t) dt \quad (2.3)$$

$$C_0 = \frac{1}{T} \int_0^T f(t) dt \quad (2.4)$$

$$RMS = \sqrt{C_0^2 + \sum_{h=1}^{\infty} \left(\frac{C_h}{\sqrt{2}}\right)^2} \quad (2.5)$$

Harmonic components are combined together so that the resultant waveform is no longer a smooth sinusoidal one. Figure 2.1 presents a typical distorted current waveform generated by a harmonic-producing load in power systems of 60Hz fundamental

frequency. The figure also depicts the associated fundamental and 5th harmonic components of this waveform.

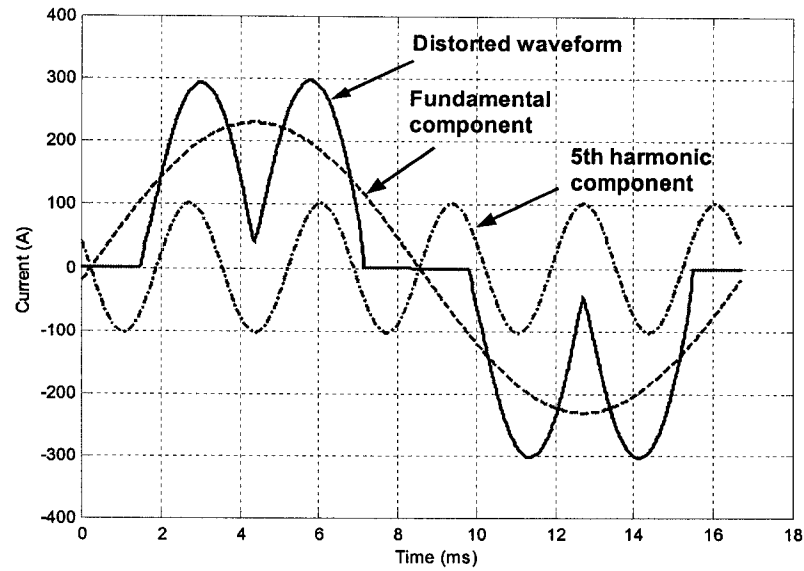


Figure 2.1: A typical distorted current waveform in electric power systems.

The most commonly used index to measure the deviation of a periodic waveform from a sine wave is called Total Harmonic Distortion (THD) [8,11,15,20]. It quantifies the harmonics content of voltage and current waveforms encountered in power systems. The THD is equal to the ratio of the RMS value of all harmonics to the RMS value of the fundamental component as a percentage. The THD of bus voltages (VTHD) and branch line currents (ITHD) can be calculated as follows:

$$VTHD = \frac{\sqrt{\sum_{h=2}^n V_h^2}}{V_1} \times 100\%, \quad ITHD = \frac{\sqrt{\sum_{h=2}^n I_h^2}}{I_1} \times 100\% \quad (2.6)$$

where

$V_1, I_1$ : RMS value of the fundamental voltage and current components,

$V_2$  to  $V_n$ : RMS value of the harmonic voltage components,

$I_2$  to  $I_n$ : RMS value of the harmonic current components,

$h$ : harmonic order,

$n$ : highest order of interest for harmonic distortion calculation.

Evidently, for a pure sinusoidal waveform, total harmonic distortion is zero. Over the past years, electric utilities have experienced an increase in the level of harmonics, therefore, most electric utility companies often assess the quality of power supplied to major customers to make sure that harmonic distortion levels are within the recommended limits [12]<sup>1</sup>.

Several other distortion indices are defined in [11], each intended to capture a specific impact of harmonics. Telephone Influence Factor (TIF) is used to measure telephone interference. The  $K$ -factor index is used to describe the impact of harmonics on losses and is useful in derating equipment such as transformers [20].

## 2.2 Modeling of Harmonic Sources

Harmonic sources are most commonly represented by a simple ideal current source at different harmonic frequencies as shown in Figure 2.2. This is due to the fact that a harmonic-producing load acts as an injection current source to the system in the steady-state condition [21]. Periodic steady-state distortion can be very effectively studied by examining the components of a Fourier series representation of the waveforms [10]. The current spectrum of the harmonic source can give the amplitude of the harmonic current components in percent of the fundamental one. Figure 2.3 presents a typical harmonic current spectrum magnitude of an adjustable speed drive (ASD) load. The characteristics of the harmonic source currents can be obtained from field measurements, specified manufacturer data or simulation programs. These characteristics are vital and should be carefully considered when performing harmonic analysis to evaluate the harmonic distortion level for systems equipped with harmonic-producing loads.

---

<sup>1</sup> For a voltage level less than 69 kV, the voltage THD standard limit is 5%. The current THD standard limit depends on the ratio of the short circuit current level available at the point of common coupling to the maximum fundamental load current ( $I_{sc}/I_L$ ). For a voltage level between 120 V and 69 kV, the current THD limit varies between 5% and 20% for  $I_{sc}/I_L$  ratio less than 20 and greater than 1000 respectively.

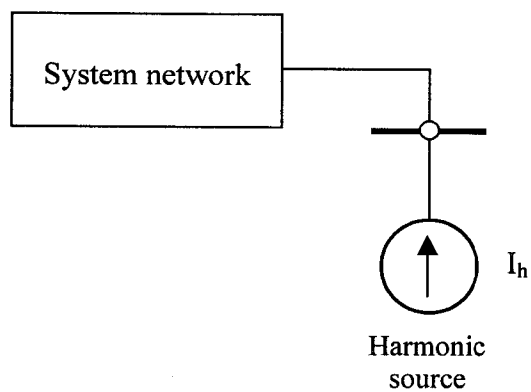


Figure 2.2: Harmonic source modeling.

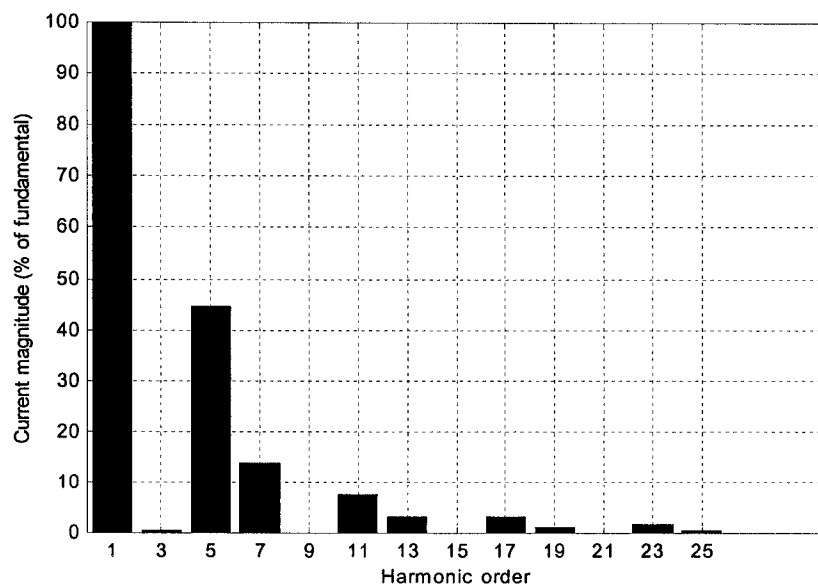


Figure 2.3: A typical harmonic current spectrum magnitude of an ASD load.

### 2.3 Power System Harmonic Analysis

Quality of power supply is now a major issue worldwide making harmonic analysis an essential aspect in power system planning and design. Harmonic analysis is the process of measuring or calculating the relative amplitudes of all the significant harmonic components present in a given voltage and current complex waveforms in order to



quantify their distortion level [22,23]. Therefore, it can determine the state and performance of the system at harmonic frequencies and can help analyze the consequences of waveform pollution.

The need for harmonic study may be indicated by excessive distortion in existing systems or by installation of new harmonic-producing equipment. It is a key element to assess the power system supply quality. Standards such as the IEEE 519-1992 [11] are referred to for guidelines of operation under harmonic conditions, and for developing and evaluating mitigation measures [10].

A harmonic analysis numerical tool is usually applied to study the generation and propagation of harmonics in an arbitrary topology network. This is an important task due to the following reasons [7,11]:

- 1) To assess the existing harmonic distortion levels and check if they are within the harmonic standards.
- 2) To judge if the produced harmonics can cause system problems such as harmonic resonance. Resonance is the indication of high harmonic voltage while the injected harmonic current is of small amplitude. This may result in improper electric equipment operation.
- 3) To evaluate the impact of adding new harmonic sources on the system. If certain system will expand by adding new nonlinear loads, it is of concern to assess whether the new loads will cause harmonic problems or not.
- 4) To help in the proper design of harmonic filtering without filter overloading or overestimation, i.e., help in the proper selection of harmonic filter components.

Different techniques have been proposed for power system harmonic analysis. These techniques vary in terms of data requirements, modeling complexity, problem formulation and solution algorithms [20]. The objective is to find the steady-state solution of distribution system voltages and currents in the presence of one or more nonlinear loads. The harmonic analysis methods can be grouped in two general categories: time domain analysis methods and frequency domain analysis methods [24].

### 2.3.1 Time Domain Analysis Methods

Time domain methodologies are primarily based on numerical integration techniques where the system model is in the form of differential equations. The solution is obtained by assuming a set of initial conditions and integrating the system equations over time. After the system has reached steady-state condition, the voltage and current waveforms of interest are subjected to Fourier analysis in order to derive the harmonic spectrum [13,25]. Time domain formulations have the advantage of dealing directly with real physical phenomena. This property greatly facilitates the modeling of nonlinear elements, which are the sources of harmonics [26,27].

One of the main disadvantages of the time domain based method is the lack of load flow constraints (such as constant power specification at load buses) at the fundamental frequency [20]. In addition, with time domain methods, it is difficult to accurately model the frequency-dependence of the AC network. Moreover, it is computationally demanding and time consuming for lightly damped circuits and an exhaustive process for large size network [27]. Accordingly, it is practically limited to the study of small systems and few numbers of case studies. Many of the most time domain simulation programs, like Electromagnetic Transients Program (EMTP) [28] and Alternative Transient Program (ATP), require significant experience on the part of the user to get reliable results [26].

### 2.3.2 Frequency Domain Analysis Methods

For a linear system, the steady-state response possesses a linear relationship with sinusoidal excitations [11]. This feature has made the frequency domain approaches very attractive for steady-state analysis on top of its simplicity in implementation. In addition, it can handle the frequency-dependence of power system elements [27]. The limitation of the frequency domain-based methods is the inability to simulate accurately high harmonic orders because the models of transformers and loads become inaccurate at higher frequencies. Besides, the power system nonlinearities are managed more precisely

using time domain methods [26]. Different techniques of the frequency domain analysis are presented in the following.

#### 2.3.2.1 Frequency Scan Method

Frequency scan is the simplest and most commonly used frequency domain technique for harmonic analysis. The input data requirements are minimized. It calculates the frequency response of a network seen at a particular bus or node. Typically a 1 per unit sinusoidal current (or voltage) is injected into the bus of interest and the voltage (or current) response is calculated. This calculation is repeated using discrete frequency steps throughout the range of interest [20]. The result is generally the input impedance or admittance at a particular point in the network.

In a typical frequency scan analysis, only harmonic currents at the concerned bus are nonzero and the driving point impedance versus frequency plot is provided to give a quick visual indication of the natural frequencies at that bus. Therefore, frequency scan simulations can identify system configuration that may cause potential harmonic problems due to resonance conditions, even though no specific sources are being considered [7]. Then, harmonic analysis is conducted to evaluate the effectiveness of harmonic filters or other harmonic reduction technique [9].

While the frequency scan can provide some useful insight into the system response at harmonic frequencies, it is not a substitute for formal harmonic power flow studies, which model the actual harmonic generation from sources in the presence of distortion [10]. Additionally, with a large number of harmonic source locations, it is difficult to determine the frequency scan buses [22].

#### 2.3.2.2 Direct Injected Current Method

If more data are available on the harmonic source characteristics, the frequency scan can be extended to determine additional harmonic distortion information. For example, 1 per unit injection current can be replaced by a specific harmonic current while all harmonic

sources are considered at the same time. The harmonic current has a magnitude determined from the typical harmonic spectrum and rated load current of the corresponding harmonic-producing equipment [20].

The injected harmonic currents would result in nonsinusoidal bus voltage wave shape due to the nonzero driving point bus impedance at the load. For a network with  $m$  buses, the harmonic bus voltages can be obtained by solving the following network nodal equation at each harmonic frequency:

$$[V_h] = [Z_h][I_h] = [Y_h]^{-1}[I_h],$$

$$\begin{bmatrix} V_{h-1} \\ V_{h-2} \\ \cdot \\ \cdot \\ V_{h-m} \end{bmatrix} = \begin{bmatrix} Y_{h-11} & Y_{h-12} & 0 & \cdot & \cdot & Y_{h-1m} \\ Y_{h-21} & Y_{h-22} & 0 & \cdot & \cdot & Y_{h-2m} \\ 0 & 0 & \cdot & 0 & \cdot & \cdot \\ \cdot & \cdot & 0 & \cdot & \cdot & \cdot \\ \cdot & \cdot & \cdot & \cdot & \cdot & 0 \\ Y_{h-m1} & Y_{h-m2} & \cdot & \cdot & 0 & Y_{h-mm} \end{bmatrix}^{-1} \begin{bmatrix} I_{h-1} \\ I_{h-2} \\ \cdot \\ \cdot \\ I_{h-m} \end{bmatrix} \quad (2.7)$$

where  $[V_h]$  is the nodal harmonic voltage vector to be solved,  $[I_h]$  is the known harmonic current vector, and  $[Z_h]$  and  $[Y_h]$  are the system bus impedance and admittance matrices at the  $h$ -th harmonic order. To compute the THD of the voltage, the nominal bus voltage at fundamental frequency is used [20]. The resultant voltage waveform is synthesized according to the following equation:

$$v(t) = \sum_{h=1}^n \sqrt{2} V_h \sin(h\omega t + \phi_h) \quad (2.8)$$

Knowing the harmonic voltages at every bus, it is possible to determine the harmonic current flow on any link as follows:

$$I_{h-(i,j)} = \frac{V_{h-i} - V_{h-j}}{Z_{h-(i,j)}} \quad (2.9)$$

where

- $I_{h-(i,j)}$ : harmonic current flowing on link between buses  $i$  and  $j$ ,
- $V_{h-i}, V_{h-j}$ : harmonic voltages at buses  $i$  and  $j$ ,
- $Z_{h-(i,j)}$ : harmonic impedance of link between buses  $i$  and  $j$ .

A fundamental frequency load flow is needed to accurately model multiple harmonic sources. Typical phase relationships between the fundamental frequency current and the harmonic currents of the nonlinear elements must be available. This approach is very effective for analyzing power systems with power electronic devices. The load flow, modeling the harmonic-producing devices as constant power loads, calculates the fundamental frequency current drawn by the load. The magnitudes of harmonic current sources tend to be more accurate since the fundamental current given by the load flow, not the rated current, is used to calculate the harmonic current magnitudes. Consequently, more accurate current THD assessment is obtained [20]. The fundamental frequency load flow solution is also beneficial for providing more accurate information for fundamental voltages that can be used for THD calculations.

The direct injected current method is easy for implementation and computationally efficient so that it can be used to handle large size systems. It has the ability to consider simultaneously the injected harmonic currents from different harmonic sources. The main disadvantage of the method is the use of typical harmonic spectra to represent harmonic-producing devices. This prevents an adequate assessment of cases involving non-typical operating conditions. Such conditions include partial loading of harmonic-producing devices and excessive harmonic voltage distortions. Even under typical conditions, the voltage-dependent harmonic producing nature of nonlinear devices may make the accuracy of typical spectrum based methods unacceptable. For some devices with nonlinear  $v-i$  relationships, the voltage-dependency is so strong that no typical spectra exist. These conditions promoted the development of a number of advanced harmonic analysis methods. One of the well-known methods is the so-called “harmonic iteration” method [20,21].

### 2.3.2.3 Harmonic Iteration Method

Harmonic iteration method is one of the methods in which a harmonic-producing device is modeled as a supply voltage-dependent current source as follows [20,29]:

$$I_h = F(V_1, V_2, \dots, V_n, C_s), \quad h = 1, \dots, n \quad (2.10)$$

where  $(V_1, \dots, V_n)$  are the harmonic phasors of the supply voltage and  $C_s$  is a set of control variables such as converter firing angles or output power. This equation is first solved using an estimated supply voltage. The results are used as the current sources in equation (2.7) from which bus harmonic voltages are then solved. By running the load flow to get the solution at the fundamental frequency, the voltages are in turn used to calculate more accurate harmonic current sources from equation (2.10). This iterative process is repeated until convergence is achieved. One of the main advantages of this “decoupled” approach is that the device model can be in a closed form, a time domain simulation process, or any other form. Iterative harmonic methods can easily model the network frequency-dependence and reliable convergence has been reported in many case studies [29], although difficulties in convergence may occur near sharply tuned resonance [20,27]. Convergence can be improved by including the equivalent admittance of nonlinear devices into the admittance matrix equation (2.10) [14].

Another method that takes into account the voltage-dependent nature of nonlinear devices is to solve system equation (2.7) and device equation (2.10) simultaneously using Newton type algorithms [27,30]. This method generally requires that the device models be available in a closed form or in a form wherein derivatives can be efficiently computed. In theory, convergence of this method is better than that of the harmonic iteration scheme if the starting point is close to the solution point [20,27]. A variation of this method is the formulation of the system equation. In [31], equation (2.7) is formulated as a power flow equation and the control variables (firing angles) are solved based on the converter power specifications.

In summary, the problem of harmonic analysis can be cast mathematically as the solution of a network equation and a set of device equations at fundamental and harmonic frequencies. The network equation can be formulated in an admittance matrix form or in a power flow equation form. The device equations can be as simple as known current sources or as complex as control-variable dependent circuits. Which technique to use for a particular harmonic problem is, to a large extent, determined by the available data. An important consideration in harmonic analysis is to use a method commensurate with input data accuracy [20].

## **2.4 Distributed Harmonic Sources**

Considerable knowledge has been accumulated over the past twenty years on the assessment of harmonic distortions. Harmonic analysis has been focused on systems with one or several harmonic sources of a constant load [19]. However, it has recently become more common to see systems with multiple harmonic sources of comparable sizes distributed across the systems. Serious concerns have been raised regarding the subsequent increase in voltage and current distortion levels in distribution systems [5,32,33]. Theoretically speaking, harmonic-producing loads can be represented individually in network-wide harmonic studies as harmonic current sources. The problem is that there exist a number of such loads in a typical system and detailed studies using traditional harmonic power flow programs becomes impractical because it ignores the interaction between the harmonic sources and the system. What is really of concern in distribution system harmonic analysis is the collective effects of these loads [20].

### **2.4.1 Main Concerns with the Operation of Distributed Harmonic Sources**

Two main issues should be carefully addressed when conducting harmonic analysis for systems with distributed harmonic sources. The first issue is the attenuation and diversity of harmonic currents for constant load harmonic sources. This appears in the proliferation of large computer systems into many businesses and commercial facilities and in the extensive use of ASDs in industrial distribution systems. Both loads represent typical

single-phase and three-phase harmonic-producing loads. The second issue is the randomness of harmonics generated from randomly operating harmonic sources. In both situations the harmonic current spectrum is no longer fixed. The harmonic characteristics of the harmonic-producing load input current depend on the load type, loading level, and the characteristics of the system supplying the load. With higher supply voltage distortion or higher loading level of the harmonic source, the magnitudes of the dominant harmonic currents of the injected current spectrum are attenuated which causes a reduction in the system distortion level. The phase angles are also changed so that partial harmonic cancellation may occur among different harmonic sources. The phase angle diversity can lead to an additional reduction in the system harmonic distortion.

Common harmonic analysis methods use the typical harmonic current spectrum for harmonic source modeling, therefore, can not take into account the variation of the current spectrum due to the supply voltage distortion or the random variation of loading level. Very little research has been done in the area of characterization and assessment of harmonic distortions for systems with distributed harmonic sources. It is the collective effect of individual sources that causes unacceptable harmonic distortion in the system. How to determine the collective effect of distributed harmonic sources still remains as a challenging technical problem.

From the aforementioned, it becomes necessary to extend the research on power system harmonics to develop different harmonic analysis methods for systems with distributed harmonic sources. The first method should consider the attenuation and diversity of harmonic currents to account for the interaction between the constant load harmonic sources and the supply system. The second method should be able to deal with the case of randomly varying harmonic-producing loads and the randomly generated harmonics.



### 2.4.2 Addition of Harmonics

It should be mentioned that the focus of this thesis is on harmonics, which means the voltage and current components that have frequencies of integer multiples of the system fundamental frequency, while the interharmonics that can be generated from some specific nonlinear loads are not considered. For systems with only one harmonic-producing load at bus  $i$ , the harmonic voltage at bus  $k$  can be obtained, using equation (2.7), as follows:

$$V_{h-k} = Z_{h-ki} I_{h-i} \quad (2.11)$$

In this case, the phase angles of the harmonic current sources representing this load are not a concern since the bus voltage at each harmonic order is determined completely by the magnitude of the injected harmonic current. However, if there are  $N$  harmonic sources in a system as shown in Figure (2.4), the harmonic voltage at bus  $k$  is calculated by:

$$V_{h-k} = \sum_{i=1}^N V_{h-ki} = \sum_{i=1}^N Z_{h-ki} I_{h-i} = Z_{h-k1} I_{h-1} + Z_{h-k2} I_{h-2} + \dots + Z_{h-kN} I_{h-N} \quad (2.12)$$

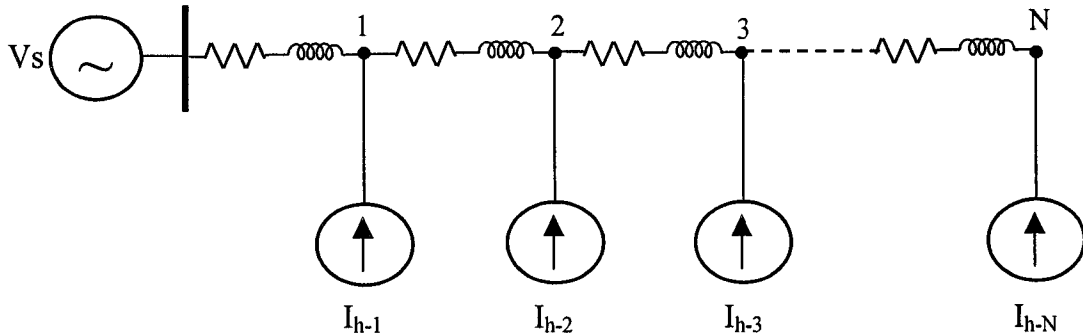


Figure 2.4: A system with multiple harmonic sources.

It can be inferred that the harmonic current produced from each source contributes to the harmonic voltage at any bus in the system. The harmonic voltage contents will add vectorially and, therefore, the combined harmonic voltage level is highly dependent on the phase angles assumed for each harmonic current source. Assuming that all current sources have the same phase angle is one of the methods to address the phase angle

problem. In most cases, this approach yields conservative estimates of the harmonic distortion level and tends to overestimate the harmonic currents by failing to account for the diversity among the phase angles. However, the results are not necessarily the worst case distortion that may be experienced by the system [10].

Rigorous addition of harmonic voltage and current contributions from multiple harmonic sources is likely to be impossible [11]. Therefore, it is sometimes worthwhile to estimate the worst case combination of the phase angles. The results can be obtained by performing harmonic studies with one harmonic-producing element being modeled at a time. The worst case harmonic level, voltage or current, is the arithmetic summation of the harmonic magnitudes calculated in each study [10].

The addition of harmonics arises when studying the connection of a new harmonic source because the distortion levels are a consequence of the way in which the harmonics will add up to the ones generated by other existing or future loads. Considering the variety and complexity of situations, it is difficult to give generally valid guidelines. Such guidelines are however necessary for practical applications and it seems worth trying to suggest some relying on all the available theoretical and practical information [34].

### **2.4.3 Attenuation and Diversity of Harmonic Currents**

Harmonic currents produced by constant load harmonic sources are normally derived on the assumption of a perfectly sinusoidal supply voltage. This assumption ignores the interaction between harmonic current injections and the supply voltage and consequently is not adequate for buses where the voltage distortion is significant. The voltage distortion always appears with more flattened waveform due to the associated reduction in the fundamental component. When the harmonic sources implementing power electronic components supplied by such waveform, the drawn current pulses or humps becomes wider and skewed to the right. This waveform change causes the magnitude of the harmonic contents to be less with more phase angle delay. The reduction in the magnitude is an indication of the harmonics attenuation and the change in the phase angle

is an indication of the phase angle diversity among different harmonic source currents subjected to different voltage distortion levels. This means that the current magnitudes and phase angles are susceptible to the supply voltage distortion due to the attenuation and diversity effects. Therefore, the commonly used fixed current injection method, using the arithmetic sums of harmonic current magnitudes, can significantly overestimate the cumulative harmonic currents produced by multiple harmonic sources.

The input current of multiple harmonic-producing loads connected through different impedances, and all are fed through a common impedance is subjected to harmonic distortion reduction [17,35]. The first cause of this reduction is found related to the attenuation of harmonic currents. The basic definition of the attenuation factor of the resultant  $h$ -th harmonic current with the operation of  $N$  PCs sharing a common supply impedance is defined in [17] as follows:

$$AF_{h,N} = \frac{I_{h,N}}{N \times I_{h,1}} \quad (2.13)$$

where

$I_{h,N}$ : the resultant  $h$ -th harmonic current when  $N$  PCs are in operation,

$I_{h,1}$ : the  $h$ -th harmonic current when 1 PC is in operation.

A small value of the attenuation factor means a high degree of attenuation. Conversely, when the attenuation factor approaches unity, a negligible attenuation is indicated. If the attenuation factor becomes more than unity, it simply means that the variation of the input current waveform occurs such that the relative proportion of the resultant harmonic current increases with the connection of more loads. The attenuation mainly depends on the number of connected harmonic sources and the shared impedance magnitude.

The second cause of the cumulative harmonic current reduction with the operation of multiple nonlinear loads is related to the phase angle disparity of the individual harmonic currents. This is caused by the discrepancy of the individual supply impedances, load

sizes, and load circuit parameters. All these factors cause the supply voltage waveform to be different at each load, thus the individual harmonic current phase angles would have small differences. The diversity factor is defined in [17,36] as follows:

$$DF_h = \frac{\left| \sum_{i=1}^N I_h^i \right|}{\sum_{i=1}^N |I_h^i|} \quad (2.14)$$

where  $I_h^i$  is the  $h$ -th harmonic current injected by the  $i$ -th load or group of loads. The diversity factor ranges between 0 to 1. Small values indicate significant harmonic cancellation due to the phase angle dispersion of the harmonic currents injected from the individual loads. On the other hand, values close to unity indicate the lack of harmonic cancellation. It means that the cumulative harmonic current is almost equal to the arithmetic sum of the harmonic currents in the individual loads.

The research work conducted to characterize the harmonics attenuation and diversity was concerned mainly with single-phase harmonic sources. Therefore, there is a need to explore the situation with three-phase harmonic sources where industrial distribution systems started to be equipped with a large number of these loads.

In [32], measurements of harmonic levels of many single-phase distorting loads as well as branch feeder and building current were presented for a typical commercial load. This work clarified the cancellation effect due to phase angle diversity among different load types. The cancellation of harmonic currents starts to be noticeable as the harmonic order rises above the 5th. The work only analyzed the obtained measurements and did not show or investigate the impact of the supply voltage waveform on the harmonic source current magnitudes and phase angles.

An analytical model was derived in [17] for calculating the harmonic components of the input current of a single-phase power electronic load. The time domain based model was used to investigate separately the harmonics attenuation and diversity. It was found that there is significant attenuation of harmonic currents above the 3rd order when a

number of the considered loads share a common system impedance. The harmonics diversity was obtained due to the variations in circuit parameters for harmonic sources connected in parallel through individual impedances to the supply point. It was shown that the cumulative harmonic currents for the 9th order and above experience appreciable phase cancellation.

The work in [35] expanded the analytical model presented in [17] to find the combined effect of attenuation and diversity on the net harmonic current produced by a large number of distributed single-phase power electronic loads. It was concluded that the harmonics reduction due to diversity is relatively independent of voltage distortion and the main reason is the discrepancy among load circuit parameters. In addition, the harmonics reduction due to attenuation is highly dependent on the interaction with system voltage. The derived analytical time domain based model proved that modeling each nonlinear load as a fixed harmonic current source determined from the typical current spectrum leads to an overestimation of the resulting harmonic voltages. This is because the use of the typical current spectrum of the nonlinear load can not take into account the harmonics attenuation and diversity. Accordingly, the results can be quite conservative since both effects help to reduce the overall harmonic levels.

It is worth mentioning that any time domain simulation can accurately solve this problem. For example, EMTP or similar programs could be used. This approach models all harmonic sources as they are. In other words, the topologies of the harmonic-producing loads are modeled. As a result, the diversity and attenuation effects are included automatically. However, this approach has two problems. Firstly, it is very difficult to set up such a detailed model and to conduct simulation studies for multiple cases. Secondly, it is difficult to understand the impact of modeling inaccuracy and the attenuation/diversity effects on the results. Because of these limitations, time domain based harmonic analysis methods are commonly used for special cases only.

There is, therefore, a need to develop a method that can take into account the diversity and attenuation effects on one hand and can maintain the simplicity of the

popular frequency domain based harmonic analysis tools on the other hand. The nature of such a method would also help users understand the effects of the attenuation/diversity factors on the overall harmonic distortion levels in a system.

#### 2.4.4 Randomly Varying Harmonic-Producing Loads

The other concern related to the operation of distributed harmonic sources is the random change in the harmonic current injections of randomly varying loads. Power system harmonic programs have been inherently deterministic with input parameters controlling the harmonic currents represented by fixed values. However, in practice, it has been recognized that power system harmonic voltages and currents may be randomly varying due to stochastic changes in the operating mode of nonlinear loads such as arc furnaces and adjustable speed drives. Consequently, probabilistic models of harmonic current injection and propagation are highly desirable for a more realistic prediction of harmonic current flows and resulting harmonic voltages [37].

With the operation of randomly varying harmonic source loads, the injected harmonic current magnitudes and phase angles vary in a random way. As a result, the sum of these harmonic currents is less than the arithmetic sum of the maximum values [38]. This behavior calls for statistical techniques to quantify harmonic levels correctly avoiding the harmonic voltage and current overestimation that could be obtained using deterministic approaches [39]. What is required is to get the probability that the summation magnitude will exceed a specific value. In the following, the summation technique of random harmonic vectors is presented.

##### 2.4.4.1 Summation Procedure of Random Harmonic Vectors

The summation of  $N$  random harmonic vectors is presented in [18,40,41]. Let a general vector be designated by  $A_i \angle \phi_i$ ,  $i=1,2,\dots,N$ , where  $A_i$  and  $\phi_i$  are random variables characterized by probability density functions. The resolution of vectors along the same

pair of mutually perpendicular axes is depicted in Figure 2.5, accordingly, the following equations can be written:

$$x_i = g(A_i, \phi_i) = A_i \cos \phi_i \quad (2.15.a)$$

$$y_i = h(A_i, \phi_i) = A_i \sin \phi_i \quad (2.15.b)$$

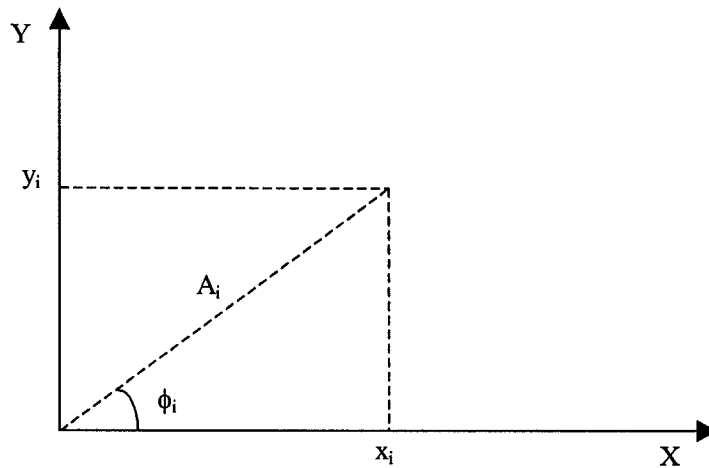


Figure 2.5: Perpendicular components of random vector.

Each of the components  $x_i$  and  $y_i$  is itself a random variable that is a function of two random variables  $A_i$  and  $\phi_i$ . The individual sums of  $x$  and  $y$  components ( $s$  and  $w$ ) are given by:

$$s = \sum_{i=1}^N x_i = \sum_{i=1}^N A_i \cos \phi_i \quad (2.16.a)$$

$$w = \sum_{i=1}^N y_i = \sum_{i=1}^N A_i \sin \phi_i \quad (2.16.b)$$

For a large number  $N$  of harmonic vectors, it follows from the Central Limit Theorem that the sums of independent resolved components are normal distribution functions regardless of the nature of the probability distribution functions of components. A normal distribution function is characterized by just two parameters, mean and variance. Hence, it is necessary to obtain these two components for each sum of

components. For the  $x$  components, let  $\mu_{xi}$  and  $\sigma_{xi}^2$ , respectively, be the mean value and the variance of each random variable  $x_i$ ,  $i=1, \dots, N$ . For the  $y$  components, let  $\mu_{yi}$  and  $\sigma_{yi}^2$  be the mean and the variance, respectively, of each random variable  $y_i$ ,  $i=1, \dots, N$ . The means and the variances of the resolved components,  $x_i$  and  $y_i$ , can be obtained by employing the following equations:

$$\mu_{xi} = \int_{-\infty}^{\infty} \int_{-\infty}^{\infty} g(A_i, \phi_i) f(A_i, \phi_i) dA_i d\phi_i \quad (2.17.a)$$

$$\mu_{yi} = \int_{-\infty}^{\infty} \int_{-\infty}^{\infty} h(A_i, \phi_i) f(A_i, \phi_i) dA_i d\phi_i \quad (2.17.b)$$

$$\sigma_{xi}^2 = \int_{-\infty}^{\infty} \int_{-\infty}^{\infty} (g(A_i, \phi_i) - \mu_{xi})^2 f(A_i, \phi_i) dA_i d\phi_i \quad (2.17.c)$$

$$\sigma_{yi}^2 = \int_{-\infty}^{\infty} \int_{-\infty}^{\infty} (h(A_i, \phi_i) - \mu_{yi})^2 f(A_i, \phi_i) dA_i d\phi_i \quad (2.17.d)$$

where  $f(A_i, \phi_i)$  is the joint probability density function (jpdf) of amplitude and angle of random vector  $A_i \angle \phi_i$ .

The means of the summation of  $x$  and  $y$  components are given by:

$$\mu_s = \sum_{i=1}^N \mu_{xi}, \quad \mu_w = \sum_{i=1}^N \mu_{yi} \quad (2.18)$$

The variances of the summation of  $x$  and  $y$  components are given by:

$$\sigma_s^2 = \sum_{i=1}^N \sigma_{xi}^2, \quad \sigma_w^2 = \sum_{i=1}^N \sigma_{yi}^2 \quad (2.19)$$

As  $N$  gets larger, by virtue of the Central Limit Theorem, the random variables  $s = \sum_{i=1}^N x_i$  and  $w = \sum_{i=1}^N y_i$  can be considered normally distributed with marginal pdfs  $f(s)$  and  $f(w)$  respectively irrespective of the nature of the pdfs of the individual  $x$  and  $y$  components.



$$f(s) = \frac{e^{-\frac{(s-\mu_s)^2}{2\sigma_s^2}}}{\sigma_s \sqrt{2\pi}}, \quad f(w) = \frac{e^{-\frac{(w-\mu_w)^2}{2\sigma_w^2}}}{\sigma_w \sqrt{2\pi}} \quad (2.20)$$

The random variables  $s$  and  $w$  are also jointly distributed with normal jpdf  $f(s, w)$ . This jpdf is characterized by the means and the variances of  $s$  and  $w$  as well as their correlation  $\rho_{sw}$  as follows:

$$f(s, w) = \frac{e^{-\frac{\eta}{2(1-\rho_{sw}^2)}}}{2\pi\sigma_s\sigma_w\sqrt{1-\rho_{sw}^2}} \quad (2.21)$$

where

$$\eta = \frac{(s-\mu_s)^2}{\sigma_s^2} - \frac{2\rho_{sw}(s-\mu_s)(w-\mu_w)}{\sigma_s\sigma_w} + \frac{(w-\mu_w)^2}{\sigma_w^2}, \quad \rho_{sw} = \frac{\sigma_{sw}^2}{\sigma_s\sigma_w} \quad (2.22)$$

$\sigma_{sw}^2$  is the covariance of the sums of  $x$  and  $y$  components ( $s$  and  $w$ ).

The covariance of the sums of resolved components of statistically independent random vectors is equal to the sum of covariances of corresponding components. Therefore,

$$\sigma_{sw}^2 = \sum_{i=1}^N \sigma_{x_i y_i}^2 \quad (2.23)$$

where  $\sigma_{x_i y_i}^2$  is the covariance of  $x_i$  and  $y_i$  and is given by:

$$\sigma_{x_i y_i}^2 = E(x_i y_i) - \mu_{x_i} \mu_{y_i} \quad (2.24)$$

$$E(x_i y_i) = \int_{-\infty}^{\infty} \int_{-\infty}^{\infty} x_i y_i f(x_i, y_i) dx_i dy_i \quad (2.25)$$

where  $f(x_i, y_i)$  is the jpdf of  $x_i$  and  $y_i$ . This jpdf is derivable from the probability distributions of  $A_i$  and  $\phi_i$ .

The magnitude of the sum of random vectors is given by:

$$z = \sqrt{\left(\sum_{i=1}^N x_i\right)^2 + \left(\sum_{i=1}^N y_i\right)^2} = \sqrt{s^2 + w^2} \quad (2.26)$$

Since  $s$  and  $w$  are random variables,  $z$  is also a random variable. In order to determine the pdf of the random magnitude of the random vector summation, the joint pdf  $f(s, w)$  is transformed into the polar form by expressing the resultant vector rectangular components through the magnitude  $z$  and phase  $\theta$ , where  $s = z \cos \theta$  and  $w = z \sin \theta$ . As derived in [40], the pdf  $f(z)$  of the magnitude of vectorial sum can be given by:

$$f(z) = \int_0^{2\pi} f(z \cos \theta, z \sin \theta) z d\theta \quad (2.27)$$

The probability of exceeding a level  $z_1$  is given by:

$$P(z > z_1) = 1 - \int_0^{z_1} f(z) dz \quad (2.28)$$

The presented procedure showed how the probability density function of the summation of randomly varying harmonic vectors can be obtained. This would help in determining the probability that harmonic voltage or current in power systems can exceed a specified level with the operation of harmonic sources of randomly varying load.

#### 2.4.4.2 Research Work Dealing with Random Harmonic Vectors

There are some publications dealing with the probability characteristics of harmonic injections generated by some specific nonlinear loads including traction drives [42], electric vehicle battery chargers [43,44,45], and electric power converters [18,46]. Other researchers analyzed the summation of random phasors with uniformly distributed magnitudes and/or phase angles [47,48,49]. In addition, research work was done considering the propagation of random harmonic currents in power networks [37,40,41].

The determination of the probability density function (pdf) of the resultant harmonic levels due to several varying harmonic sources has an analytical expression, which can

hardly be expressed [50]. This entails summation of random harmonic vectors of currents and voltages. The problem of summation of random vectors was first tackled by two researchers, Sherman and Rowe. Sherman [48] described a technique that can be used to sum a large number of similar-order random vectors. He presented a Fourier Series solution for the pdf of the summation magnitude; the harmonic vectors that can be summed have to satisfy the following requirements:

- 1) Uniformly distributed phase angle ( $0 - 2\pi$ ).
- 2) Component phasors are statistically independent.
- 3) Fixed magnitudes.

It was concluded in [48] that for random vectors  $N$  greater than about 8, the resultant summation magnitude very closely approximates to the normal probability distribution when the amplitudes are all close in values. With more diverse amplitude values,  $N$  would have to be at least 10 or 12.

Sherman's work was extended by Rowe [47] to cover the summation of random vectors whose magnitudes could vary uniformly between zero and a maximum. However, the first two above requirements still had to be met. In addition, the random variables of magnitude and phase angle have to be statistically independent, i.e., their probability distribution functions do not depend on each other. Rowe found that by resolving harmonic vectors into two components along the real and imaginary axes ( $X$  and  $Y$ ), the Central Limit Theorem could be applied to the two sums of the resolved components. It was concluded that as the number of random vectors  $N$  is large enough, the magnitude of the resultant follows a Rayleigh distribution.

However, for harmonics in actual power systems, phase angle variation is limited and rarely to cover the  $2\pi$  range. Besides, the magnitude is expected to change from a minimum limit, which is not zero to the maximum value. Hence, more refined tools are needed. A numerical solution procedure for the pdf in a general case was first presented by Baghzouz and Tan [37] using the convolution integral. For the solution, they assumed

that the component vectors can be resolved along the perpendicular axes and that the sums of the resolved components may be regarded as independent of each other, particularly with a large number of nonlinear loads.

It was mentioned in [34] that when the phase angle (and generally also the amplitude) may be considered as randomly varying for nonlinear loads, the best assumption seems to be a uniform distribution for a satisfactory agreement between calculations and measurements. Considering the statistical distributions of amplitudes and phases as independent may not be correct, but the resulting calculation errors are small.

Since the two sums of the resolved  $x$  and  $y$  components approach normal distributions as the number of random harmonic vectors  $N$  is sufficiently large, a bivariate normal distribution (BND) applies to the summation problem very well [18]. The BND has been used by Kazibwe et al. [40] who presented a general method of determining the pdf of the magnitude of the vectorial sum of random vectors of arbitrary probability characteristics. The pdf has been given in an integral form, which must be solved by a numerical method. The method covers summation of vectors whose components, magnitude and angle, are either statistically independent or dependent.

It should be mentioned that although the BND model is an asymptotic model based on the Central Limit Theorem that holds for sufficiently large  $N$ , several studies have shown that the model gives satisfactory results even for small  $N$ . Comparison of the pdfs calculated by the BND model and the empirical histograms obtained from Monte Carlo simulation in [40] clearly showed that for  $N \geq 5$  the pdfs obtained from the BND model agree closely with those from the simulation. Greater discrepancy has been observed for the case  $N=3$  since the Central Limit Theorem is not practically applicable to a so small number of random harmonic vectors.

In [34], it has been found that the summation of randomly varying  $N$  vectors may be given by one of the following three methods to take into account the harmonic cancellation effect:

$$\text{Method 1:} \quad A = k \sqrt{\sum_{i=1}^N A_i^2}, \quad k \leq 1 \quad (2.29.a)$$

$$\text{Method 2:} \quad A = \sqrt[\alpha]{\sum_{i=1}^N A_i^\alpha}, \quad 1 \leq \alpha \leq 2 \quad (2.29.b)$$

$$\text{Method 3:} \quad A = K \sum_{i=1}^N A_i, \quad K \leq 1 \quad (2.29.c)$$

where  $A_i$  can be the harmonic voltage (at any bus) produced by the  $i$ -th harmonic source alone,  $A$  is the total harmonic voltage produced by all harmonic sources, and  $k$ ,  $\alpha$ , and  $K$  are aggregation factors which are functions of the harmonic source characteristics (variation range for both magnitudes and phase angles).

In method 1, the value of  $k$  determines the value of the non-exceeding probability  $P_r$ . If  $k=1$  for example, fixed amplitudes and random phases give  $P_r=63\%$  (for  $N \geq 3$ ) while random amplitudes and random phases give  $P_r=95\%$  [47]. Method 2 has been proposed as a general law for the summation of individual harmonic currents or voltages. For the summation of harmonics from different groups of domestic appliances,  $\alpha=1.2$ . More generally,  $\alpha=1$  for low order harmonics and  $\alpha=2$  for higher order ones from the 11th. Method 3 is given to get a simple rule for practical applications for the diversity factor  $K$  concerned with multiple loads [34].

## 2.5 Summary

An overview on harmonics in electric power systems was given in this chapter. Harmonics representation and harmonic sources were presented. The importance of harmonic analysis was highlighted. The different techniques widely used for harmonic analysis were reviewed. These techniques are mainly classified as time domain methods and frequency domain methods. The main features of each technique were identified showing the cons and pros of each one.

The recent trend of using distributed harmonic sources in distribution systems was discussed clarifying how it is different from the traditional trend of employing one or several harmonic sources. The main two issues related to the distributed harmonic sources are the attenuation and the diversity of the produced harmonic currents from constant load harmonic sources and the random harmonic currents produced by randomly operating harmonic source loads. Both cases imply that the direct current injection method, which is the simplest and most common frequency domain method used for harmonic analysis, is not the appropriate one for implementation and more advanced methods are needed to deal with such situations.

The definitions of the attenuation and diversity factors were presented to illustrate how they can contribute to the reduction of the cumulative harmonic current with the presence of multiple harmonic sources. The summation of randomly varying harmonic vectors was discussed showing the procedure needed to get the probability density function of the summation magnitude. This would help in the realistic assessment of harmonic levels in power systems.

The mentioned concerns are the motivation to search for developing harmonic analysis methods that can deal with the two situations encountered in the presence of distributed harmonic sources and overcome the limitations of the traditional methods. The interaction between the supply voltage and the harmonic source current spectrum will be examined in order to extract reliable relationships that can correlate the harmonic current magnitudes and phase angles with the distortion of the supply voltage waveform. Accordingly, harmonic analysis can be performed taking into account the attenuation and diversity effects. Regarding the case of distributed harmonic sources with randomly varying load, the variation of the harmonic current spectrum with loading level will be investigated. Based on the obtained characteristics, an analytical method will be implemented utilizing the Central Limit Theorem to get the probabilistic magnitude of system harmonic voltages and currents considering the randomness in the loading level of the harmonic sources.

# Chapter 3

## Harmonics Attenuation and Diversity for Single-Phase Power Electronic Loads

In this chapter, a personal computer (PC) load, one of the most common single-phase loads employing a capacitor-filtered diode bridge rectifier, is considered to investigate the harmonics attenuation and diversity. The variation of measured PC harmonic current magnitudes and phase angles with supply voltage distortion is presented. This is carried out with the change of both the supply impedance and the background voltage distortion. A comparison between the results obtained in the two cases is illustrated. A justification is made to account for choosing the voltage total harmonic distortion (THD) of the harmonic source as the proper indicator of the harmonic source current spectrum. This constitutes the basis to propose a harmonic analysis method that can deal with the harmonics attenuation and diversity to overcome the limitation of the traditional method.

### 3.1 Introduction

Most harmonic studies dealt with power electronic equipment, to predict the impact of the harmonic currents produced by the equipment on the associated system, are generally based on the assumption that the harmonic current injection is fixed and independent of the supply voltage distortion. The injected harmonic currents utilize the typical spectrum of the harmonic source, which may be obtained from harmonic measurements or published data [51]. This traditional method is accurate only when the supply voltage

waveform is reasonably sinusoidal. However, with the presence of many harmonic sources in the distribution systems, the bus voltage supplying any harmonic source is usually distorted. Therefore, the harmonic source will inject harmonic currents that are different from those obtained in the case of nondistorted supply voltage due to the harmonics attenuation and diversity. The traditional method can not take into account these effects which would cause overestimation of the resultant system distortion level.

In order to construct a harmonic analysis method that can consider the influence of the supply voltage waveform on the harmonic source current spectrum, it is necessary to investigate the behavior of the harmonic current magnitudes and phase angles under different supply voltage waveforms. A PC load is considered for such a study as one of the most commonly used single-phase power electronic loads. Controlled measurements are conducted to characterize the variation of the PC load harmonic currents with the supply voltage waveform. Two experiments are carried out; in the first one the supply impedance is changed and the corresponding supply voltage and current are recorded. In the second one the background voltage distortion is changed by connecting external harmonic sources and the subsequent effect on the harmonic currents is investigated. The objective is to characterize the interaction between the supply voltage waveform and the harmonic source current. Then, the response of the system voltage waveform to the current distortion of the harmonic source is investigated. Both harmonic source characteristic and system characteristic are examined to determine the reliable voltage index that should be adopted to characterize the harmonic currents produced by a harmonic source taking into account the impact of the supply voltage waveform. This in turn can be utilized on conducting harmonic analysis for systems with distributed single-phase power electronic loads to provide improved results due to the consideration of the harmonics attenuation and diversity.



### 3.2 Single-Phase Capacitor-Filtered Diode Bridge Rectifier

The single-phase power electronic load is the most common harmonic source in residential and commercial distribution systems. The switch-mode power supplies of personal computers and television sets are typical examples of such a load [17,51]. The load uses a capacitor-filtered diode bridge rectifier shown in Figure 3.1. The rectifier consists of a circuit that rectifies a sinusoidal voltage from a power line, a DC-link capacitor, and an equivalent DC current source. The various circuit components are:

- $V_{th}$ : Thevenin equivalent system voltage,
- $R_{th}, L_{th}$ : Thevenin equivalent system impedance parameters,
- $R_s, L_s$ : local supply impedance parameters,
- $C$ : DC-smoothing capacitor,
- $I_{dc}$ : equivalent DC load.

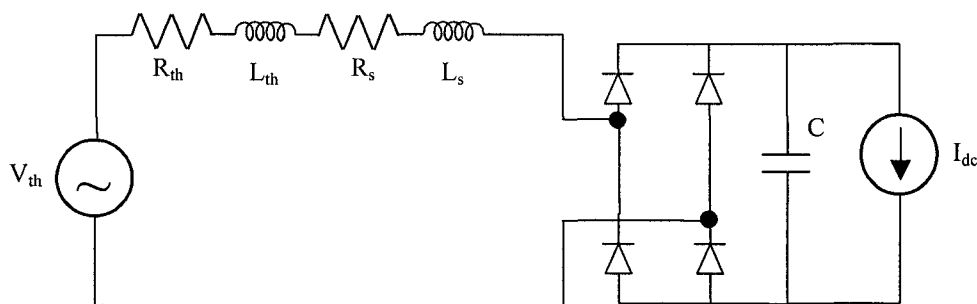


Figure 3.1: Capacitor-filtered diode bridge rectifier Circuit.

The input current of the capacitor-filtered rectifier is not taken from the power line in a sinusoidal form, but instead it is taken in short pulses. Figure 3.2 illustrates a typical measured PC input current waveform and Figure 3.3 shows the corresponding harmonic current spectrum magnitude in percent of the fundamental component. The waveform pulses occur when the AC source is at a higher voltage than the DC link of the rectifier, therefore, the capacitor starts being charged. During this time, the diodes are forward biased and the current flows [26]. The drawn current is highly distorted and its spectrum

consists mainly of odd harmonics with magnitudes depending on the shape of the pulse. The PC load input current THD is typically between 100% and 150%. The width of the current pulse depends on the rectifier circuit parameters. When the current pulse is wider, its THD becomes lower and vice versa.

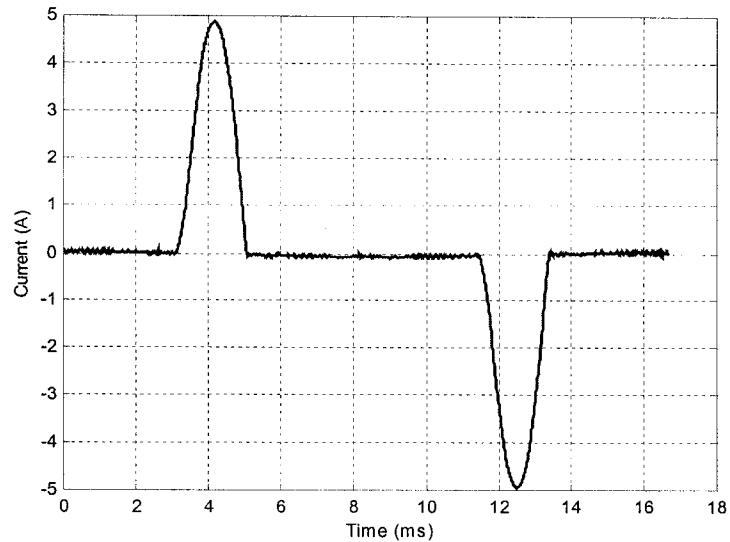


Figure 3.2: A typical measured input current waveform for a PC load with 135% current THD.

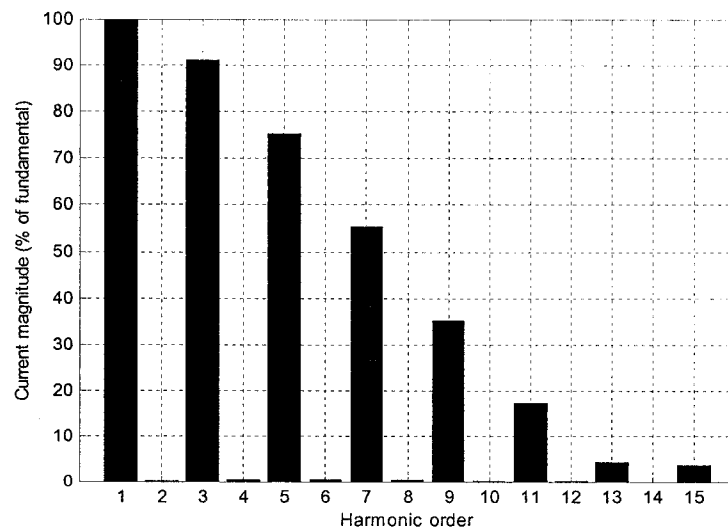


Figure 3.3: Harmonic spectrum of the typical PC current waveform.

### 3.3 Characterization of Single-Phase Harmonic Sources

An office building with a lot of PCs is a typical distribution system with a number of single-phase harmonic-producing loads of comparable sizes. It is of importance to determine the harmonic distortion level for this type of systems. As previously mentioned, using the typical harmonic current spectrum would overestimate the distortion level since it ignores the reduction of the collective harmonic currents due to the attenuation and diversity effects. No relationship could be extracted between the input harmonic currents and the parameters of the capacitor-filtered rectifier circuit. Therefore, it is not easy to predict the current waveform from circuit parameters [51]. Rather, the distortion of the terminal voltage waveform in this research work is adopted to predict the magnitude and the phase angle of the input harmonic currents to reflect the impact of the supply impedance or other system connected harmonic sources.

The aim of this part is to characterize the interaction between the PC harmonic currents and feeding voltage waveform. Two experiments are conducted for this purpose where the voltage waveform variation is produced by two ways. The design of the first experiment is such that different PC supply impedance magnitudes are provided to create different voltage distortion levels and the design of the second experiment is such that external harmonic-producing loads are connected sequentially to the concerned PC to create different background voltage distortions. In both cases, the feeding voltage and supply current are recorded to search for the reliable voltage waveform index that can be considered as a good indicator of the harmonic current spectrum. Then, the obtained relationships will be embedded in the harmonic source model in order to account for the supply voltage waveform effect on the harmonic current magnitudes and phase angles. This would help adjust the injected current spectrum from different harmonic sources considering the attenuation and diversity effects. Hence, a reliable assessment of the harmonic distortion level for systems with distributed harmonic sources can be obtained.

The measurements are conducted using a Data Acquisition Nicolet Transient Recorder BE256-LE. This instrument has eight channels for simultaneous recording with

an adjustable sampling rate. The voltage and current waveforms are measured using voltage and current probes. The waveform data can be acquired by connecting the recorder to a laptop via IEEE-488 interface unit. The recorder has special software called “TEAM256” (Transient Evaluation and Analysis Manager) which is installed on the laptop to control the recording process. The main set up of the conducted experiments and the instruments used in the measurements are described in Appendix A.

### 3.3.1 Effect of Supply Impedance Variation

The circuit configuration used for this test is shown in Figure 3.4 where the PC load is supplied through variable impedance components  $R_s$  and  $L_s$ . The supply impedance is changed in many steps for a specific  $X/R$  ratio. 10 measurements are taken and the feeding voltage “ $V_f$ ” and the supply current “ $I_s$ ” waveforms are obtained using Nicolet Transient Recorder with a sampling rate of 7.5 kHz (125 samples/60 Hz cycle). This process is repeated for different cases of the supply impedance  $X/R$  ratio. The chosen supply impedance values are listed in Appendix A. The impedance magnitudes with the PC fundamental current cause voltage drop up to 3.15%. Data processing is performed using MATLAB software to extract the harmonic current magnitudes and phase angles as well as the total harmonic distortion (THD) and crest factor<sup>1</sup> (CF) of the feeding voltage.

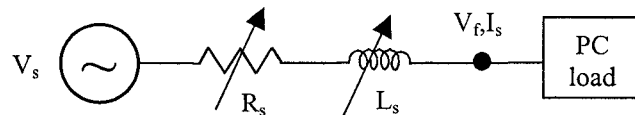


Figure 3.4: Circuit connection to investigate the effect of supply impedance variation.

Figure 3.5 shows the variation of the supply current THD with the feeding voltage THD and CF. It can be seen that the current THD becomes lower with the increase in

---

<sup>1</sup> The crest factor is a measure of the peak value of the waveform compared to the true RMS value. A perfect sine wave, by definition, will have a crest factor of 1.414. The logic behind this definition is that any deviation from 1.414 represents a distorted waveform.

voltage THD and the decrease in voltage CF. This implies that as the voltage distortion increases due to the supply impedance increase, the voltage waveform becomes more flattened, and the current pulse becomes wider. Figure 3.6 depicts the variation of the individual harmonic current magnitudes in percent of the fundamental component with voltage THD and CF. Figure 3.7 presents the corresponding variation of the individual harmonic current phase angles with respect to the phase angle of the fundamental component of the feeding voltage. The figures show that the harmonic current spectrum can no longer be assumed fixed and the effect of the voltage waveform should be included in the harmonic analysis.

From all conducted measurements for different  $X/R$  ratios of the supply impedance, the correlation coefficients between the current THD and both voltage THD and voltage CF are -0.9485 and 0.9872 respectively. This reveals the good negative and positive linear relationships between the PC current THD and both voltage indices. Figure 3.6 shows that the individual harmonic current magnitudes are strongly characterized by the THD and CF of the voltage waveform. Also, from Figure 3.7, it can be observed that the variation of the individual harmonic current phase angles, even they are slightly scattered, has a specific trend where the phase angles have more delay with the increase in voltage THD and the decrease in voltage CF.

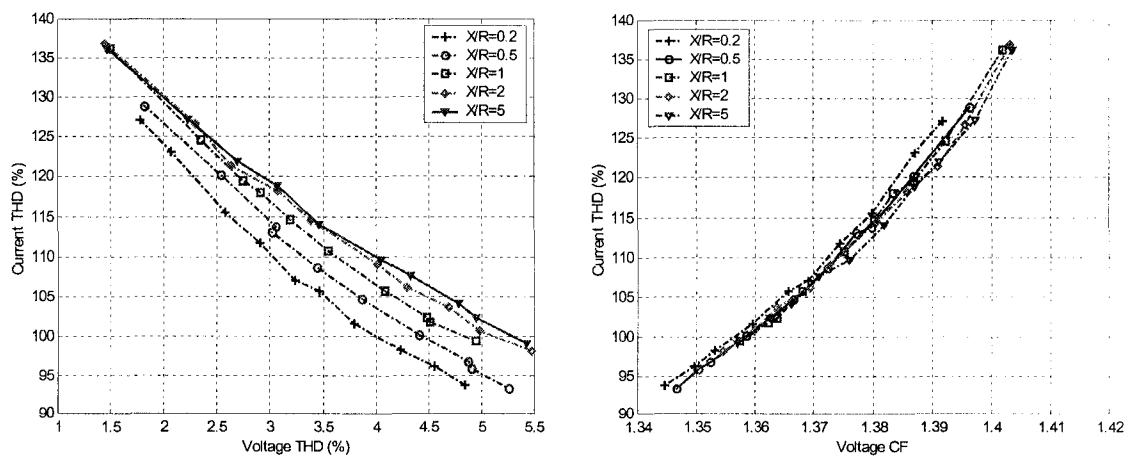


Figure 3.5: Variation of PC current THD with voltage THD and CF due to supply impedance variation.

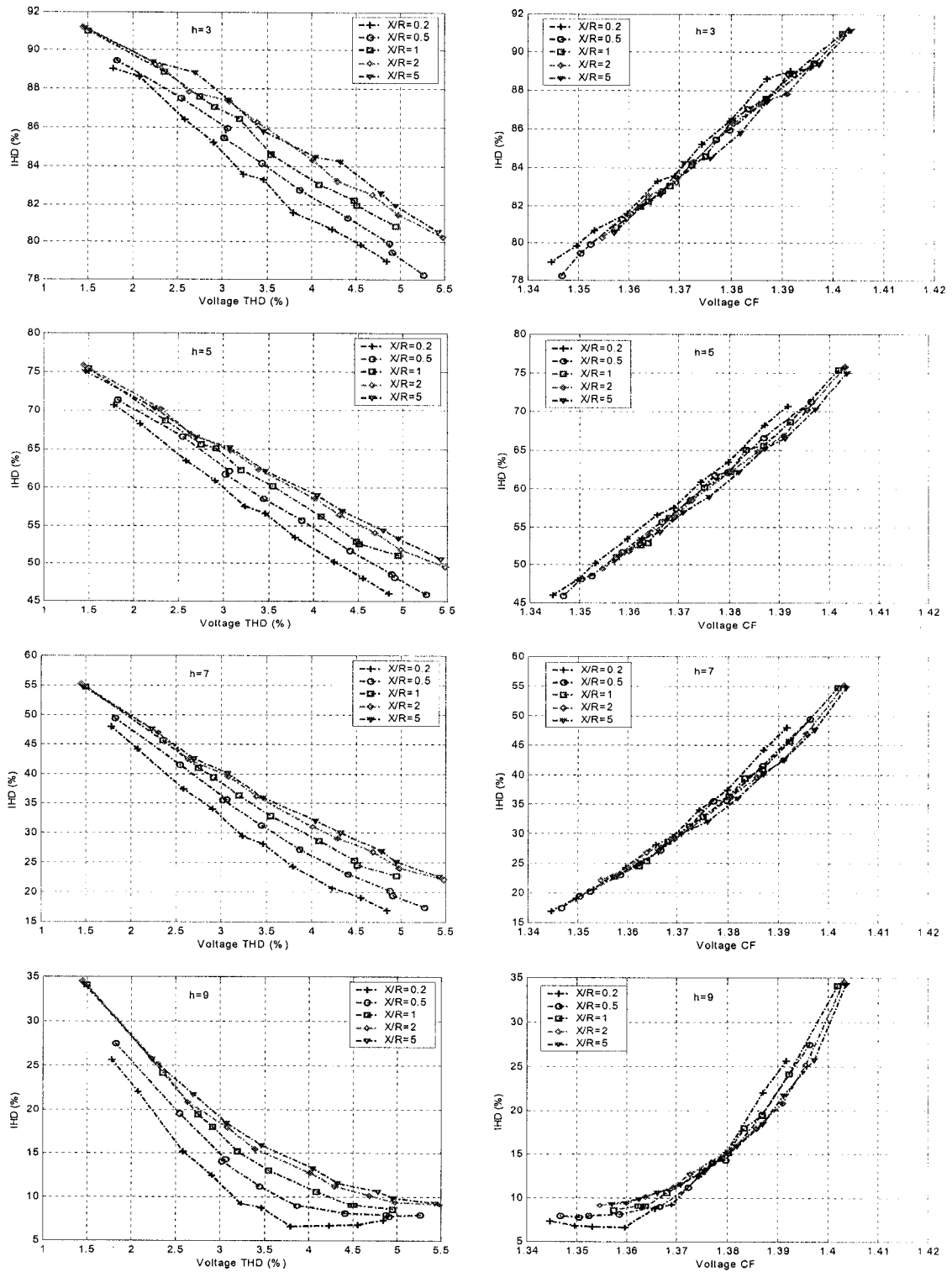


Figure 3.6: Variation of PC individual harmonic current magnitudes with voltage THD and CF due to supply impedance variation.

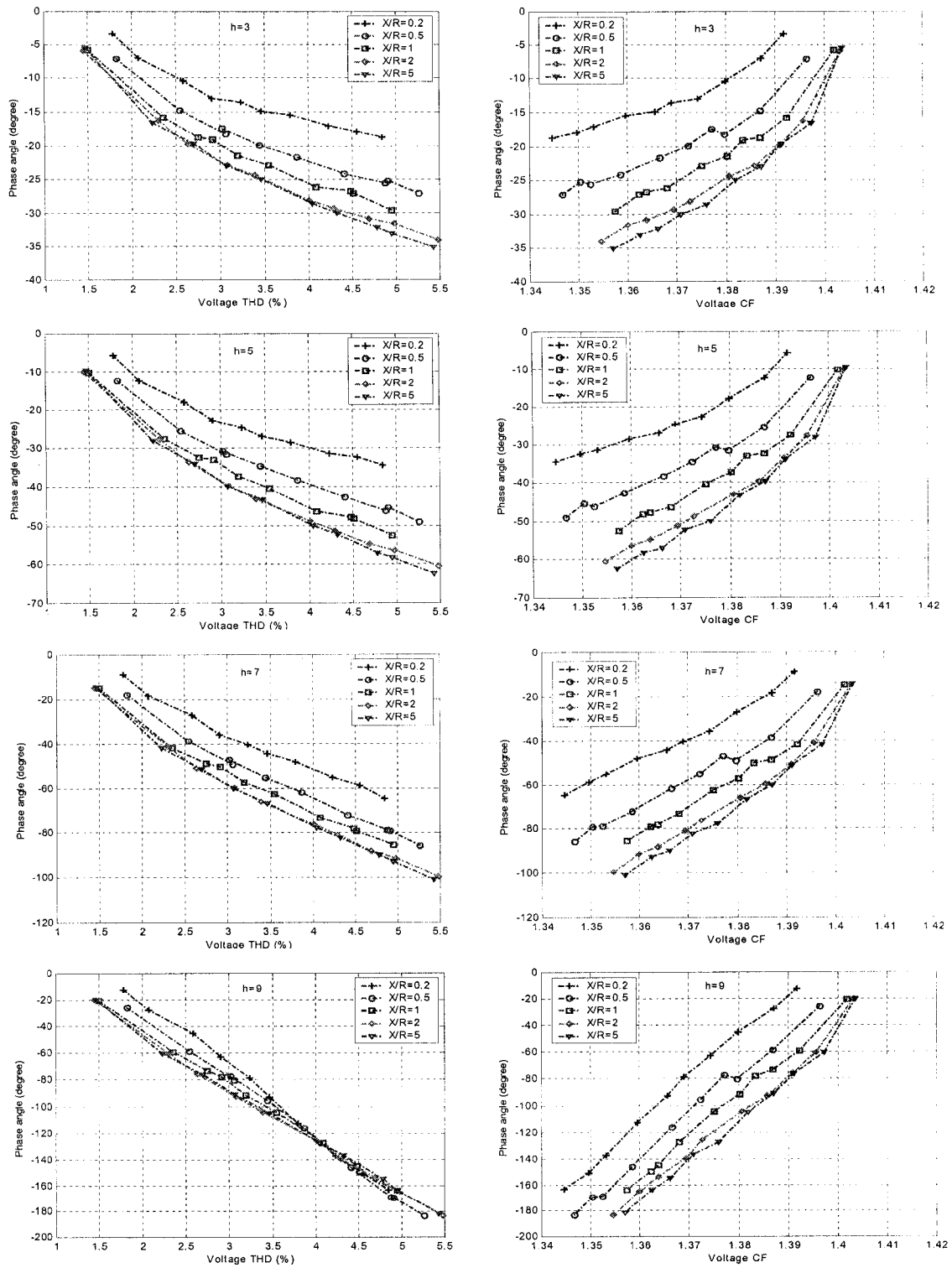


Figure 3.7: Variation of PC individual harmonic current phase angles with voltage THD and CF due to supply impedance variation.

### 3.3.2 Effect of Background Voltage Distortion Variation

The circuit configuration used for this test is shown in Figure 3.8. The purpose is to create different background voltage distortions and see the influence on the PC harmonic currents. Seven external computer and monitor loads are connected in sequence to the common point of the concerned PC and the feeding voltage and supply current waveforms are recorded. The first measurement recording point is taken when none of the external loads is connected so that we get a total of eight measurements of the voltage and current for the same supply impedance. This is performed for different  $X/R$  ratios of the supply impedance and repeated for four different supply impedance steps of multiple magnitudes as listed in Appendix A to get higher values of the voltage distortion. The presented results are those obtained with the smallest supply impedance magnitude.

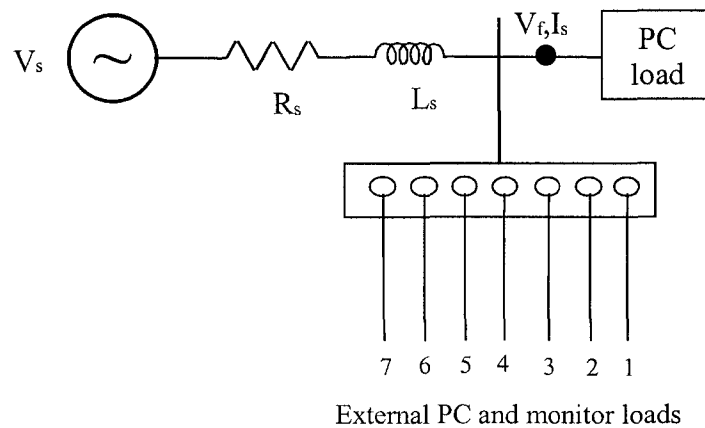


Figure 3.8: Circuit connection to investigate the effect of background voltage distortion variation.

Figure 3.9 shows the variation of the current THD with the feeding voltage THD and CF. It can be seen that with the variation of the voltage waveform caused by external loads, there is also a good correlation between the current THD and both voltage indices. Figure 3.10 depicts the variation of the individual harmonic current magnitudes in



percent of the fundamental component with voltage THD and CF while Figure 3.11 illustrates the variation of the individual harmonic current phase angles with respect to the phase angle of the fundamental component of the feeding voltage. Both figures show similar trends to those in the impedance variation case. From the conducted measurements with different  $X/R$  ratios of the supply impedance and with different impedance magnitudes, the correlation coefficients between the current THD and both voltage THD and voltage CF are  $-0.9037$  and  $0.9667$  respectively. This assures the linear relationships between the PC current THD and the voltage indices irrespective of the cause of the voltage waveform change.

The plateau of the current THD and individual harmonic currents appeared between some points because the measurements at these points are taken when monitor loads are connected to have more voltage distortion level. However, after these points with adding more PC loads, the general trend of the curves is restored as an extension of the previous points to represent the characteristics of the PC loads.

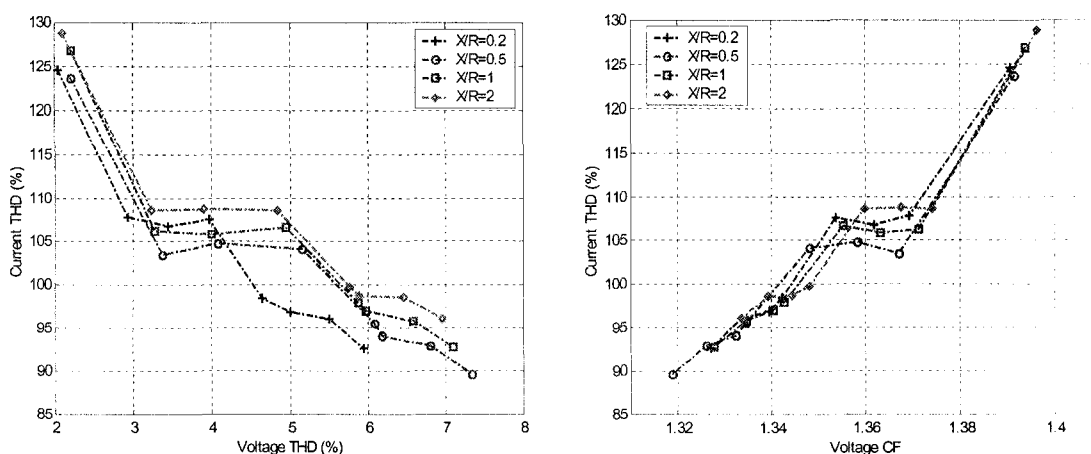


Figure 3.9: Variation of PC current THD with voltage THD and CF due to background voltage distortion variation.

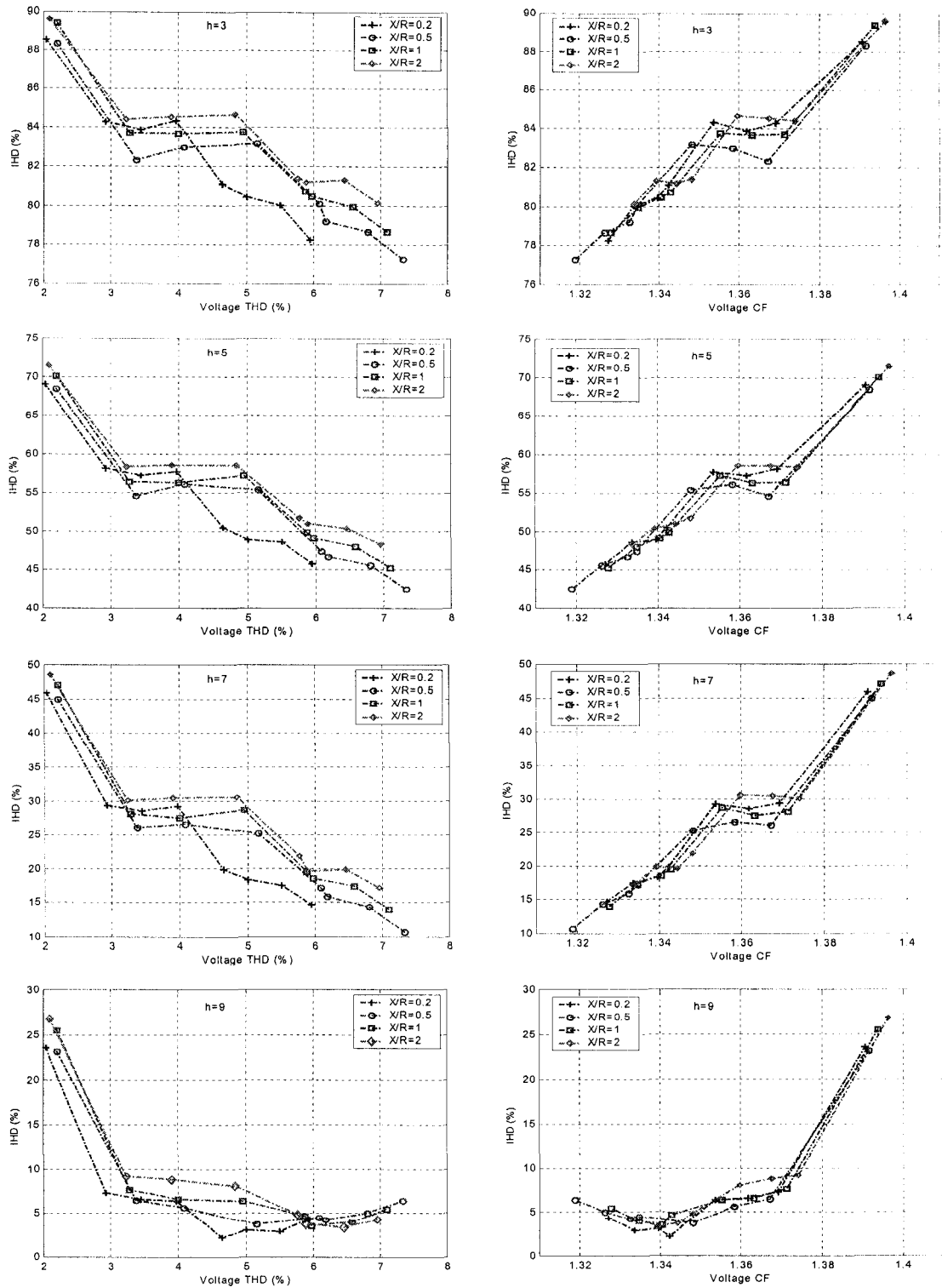


Figure 3.10: Variation of PC individual harmonic current magnitudes with voltage THD and CF due to background voltage distortion variation.

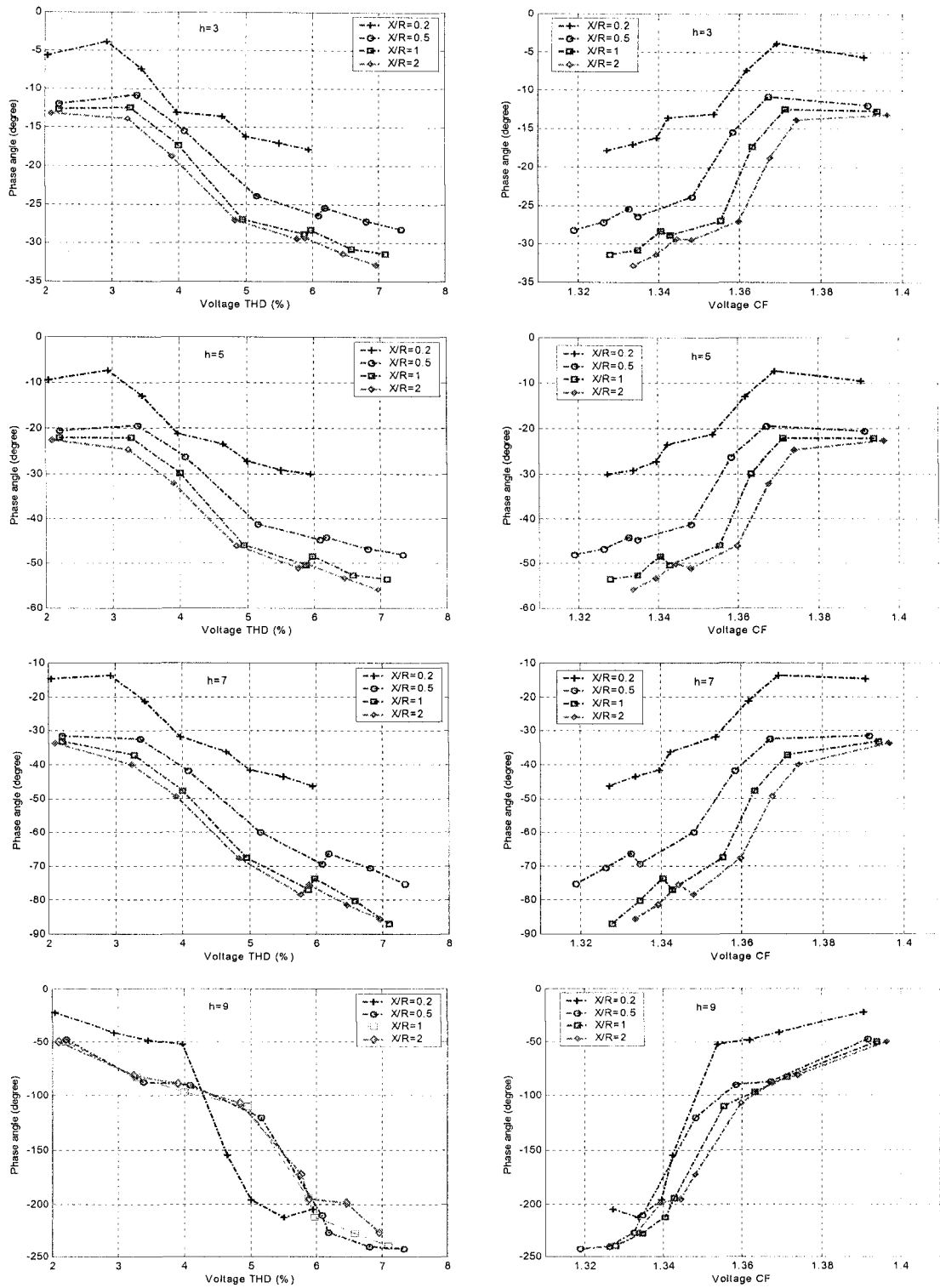


Figure 3.11: Variation of PC individual harmonic current phase angles with voltage THD and CF due to background voltage distortion variation.

### 3.3.3 Comparison between the Results Obtained due to the Variation of Supply Impedance and Background Voltage Distortion

In this part, the variation of the magnitudes and phase angles of the individual harmonic currents with voltage THD and CF due to the supply impedance change ( $Z_{change}$ ) is compared with the corresponding variation due to the background voltage distortion change ( $V_{background}$ ). Since the measurements obtained from the impedance change were taken in the range up to voltage THD of 5.5%, the background distortion case will consider only the step of the supply impedance magnitude that produces voltage THD up to approximately 7% so that results can be compared. Figure 3.12 shows the variation of the current THD with the voltage THD and CF under the two concerned conditions. Figures 3.13 and 3.14 illustrate the variation of the individual harmonic current magnitudes and phase angles. It can be observed how the results are comparable which indicates that the harmonic current spectrum can be fairly characterized upon the voltage waveform regardless the cause of the waveform change.

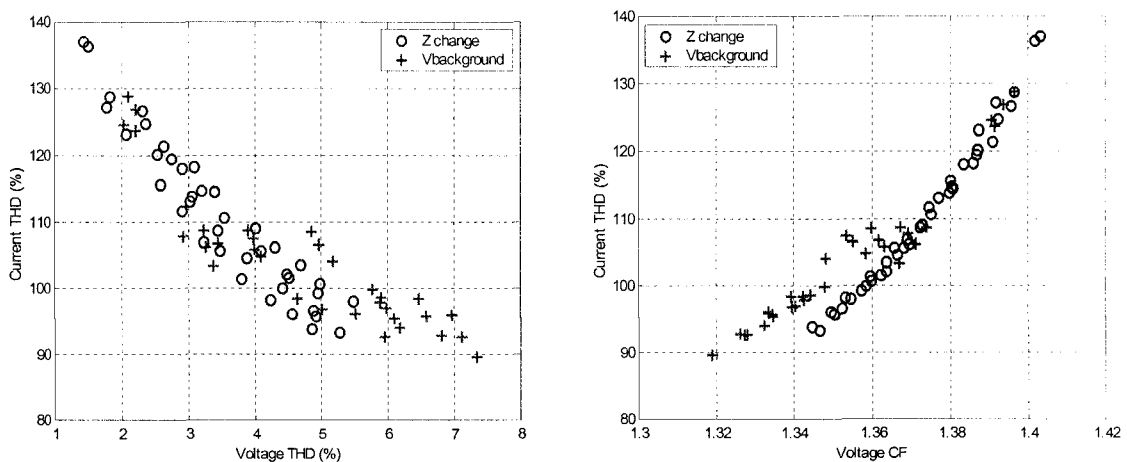


Figure 3.12: Variation of PC current THD with voltage THD and CF due to the change of supply impedance and background voltage distortion.

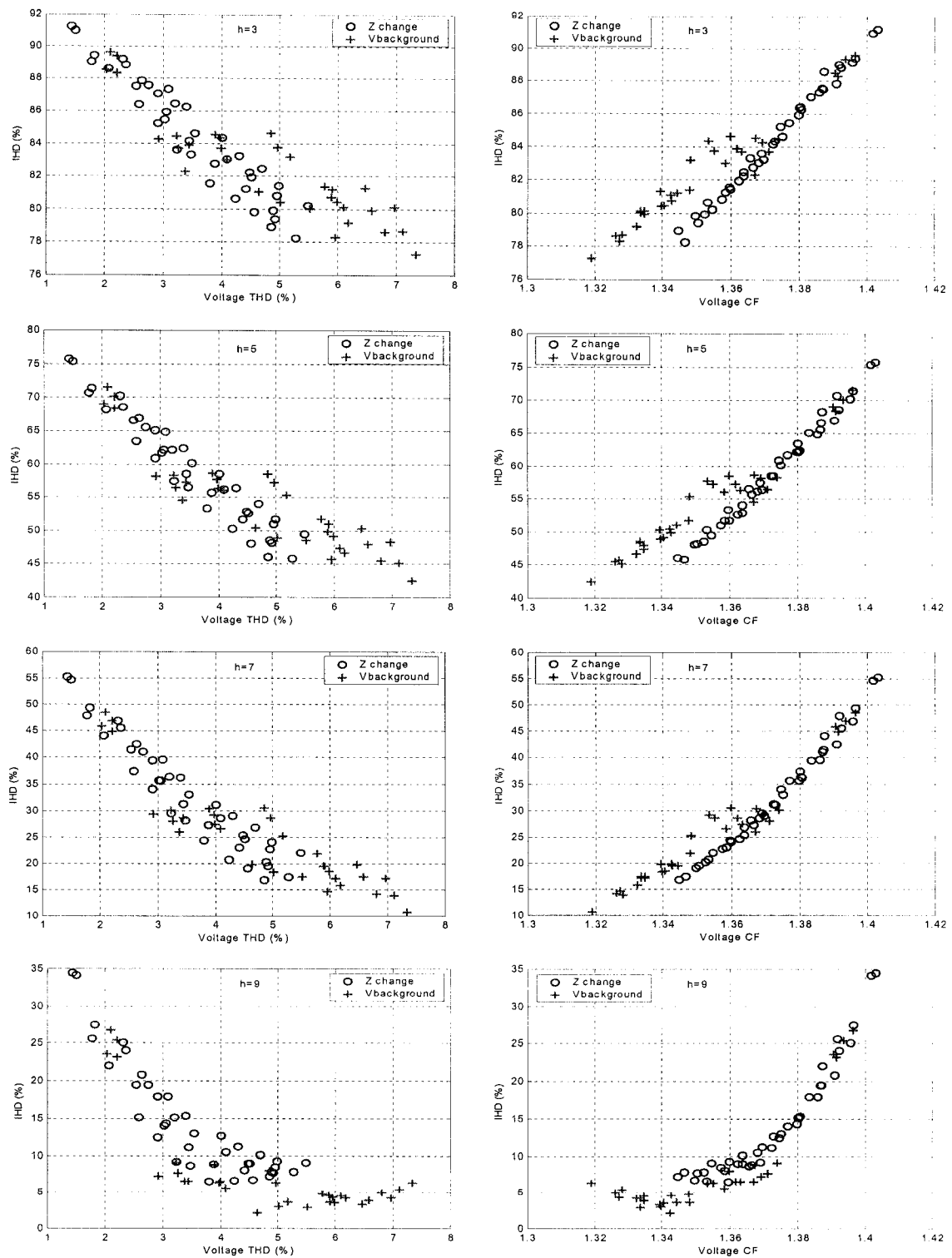


Figure 3.13: Variation of PC individual harmonic current magnitudes with voltage THD and CF due to the change of supply impedance and background voltage distortion.

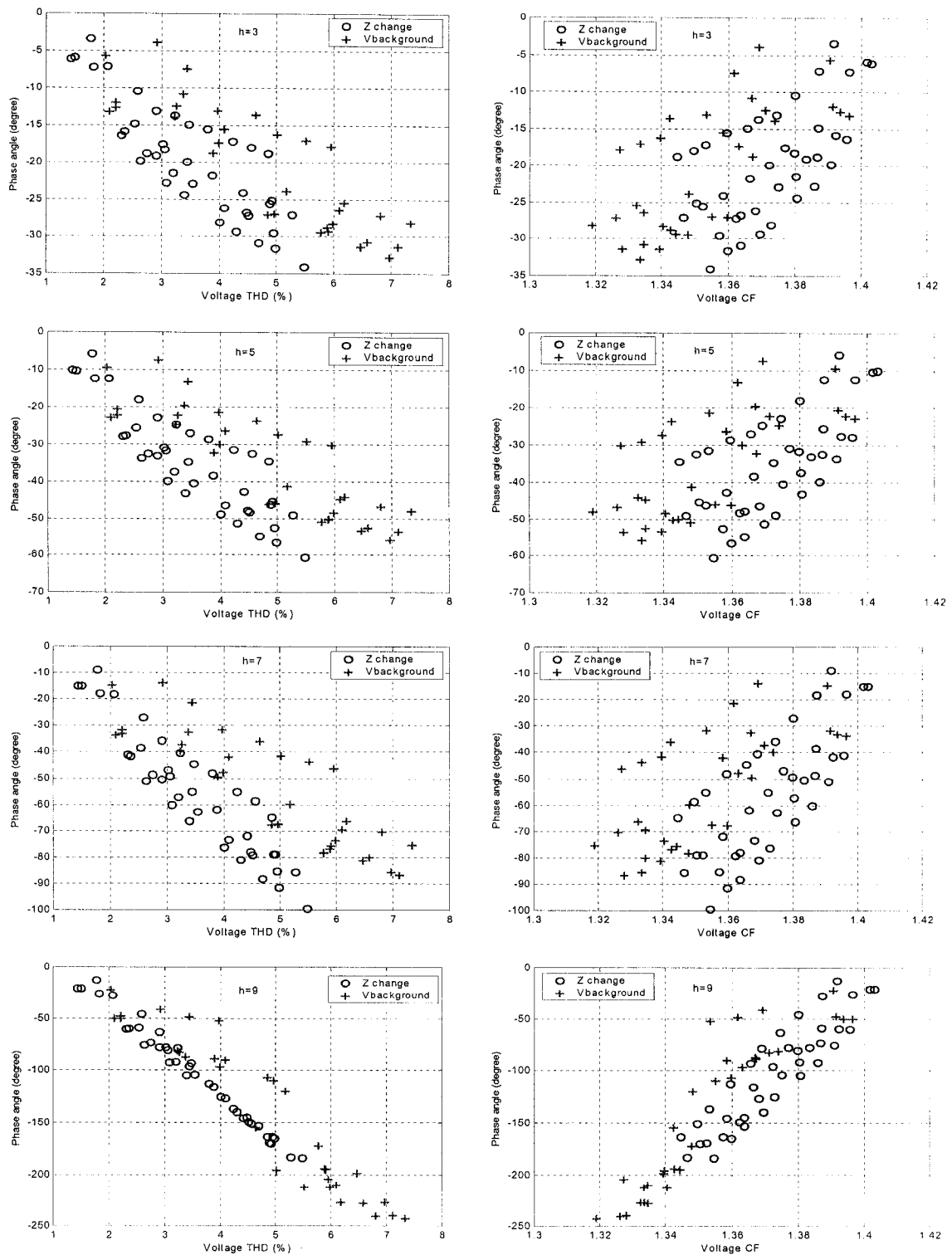


Figure 3.14: Variation of PC individual harmonic current phase angles with voltage THD and CF due to the change of supply impedance and background voltage distortion.

### 3.3.4 Results Justification

In order to justify the measurement results and the obtained relationships between the harmonic currents and feeding voltage THD and CF, the effect on the resultant voltage waveform and the harmonic voltage components is scrutinized under the following different conditions: 1) changing the supply impedance magnitude with the same  $X/R$  ratio; 2) changing the background voltage distortion with the same supply impedance; and 3) changing the supply impedance  $X/R$  ratio with the same fundamental impedance magnitude.

For the first condition, Figure 3.15 shows the results when the supply impedance of  $X/R$  ratio of 0.2 is increased from  $Z_1$  ( $4.712+j0.942$  ohm) to  $Z_2$  ( $10.36+j2.073$  ohm). The associated voltage THD is increased and the magnitudes and phase angles of the harmonic voltage components are obtained such that the voltage CF is decreased. On the other hand, the current THD is reduced from 111.69% to 93.83%.

For the second condition, Figure 3.16 shows the variation of the harmonic voltage components when the background voltage distortion is increased from  $V_{bg1}$  (3.969%) to  $V_{bg2}$  (5.943%) with supply impedance of  $X/R$  ratio of 0.2. It is found that with the increase in the background voltage distortion, the voltage CF becomes lower and the current THD is reduced from 107.94% to 100.26%. This gives the same relationships between the current THD and both voltage THD and CF as those obtained with the supply impedance variation condition.

In order to investigate the effect of the supply impedance  $X/R$  ratio for the third condition, the same fundamental impedance magnitude with different  $X/R$  ratios should be chosen. This could be obtained from the available impedance components used in the measurements with  $X/R$  ratios of 0.5 ( $1.885+j0.942$ ) and 2 ( $0.942+j1.885$ ). Figure 3.17 shows the obtained results where the magnitude of the harmonic voltage components is found slightly higher for the case of higher  $X/R$  ratio. This is because the increase in the reactance at harmonic frequencies when  $X/R$  is higher can make up the increase in the

resistive part for the case of lower  $X/R$  ratio. Therefore, the voltage THD is increased and the voltage CF is slightly reduced with  $X/R$  ratio of 2. As for the current, its THD has a little reduction from 120.14% to 118.22% with the increase in  $X/R$  ratio.

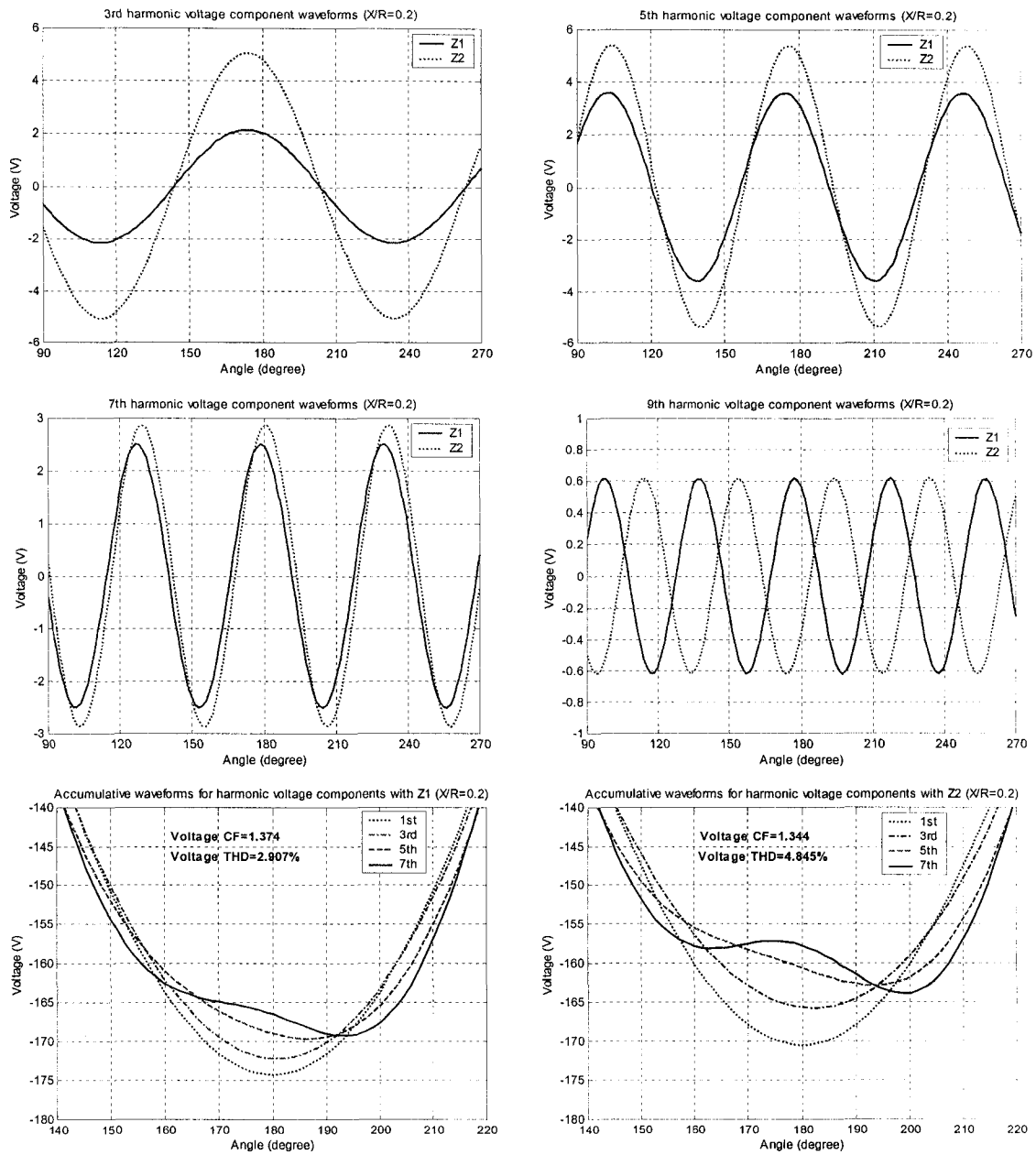


Figure 3.15: Variation of harmonic voltage components and accumulative waveforms with different supply impedance magnitudes.



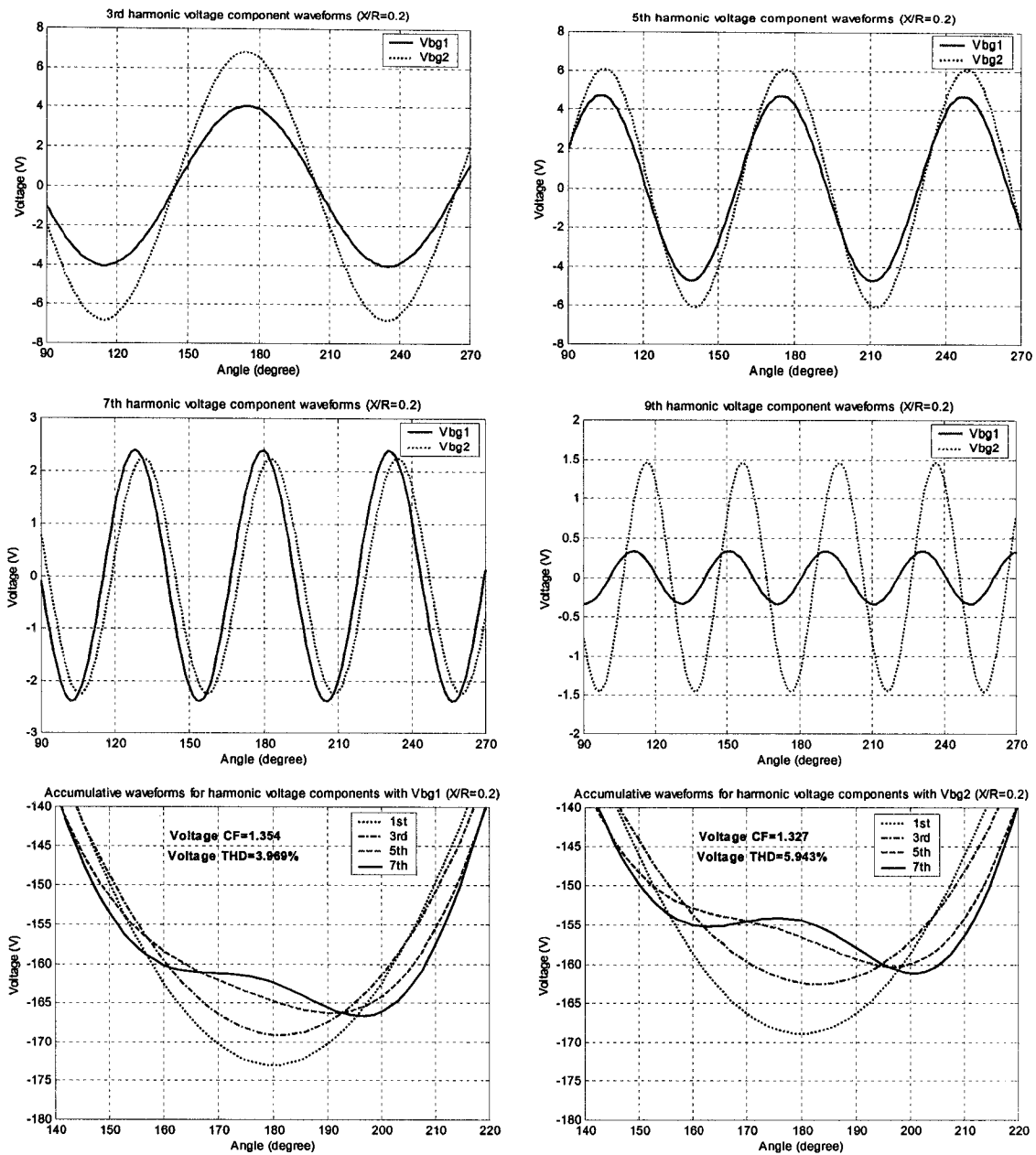


Figure 3.16: Variation of harmonic voltage components and accumulative waveforms under different background voltage distortions.

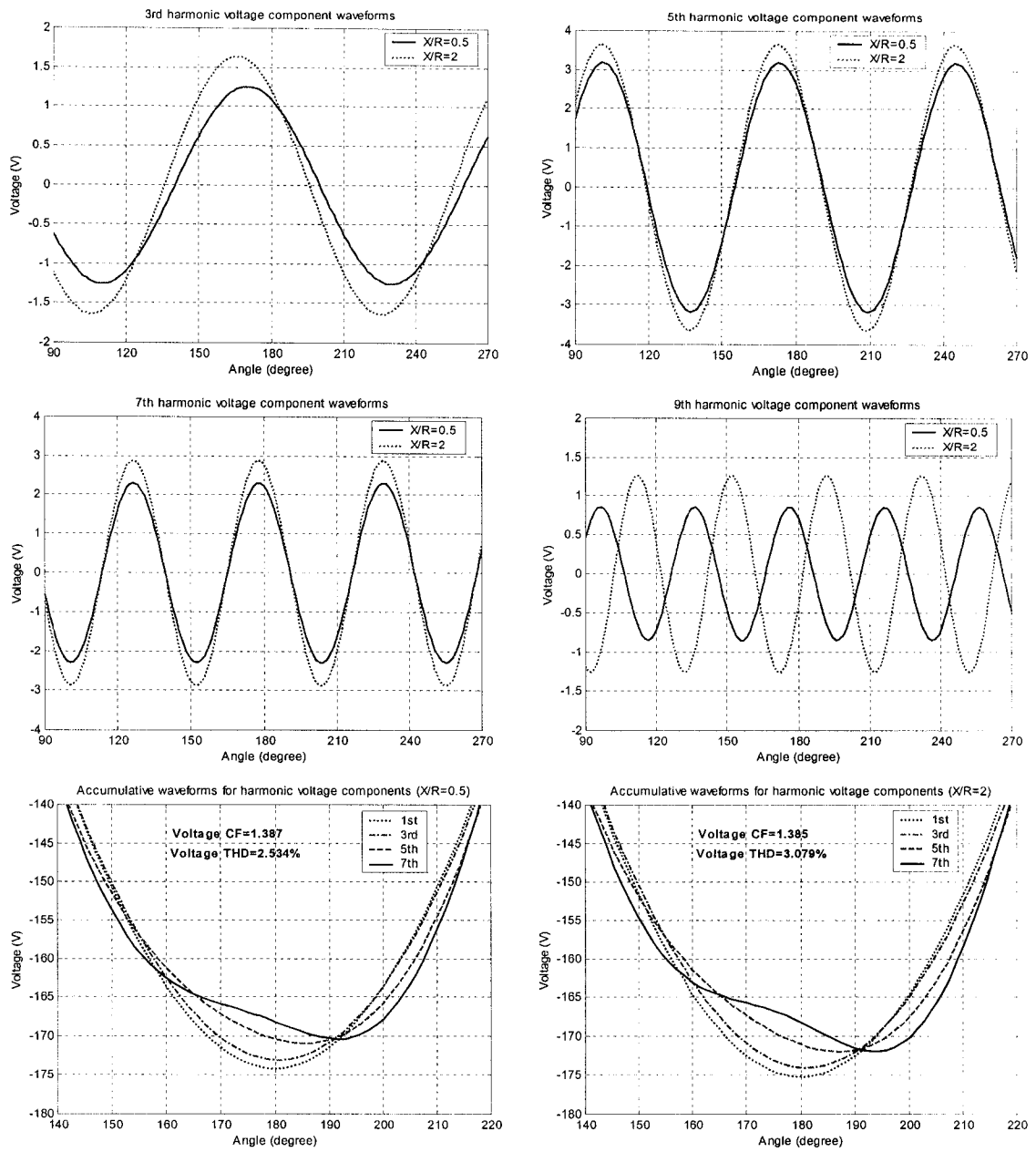


Figure 3.17: Variation of harmonic voltage components and accumulative waveforms with different supply impedance  $X/R$  ratios.

By examining the results of the conducted experiments, the interaction between the PC voltage and harmonic current offers the following findings:

- The phase angles of the lower harmonic order components of the voltage that have dominant magnitudes (3rd, 5th, and 7th) are such that the waveforms have positive peaks so close to the negative peak of the fundamental voltage component and vice versa. Therefore, the increase in the magnitude of these components reduces the peak of the resultant waveform to be more flat with lower CF besides the increase in the voltage THD.
- The harmonic current magnitudes are strongly affected by the voltage waveform. The impact is similar whether the waveform change is caused by the supply impedance variation or the connection of other harmonic sources.
- The harmonic current phase angles with respect to the phase angle of the fundamental voltage component are slightly diversified with the variation of supply impedance or background voltage distortion. However, they do have a specific pattern, which is more delay with the voltage THD increase or the voltage CF decrease. Additionally, the harmonic current phase angles of the lower harmonic orders (dominant ones) are not scattered like higher orders so that they can be reasonably characterized.

From the aforementioned, developing accurate relationships between the harmonic current magnitudes and the voltage THD or CF is feasible. This, combined with the development of approximate relationships for the harmonic current phase angles, will enable to correlate the harmonic current spectrum with the voltage waveform to identify the harmonic source characteristic.

### **3.3.5 Investigating the Reliable Voltage Index on Characterizing the Harmonic Source Current Spectrum for Harmonic Analysis**

The previous research work conducted in [17,33,35] was limited to merely characterize the harmonics attenuation and diversity among distributed single-phase power electronic loads. But the ultimate goal of the research work in this thesis is to expand this study and

develop a methodology for harmonic analysis that can consider the harmonics attenuation and diversity in order to overcome the shortcoming of the traditional harmonic analysis method. This would be accomplished by utilizing the harmonic source characteristic in conjunction with the distribution system characteristic to accurately evaluate the distortion level with distributed harmonic sources while taking into account the effect of the voltage waveform on the harmonic source currents.

It is found that the harmonic current magnitudes and phase angles can be characterized by the CF or THD of the supply voltage waveform. It is also found that the PC current THD has a strong correlation with the two voltage waveform indices. What is required now is to determine the voltage index that should be used as an indicator of the harmonic source current spectrum and moreover can be successfully implemented in the harmonic analysis for the associated distribution system. In order to achieve this purpose, the characteristic of the system voltage with the presence of the harmonic source should be investigated. This means finding the response of the voltage waveform to the PC current distortion. The investigation would tell which voltage index is reliable and should be chosen on characterizing the harmonic source current spectrum to conduct harmonic analysis while considering the harmonics attenuation and diversity. This can be realized according to the following procedure:

- 1) A PC load current is applied to an equivalent system as shown in Figure 3.18. 10 cases with PC current waveforms of different THD levels are carried out. A sample of the used waveforms is depicted in Figure 3.19.
- 2) The traditional harmonic analysis is performed for the considered PC current waveforms and the voltage at the PC node " $V_f$ " is obtained. The voltage CF and THD in each case are extracted to get the system characteristic curves of the current THD and both voltage indices.
- 3) Different  $X/R$  ratios of the supply impedance are tried in this analysis with different impedance magnitudes for each ratio where  $Z_4 > Z_3 > Z_2 > Z_1$ .
- 4) The previous steps are tried with other 8 PC current waveforms but with higher supply impedance magnitude to explore the results for a higher range of the voltage

CF and THD. The chosen impedance magnitudes are such that the resultant voltage drop is up to 3% for lower voltage THD range and up to 10% for the higher voltage THD range. This would help get the general trend of the system characteristic so that a firm conclusion can be drawn on determining the proper voltage index for harmonic source characterization.

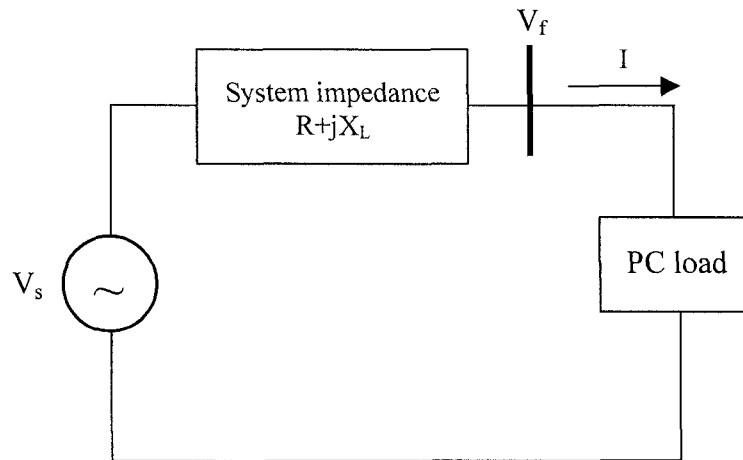


Figure 3.18: Equivalent system to investigate the voltage response to the PC current distortion.

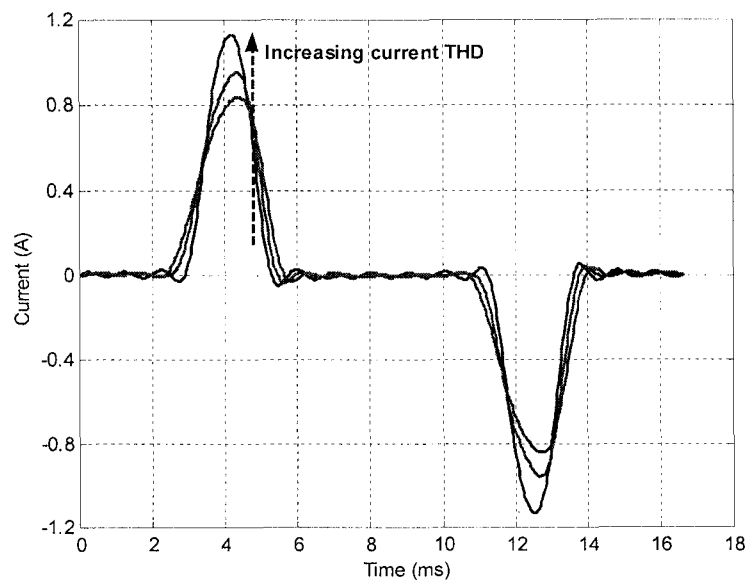


Figure 3.19: A sample of PC current waveforms with different THD levels.

Figures 3.20 and 3.21 present the obtained system voltage characteristic curves of the current THD and both voltage CF and THD respectively following the described procedure. The figures also show the characteristic of the harmonic source. Figure 3.20 shows that generally no solution exists with the voltage CF index since there is no intersection between the system and harmonic source characteristic curves. As a result, the voltage CF can not be taken as a reliable indicator of the harmonic source current spectrum to provide a solution for the harmonic analysis taking into account the harmonics attenuation and diversity. This conclusion is extracted from all results aside from those obtained with  $X/R=0.2$  with impedance  $Z_l$  for the lower voltage CF range at which an intersection may occur. This case is actually not of concern to our study because the associated voltage distortion level is less than 1% and, therefore, no need to consider the harmonics attenuation and diversity. Consequently, the typical harmonic current spectrum can be used directly for harmonic analysis. What is of concern is the higher distortion level where the attenuation and diversity effects start to be pronounced.

The harmonic source and system characteristic curves of the current THD and voltage THD usually have an intersection point and a solution exists as illustrated in Figure 3.21. This implies that the voltage THD should be considered as the proper indicator of the harmonic source currents while conducting harmonic analysis. Therefore, the voltage THD will be adopted in this research work to determine the harmonic source current spectrum and the system distortion level in the harmonic analysis method proposed in the next chapter. From figure 3.21, the following can be inferred:

- 1) With increasing the supply impedance magnitude, the system characteristic curve is rotated to have lower slope. The chosen impedance magnitudes are actually exaggerated for PC systems to have a voltage drop up to 10%.
- 2) Theoretically, if the supply impedance magnitude is allowed to have higher values, a situation of non-convergence can be reached. For the harmonic source and system characteristic curves with slopes  $c_1$  and  $c_2$  in finite interval, the general criterion of convergence is that  $c_1 c_2 < 1$  [52].

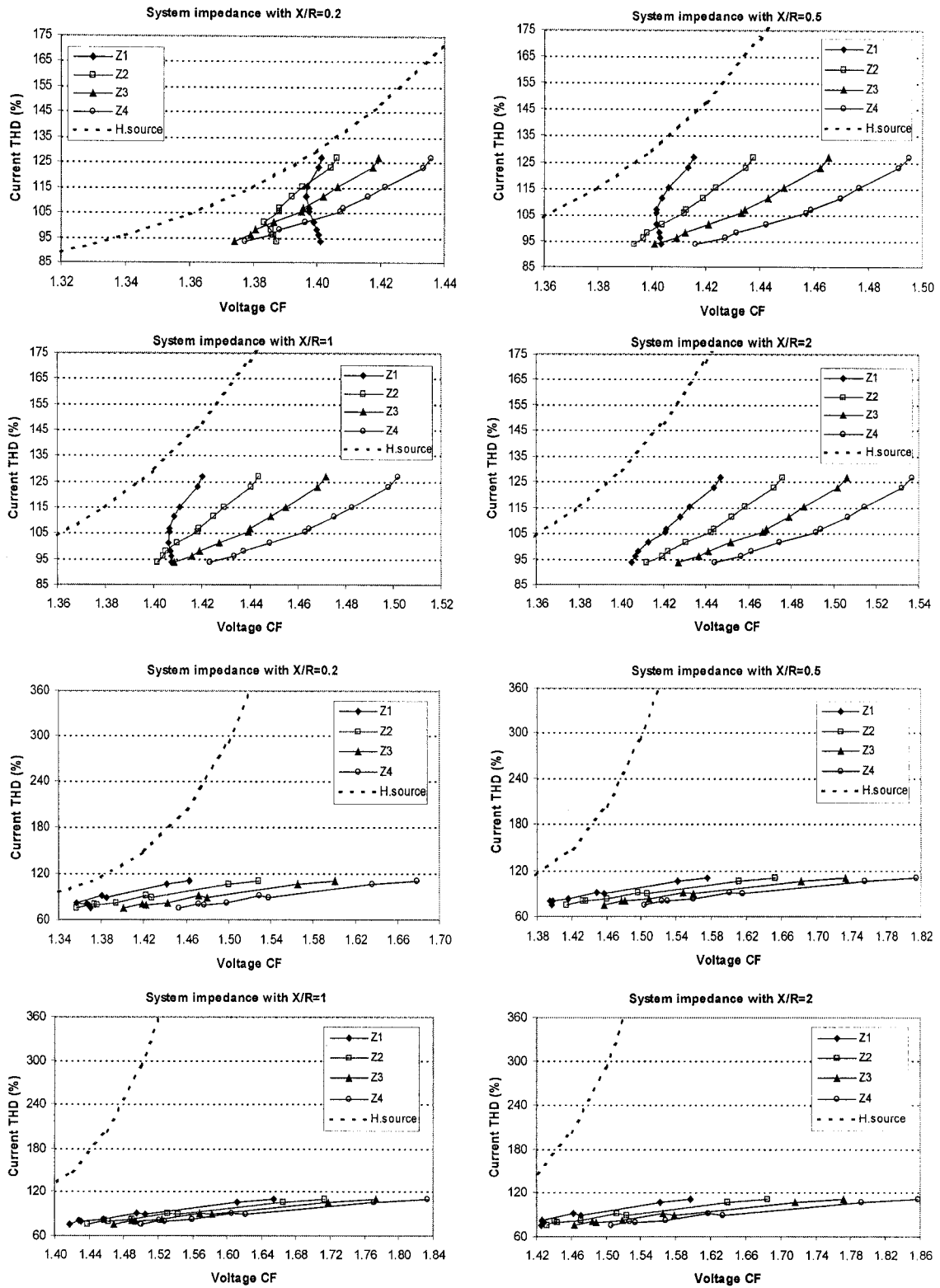


Figure 3.20: System voltage CF response to the PC current distortion.

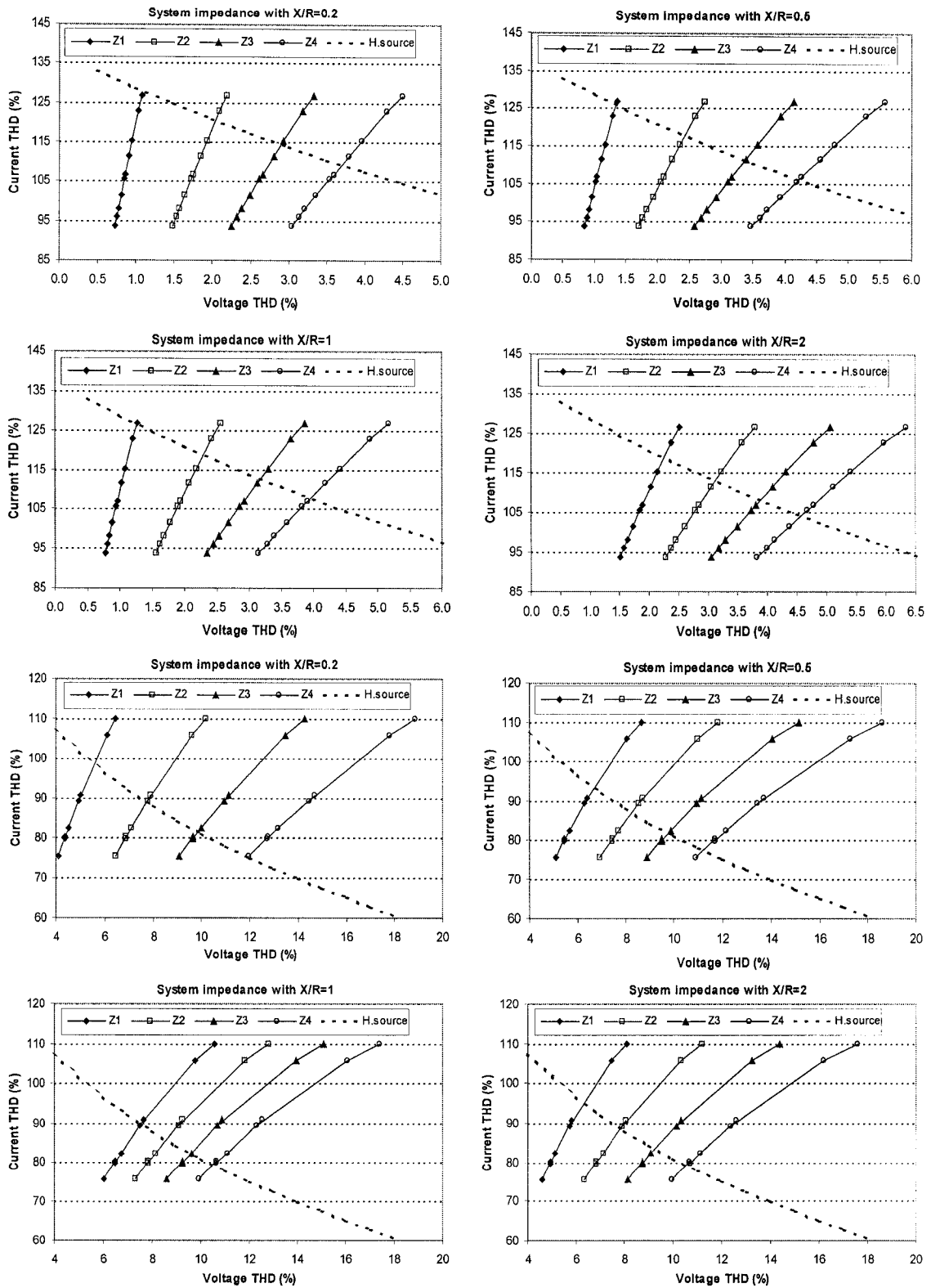


Figure 3.21: System voltage THD response to the PC current distortion.



Justification of the Peaked Voltage Waveform with Increasing the Current Distortion

In order to justify the response of the system voltage waveform towards the current distortion, the instantaneous steady-state equation is used to express the PC voltage  $v_f(t)$  of the system shown in Figure 3.18 as follows:

$$v_f(t) = v_s(t) - [Ri(t) + L(di(t)/dt)] \quad (3.1)$$

The waveform of the supply voltage  $v_s(t)$  is a pure sinusoidal one with a frequency of 60 Hz. Referring to the PC current waveforms shown in Figure 3.19,  $di(t)/dt$  can be extracted, then the waveform of the voltage drop across the system impedance elements (resistance and inductance) can be obtained. This serves to get the PC voltage waveform according to equation (3.1). The variation of the different voltage waveforms with the PC current THD level is depicted in Figure 3.22. It can be noticed that the negative part of the voltage drop across the system impedance that appears in the interval of the positive part of the supply voltage waveform is produced due to the voltage across the inductance. The voltage across the resistance follows the current waveform but scaled with the resistance magnitude.

With the PC current THD increase in the form of peaked and narrower current pulse width, the current will in turn have more sloped waveform. Therefore,  $di(t)/dt$  curve will have increased positive and negative peaks and the resultant PC voltage waveform will be more distorted and skewed to the right with higher peak as shown in Figure 3.22. This explains the response of the system voltage to the current distortion. With increasing the current THD, the harmonic source voltage will have higher CF. Also, when the impedance magnitude increases for the same  $X/R$  ratio, both positive and negative peaks of the voltage drop across the system impedance will accordingly increase. This will provide more distorted and peaked PC voltage waveform skewed to the right. Hence, higher voltage CF is obtained. These justifications fully comply with the results obtained in Figures 3.20 and 3.21.

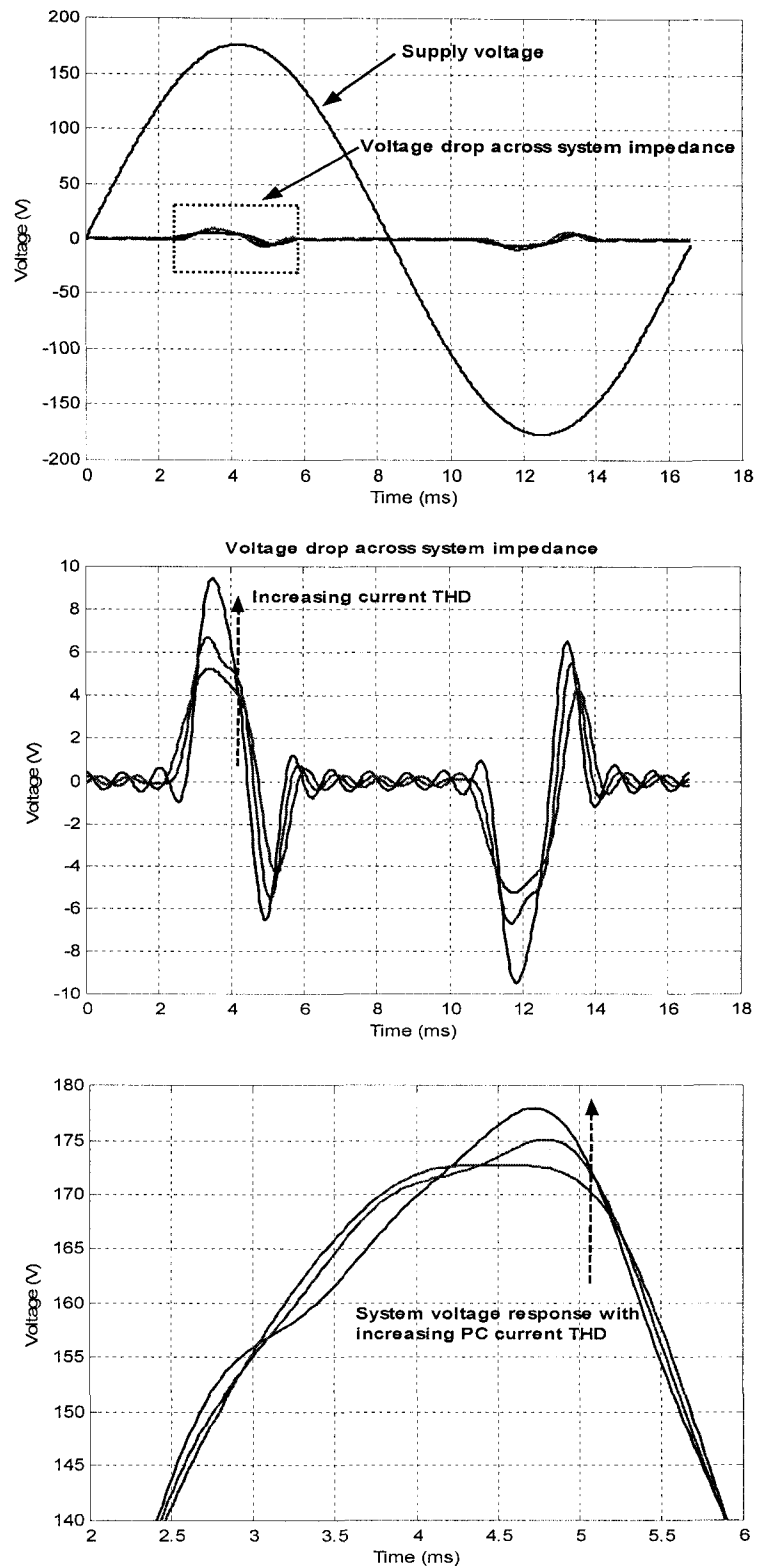


Figure 3.22: Justification of system voltage response to the PC current distortion.

### 3.3.6 Attenuation Factor for PC loads Based on the Supply Voltage Distortion

It can be concluded that the ultimate cause of harmonics attenuation is the distortion of the supply voltage waveform. The definition of the attenuation factor in equation (2.13) considers the effect on harmonic currents in the presence of different number of PC units with respect to the base case of only one PC. The use of more PCs actually affects the voltage distortion seen by the loads. Therefore, the attenuation factor definition is modified to be dependent on the voltage distortion with a base case when the supply voltage has little or no distortion. This base case provides the typical harmonic current spectrum of the harmonic source. Accordingly, the modified attenuation factor definition can be in the following form:

$$AF_{h,V-dist} = \frac{I_{h,V-dist}}{I_{h,typ}} \quad (3.2)$$

where

- $AF_{h,V-dist}$ : the current attenuation factor for the  $h$ -th harmonic order at a specific distorted supply voltage waveform,
- $I_{h,V-dist}$ : the magnitude of the  $h$ -th harmonic current spectrum in percent of the fundamental component at a specific distorted supply voltage waveform,
- $I_{h,typ}$ : the magnitude of the  $h$ -th typical harmonic current spectrum in percent of the fundamental component at a little or nondistorted supply voltage waveform.

The variation of the attenuation factor for each harmonic order with voltage THD is shown in Figure 3.23. The results are obtained from the conducted measurements via equation (3.2). It can be noticed that the attenuation factor for the lower harmonic orders (dominant ones) is less than unity. However, it can be more than unity for the higher harmonic orders, which normally have small magnitudes. This is due to the probable increase in the harmonic current magnitude portion of these orders in the current waveform with the increase in the supply voltage distortion.

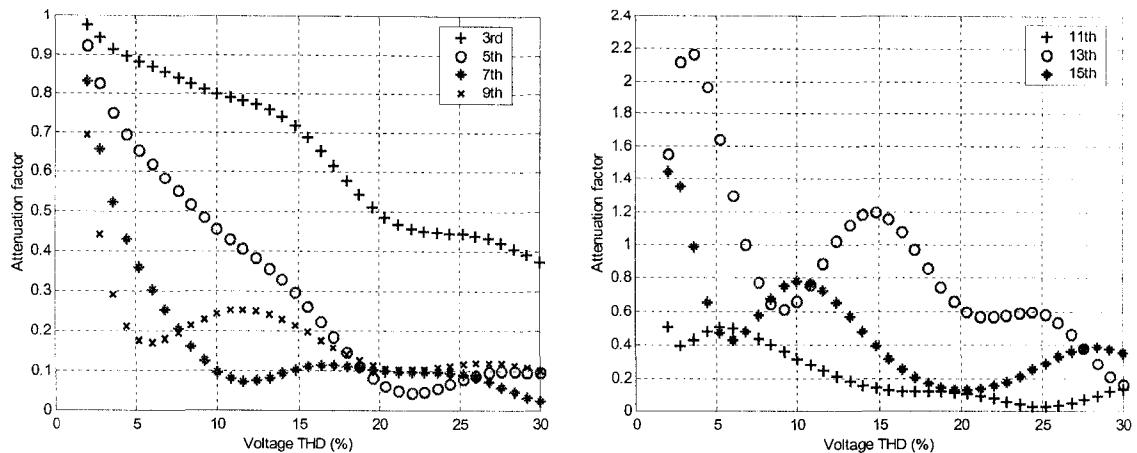


Figure 3.23: Attenuation factor variation for PC harmonic current magnitudes with the supply voltage THD.

### 3.4 Summary and Conclusions

The attenuation and the diversity of harmonic currents produced from a PC load were investigated. The PC load is one of the most commonly used single-phase power electronic loads in commercial systems. Extensive measurements showed how the PC harmonic currents are susceptible to the supply voltage waveform and the current spectrum can no longer be the same as the one obtained with little distorted supply voltage. Therefore, the assumption of fixed harmonic current injection using the typical spectrum will not provide accurate results for harmonic analysis with considerably distorted supply voltage.

The conducted measurements revealed that the supply voltage waveform could be used to characterize the PC harmonic current magnitudes and phase angles. Hence, the current spectrum can be made adaptive to the variation of the supply voltage waveform reflecting the effect of the supply impedance and the background voltage distortion. It was concluded that both voltage THD and CF indices had a good correlation with the harmonic current magnitudes and phase angles.

However, further investigation was made to determine which index could be counted upon to serve for conducting harmonic analysis while considering the harmonics attenuation and diversity. By examining the system voltage response to the PC current distortion to determine the system voltage characteristic, the voltage THD was found as the appropriate index that should be used for this purpose. According to the findings in this chapter, harmonic analysis will be proposed in the next chapter with the capability to handle the attenuation and diversity effects for more accurate and reliable results.

# Chapter 4

## An Iterative Method for Harmonic Distortion Assessment with Distributed PC Loads

The previous chapter showed that the harmonic current magnitudes and phase angles of the PC load are not constant and change with the supply voltage distortion. Therefore, the traditional harmonic analysis method that implements the typical current spectrum will not provide reliable results since it overlooks the variation of harmonic currents. This chapter, based on the results obtained in the previous chapter, proposes an iterative harmonic analysis method for harmonic distortion assessment for systems with distributed harmonic sources while considering the harmonic currents attenuation and diversity. The difference between the proposed method and the traditional one is discussed. Case studies for systems with distributed PC loads are performed and harmonic measurements are carried out to verify the proposed method. Sensitivity studies are conducted to evaluate the performance of the method and the extension possibility to other harmonic source loads.

### 4.1 Introduction

The most common technique for harmonic calculation of power electronic devices is to treat the devices as known sources of harmonic currents with or without including phase angle information. This is due to the fact that the device rectifier circuit acts as an injection current source to the system [21]. The assumption that permits this

representation is that the system voltage distortion is not considerable. This representation, for most nonlinear devices, is quite accurate up to harmonic voltage distortion level of 10% [7].

The advantages of the harmonic current injection method are that the solution can always be obtained directly and it is computationally efficient so that it is capable of accommodating large size distribution systems. Ideally, this method is able to handle several harmonic sources simultaneously. The drawback of this traditional method is that the typical spectrum is often used to represent the harmonic currents generated by the nonlinear loads, which ignores the interaction between the network and the loads. This prevents an adequate harmonic source current assessment of cases involving excessive harmonic voltage distortion. When the harmonic source voltage THD is on the order of 10% or more, modeling the nonlinear elements as constant harmonic current sources introduces inaccuracies, which may be significant and consequently this current injection model should be used carefully [21]. To improve the harmonic analysis accuracy, the phase angles of the harmonic current produced by a nonlinear element should be fairly characterized. Correct representation of the phase angles is important in the presence of a considerable number of harmonic sources to take care of the diversity effect. On the other side, accurate assessment of the harmonic current magnitudes is of a great concern to account for the attenuation effect.

In [53], the impact of the supply voltage distortion is ignored although the distortion level is considerable and can affect the harmonic current spectra of the harmonic sources. In [32], the phase angle diversity among different loads is just investigated without addressing the effect of the supply voltage waveform. The influence of the voltage waveform on harmonic currents injected from multiple single-phase harmonic sources using an analytical time domain based model is examined in [17,33,35] to show the harmonics attenuation and diversity. However, no research work has been reported on how to utilize the findings of the attenuation and diversity studies in harmonic analysis using the common frequency domain based methods to predict the resultant distortion level for systems with distributed harmonic sources.

In this chapter, an iterative frequency domain based harmonic analysis method is proposed to deal with distributed single-phase harmonic source loads. The proposed method is motivated by the mentioned considerations to include the attenuation and diversity of harmonic currents. The method considers the voltage THD as the unique index that can characterize the degree of harmonics attenuation and diversity as concluded in Chapter 3. Using this index in an iterative process, the current spectrum of the system harmonic sources can be modified for reliable system distortion level assessment. Different case studies with distributed PC loads are conducted in order to verify the proposed method and show its advantage over the traditional one. In addition, sensitivity studies are performed to explore the performance of the method.

## 4.2 Traditional Harmonic Analysis Method

Basically, there is a need to solve the fundamental frequency load flow when implementing the traditional harmonic analysis method. Load flow provides the fundamental current of harmonic sources, which affects the magnitudes and phase angles of the injected harmonics. The magnitude of the  $h$ -th harmonic current injected into any bus  $k$  is determined from the typical spectrum and fundamental load current of the harmonic source according to the following equation [20]:

$$I_{h-k} = I_{1-k} \frac{I_{h,spect-k}}{I_{1,spect-k}} \quad (4.1)$$

where  $I_{1-k}$  and  $I_{h-k}$  are the calculated magnitudes of the fundamental and  $h$ -th harmonic current components, and  $I_{1,spect-k}$  and  $I_{h,spect-k}$  are the magnitudes of the fundamental and  $h$ -th harmonic components of the typical current spectrum of the harmonic source.

From the load flow solution, the fundamental frequency phase angle of the harmonic source current is provided, then the phase angle of the  $h$ -th harmonic current injected into bus  $k$  is determined by [20]:

$$\theta_{h-k} = \theta_{h,spect-k} + h(\theta_{1-k} - \theta_{1,spect-k}) \quad (4.2)$$



where  $\theta_{l-k}$  and  $\theta_{h-k}$  are the calculated phase angles of the fundamental and  $h$ -th harmonic current components, and  $\theta_{l,spect-k}$  and  $\theta_{h,spect-k}$  are the phase angles of the fundamental and  $h$ -th harmonic components of the typical current spectrum of the harmonic source. The frequency domain nodal equations for each harmonic order are then used to compute the network harmonic voltages by knowing the system harmonic admittance matrix.

For harmonic studies involving one harmonic source, the harmonic current phase angles can be ignored and only the magnitudes are used in the harmonic calculation. However, harmonic phase angles need to be included when multiple harmonic sources are considered simultaneously in order to take the harmonic cancellation effect into account. Considering two loads connected at buses  $k$  and  $k+1$  and having the same typical harmonic current spectrum, the phase angle difference between the  $h$ -th harmonic current components of the two loads, using equation (4.2), can be obtained by:

$$\Delta\theta_{h-(k,k+1)} = h(\theta_{1-k} - \theta_{1-(k+1)}) \quad (4.3)$$

The fundamental current phase angle of the harmonic sources depends on the phase angle of the fundamental voltage at the buses where the harmonic sources are connected. Assuming the loads are identical, the phase angle difference between the fundamental current components is equal to the phase angle difference between the associated fundamental voltage components, therefore, equation (4.3) can be written as follows:

$$\Delta\theta_{h-(k,k+1)} = h(\phi_{1-k} - \phi_{1-(k+1)}) = h\Delta\phi_{1-(k,k+1)} \quad (4.4)$$

where  $\phi_{1-k}$  and  $\phi_{1-(k+1)}$  are the phase angles of the fundamental voltages at buses  $k$  and  $k+1$  and  $\Delta\phi_{1-(k,k+1)}$  is the phase angle difference between these two components. This shows how the diversity among the harmonic source currents is determined only by the diversity among the fundamental voltage phase angles at the respective buses.

### 4.3 Proposed Iterative Harmonic Analysis Method

From the extensive measurements conducted to the PC load, it is found that the harmonic current spectrum is highly affected by the supply voltage distortion. Figure 4.1 depicts the measured PC harmonic current magnitudes in percent of the fundamental component and the harmonic current phase angles with respect to the corresponding fundamental component phase angle of the supply voltage under two different distortion levels of the supply voltage (1.77% and 4.23%). It is obvious how the harmonic current spectra are not the same. The dominant harmonic currents have less magnitude with the higher voltage distortion case, which accounts for the attenuation effect. Besides, the harmonic current phase angles exhibit sensible difference in the two cases, which accounts for the phase angle diversity among distributed harmonic sources having different bus voltage distortion levels.

Based on the above findings, the individual harmonic current components are considered dependent on the voltage total harmonic distortion at the associated bus. Therefore, an iterative procedure can be proposed to assess the distortion level for systems with distributed harmonic sources taking into account the attenuation and diversity of the generated harmonic current spectrum. From the PC load experiments described in Chapter 3, the individual harmonic current magnitudes and phase angles are characterized using curve fitting as a function of the supply voltage THD as shown in Figures 4.2 and 4.3. These curves can be used to get the harmonic current spectrum at a specified voltage THD.

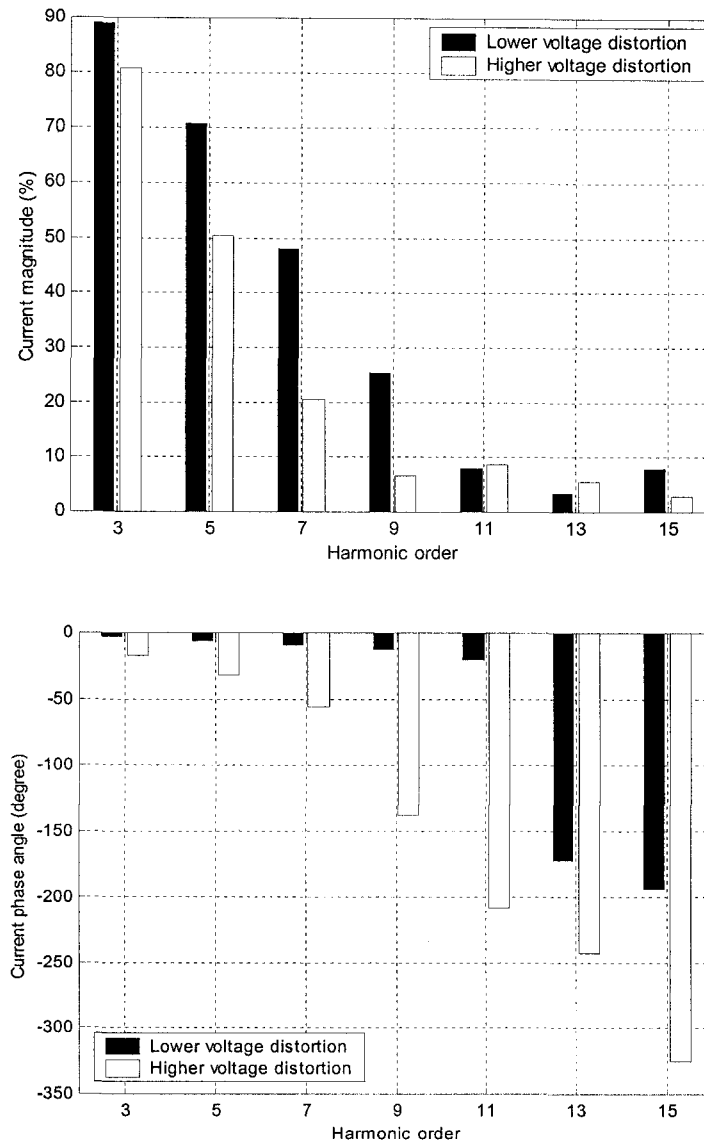


Figure 4.1: Measured harmonic current spectra for a PC load under different supply voltage distortion levels.

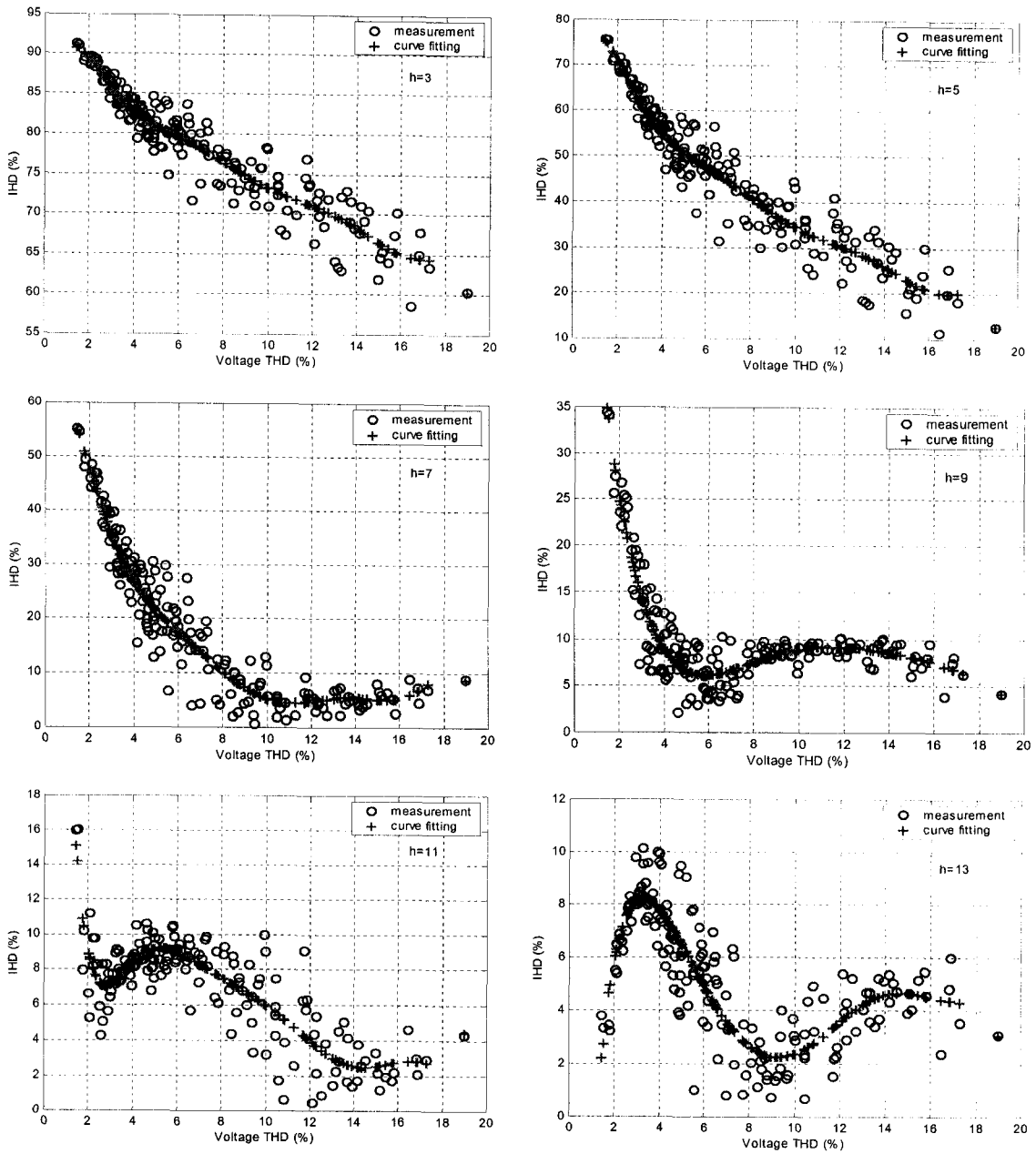


Figure 4.2: Variation of PC individual harmonic current magnitudes as a function of supply voltage distortion.

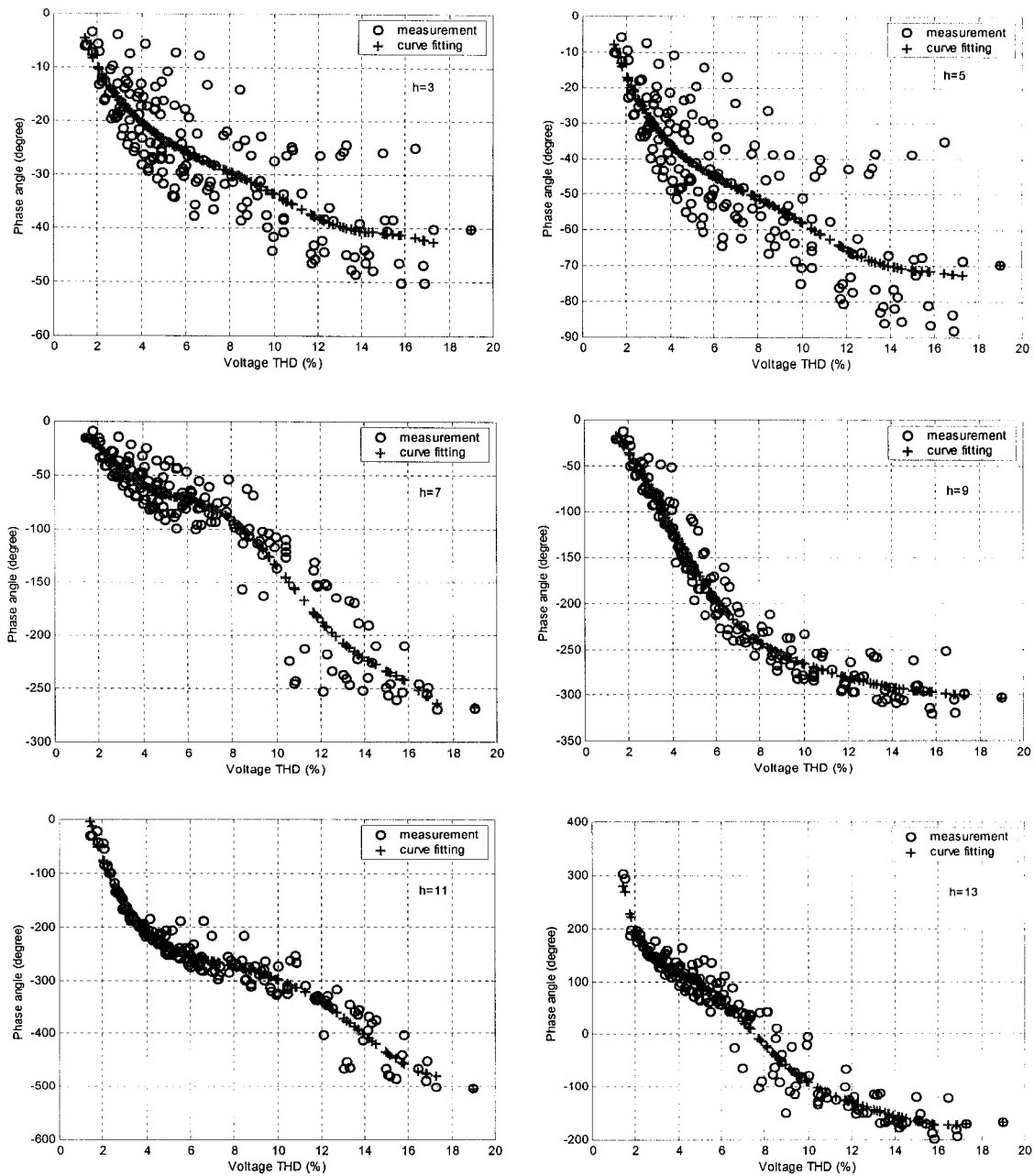


Figure 4.3: Variation of PC individual harmonic current phase angles as a function of supply voltage distortion.

According to the PC load measurements, the harmonic current spectrum is expressed as a function of the voltage THD using the following equations:

$$I_h = \alpha_h(VTHD) \quad (4.5)$$

$$\theta_h = \beta_h(VTHD) \quad (4.6)$$

where  $\alpha_h$  (VTHD) denotes the magnitude of the  $h$ -th harmonic current in percent of the fundamental component as a function of the voltage THD.  $\beta_h$  (VTHD) denotes the phase angle of the  $h$ -th harmonic current with respect to the fundamental voltage phase angle as a function of the voltage THD.

In order to implement the proposed method for harmonic analysis, initial values of the voltage THD should be assumed to start the iterative process. This is because the harmonic voltages at different locations are not known yet to determine the harmonic current spectrum of each harmonic source. One possible way for initializing the voltage THD is by utilizing the harmonic power flow results obtained from the traditional method employing the typical harmonic current spectrum. In addition, the fundamental frequency load flow provides the fundamental voltage and current components of the different harmonic sources.

Using the voltage THD results, the harmonic current spectrum of the harmonic source at bus  $k$  is adjusted, with the help of the developed relationships, as follows:

$$I_{h,adj-k} = I_{1-k} \times \frac{\alpha_h(VTHD_k)}{100} \quad (4.7)$$

$$\theta_{h,adj-k} = \beta_h(VTHD_k) + h\phi_{1-k} \quad (4.8)$$

This adjustment considers the attenuation and diversity of harmonic currents. Then, the adjusted harmonics are re-injected into the system to get the new and improved system harmonic voltages using the harmonic nodal equations and the voltage THD can be calculated. Since the harmonic currents are influenced by the new system voltage distortion, new adjusted harmonic currents are obtained and the process is sequentially repeated until convergence in the voltage THD at all system buses is reached. As a result,

the interaction between the harmonic-producing loads and system voltage is taken care of to yield more precise and reliable results.

According to equation (4.8), the phase angle difference between the  $h$ -th harmonic current components for two loads connected at buses  $k$  and  $k+1$  is obtained by:

$$\begin{aligned}\Delta\theta_{h-(k,k+1)} &= \beta_h(VTHD_k) - \beta_h(VTHD_{k+1}) + h(\phi_{1-k} - \phi_{1-k+1}) \\ &= \beta_h(VTHD_k) - \beta_h(THD_{k+1}) + h\Delta\phi_{1-(k,k+1)}\end{aligned}\quad (4.9)$$

It can be inferred that by implementing the proposed method, the phase angle difference between the injected harmonic source currents at different locations is determined by the phase angle difference between the fundamental voltages and also by the effect of the voltage distortion at the harmonic source buses. However, by using the traditional method, the phase angle difference between the harmonic currents is determined only by the phase angle difference between the fundamental voltages as implied in equation (4.4). This reflects how the supply voltage waveform can contribute to the harmonic current phase angle diversity among distributed harmonic sources and consequently can affect the degree of harmonic cancellation. Regarding the magnitude of the harmonic current spectrum, its adjustment using equation (4.7) reflects the attenuation impact, while the traditional method uses fixed harmonic current magnitude determined from the typical spectrum.

With small values of the voltage THD, it is not expected to have considerable attenuation and diversity effects. Therefore, the traditional harmonic analysis method should give close results to those obtained using the proposed method. This is due to the insignificant impact of the small values of the supply voltage distortion on the magnitudes and the phase angles of the injected harmonic current spectrum. With significant harmonic voltage distortion levels, the iterative algorithm is mandatory to get the resultant system distortion. The flow chart in Figure 4.4 shows how the proposed iterative harmonic analysis method can be implemented for harmonic distortion assessment for distribution systems with distributed harmonic sources.

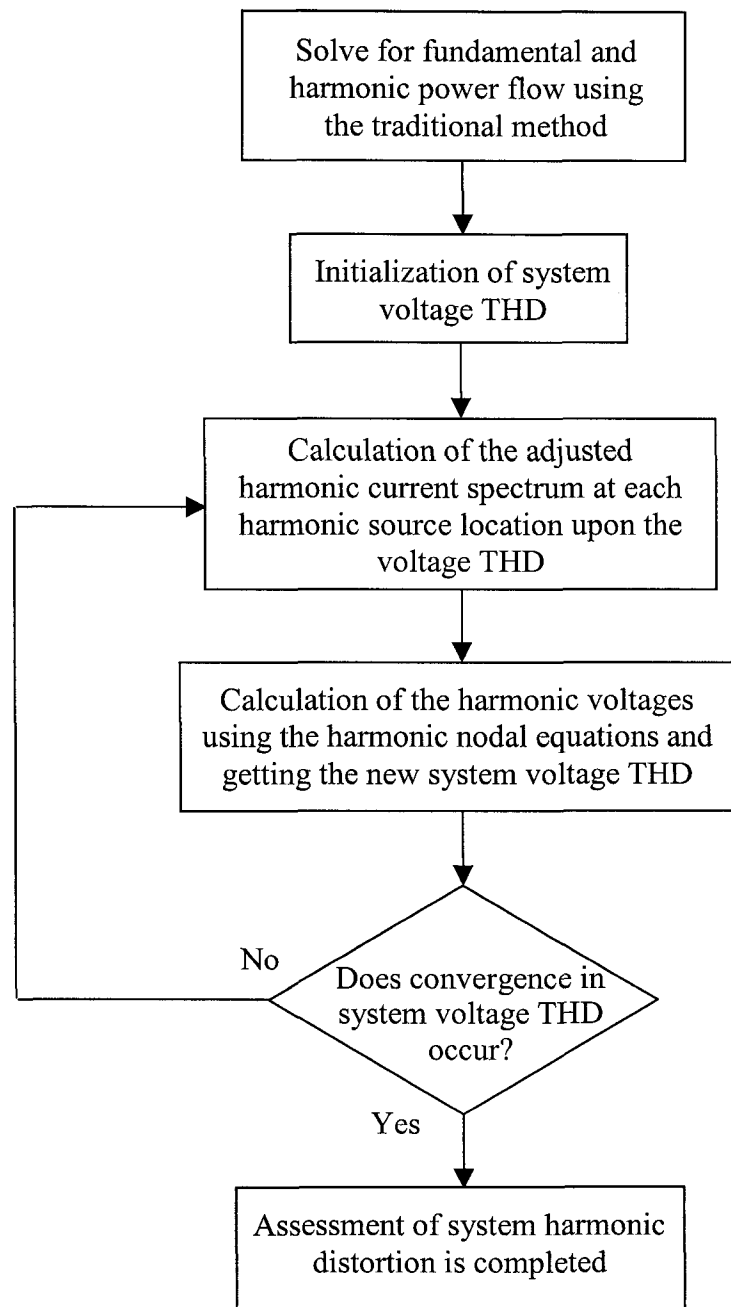


Figure 4.4: Flow chart of the proposed iterative method for harmonic distortion assessment for systems with distributed harmonic sources.



#### 4.4 Case Studies for Distributed PC Loads

In order to verify the proposed iterative method, harmonic measurements are conducted on two PC systems with multiple PC loads in the power laboratory in the Electrical and Computer Engineering Research Facility at the University of Alberta. The two PC systems shown in Figure 4.5 are constructed such that they have different configurations and number of PC units in order to determine the general applicability of the proposed method. The magnitude of the supply impedance " $Z_s$ " is increased in many steps to vary the system distortion level and voltage and current measurements are performed. Calculations are carried out for harmonic analysis using the traditional and iterative methods. The results are compared with the measurements to verify the proposed method and clarify the inaccuracy introduced in system distortion evaluation when the traditional method is applied.

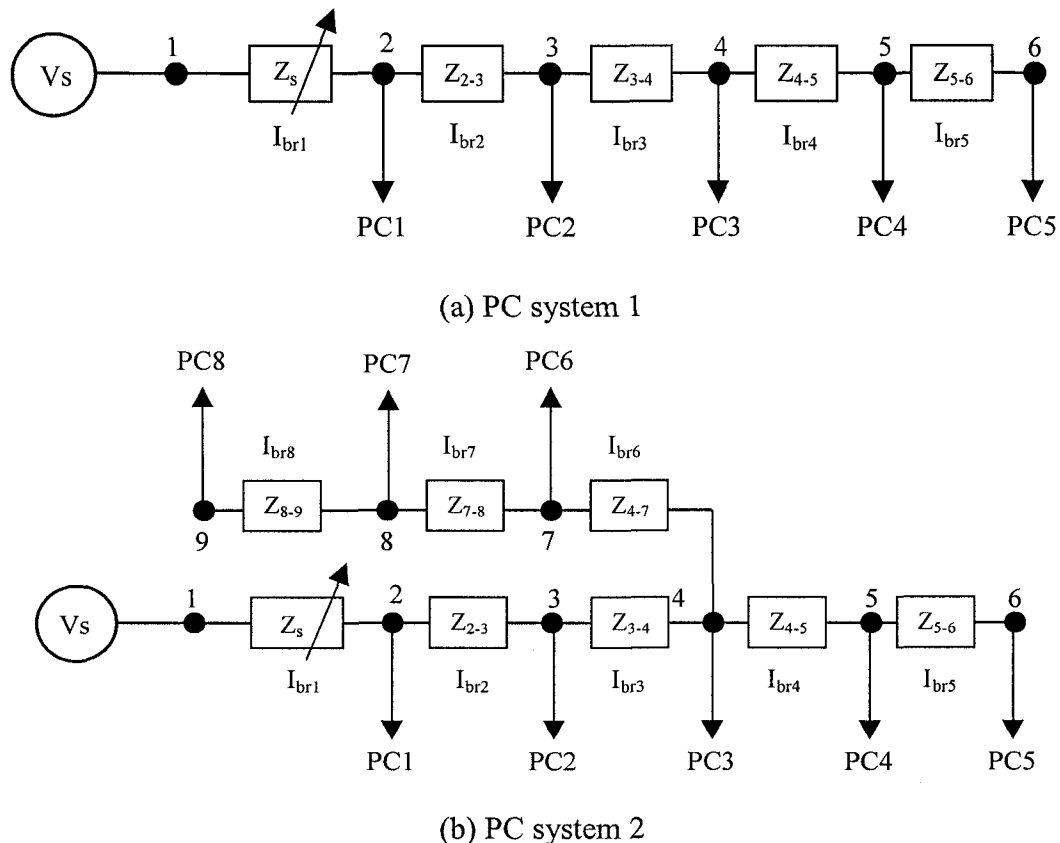


Figure 4.5: Single-line diagram of the two PC systems under study.

#### 4.4.1 Measurement and Calculation Results for PC system 1

The size of the supply impedance is increased in seven steps for PC system 1. The study cases have resistance values of 0.5, 1.25, 1.75, 2.5, 3, 3.75, and 4.25 ohm respectively with X/R ratio of 0.754. The voltage and PC current are measured at nodes 2 and 3 in addition to the current through branches 1 and 2. The convergence criterion of the iterative method is set at 0.05% of the maximum absolute difference of the voltage THD at all nodes between two successive iterations. Figure 4.6 depicts the voltage and current THD results obtained from the measurements and the results obtained by the proposed iterative method and the traditional method that employs the typical harmonic current spectra of the PC loads. The results are presented for different study cases of the supply impedance magnitude in ascending order and the following conclusions can be drawn:

- 1) The calculation using the typical harmonic current spectra by injecting fixed harmonic currents would give voltage distortions that are not accurate and far from the measurements. As the system distortion level increases, the difference becomes significant. This ensures that using the typical harmonic current spectrum can lead to considerable overestimation of system distortion due to ignoring the attenuation and diversity of harmonic currents.
- 2) The measured current THD through different branches decreases when the supply impedance increases. This is due to the impact of the voltage waveform distortion at each node on the spectrum of the harmonic current injected from the associated PC. Due to the attenuation and diversity effects, the resultant current THD is highly reduced compared with the case when the typical harmonic current spectrum is used.
- 3) The calculation using the iterative method predicts the distortion level reasonably well and the results are generally in a good agreement with the measurements. This shows how the proposed method can consider the influence of the supply voltage waveform on the harmonic currents by taking into account both the attenuation and diversity effects, thus providing reliable harmonic distortion for systems with distributed harmonic sources.

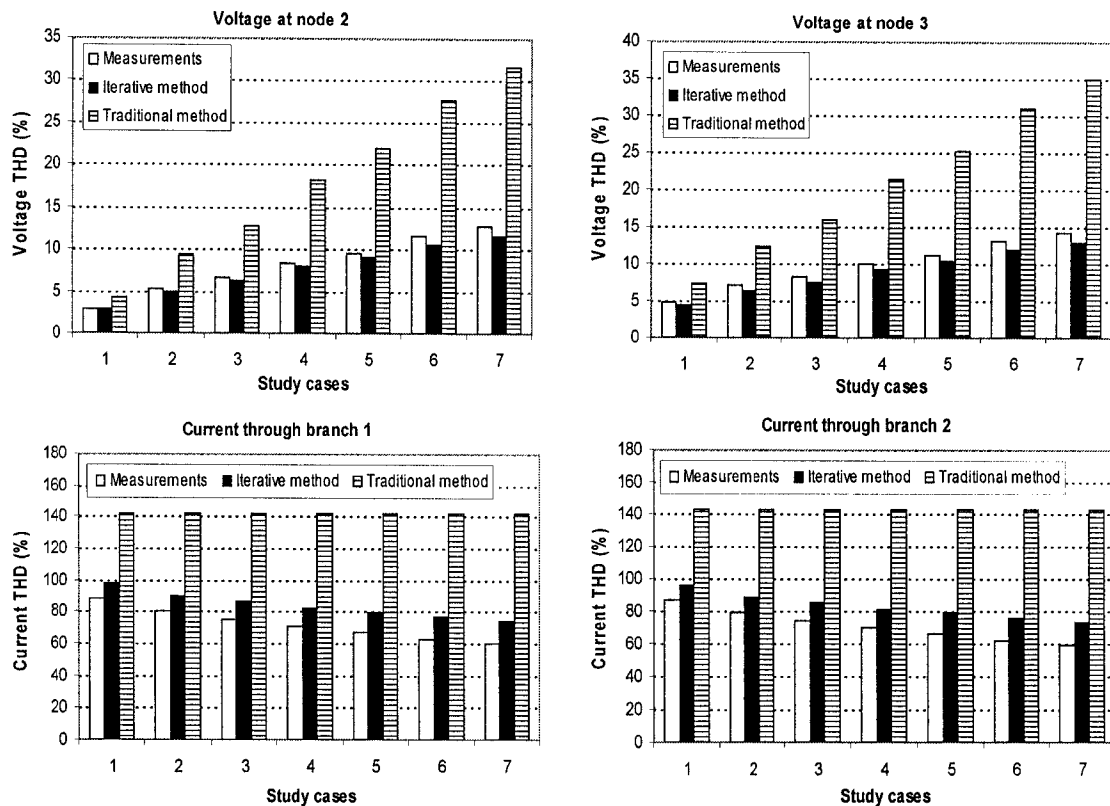


Figure 4.6: Measurement and calculation results of the voltage and current THD for PC system 1.

In order to assert the validity of the proposed iterative method, a comparison between the measurements and calculation results is made for the individual harmonic source voltage and current magnitudes in percent of the fundamental component. A comparison is also made for the individual harmonic voltage and current phase angles with respect to the fundamental voltage phase angle at the corresponding node. Figure 4.7 shows the results of the harmonic voltages at nodes 2 and 3 and Figure 4.8 shows the results of the harmonic currents produced from the PCs at the same nodes. It can be inferred that using the traditional method gives inaccurate harmonic voltage and current components. On the contrary, the iterative method has the capability of adjusting the harmonic current spectrum according to the voltage distortion and, therefore, is an improved and more accurate method to assess the system distortion level.

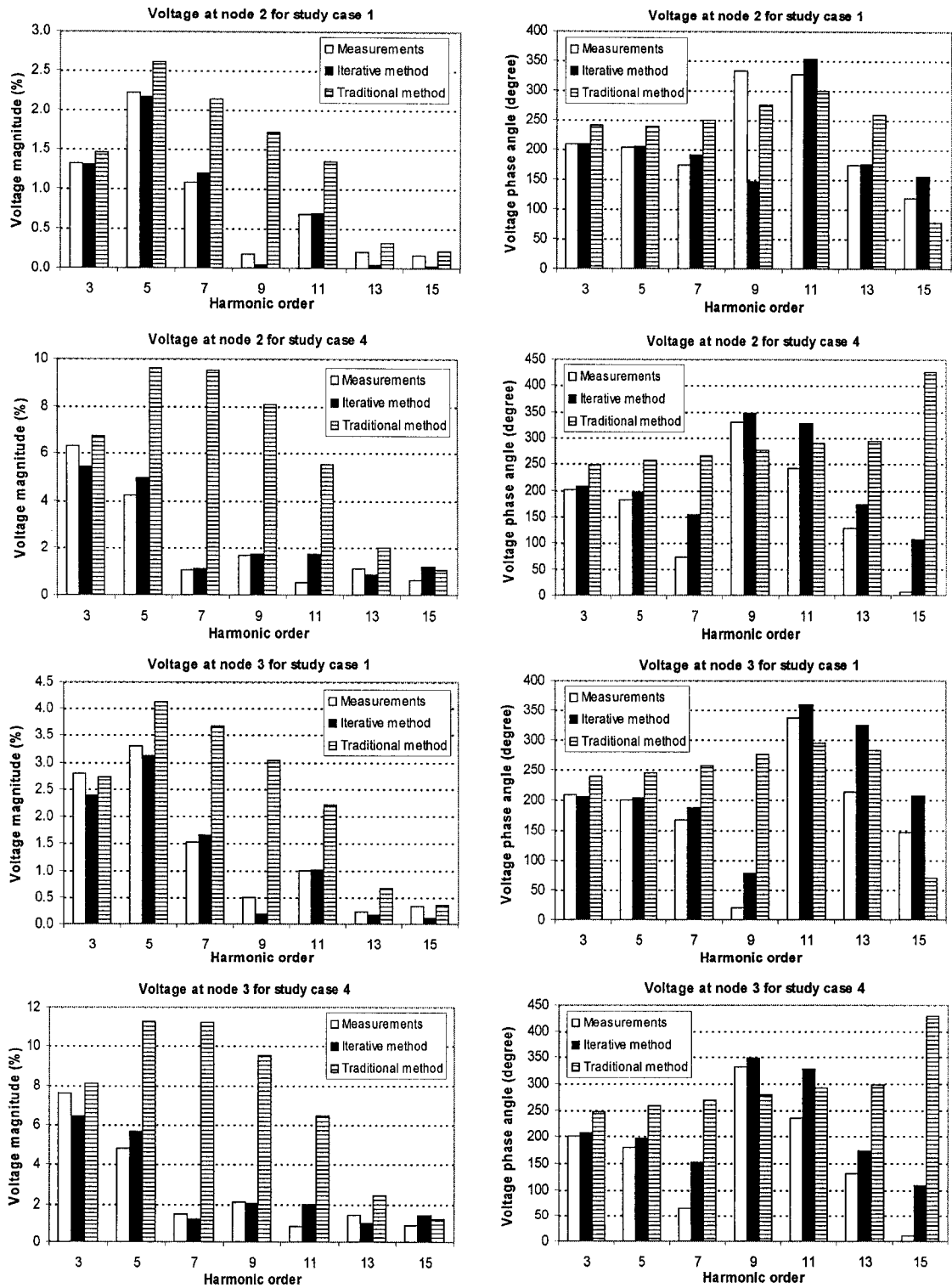


Figure 4.7: Measurement and calculation results of the individual harmonic magnitudes and phase angles of system node voltages (PC system 1).

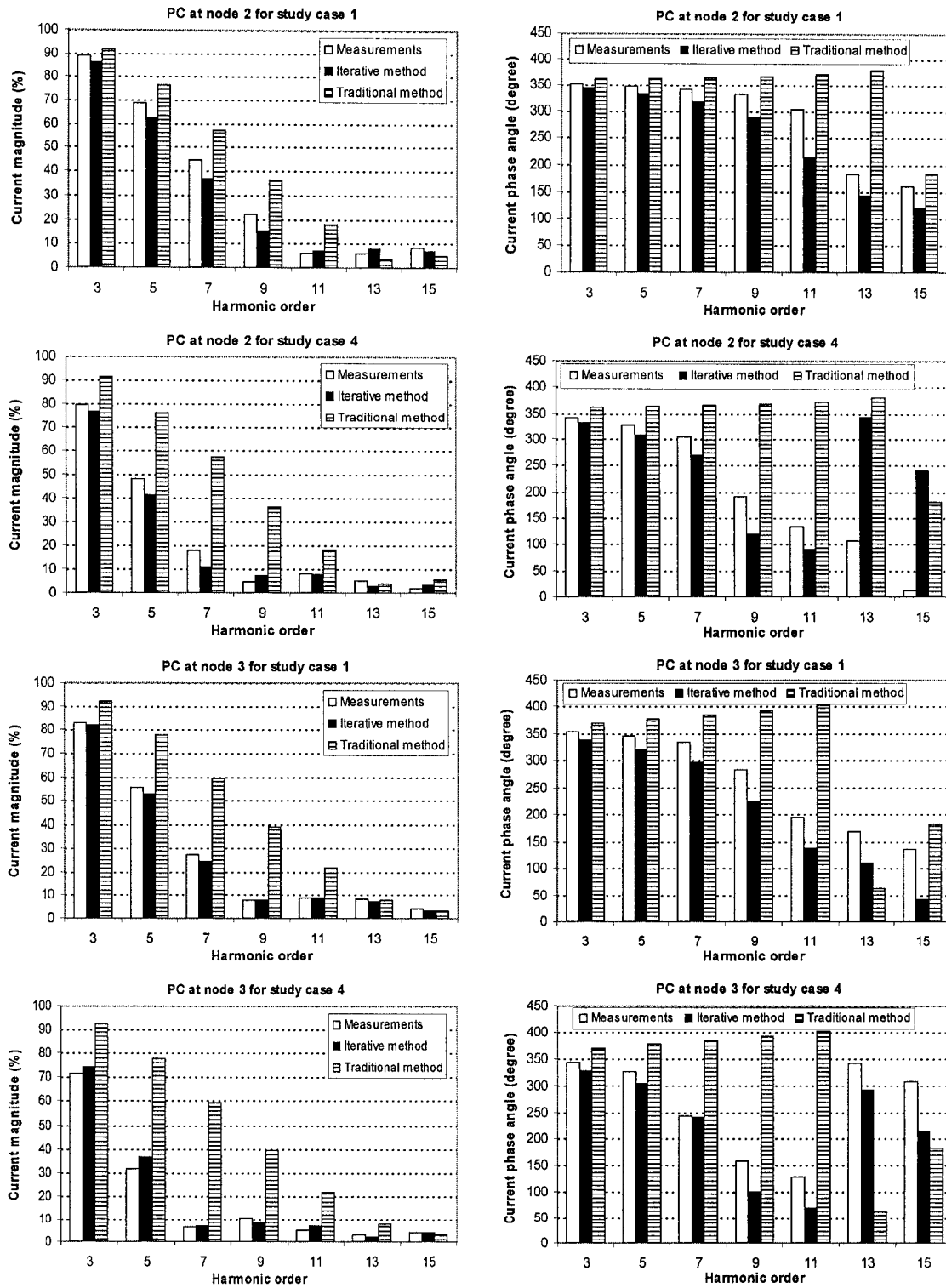


Figure 4.8: Measurement and calculation results of the individual harmonic magnitudes and phase angles of system harmonic source currents (PC system 1).

#### 4.4.2 Measurement and Calculation Results for PC system 2

The size of the supply impedance is increased in three steps for PC system 2. The study cases have resistance values of 0.5, 1.25, and 1.75 ohm respectively with X/R ratio of 0.754. Measurements are taken for the voltage and PC current at node 2 in addition to the current through branch 1. The convergence criterion of the iterative method is set at 0.05% similar to PC system 1. Figure 4.9 presents the measurement and calculation results of the node voltage and branch current THD for different study cases of the supply impedance magnitude. The results provide the same conclusions drawn for PC system 1. Figure 4.10 shows the individual harmonic voltage magnitudes and phase angles at node 2 as well as the harmonic current spectrum of the PC at the same node.

The overestimated results of the voltage and current THD can be noticed in case of applying the traditional harmonic analysis method. Also, it can be shown how the harmonic current spectrum using the iterative method is properly adjusted to account for the effect of the supply voltage distortion. Accordingly, reasonable individual harmonic voltage magnitudes and phase angles are obtained. The traditional method uses the typical harmonic current spectrum, which is constant irrespective of the system distortion level, thus producing inaccurate harmonic voltage components. The obtained results emphasize that the proposed iterative method should be adopted to take into account the interaction between the PCs and system voltage.

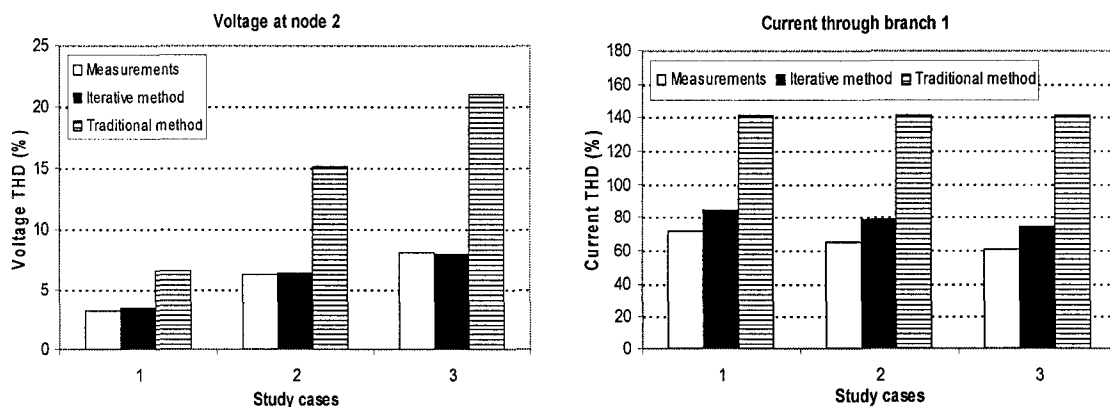


Figure 4.9: Measurement and calculation results of the voltage and current THD for PC system 2.

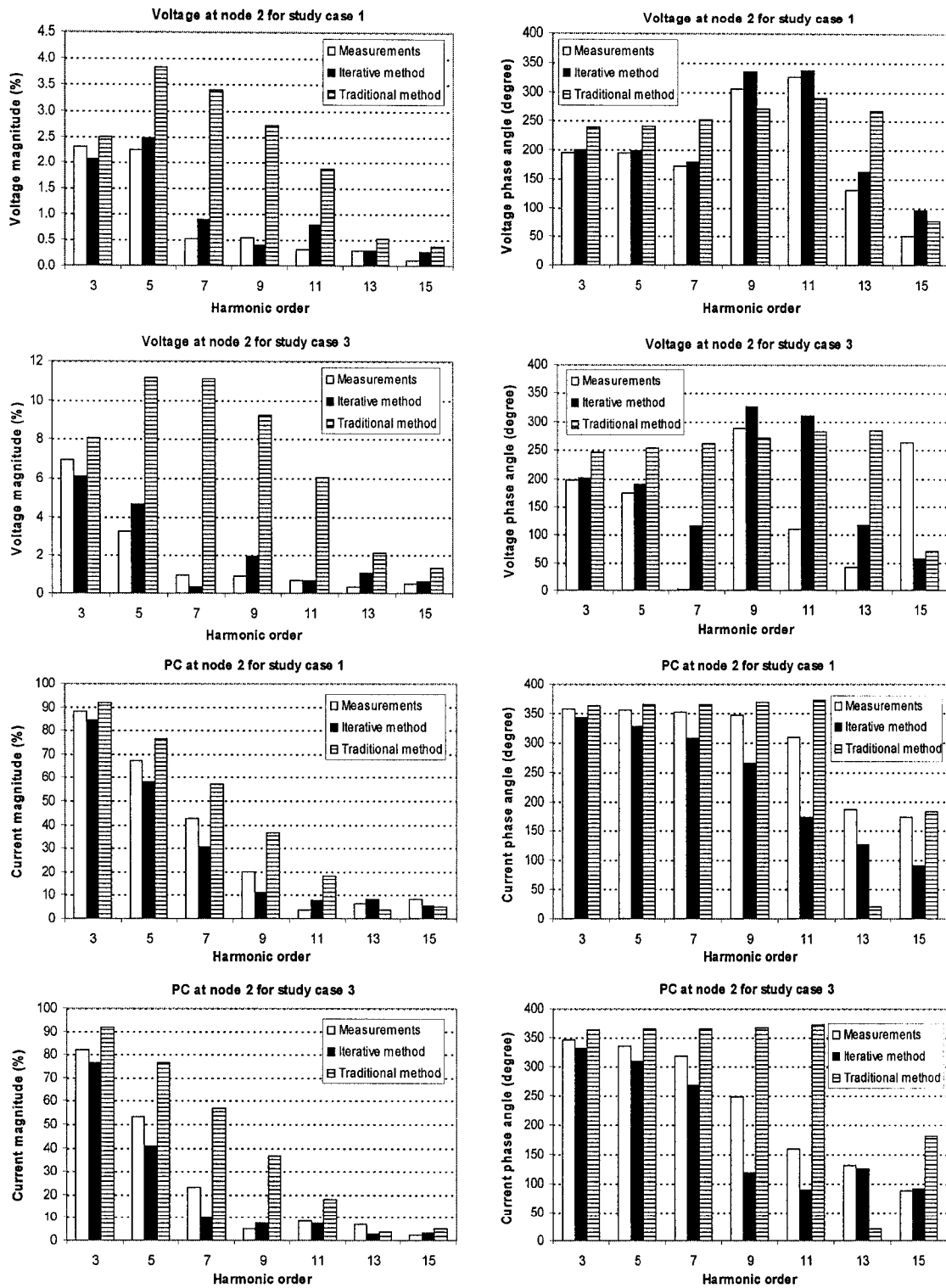


Figure 4.10: Measurement and calculation results of the individual harmonic magnitudes and phase angles of the voltage and the harmonic source current at node 2 (PC system 2).

### 4.4.3 Sensitivity Studies

Sensitivity studies are conducted to examine the convergence behavior of the iterative method in addition to some approximations on the assessment of harmonic distortion as follows:

- 1) System characteristics of the current THD and both voltage THD and voltage CF are extracted to show how the proposed iterative method can converge only when the voltage THD is considered to estimate the harmonic source current.
- 2) The implementation of the iterative method without considering the diversity of harmonic currents due to the voltage distortion is investigated, i.e., the harmonic current spectrum adjustment is performed only on the magnitudes while the phase angles are determined using the traditional method.
- 3) The impact of system distortion level on solution convergence speed is determined with and without considering the harmonics diversity.
- 4) Finally, a simplified and approximate way to get a round figure of the system distortion level without the need to perform the complete iterative procedure is investigated.

#### 4.4.3.1 Convergence Process of the Iterative Method

Figure 4.11 shows the system characteristics of the current THD of the PC at node 2 in PC system 1 and the corresponding voltage THD and CF which are obtained for study case 4 of the supply impedance magnitude. Besides, the harmonic source characteristics for both voltage indices are presented to clarify the iterative method. It can be seen that when the system voltage THD is used to determine the harmonic source current, the iterative method converges to the intersection point between the two curves to provide the resultant distortion. On the contrary, the two characteristic curves of the current THD and voltage CF have no intersection, therefore, the system voltage CF can not lead to solution convergence. Even if theoretically the two curves are extended to have an intersection point, the iteration will diverge because the slope of the system characteristic



is less than that of the harmonic source characteristic, which provides unstable solution point. This clarification reinforces the conclusions drawn in Chapter 3 regarding the choice of the voltage THD as the appropriate index to characterize the harmonic source current spectrum.

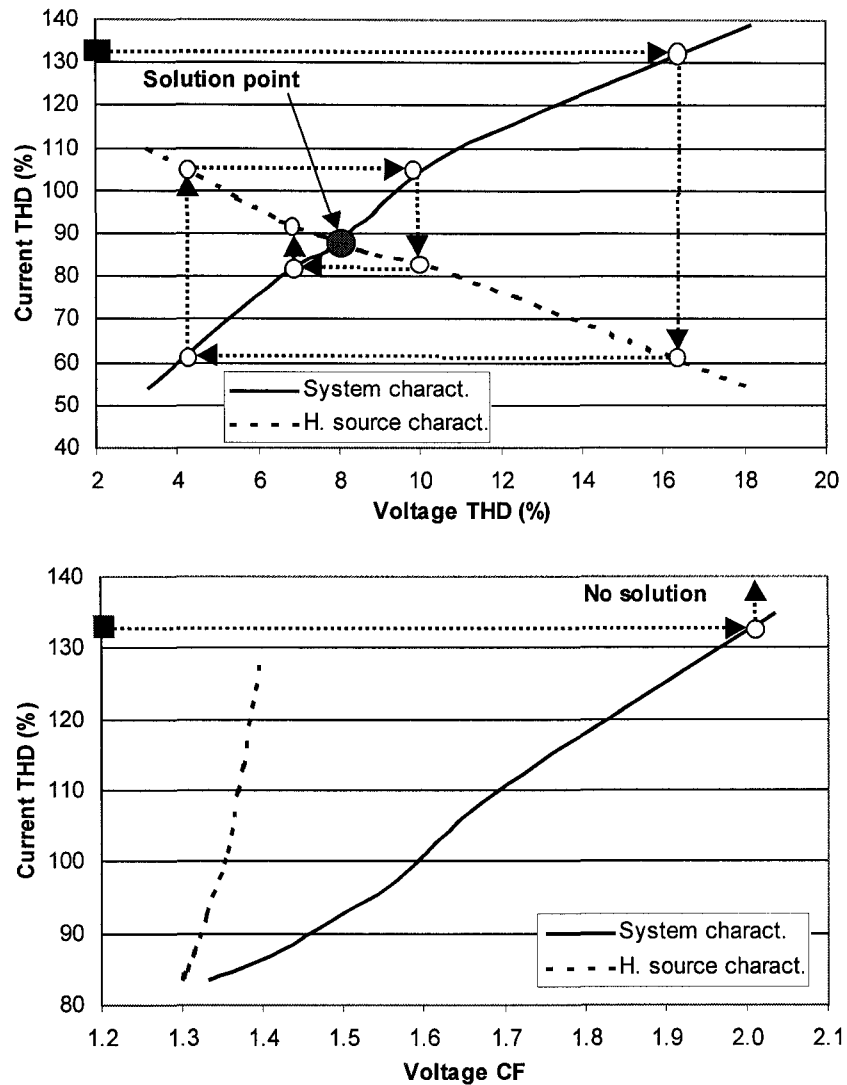
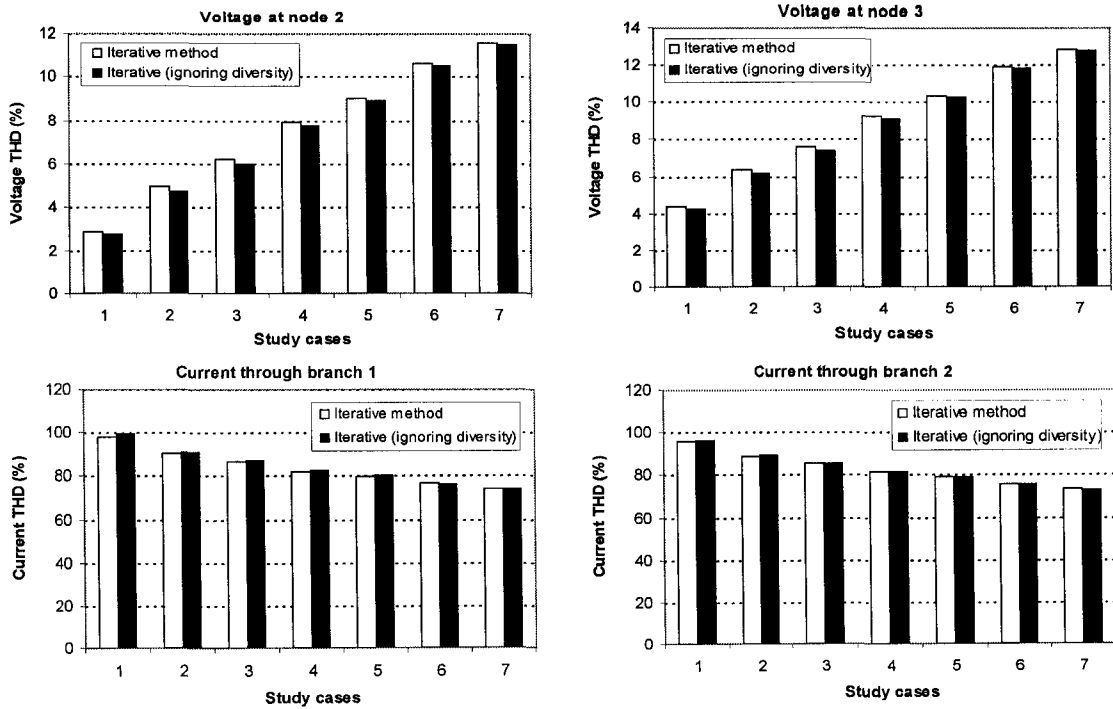


Figure 4.11: Iterative process with voltage THD and CF indices.

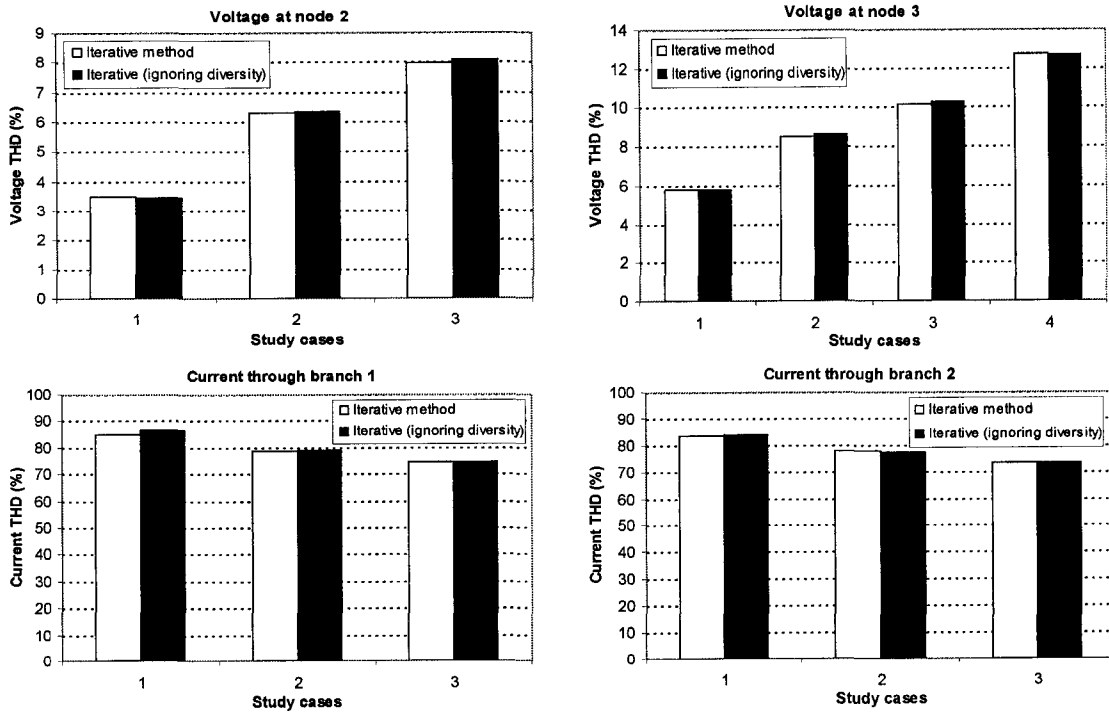
#### 4.4.3.2 Effect of Ignoring the Harmonic Currents Diversity

When the complete iterative process considers the adjustment of harmonic current magnitudes and phase angles, both attenuation and diversity effects are taken into account. In order to see how significant is the harmonics diversity introduced due to the voltage distortion and if it is possible to be overlooked, the modification of the harmonic current spectrum will be applied only on the magnitudes according to the voltage THD at each associated node using equation (4.7). As for the harmonic current phase angles, the adjustment is performed according to the traditional harmonic power flow method using equation (4.2). Following this approximation, the diversity among harmonic current phase angles is determined upon the fundamental voltage phase angle at harmonic source nodes as shown in equation (4.4) provided the harmonic sources have the same harmonic current spectrum. However, by using the complete iterative method, the harmonic current phase angles are adjusted such that their diversity is dependent on the fundamental voltage phase angles besides an additional component that takes into account the effect of the supply voltage waveform distortion as indicated in equation (4.9).

Figure 4.12 shows the calculated distortion level using the proposed iterative method with and without considering the harmonics diversity for both PC systems. It can be inferred that there is no noticeable difference between the results for the different study cases of the supply impedance. This is mainly due to the small diversity that the voltage waveform distortion introduced among the harmonic current phase angles of different PCs. Therefore, considering the attenuation effect for PC loads is the main issue and more vital in determining the resultant distortion level since the diversity effect is not pronounced.



PC system 1



PC system 2

Figure 4.12: Comparison of distortion results to show the impact of ignoring the harmonic currents diversity.

4.4.3.3 Sensitivity of Solution Convergence to System Distortion Level

The sensitivity study in this part provides an idea about the number of iterations required for solution convergence and how it is affected by system distortion level, i.e., with different sizes of the supply impedance. Figure 4.13 presents the convergence process of the voltage THD at different nodes for PC system 1. Results of iteration round “0” are the initial values obtained from the typical harmonic current spectrum. The distortion oscillates during the adjustment of the harmonic currents towards solution convergence. It can be inferred that with the increase in the initial distortion level, the oscillation range is wider and, therefore, more iterations are needed to reach the steady-state solution as shown for study case 4 of the supply impedance. The variation of the number of iterations required for convergence for different study cases is depicted in Figure 4.14 with and without considering the diversity effect. As the system distortion level becomes higher by increasing the supply impedance magnitude, the number of iterations increases significantly for both PC systems. It can also be noticed that the convergence is faster when the diversity effect is ignored.

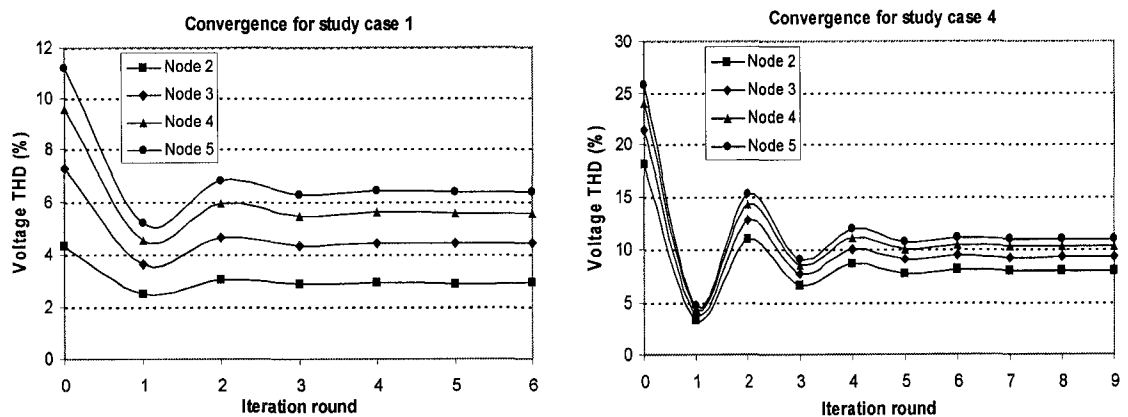


Figure 4.13: Convergence process of the voltage THD for different study cases of the supply impedance for PC system 1.

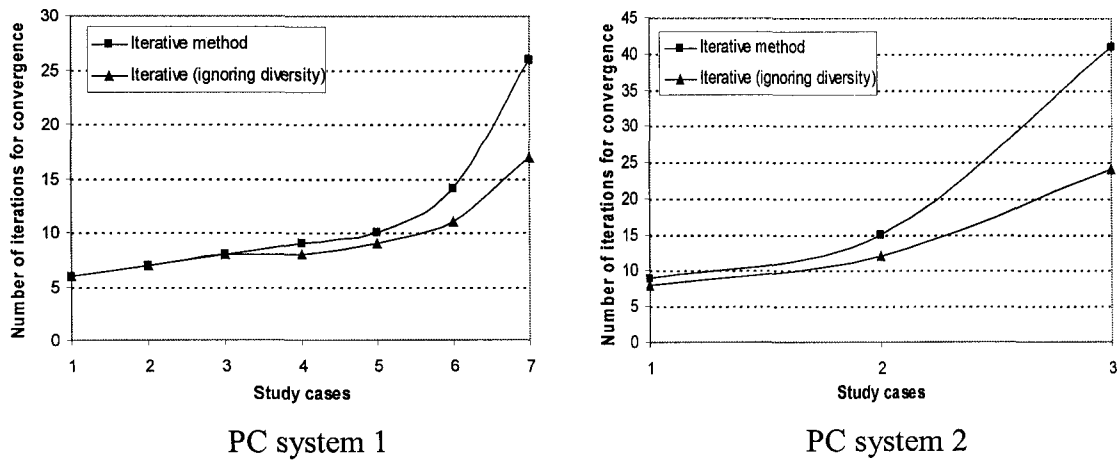


Figure 4.14: Variation of the number of iterations for convergence for different study cases of the supply impedance.

#### 4.4.3.4 A Simplified Way to Estimate System Distortion Level

A simplification is investigated to get directly a round figure or a range of the resultant distortion of system bus voltages or harmonic source currents without resorting to the complete iterative process. Results of PC systems 1 and 2 are considered for the first three and two study cases respectively of the supply impedance magnitude. Two multiplier factors are proposed for this purpose:

- 1) The first multiplier factor “ $MF_1$ ” is the ratio of the final converged solution ( $THD_{conv}$ ) to the summation of the typical distortion ( $THD_{typ}$ ) and the distortion obtained from the first iteration ( $THD_{itr-1}$ ). The typical distortion is that obtained using the traditional method with the typical harmonic current spectrum and considered as an initial value in the iterative process. Therefore, the “ $MF_1$ ” can be defined by:

$$MF_1 = \frac{THD_{conv}}{THD_{typ} + THD_{itr-1}} \quad (4.10)$$

- 2) The second multiplier factor “ $MF_2$ ” is the ratio of the final converged solution to the typical distortion as follows:

$$MF_2 = \frac{THD_{conv}}{THD_{typ}} \quad (4.11)$$

where the THD can be of system bus voltages or harmonic source currents. Figure 4.15 shows the relationships of the different multiplier factors with system voltage THD obtained using the traditional method and with typical current THD of different harmonic sources. It can be shown that the range of the first multiplier factor for voltage THD is between 0.35 and 0.55 and the range of the second multiplier factor is between 0.35 and 0.9. The same range of the two multiplier factors can be approximately applied to the harmonic source current THD. The following conclusions can be drawn:

- 1) The  $MF_1$  depends on the typical solution and the solution of the first iteration, which is obtained from the typical one using the developed harmonic source characteristic curves. The converged solution usually lies in the middle one third between the typical and first iteration values irrespective of the typical distortion level, therefore, the  $MF_1$  has limited variation with the change of the typical voltage and current THD values.
- 2) The  $MF_2$  depends on the typical distortion value, which has no relation with the harmonic source characteristics and it does not have a direct relation with the converged solution. Therefore, the  $MF_2$  values are more scattered with noticeable discrepancy according to the typical distortion level.

Hence, a simplification using the  $MF_1$  is better to be selected to get an approximate figure of the distortion level. This can be done using the traditional harmonic analysis programs to get the initial distortion values utilizing the typical harmonic source current spectrum. Besides, the results for only one iteration can be obtained by using the attenuation curves in Figure 3.23 without the need to apply the complete iterative process of the proposed method. In this case, a value of 0.5 for the first multiplier factor can be considered to give conservative results.

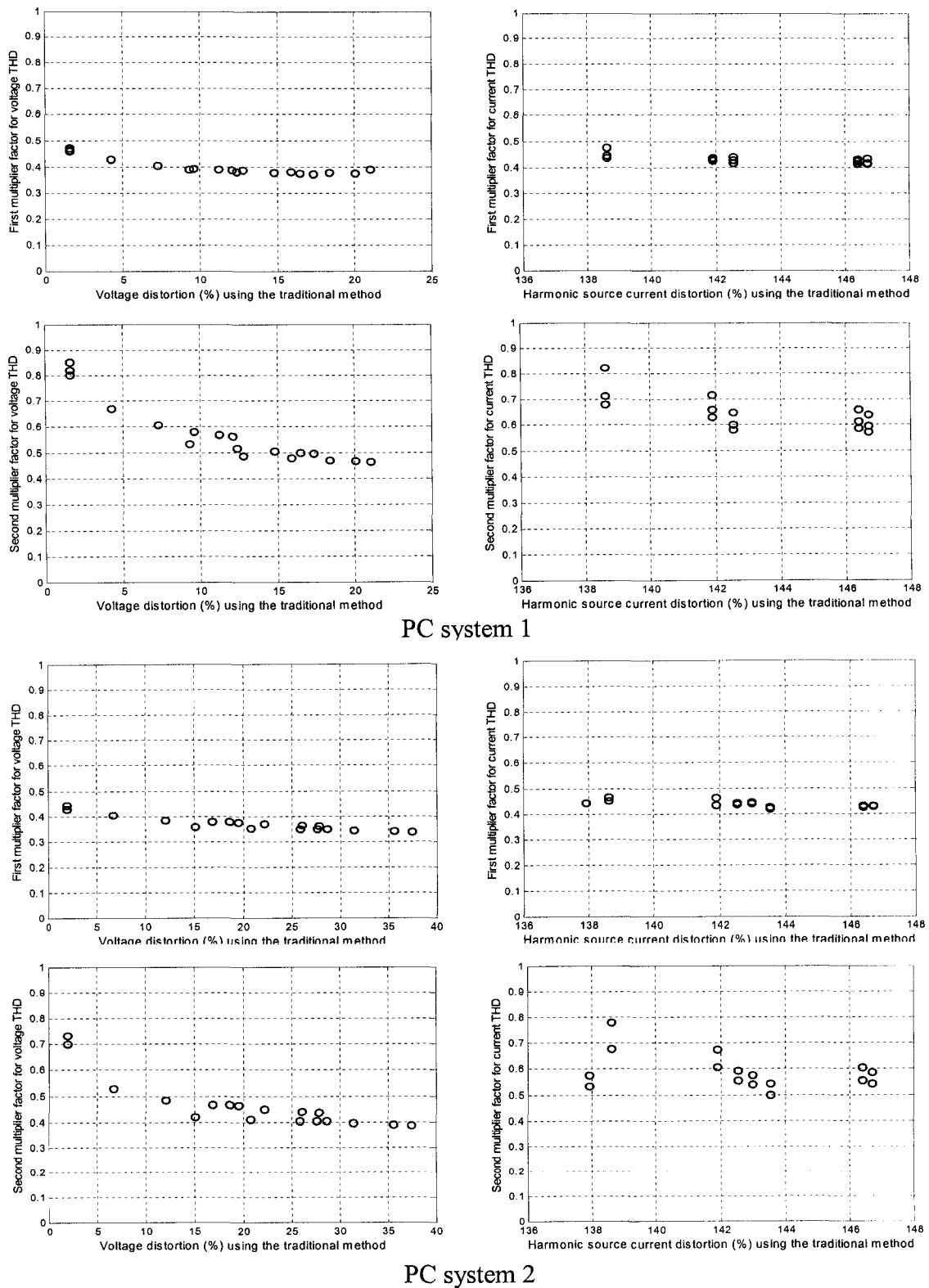


Figure 4.15: Multiplier factors for voltage and current THD.

## 4.5 Summary and Conclusions

Conventionally, the nondistorted input voltage to the harmonic sources is assumed when conducting harmonic analysis. Therefore, the ideal current source model is sufficient for the representation of the harmonic source. However, with the distributed nature of harmonic sources, the system voltage distortion may arise. Consequently, the harmonic current spectrum will vary and more advanced models of harmonic sources are necessary for accurate harmonic penetration studies. The traditional frequency domain harmonic analysis programs with a one-step computation using the typical current spectrum can not deal successfully with systems of considerable distortion level since they do not have the capability to consider the harmonics attenuation and diversity.

In Chapter 3, the conducted extensive measurements for a PC load revealed that the supply voltage THD can fairly characterize the harmonic magnitudes and phase angles of the current spectrum. The obtained harmonic source characteristics paved the way to propose an iterative frequency domain based method for harmonic analysis to predict the distortion level in the presence of distributed harmonic sources. The developed method takes into account the interaction between the harmonic sources and the system voltage. Hence, it overcomes the limitations of the fixed current injection method used by the traditional harmonic analysis programs.

Official electrical systems with a considerable number of PCs are example systems with distributed harmonic sources. The proposed method was verified by conducting measurements for PC systems. Reliable results could be obtained showing the effectiveness of the proposed method in handling the attenuation and diversity issues. Sensitivity studies were performed. It was concluded that the attenuation is the main factor contributing to distortion reduction since the diversity effect is not that significant for the PC systems. Multiplier factors were investigated to provide an approximate way to get a range of system distortion level using the traditional harmonic analysis programs for only one iteration to modify the current spectrum. This can be done by utilizing the attenuation factor curves without turning to the complete iterative process.



# Chapter 5

## Harmonics Attenuation and Diversity for Three-Phase Power Electronic Loads

Chapter 3 dealt with the characterization of single-phase power electronic loads employing a capacitor filtered-diode bridge rectifier. This chapter extends the work to include three-phase power electronic loads where the rectifying topology is similar to that of single-phase rectifiers but with a front end for connection of three phases. The application of adjustable speed drives (ASDs) in industrial distribution systems is discussed. ASD modeling and harmonic characteristics are presented. The variation of the ASD harmonic currents with the supply voltage distortion is investigated. Choosing the voltage total harmonic distortion (THD) to characterize the ASD current spectrum is justified. The findings will serve to conduct harmonic analysis while considering the attenuation and diversity of harmonic currents injected from distributed ASD loads as will be shown in the next chapter.

### 5.1 Introduction

The load history of the industrial plants points to the fact that ASDs became highly proliferated in industrial facilities and they are going to be the most dominant load in the near future [54,55]. The interaction of harmonic currents generated by ASDs with system impedance versus frequency results in the threat of potential distortion level in a distribution system due to the installation of ASD loads [56]. Thus, there is an impending need to quantify the distortion in voltage and current waveforms in such a system.

One difficulty on evaluating harmonic voltages and currents throughout a distribution system is the need for accurate assessment of the injected harmonic current spectra from the distributed ASD loads. These loads not only have the potential to produce harmonic distortion, but the amount varies with the variation of supply voltage distortion and loading level. A crucial point is to address how the ASD harmonic current characteristics differ under these variations. This chapter deals with the variation of the supply voltage distortion for a constant drive load, while Chapter 7 will present the case when the loading level is considered varying.

Simulation studies are conducted to investigate the behavior of harmonic currents produced from an ASD employing a full-wave diode bridge rectifier under different supply voltage distortion levels. The change of the voltage distortion is produced by two ways. The first way is by changing the supply impedance and the second way is by connecting other ASD loads to the common point to create different background voltage distortions. The harmonic source characteristic is compared with system characteristic to justify the choice of the voltage THD as the proper voltage index that should be used to address the current spectrum of the ASD as a three-phase harmonic source. This assures the conclusion drawn in Chapter 3 for a single-phase harmonic source case. Accordingly, ASD modeling would be achieved taking into account the interaction with the system voltage when conducting harmonic analysis for distribution systems with distributed ASD loads.

## **5.2 Application of ASDs in Power Distribution Systems**

ASD is becoming a significant load component for power distribution systems. It drives a process, whether it is fluid, gas, material or air with a variable speed induction motor. Modern ASDs employ power electronic devices to generate the variable frequency power supply for AC motor speed control. Harmonics are produced in the process. Assessment and mitigation of the ASD harmonic effects on supply systems have become an important aspect of power quality management [57].

At the planning stage of the operation of ASDs, it is necessary to assess the level of harmonic current flow into the public electricity supply to ensure that no undue interference is experienced by other electricity consumers. If the harmonic distortion is excessive, installation of harmonic filters may be required [42]. It is unlikely that one ASD would draw enough harmonic currents to have pronounced effect on the power distribution system. But, if many ASD loads are connected to a specific distribution feeder, it seems reasonable to expect that harmonics drawn by these loads may cause significant harmonic pollution.

### **5.2.1 Advantages of using ASDs**

The application of ASDs has recognized advantages in industrial facilities. The main benefit is in the economics and energy reduction savings which is typically in the 20% to 50% range over that of conventional motor electromechanical drive applications. Other typical benefits include controllability to provide smooth ramp-up and ramp-down acceleration transitions, optimized mechanical load characteristics, equipment reliability, reduced mechanical related maintenance, increased product qualities, reduced audible noise levels, and reduced physical space requirements [5,6]. On the other side, the interface of the ASDs with the distribution system has a disadvantage of injecting harmonic currents into the system, which can have detrimental effects on the system elements [58].

### **5.2.2 ASDs Structure and Classification**

An ASD consists of three key components, a rectifier, an inverter, and a DC circuit that connects the rectifier and the inverter as shown in Figure 5.1. The rectifier converts the supply AC voltage into a DC voltage. The DC circuit is called the DC link and through which the DC voltage is filtered. The inverter converts the DC voltage to an adjustable frequency, adjustable AC voltage for AC motor speed control. The rectifier (converter) section of an ASD, called the front end, is typically a full-wave bridge rectifier type and

is the part that generates harmonic currents into the supply system through the switching process of its power electronic components [57].

ASDs are normally classified into different types according to the inverter design. The three most common types are the pulse-width modulated inverter (PWM) type, the voltage source inverter (VSI) type, and the current source inverter (CSI) type. For the PWM and VSI types, the DC link mainly consists of a large shunt capacitor, whereas for the CSI type, the DC link is made up of a large series inductor. For VSI and CSI types, the rectifier DC voltage output must be adjustable in order to obtain an adjustable AC voltage at the motor side. This is normally achieved by using thyristor rectifiers. The firing angle of the thyristors is varied to provide controlled voltage to the DC link and consequently the inverter will have controlled AC output voltage supplied to the motor. The control of the motor frequency is performed through the inverter [26].

On the other hand, the PWM type is used with a diode bridge rectifier that puts a constant amplitude rectifier AC voltage on the DC link, which has a DC link capacitor. The frequency and the voltage magnitude supplied to the AC motor are adjusted through the inverter, therefore, there is no need to control the rectifier output. Among the three types of ASDs, the PWM type is the most common one in the low horse power applications and is used for rating up to 1500 HP. Most CSI type is applied for large horse power AC motor drives (1500HP and above) [57].

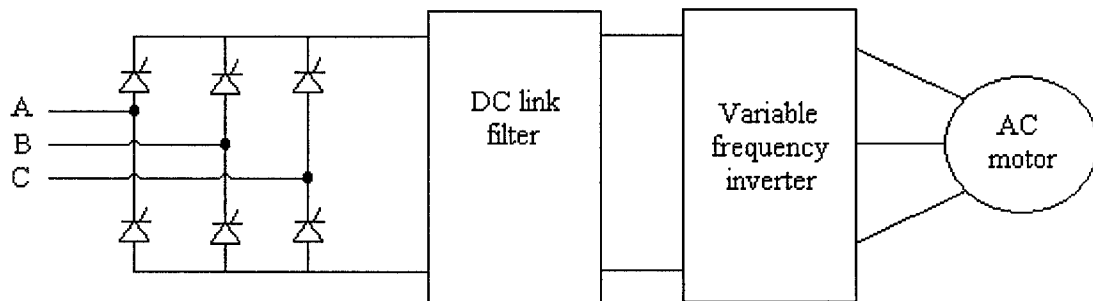


Figure 5.1: Basic structure of an adjustable speed drive.

### 5.3 ASD Modeling and Harmonic Characteristics

Computer simulation is one of the effective ways to assess the harmonic effects of ASDs. The usefulness of simulation techniques relies heavily on adequate models of the drive and a good understanding of the sensitivity of the models with respect to the data available for model construction. In spite of its importance, research on the modeling of ASDs for harmonic analysis is limited [57]. It has been commonly assumed that the ASD can be modeled as ideal harmonic current sources, which inject harmonic currents into the AC power system. This assumption is reasonable only for cases when the supply voltage waveform exhibits little or no distortion [53]. The source magnitudes are either calculated as the  $1/h$ -th of the fundamental frequency current for the  $h$ -th harmonic or measured from a particular drive operating condition [57,59].

#### 5.3.1 An Equivalent Circuit Model for ASD

Harmonic currents injected by an ASD load are generated due to mainly the electronic switching process of the converter operation. The inverter can introduce additional ripples into the DC link current. These ripples in turn can penetrate into the supply system side. The extent and the frequency of inverter-caused ripples are largely a function of inverter design and motor parameters. An ASD can therefore be represented with a generic three-phase bridge converter circuit as shown in Figure 5.2. A significant feature of this circuit is that the inverter and the motor are collectively modeled as a direct current source [57].

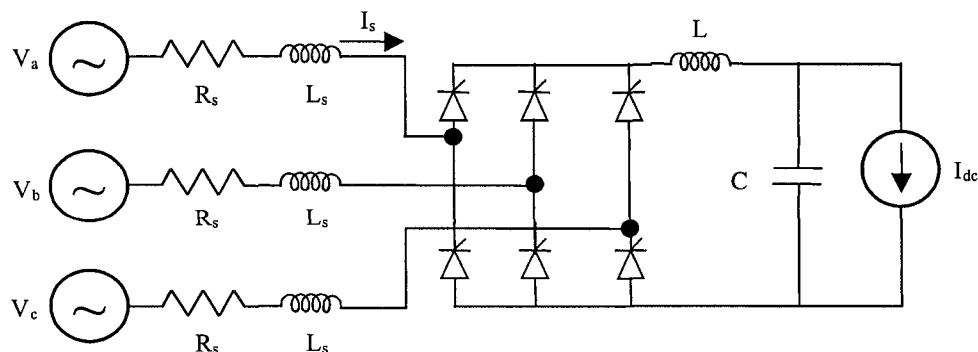


Figure 5.2: Generic converter circuit for ASD.

Theoretically speaking, the inverter and motor should be represented as a harmonic current source. The magnitudes and phase angles should be determined from the inverter design and motor operating conditions. Attempts were made to develop a procedure that automatically determines the harmonic current source. However, the complexity and variety of the inverters make the work extremely difficult. Extensive sensitivity studies performed in [57] concluded that there is a little need to model the current source as a harmonic source. Namely, the inverter harmonics are negligible as seen from the converter AC side. This is because, in the case of PWM and VSI type ASDs, the inverter harmonics are largely bypassed by the DC link capacitor before they can penetrate into the supply system side. In the case of CSI type ASD, the series inductor serves as a large impedance to block inverter harmonics from ever getting into the converter. The direct current into inverter can be estimated from the motor load as:

$$I_{dc} = \frac{\pi}{3\sqrt{2}} \left[ \frac{P}{V_{L-L} \cos \alpha} \right] \quad (5.1)$$

where  $P$  is the motor load including losses,  $V_{L-L}$  is the RMS line to line voltage of the supply system, and  $\alpha$  is the firing angle in case of using a thyristor bridge rectifier.

### 5.3.2 ASD Input Harmonic Current Characteristics

The characteristics of the input current for ASDs depend on the drive type, drive loading, and the characteristics of the system supplying the drive. The harmonic distortion in these currents can vary over a wide range. However, it is possible to identify two basic waveform types produced by three-phase full-wave converters for harmonic analysis purposes [56].

#### Type 1: High Distortion Current Waveform

A typical high distortion current waveform and the associated harmonic spectrum are shown in Figure 5.3. This is the characteristic of virtually all ASDs of VSI or PWM types where the DC link mainly consists of a large shunt capacitor. The shunt capacitor causes

large ripples in the DC link current in the form of two pulses in each half cycle. These drive types usually do not have additional choke inductance for current smoothing and, therefore, the input current THD is high, for instance, the total harmonic distortion for the selected waveform is 78.5%.

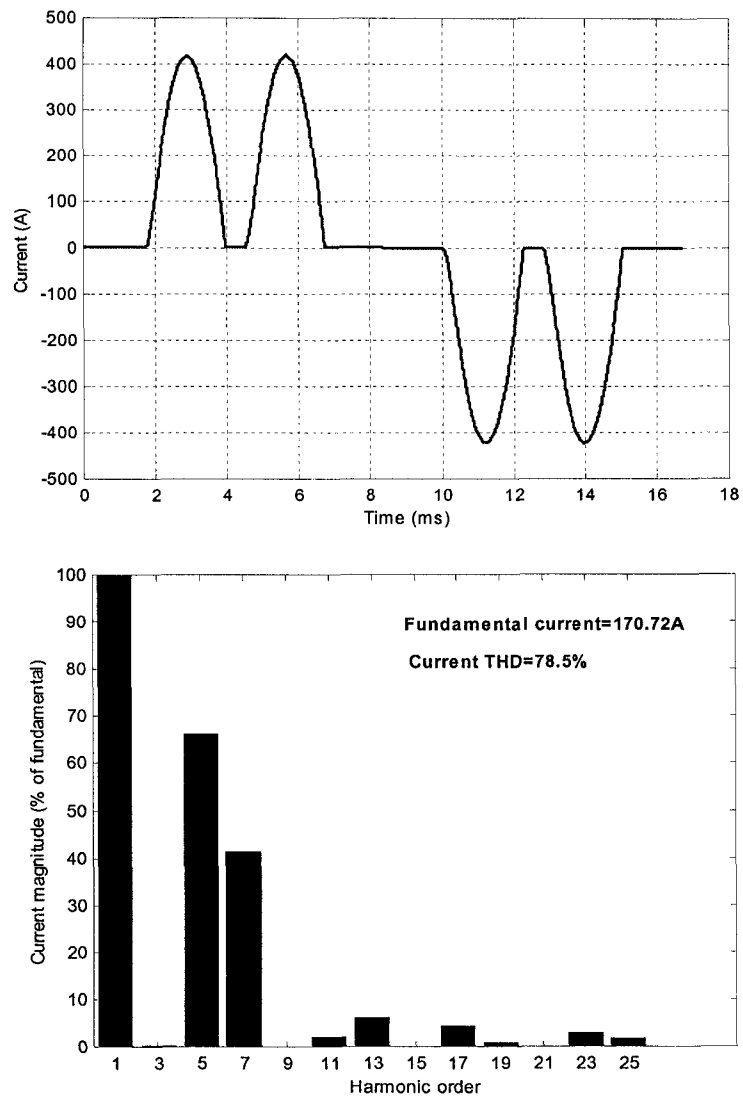


Figure 5.3: ASD high current distortion waveform and the harmonic spectrum.

Type 2: Normal Distortion Current Waveform

A typical normal distortion current waveform and the associated harmonic spectrum are depicted in Figure 5.4. The waveform has two humps in each half cycle. This current waveform represents DC drives, large AC drives with current source inverters, and smaller AC drives of VSI or PWM types and added inductance for current smoothing. The presented current waveform has a distortion level of 32.3%.

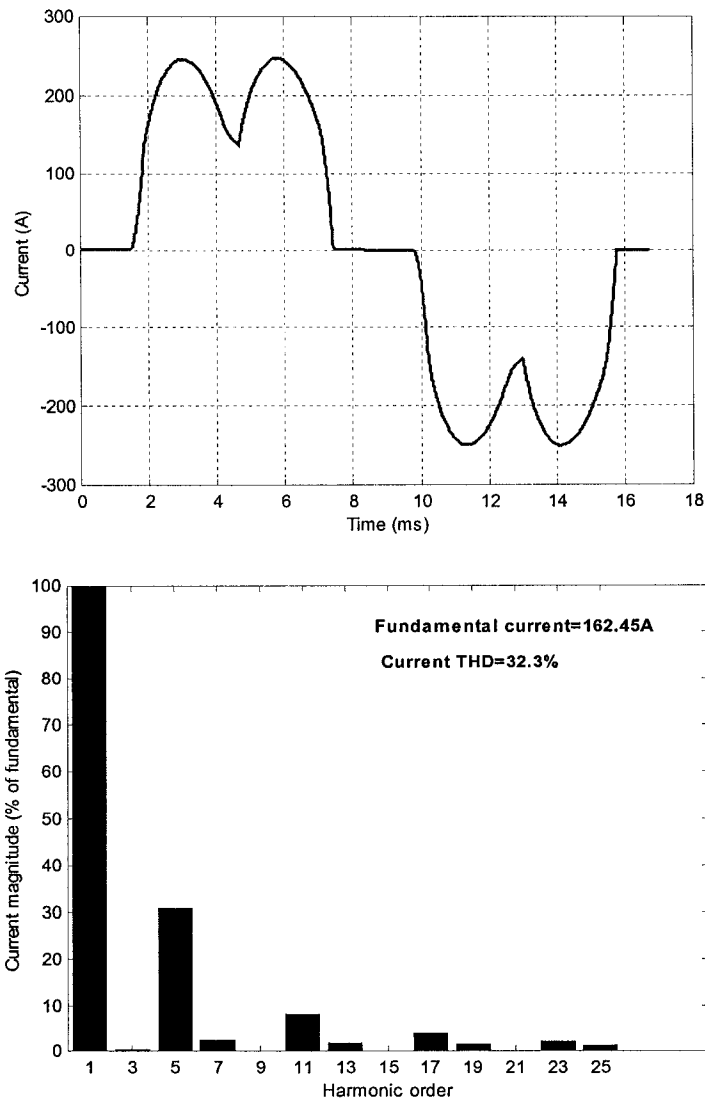


Figure 5.4: ASD normal current distortion waveform and the harmonic spectrum.



Generally, the current flows through the rectifier diodes for the time period when the input voltage exceeds the DC link voltage. Peak input current into the rectifier is limited by the line impedance feeding the circuit and by the DC link inductance in the drive. As a result, inverters of mainly capacitor in the DC link will have a current waveform of narrowed width and high peak pulses as shown in Figure 5.3. Figure 5.4. illustrates the significant reduction in the current distortion that can be obtained for PWM type ASDs just by adding a choke inductance in the DC link of the drive. The same reduction benefit can be obtained by adding the inductance at the input AC line [56,59]. Representation of the DC link is essential for the correct simulation of ASDs and can affect significantly the ASD current waveforms and the magnitude of the harmonic contents.

Both waveform types produce harmonic currents of orders determined by:

$$h = 6k \pm 1, \quad k = 1, 2, 3, \dots \quad (5.2)$$

This shows that the spectrum mainly includes odd harmonics excluding the triplen harmonics (multiples of three). The use of equation (5.2) results in harmonic orders or multiples of the fundamental frequency of the 5th, 7th, 11th, 13th, etc., which corresponds to 300, 420, 660 and 780 Hz respectively with 60 Hz fundamental frequency.

#### 5.4 Characterization of Three-Phase Harmonic Sources

Harmonic studies were primarily dealing with industrial distribution systems having one or several ASDs [15,56,60,61], which are the most common three-phase harmonic sources. But now with the continuous use of power electronic devices, distribution systems start to employ a large number of these loads. A typical fully-loaded ASD current spectrum was adopted to model the drives as ideal harmonic current sources. The traditional method for harmonic analysis assumes that the supply voltage distortion has no impact on the current spectrum and the magnitudes and phase angles of the harmonic current are automatically established using the typical spectrum according to the fundamental frequency load flow results.

Information about the harmonic currents drawn by ASDs is the key to any harmonic analysis. This should take into account the interaction between the system and the drive itself to be able to consider the harmonics attenuation and diversity. Figure 5.5 depicts the harmonic current magnitudes in percent of the fundamental component and the harmonic current phase angles with respect to the corresponding fundamental component phase angle of the supply voltage for an ASD load under two different distortion levels of the supply voltage. It is clear that specifying the typical harmonic current spectrum, obtained with little voltage distortion, would exhibit inaccuracy and can not be adequate with ASD loads distributed across the entire distribution systems. Such systems are expected to have considerable voltage distortion levels and, therefore, the harmonics attenuation and diversity can be pronounced due to the change of harmonic currents.

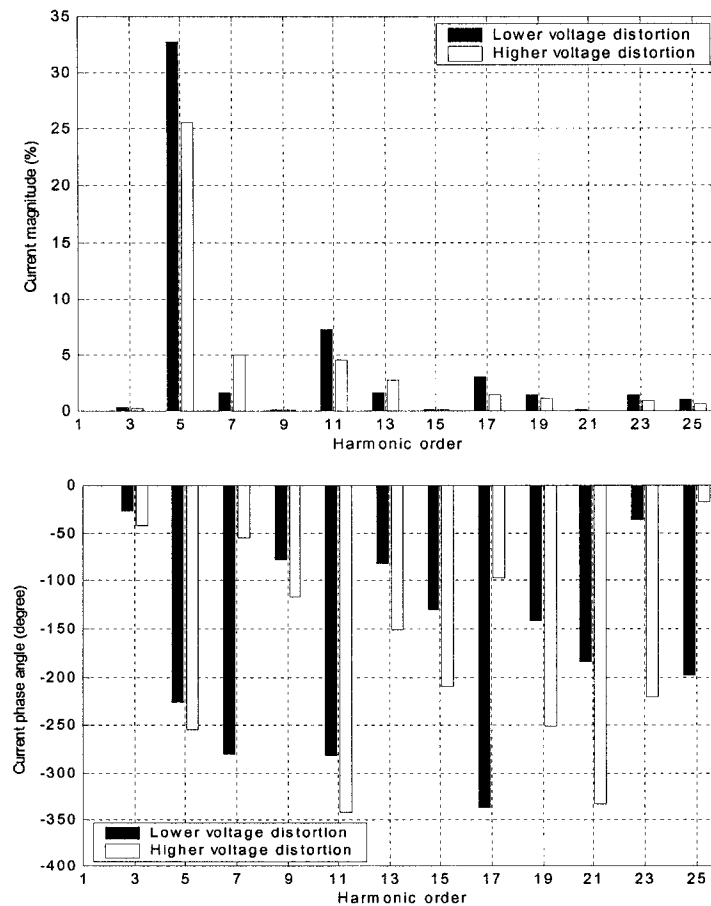


Figure 5.5: Harmonic current spectra for an ASD load under different supply voltage distortion levels.

From the extensive measurements conducted to characterize the harmonic current magnitudes and phase angles with the supply voltage waveform for a PC load, it is envisioned that the same procedure can be extended and applied to an ASD load. ASD harmonic current characteristics will be investigated under different distorted voltage waveforms to find the appropriate voltage parameter that can address the harmonic current spectrum. Consequently, the effect of the supply voltage waveform on the attenuation and diversity of the generated harmonic currents can be taken into consideration.

#### **5.4.1 Effects of the Variation of Supply Impedance and Background Voltage Distortion**

The interaction between the ASD feeding voltage waveform and the harmonic currents is investigated by performing simulation studies on an ASD load using PSCAD/EMTDC software program with its built-in libraries for the ASD model representation. PSCAD is a powerful graphical user interface that integrates with EMTDC, a general-purpose time domain program, for simulating power system transients and controls. Together they provide a fast, flexible, and accurate solution for the simulation of virtually any electrical equipment or system. The simulation results are manipulated by MATLAB program for harmonic source characterization.

The voltage waveform at the ASD terminals is changed under two cases. In the first case, the supply impedance magnitude is increased in many steps, which affects the distortion of the voltage waveform. In the second case, the background voltage distortion is changed by connecting other ASDs of different ratings and circuit parameters in sequence to the common point of the concerned ASD. In both cases, the drawn harmonic current magnitudes and phase angles are changed. Simulation studies are carried out for 150 HP ASD with a diode bridge rectifier at the front end and a shunt capacitor in the DC link in addition to an inductance so that the current waveform belongs to the normal distortion type. The voltage and current waveforms are obtained for analysis and exploring their interaction.

Figure 5.6 shows a comparison between the variation of the drawn current THD with both voltage THD and voltage crest factor (CF) due to the variation of supply impedance ( $Z_{change}$ ) and the variation of background voltage distortion ( $V_{background}$ ). The impedance, which is dominantly inductive, is changed from 0.015 ohm to 0.36 ohm corresponding to a voltage drop variation from 0.85% to 20.4%. The following conclusions can be drawn:

- 1) There is no noticeable difference in the results for the two cases and similar characteristics are obtained.
- 2) With the decrease in the current THD values till 25% (12% voltage THD), the current THD and voltage CF have negative correlation where the reduction in the current THD is associated with more peaked voltage waveform in the form of higher CF. This trend is reversed with the continuous decrease in the current THD. Therefore, the voltage CF does not have a fixed influence on the harmonic current distortion for ASD loads.
- 3) The obtained non-steady relationship between the ASD current THD and voltage CF is opposite to the constant trend found in the case of PC loads in which the voltage waveform always gets flattened (lower CF) with the decrease in the current THD. On the other side, the ASD current THD and voltage THD have negative correlation and similar trend to that obtained for the PC load and there is a steady relationship between both parameters.

In Chapter 3, an investigation was conducted to choose the voltage THD as the proper indicator of the PC harmonic current magnitudes and phase angles. As a result, harmonic analysis could be performed in Chapter 4 leading to a reliable and converged solution while taking into account the harmonics attenuation and diversity. The same investigation will be conducted in this chapter clarifying the justification on choosing the proper voltage index for the characterization of ASD harmonic currents.

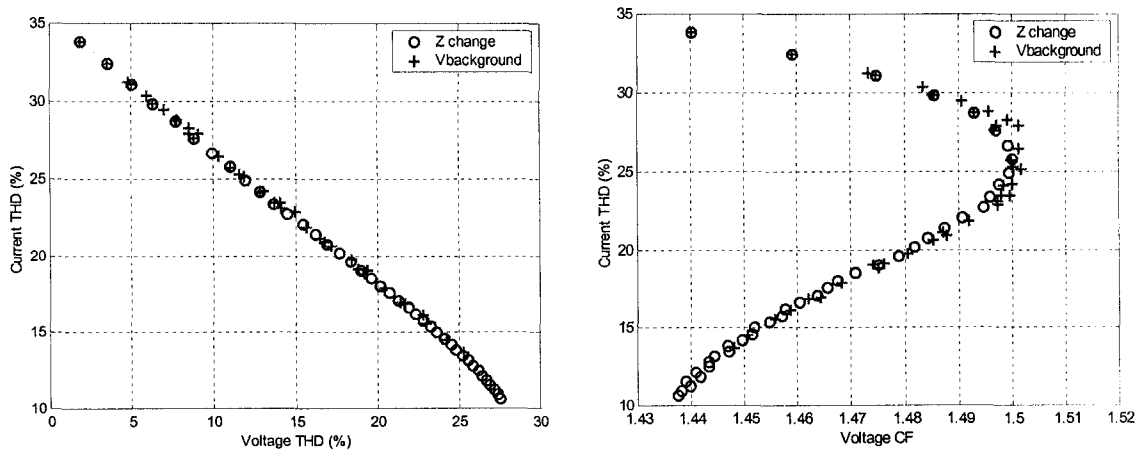


Figure 5.6: Variation of ASD current THD with voltage THD and CF due to the change of supply impedance and background voltage distortion.

Figure 5.7 presents the variation of the individual harmonic current magnitudes, in percent of the fundamental component, with the voltage THD due to the change of supply impedance magnitude and background voltage distortion. The dominant harmonic current magnitudes are attenuated with the increase in the voltage THD. Hence, the current THD is reduced as shown in Figure 5.6. Figure 5.8 depicts the corresponding variation of the individual harmonic current phase angles with respect to the fundamental voltage phase angle. It can be shown that the current of different harmonic orders is subjected to more delay with the increase in the voltage distortion. This clarifies how system buses having different voltage distortion levels could contribute to the phase angle diversity among distributed harmonic sources and consequently lower distortion level can be attained.

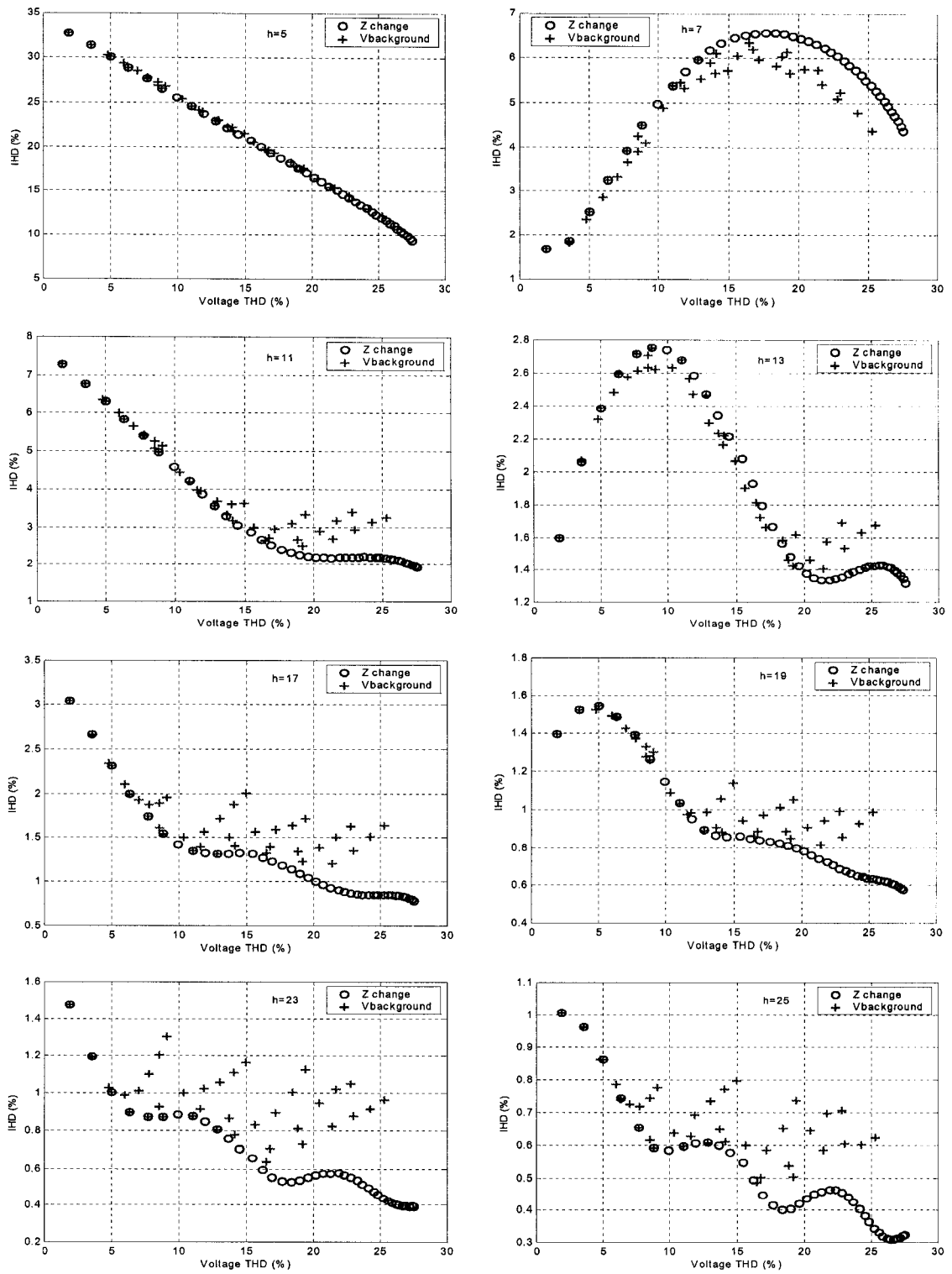


Figure 5.7: Variation of ASD individual harmonic current magnitudes with voltage THD due to the change of supply impedance and background voltage distortion.

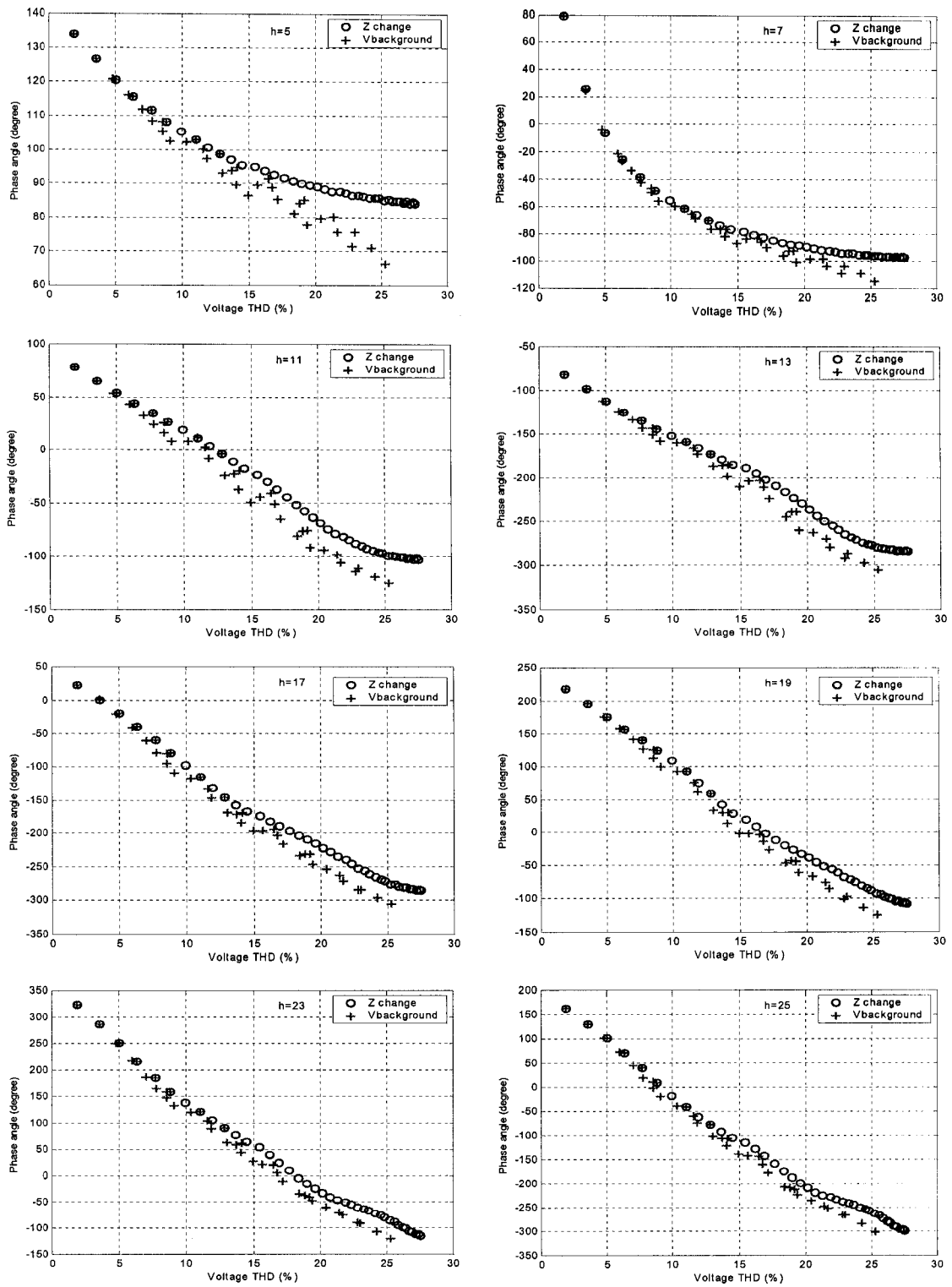


Figure 5.8: Variation of ASD individual harmonic current phase angles with voltage THD due to the change of supply impedance and background voltage distortion.

The simulation results of the harmonic currents obtained with the variation of the supply impedance magnitude and background voltage distortion are comparable. They can collectively provide reliable relationships to reflect the impact of voltage waveform on the current spectrum and to correlate the individual harmonic current magnitudes and phase angles with the voltage THD. These relationships account for the attenuation and diversity of harmonic currents and should be considered in harmonic power flow programs to modify the harmonic current spectra injected from ASD loads under the influence of the distorted voltage.

#### 5.4.2 Results Justification

Figure 5.9 illustrates the individual harmonic voltage component waveforms and the accumulative ones when the supply impedance is increased from  $Z_1$  ( $j0.015$  ohm) to  $Z_2$  ( $j0.06$  ohm). Both voltage THD and CF are increased and the current THD is decreased from 33.8% to 29.8%. Figure 5.10 presents the waveforms when the background voltage distortion is increased from  $V_{bg1}$  (3.511%) to  $V_{bg2}$  (8.769%). The voltage CF is also increased and the current THD is decreased from 32.5% to 27.6%.

It can be seen how the harmonic voltage phase angles of the dominant components (5th and 11th) are obtained such that their negative peaks coincide with the negative peak of the fundamental voltage waveform. Therefore, with the increases in the harmonic voltage magnitudes, the waveform CF becomes higher. This is in contrast to the case of PC loads where the positive peaks of the dominant harmonic voltage components coincide with the negative peak of the fundamental component to have more flat voltage waveform and lower CF. It is worth mentioning that as current THD values decreases below 25%, the voltage CF starts to reduce as in the PC load, but the CF values are still higher than that of a pure sinusoidal waveform (1.414).



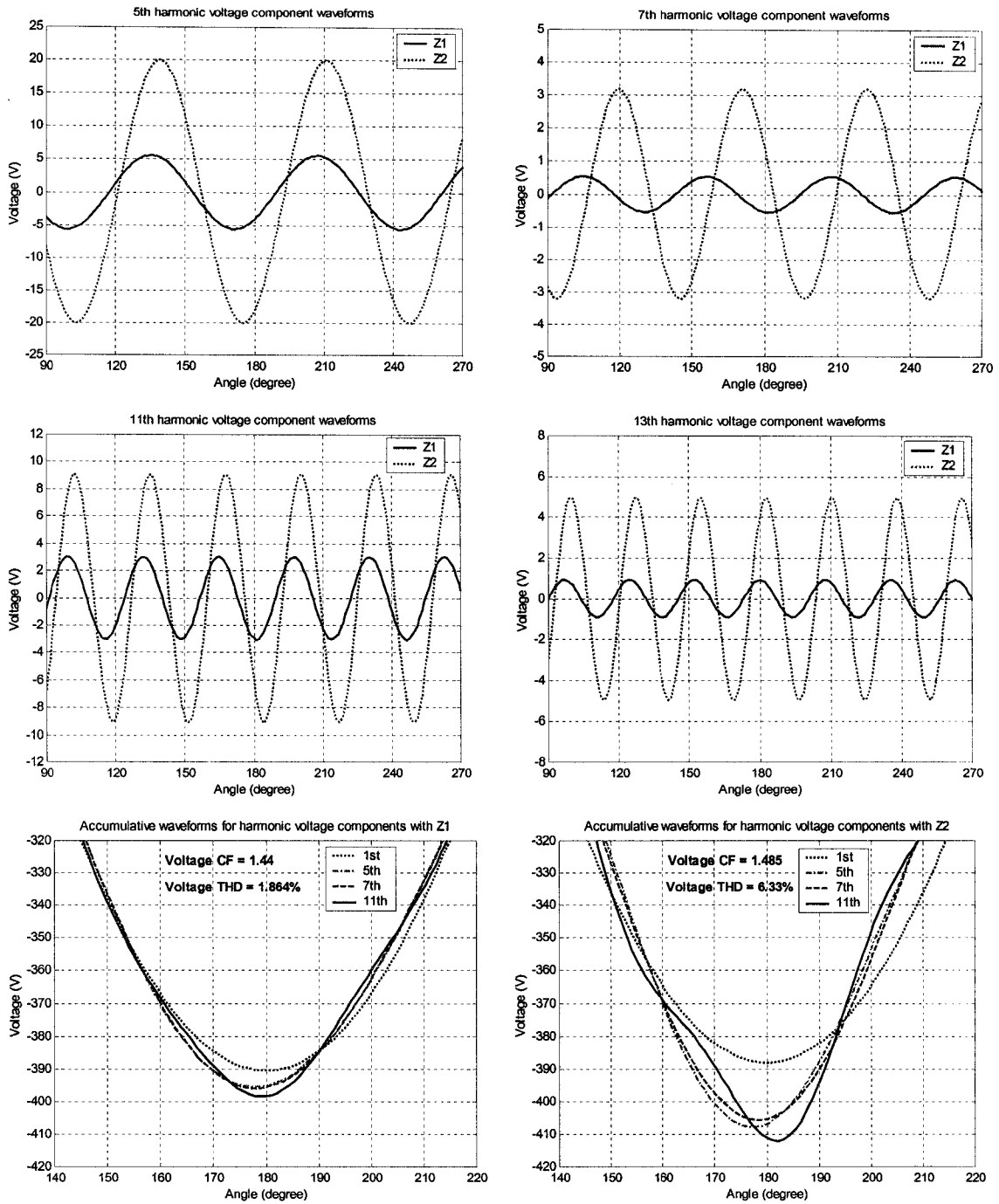


Figure 5.9: Variation of different harmonic voltage components and accumulative waveforms with supply impedance.

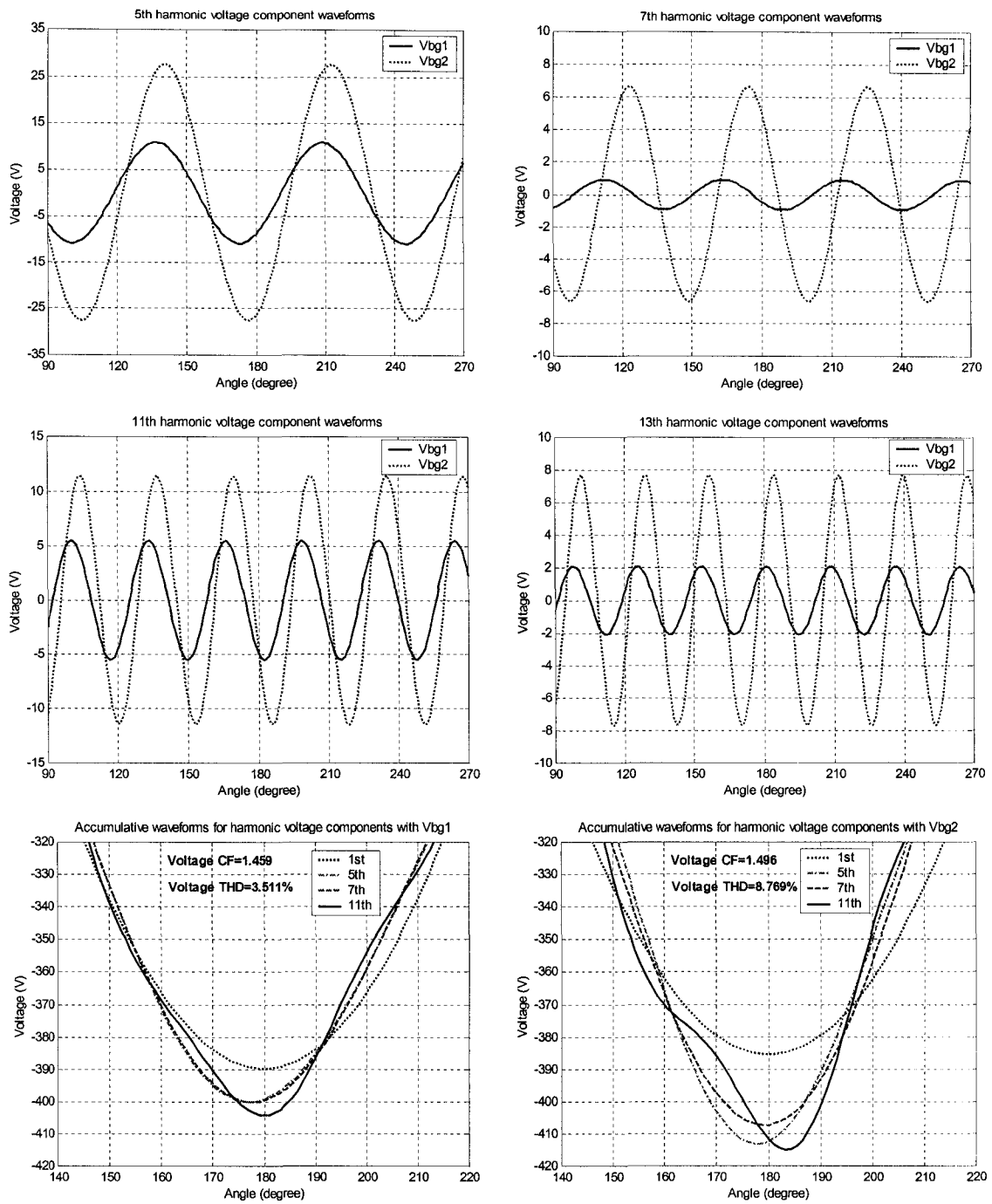


Figure 5.10: Variation of different harmonic voltage components and accumulative waveforms with background voltage distortion.

### 5.4.3 Justification of the Voltage THD Choice on Characterizing the Harmonic Source Current Spectrum for Harmonic Analysis

As mentioned before in Chapter 3, the main goal of the characterization of harmonic source currents is to utilize the obtained relationships for harmonic analysis enhancement by taking into account the harmonics attenuation and diversity in the presence of distributed harmonic sources. In order to justify the choice of the voltage THD index for this purpose, the response of system voltage waveform to the ASD current distortion is investigated. This is accomplished by applying 10 ASD current waveforms of the same load but with different distortion levels to an equivalent system as shown in Figure 5.11. The traditional harmonic analysis is performed for each case to get the voltage at the ASD bus in order to determine the system characteristic curves of the current THD and both voltage THD and voltage CF. This is repeated for different magnitudes of the dominantly inductive supply impedance where  $Z_3 > Z_2 > Z_1$ . The corresponding voltage drops are 2.36, 3.15, and 4% respectively with increasing the impedance magnitude.

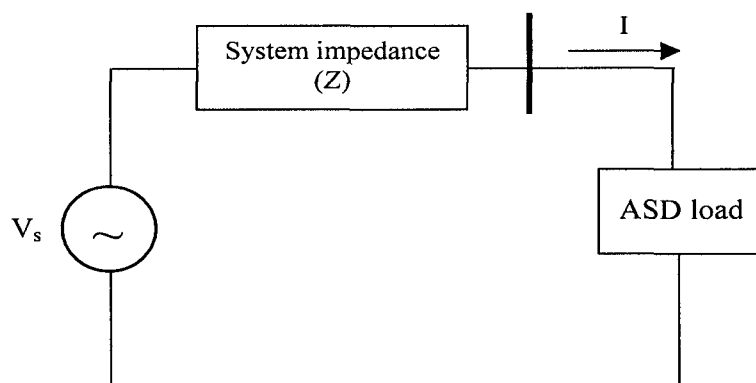


Figure 5.11: Equivalent system to investigate the voltage response to the ASD current distortion.

Figure 5.12 presents the obtained system voltage characteristics for voltage THD and voltage CF in addition to the harmonic source characteristics. Figure 5.13 clarifies the application of the proposed iterative method described in the previous chapter to the system characteristic with supply impedance  $Z_1$ . It can be noticed that, although the system and harmonic source characteristic curves of the current THD and voltage CF has

an intersection, this solution point is unstable and the iteration will not converge whatever is the initial current THD value. The reason is that the slope of the system characteristic is less than that of the harmonic source characteristic and, therefore, the criterion required for convergence is not satisfied. Moreover, the curves may not have any intersection at higher voltage distortion level, i.e., with higher impedance magnitude as shown in Figure 5.12. Therefore, the use of the voltage CF can not lead to solution convergence. As for the voltage THD, the same conclusions drawn with the PC load can be applied in this case. The nature of the system and harmonic source characteristic curves always makes them have an intersection point, which is stable and offers a converged solution.

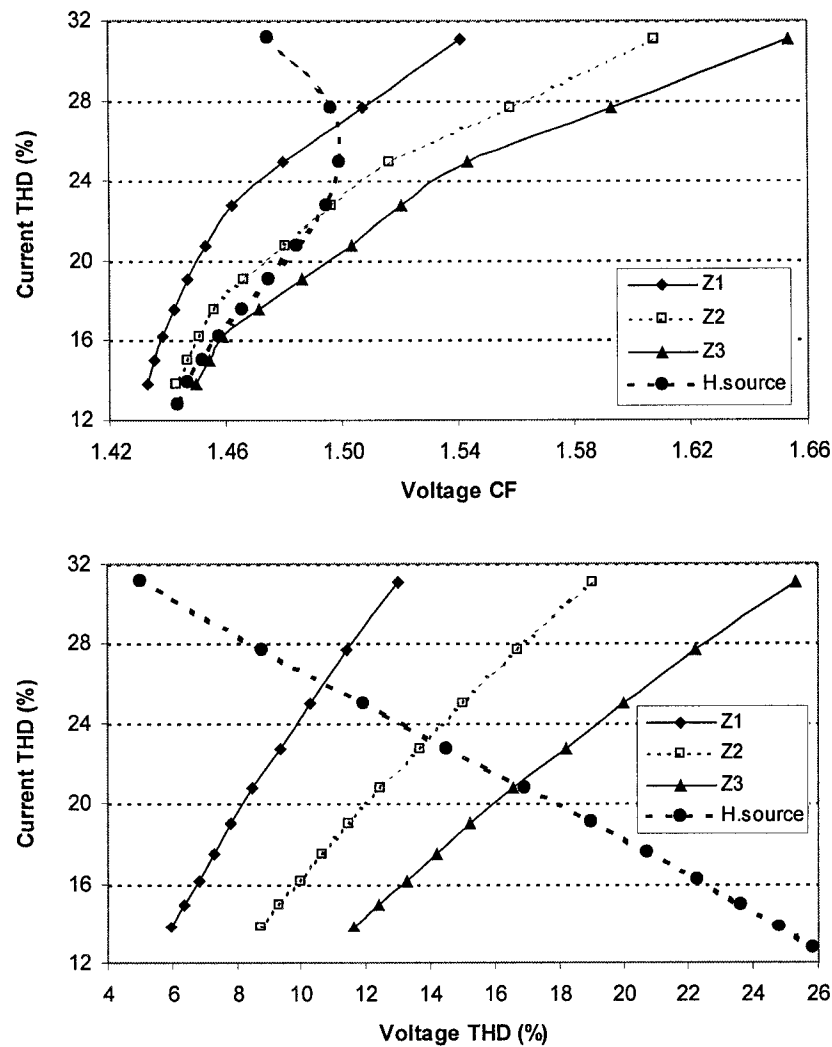


Figure 5.12: System voltage response to the ASD current distortion.

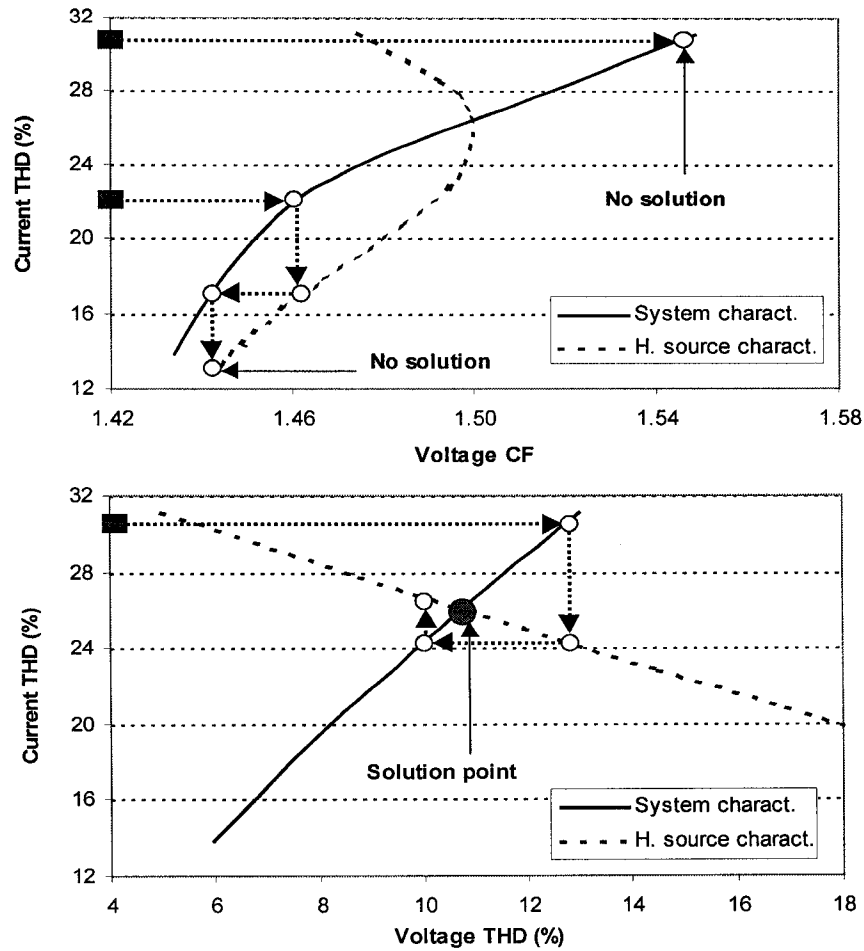


Figure 5.13: Iterative process with voltage CF and THD indices.

The same procedure followed in Chapter 3 to explain the peaked voltage waveform of system characteristic with increasing the harmonic source current THD is followed here with the ASD load. The instantaneous steady-state ASD voltage waveform is obtained by subtracting the voltage drop across the supply impedance from the sinusoidal supply voltage. A sample of the tried ASD current waveforms and the resultant different voltage waveforms are shown in Figure 5.14. With increasing the current waveform distortion, the depth of the two humps is increased. Hence, the negative slope of the current during the waveform valley is higher. This part lies so close to the instant of the supply voltage peak. By subtracting the system impedance voltage drop, which is dependent on the current slope, the ASD voltage would have higher CF and more distorted waveform with increasing the ASD current distortion.

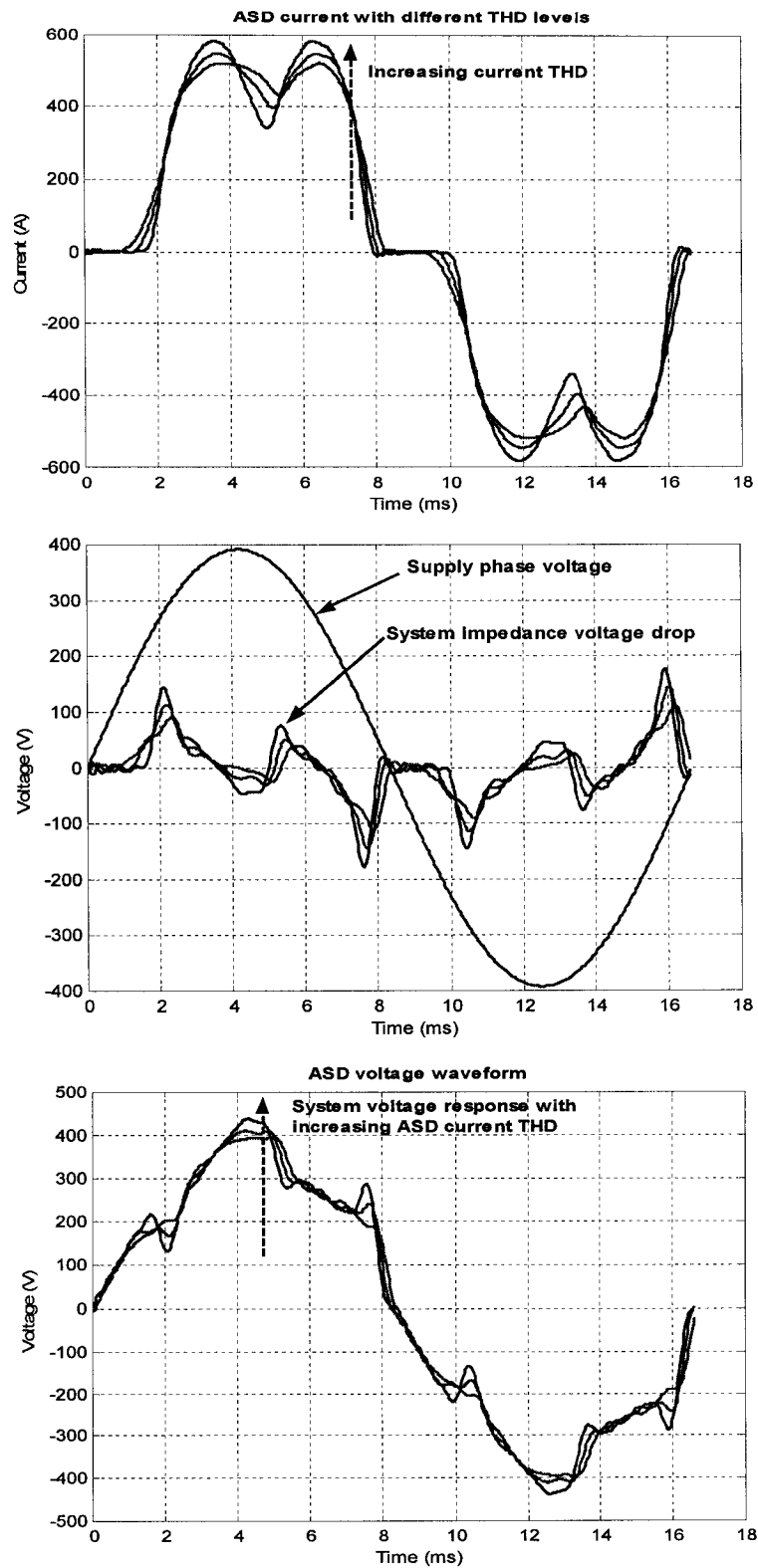


Figure 5.14: Justification of system voltage response to the ASD current distortion.

#### 5.4.4 Attenuation Factor for ASD Loads Based on the Supply Voltage Distortion

With the variation of the supply impedance and background voltage distortion, the net effect is to change the distortion of the voltage supplied to the ASD load. From the comparable results shown in Figure 5.7, a single relationship can be extracted to address the variation of the harmonic current spectrum magnitudes with the voltage THD. The attenuation factor, as obtained for the PC load, is derived for the ASD load using the simulation results by applying equation (3.2). It gives the ratio of the magnitude of the harmonic current spectrum at a specified voltage distortion to the magnitude of the typical spectrum when the voltage distortion is insignificant. Figure 5.15 shows the variation of the attenuation factor for different harmonic orders reflecting the interaction between the drive and system voltage waveform distortion and how the harmonic currents are affected.

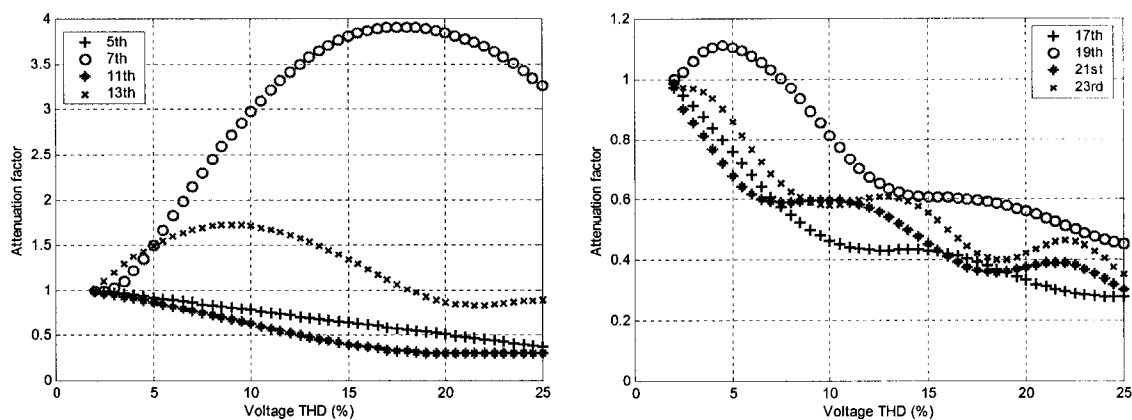


Figure 5.15: Attenuation factor variation for ASD harmonic current spectrum magnitudes with the supply voltage THD.

### 5.5 Summary and Conclusions

The attenuation and the diversity of harmonic currents produced from an ASD load were explored. The ASD is the most dominantly used three-phase power electronic load in industrial systems. It was shown that the harmonic current spectrum of ASD load is not constant and changes with the supply voltage waveform. This concept is opposite to the

traditional harmonic analysis where the ASD load is represented by the typical current spectrum determined upon little distortion of the supply voltage. The results revealed that ASD harmonic current spectrum can be characterized by the voltage distortion whether it is caused by the supply impedance or by the connection of other ASD loads in the system. Therefore, relationships can be obtained to correlate the harmonic current magnitudes and phase angles to the voltage distortion.

Considering the effect of supply voltage waveform is important for systems employing a large number of ASDs where the system voltage distortion level can be significant. A justification was made regarding the choice of the voltage THD as a predictor of the ASD harmonic current spectrum. This will be embedded in the ASD model to conduct harmonic analysis in the next chapter for systems with distributed ASD loads using the iterative method proposed in Chapter 4 that takes into account the harmonics attenuation and diversity.



# Chapter 6

## Application of the Iterative Harmonic Analysis Method with Distributed ASD Loads

Based on the encouraging results in Chapter 4 with multiple PC loads, the proposed iterative harmonic analysis method has been chosen for ASDs. Different case studies are conducted where the ASD harmonic current characteristics obtained in the previous chapter are used for the assessment of harmonic distortion for systems with distributed ASD loads. The drawback of implementing the traditional harmonic analysis method is presented showing the ensuing significant error that may appear for systems with considerable distortion levels. Time domain simulation is used to verify the iterative method and show its merit on providing more accurate and reliable results. Sensitivity studies are carried out to investigate the performance of the method and its implementation with some simplifications.

### 6.1 Introduction

Example systems with distributed harmonic sources are the oil field industrial distribution systems where ASDs are extensively used due to their high efficiency and flexibility. A typical application would be the operation of pump jacks distributed across a field. ASDs are scattered all over the distribution system and their presence contributes significantly to the system harmonic distortion level. Consequently, the attenuation and the diversity of the produced harmonic currents are expected to be considerable.

The effects of cumulative harmonics can result in poor operating performance of the drives and other connected loads. They can also damage sensitive electronic equipment connected in the system and cause telephone interference. If harmonics attenuation and diversity are ignored by using the typical current spectrum, harmonics related problems may be overestimated. Therefore, there is a need to quantify accurately the generated harmonics when distributed ASDs are in operation. Unfortunately, little work has been done on this subject, and no information was found that specifically dealt with the situation encountered in this research work.

In this chapter, the iterative frequency domain based harmonic analysis method proposed in Chapter 4 is applied to different distribution systems with a considerable number of ASDs. The results are compared with those obtained from the traditional method to show the potential of harmonic reduction due to the attenuation and diversity effects. Time domain simulation is conducted to verify the iterative method. Sensitivity studies are carried out to examine different aspects related to the method.

## **6.2 Case Studies for Distributed ASD Loads**

Three 25 kV electrical distribution systems are used as sample systems to explore the effect of the attenuation and diversity of distributed harmonic source currents on the system distortion levels. They represent typical oil field distribution systems with uniformly disseminated ASD loads across the distribution feeders. The system loads consist of linear and nonlinear kVA. The three feeders have different load levels and topologies so that the most common oil field distribution system configurations can be considered for the attenuation and diversity study. The ASD loads are operating at the 480V secondary voltage of the system transformers. The feeder loads are generally balanced, therefore, a single-phase system representation is adopted in the harmonic analysis. The supply system is modeled with its short circuit impedance at the 25kV side. Induction motors are modeled as loads at the fundamental frequency and as short circuit impedances at the harmonic frequencies. Line shunts, though small, are included in the

network representation since they have significant impact on the network harmonic frequency responses. The main methodology adopted in this investigation is conducting case studies on the representative oil field feeders. The results are then examined using time domain simulation in addition to sensitivity studies to determine their general applicability.

### **6.2.1 Goose River Oil Field System**

Goose River oil field system is one of the selected systems located in Northern Alberta where distributed ASDs already exist and future load expansion is intended. There are 21 ASDs installed in the low voltage side of the system (480V) in addition to other linear loads. 15 of the ASD transformers are YY connected, while the other six transformers are DY connected. This contributes to a partial cancellation of the 5th and 7th harmonic currents. Besides, there are nine capacitors distributed around the system for voltage support. Electric power is delivered to load buses mainly by overhead distribution lines at 25 kV level. The single-line diagram of the system is depicted in Figure 6.1 showing the rating of different ASDs and linear loads. The ASDs in operation use a diode bridge rectifier in the front end in addition to an inductance and a capacitor in the DC link. Hence, the ASD current THD is not high due to the presence of the DC link inductance that acts on current smoothing. The system total real and reactive power are 6.3 MW and 2.2 MVAR respectively. It is required to get the system distortion level taking into account the attenuation and diversity effects with the operation of the distributed ASDs.

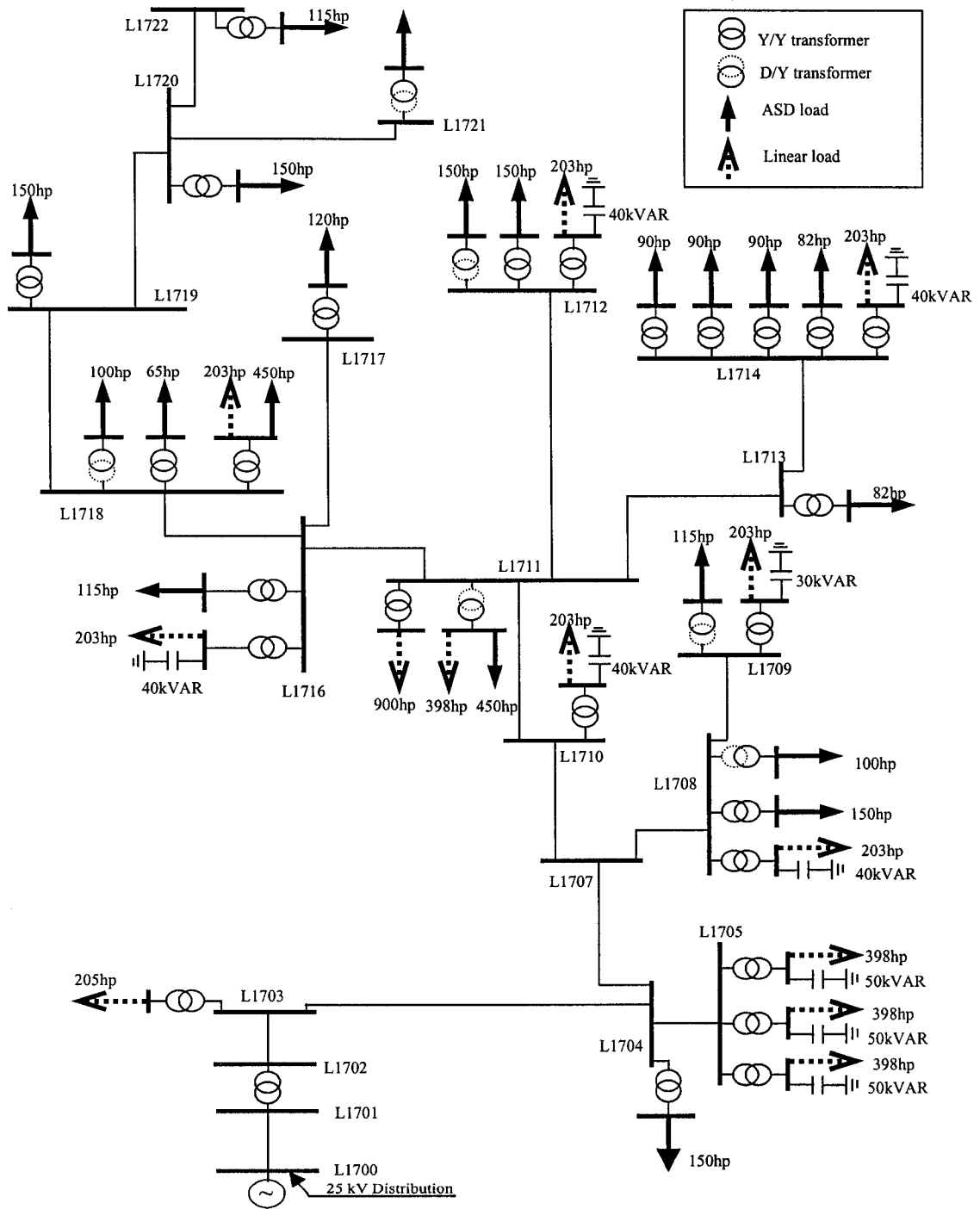


Figure 6.1: Single-line diagram of Goose River oil field distribution system.

### 6.2.1.1 Calculation Results

The relationships that characterize the variation of the harmonic current magnitudes and phase angles with the voltage THD are determined for each individual drive of different HP rating. In implementing the proposed iterative method, the initial estimate of the system voltage THD is obtained using the typical harmonic current spectrum. Next, the current spectrum of each drive is corrected upon the associated supply voltage THD using the developed relationships. Subsequently, the harmonic power flow computations are performed via the harmonic nodal equations to get the new harmonic voltages and the voltage THD is calculated. The whole process is reiterated again and exit from iteration occurs when the steady-state solution of the system voltage THD is obtained. In this way, the interaction between the harmonic current spectra of the ASD loads and the system voltage is considered. The solution is converged within 4 iterations as shown in Figure 6.2 with a convergence criterion of 0.1% of the maximum absolute difference of the system voltage THD.

Figure 6.3 shows the voltage THD at system buses as well as the current THD through system branches. It is clear how the proposed iterative method provides reduced system distortion level compared with the traditional method that uses the typical harmonic current spectrum. This is due to the consideration of the attenuation and diversity of ASD injected harmonic currents as a result of the distortion of the supply voltage waveform, which is usually ignored by the traditional harmonic analysis programs. Figure 6.4 illustrates the individual harmonic components of the voltage at buses L1701 and L1711 and of the current through branches L1700-L1701 and L1704-L1705. There is a noticeable difference in the results due to the adjustment performed on the ASD harmonic currents that in turn affects the resultant system individual harmonic voltages and the individual harmonic currents through different branches. In the next section, the impact on the harmonic current spectrum of different drives will be illustrated and verified by a time domain simulation program.

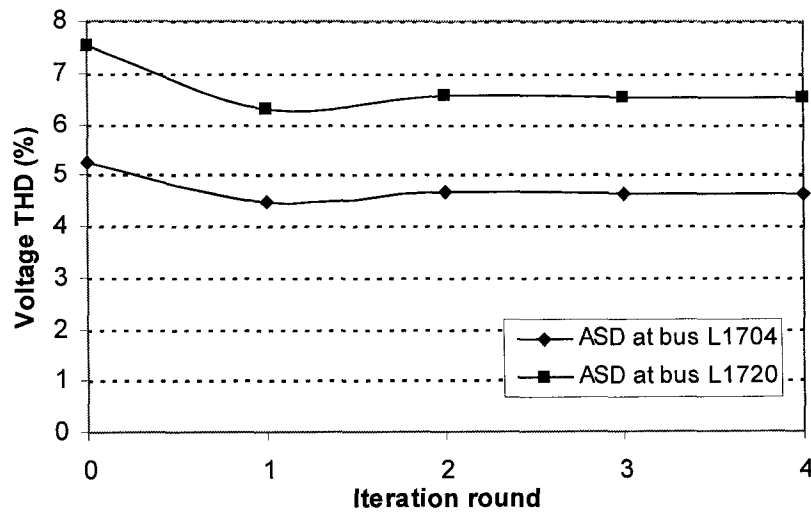


Figure 6.2: Convergence process of the voltage THD at different ASD locations.

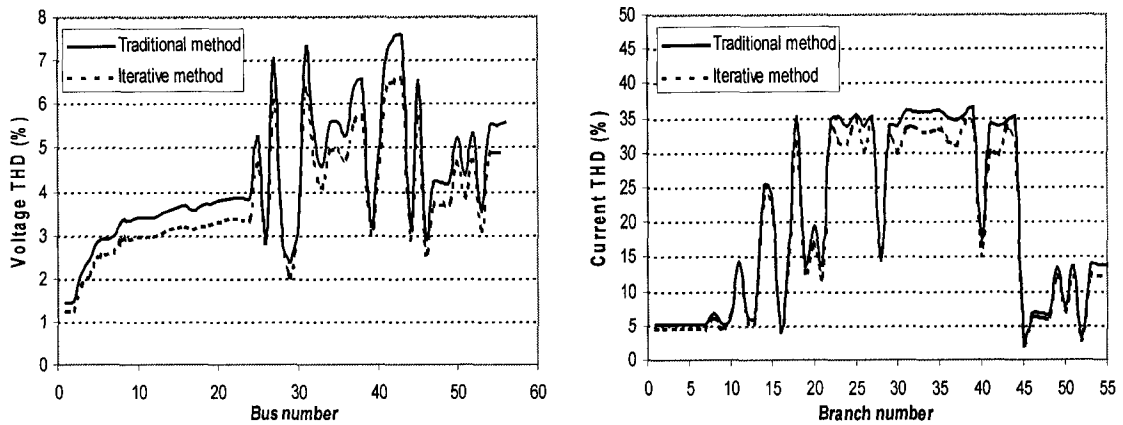


Figure 6.3: System voltage and current THD using the traditional method and the iterative method.

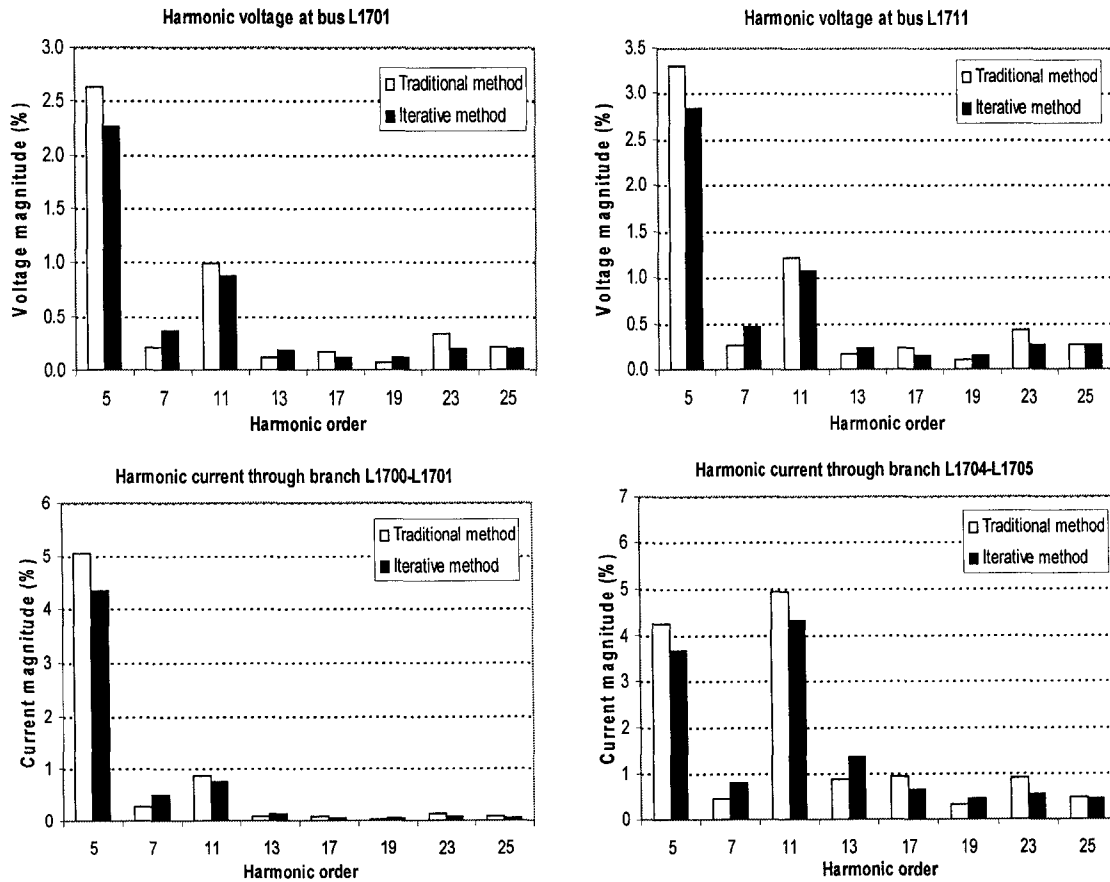


Figure 6.4: Individual harmonic voltages and currents using the traditional method and the iterative method.

### 6.2.1.2 Time Domain Simulation Results

In order to verify the proposed iterative method, harmonic analysis is performed on the Goose River system using a time domain simulation program such as PSCAD/EMTDC. This program models the topologies of the harmonic-producing loads, therefore, the attenuation and diversity effects are naturally taken care of. To clarify how the proposed frequency domain iterative method could address the harmonics attenuation and diversity, the results of the ASD harmonic current spectra are compared with the time domain simulation results. The comparison also includes the results obtained by the frequency domain traditional method that employs the typical current spectrum of the harmonic source.

Figure 6.5 presents the individual harmonic current magnitudes in percent of the fundamental component for seven ASDs of different ratings (65, 90, 100, 115, 120, 130, and 450 HP respectively). Figure 6.6 depicts the individual harmonic current phase angles with respect to the corresponding fundamental voltage phase angle for the same drives. It can be inferred how the iterative method can give results of a good consistency with those obtained by the time domain simulation. This shows its advantage on accommodating the ASD harmonic current magnitudes and phase angles over the traditional method in order to account for the harmonics attenuation and diversity.

Figure 6.7 illustrates a comparison of the ASD supply voltage THD as well as the corresponding current THD obtained by different methods. It reveals that the iterative method can closely solve the attenuation and diversity problems associated with distributed harmonic sources by dealing with the effect of the supply voltage waveform distortion. The figure also emphasizes the fact that the traditional method using the typical current spectrum would result in overestimation of the system distortion level.

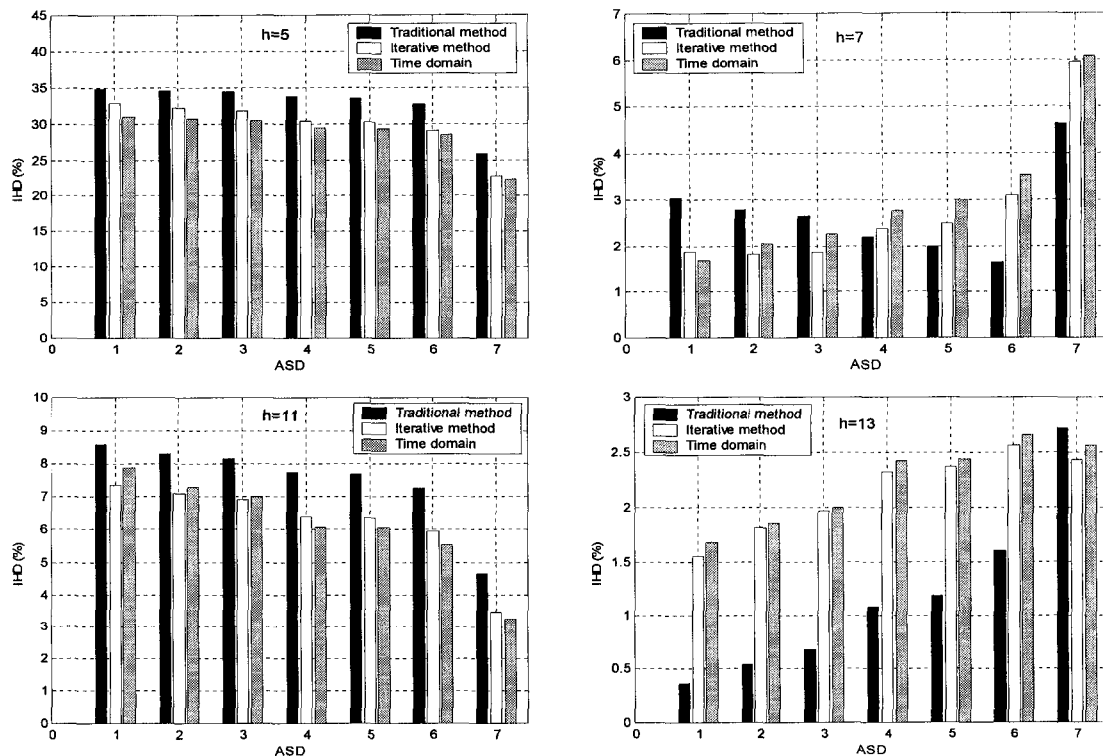


Figure 6.5: Comparison of individual harmonic current magnitudes.



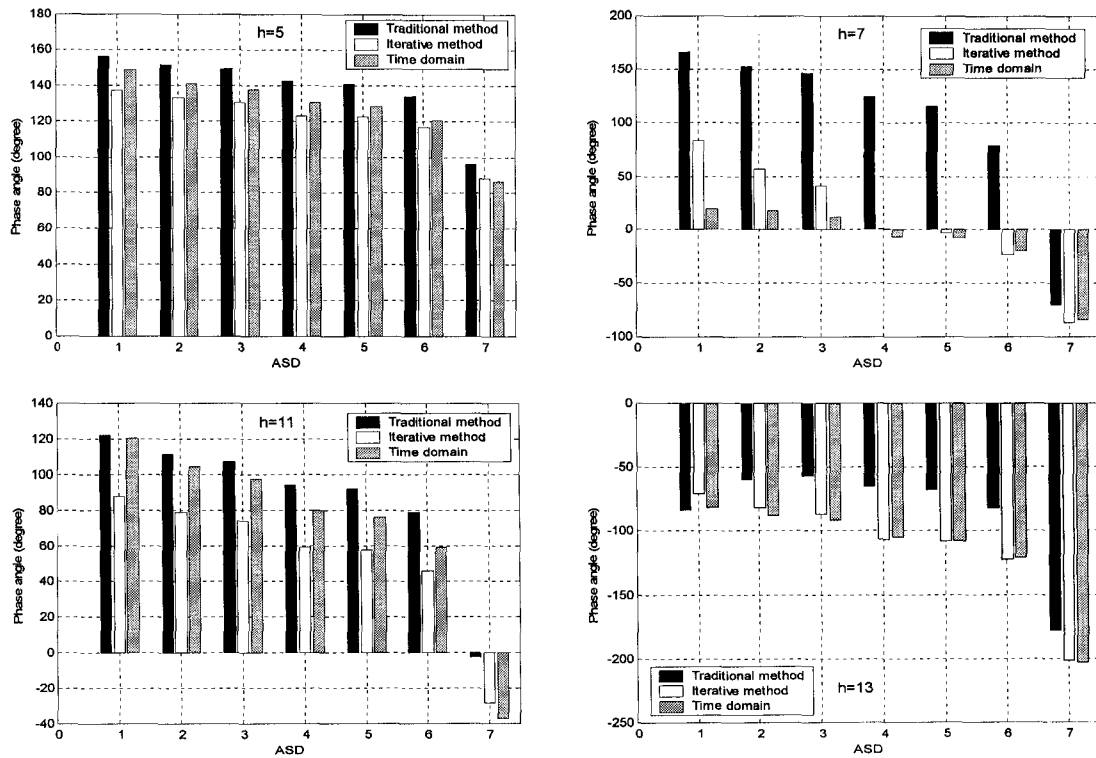


Figure 6.6: Comparison of individual harmonic current phase angles.

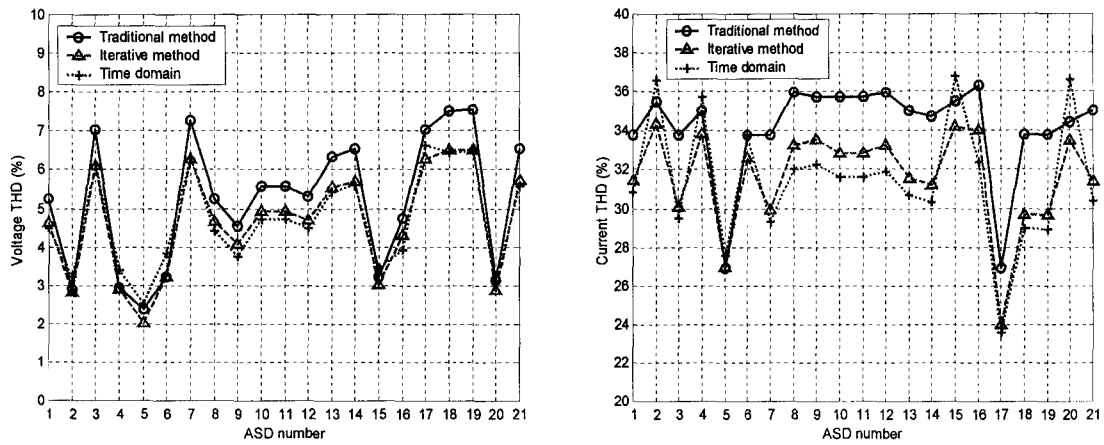


Figure 6.7: Comparison of the ASD supply voltage and current distortion levels.

### 6.2.1.3 Sensitivity Studies

Different sensitivity studies are conducted to address some approximations. The first one is ignoring the impact of the voltage distortion on the harmonic current phase angles, i.e.,

excluding the harmonics diversity. Also, the multiplier factors proposed in the case of the PC loads to get an approximate range of the distortion level without performing the complete iterative procedure are investigated. Finally, the results obtained when the same harmonic current spectrum characteristic is applied to all drives are presented.

Effect of Ignoring the Harmonic Currents Diversity

Figure 6.8 presents the THD of system bus voltages and branch currents obtained by the iterative method with and without considering the harmonic currents diversity introduced by the voltage distortion. It can be observed that ignoring the diversity has approximately no impact on the results. This is mainly because the voltage distortion at the drive buses is less than 7% so that the change of the distributed ASD harmonic current phase angles is not considerable.

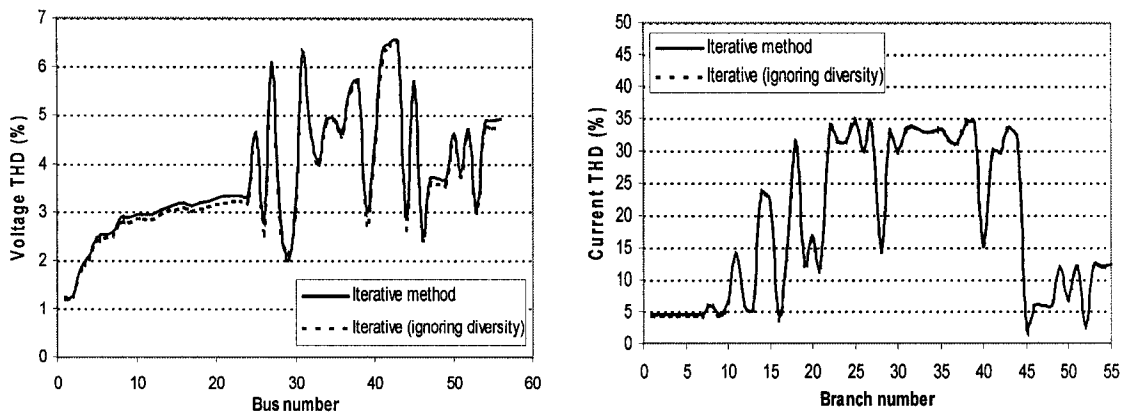


Figure 6.8: System voltage and current THD to show the impact of ignoring the harmonic currents diversity.

Summary of the Individual Harmonic Results

The results obtained by the traditional method, complete iterative method, and approximate iterative method that ignores the harmonics diversity are summarized in Figure 6.9. The results are for individual harmonic voltages at different buses and individual harmonic currents through different branches as well as injected harmonic currents from two drives at different locations. The figure shows that the implementation

of the traditional method that uses the typical harmonic current spectrum overestimates the individual harmonic distortion. It can also be seen that ignoring the diversity effect does not have pronounced impact on the results since the system distortion level is not that severe.

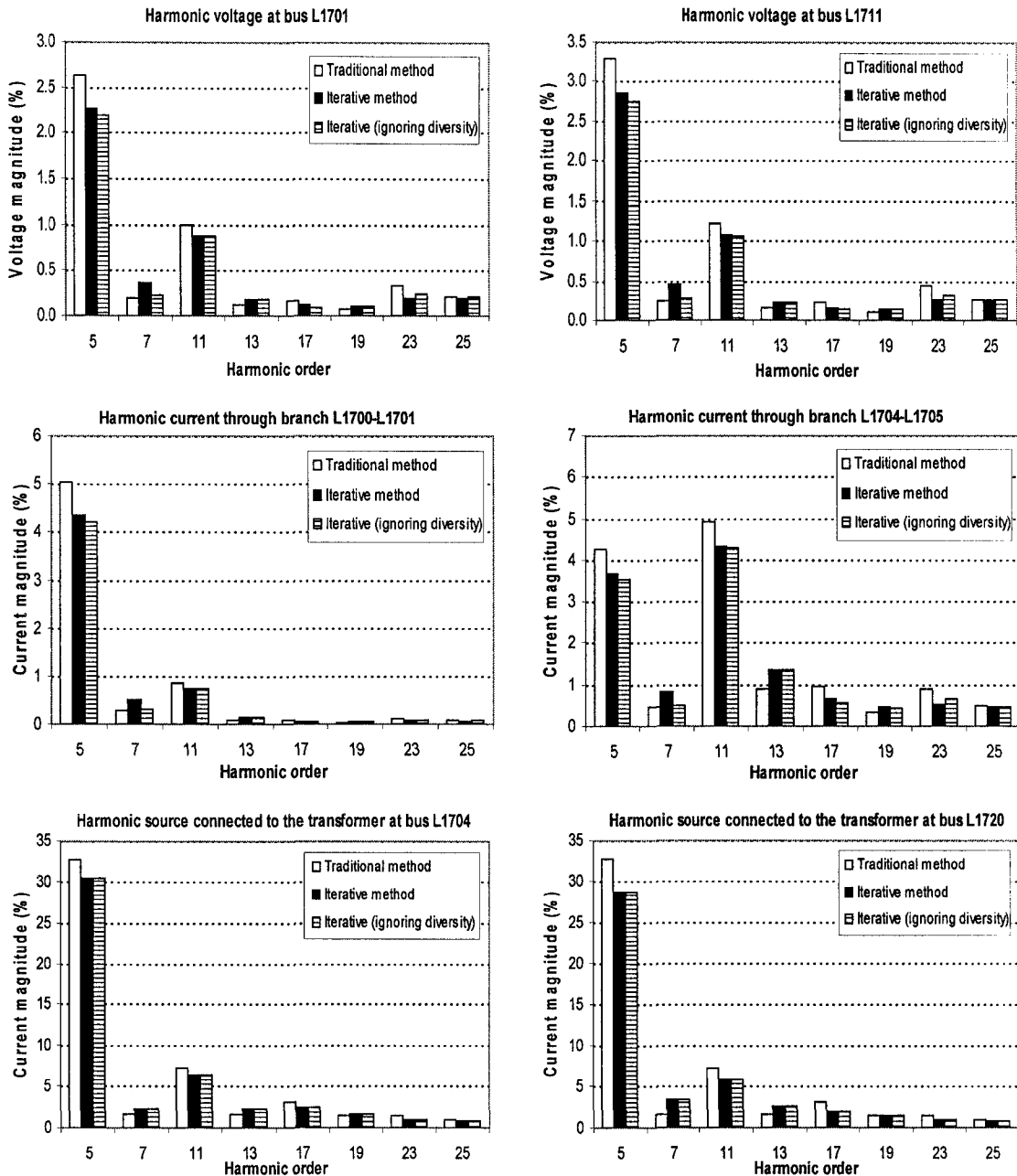


Figure 6.9: Summary of the individual harmonic voltage and current results.

### A Simplified Way to Estimate System Distortion Level

As mentioned before in the PC load case studies, two multiplier factors “ $MF_1$ ” and “ $MF_2$ ” were proposed using equations (4.10) and (4.11) to give an approximate distortion level by knowing the initial result obtained using the typical current spectrum and the result of the first iteration. This simplification provides a preliminary range of system distortion, then more precise result can be obtained using the iterative method when needed. Figure 6.10 presents the relationships between the different multiplier factors and system voltage THD and harmonic source current THD.

The results show that the values of  $MF_2$  are in the range of 0.8 to 1, which is different from the range in the case of the PC loads. This is mainly due to the difference in system characteristic and distortion level, which affects the relative value of the converged solution to the typical solution obtained by the traditional method. However, the results of the  $MF_1$  are in the range of 0.45 to 0.5, i.e., comply with the results obtained in the case of the PC loads. Accordingly, a value of 0.5 for the first multiplier factor can be adopted to give acceptable results. Consequently, approximate distortion level can be obtained in a simplified way when the attenuation factor at different distortion levels is attainable using the attenuation factor graph shown in Figure 5.15 for ASD loads to modify the harmonic currents for only one iteration. This is helpful for engineers who are interested in conducting harmonic analysis considering the voltage distortion effect without resorting to the complete iterative algorithm where the traditional harmonic analysis software programs can still be used for this purpose.

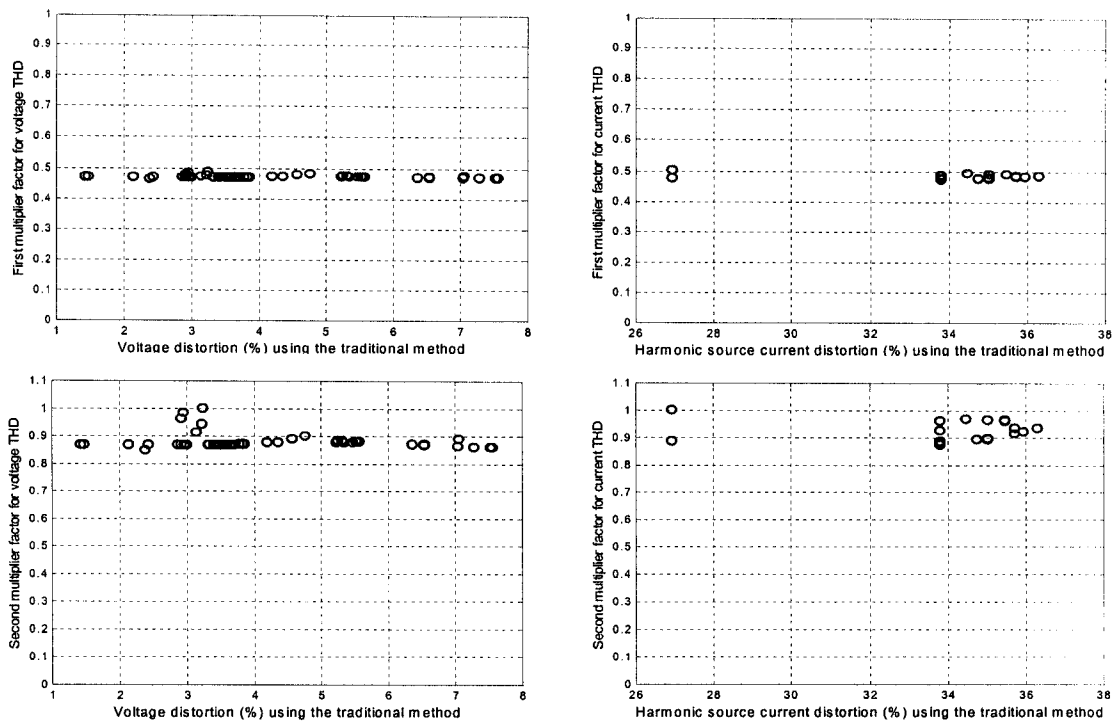


Figure 6.10: Different multiplier factors for voltage and current THD (Goose River oil field system).

Calculation Results when Applying the Same Harmonic Current Spectrum to All Drives

Goose River system has 21 ASDs of the following ratings: 65, 82, 90, 100, 110, 115, 120, 130, and 450 HP. Most of the drives are of comparable sizes between 90 and 150 HP. Therefore, when implementing the iterative method for harmonic analysis, the relationships of the harmonic current spectrum of 150 HP ASD with the voltage THD can be adopted and applied to all other drives. Figures 6.11 and 6.12 show the resultant individual harmonic current magnitudes of the spectrum in percent of the fundamental component and the individual harmonic current phase angles with respect to the fundamental voltage phase angle for five drives of the considered rating (150 HP). The figures indicate that applying the same harmonic current spectrum characteristic to all drives would give comparable results to the time domain simulation results.

This shows that assuming the same spectrum characteristic is permissible in the case under study and can be applied in similar cases. The main reason is that there is no much

discrepancy among the harmonic current characteristics for different drives due to the similarity in circuit topologies. Consequently, less effort and time are needed to develop the relationships that correlate the harmonic current spectrum for each drive with the supply voltage THD in order to conduct the iterative harmonic analysis method. On the other side, using the traditional method gives inaccurate results due to neglecting the distortion impact of the supply voltage waveform.

Figure 6.13 illustrates a comparison of the resultant ASD supply voltage THD as well as the corresponding current THD when each individual drive implements its own harmonic current spectrum characteristic and when all drives use the same spectrum characteristic of 150 HP drive. It can be confirmed that using the same spectrum produces acceptable voltage distortion levels due to the same circuit topology for all ASDs.

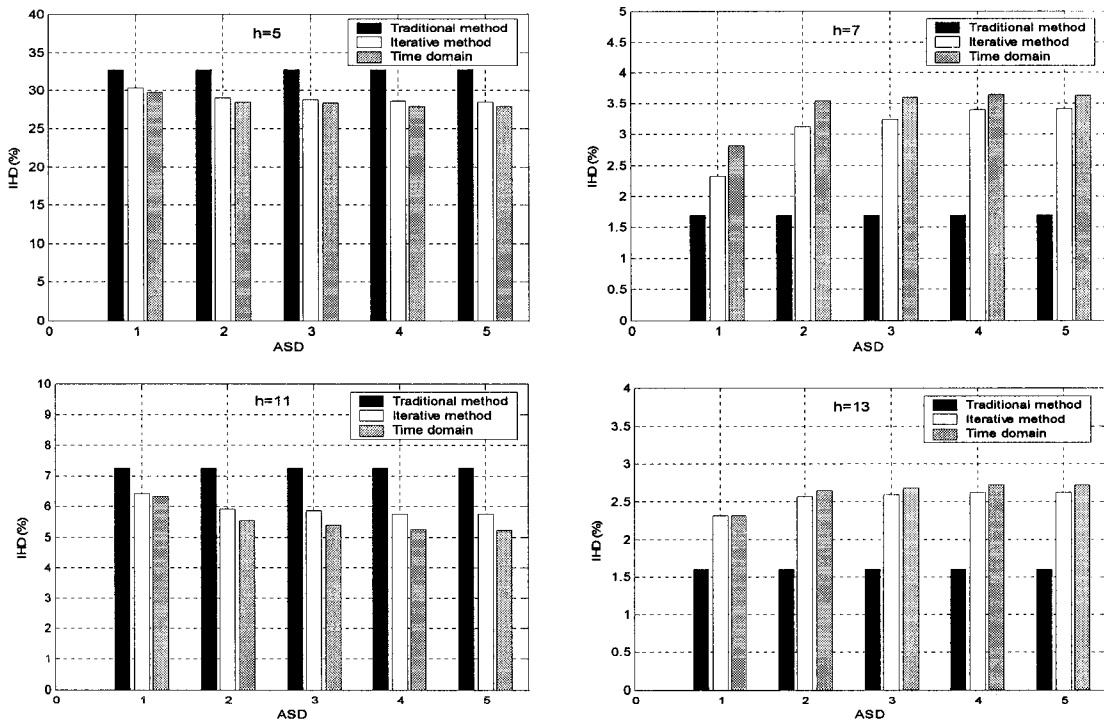


Figure 6.11: Individual harmonic current magnitudes (same spectrum case).

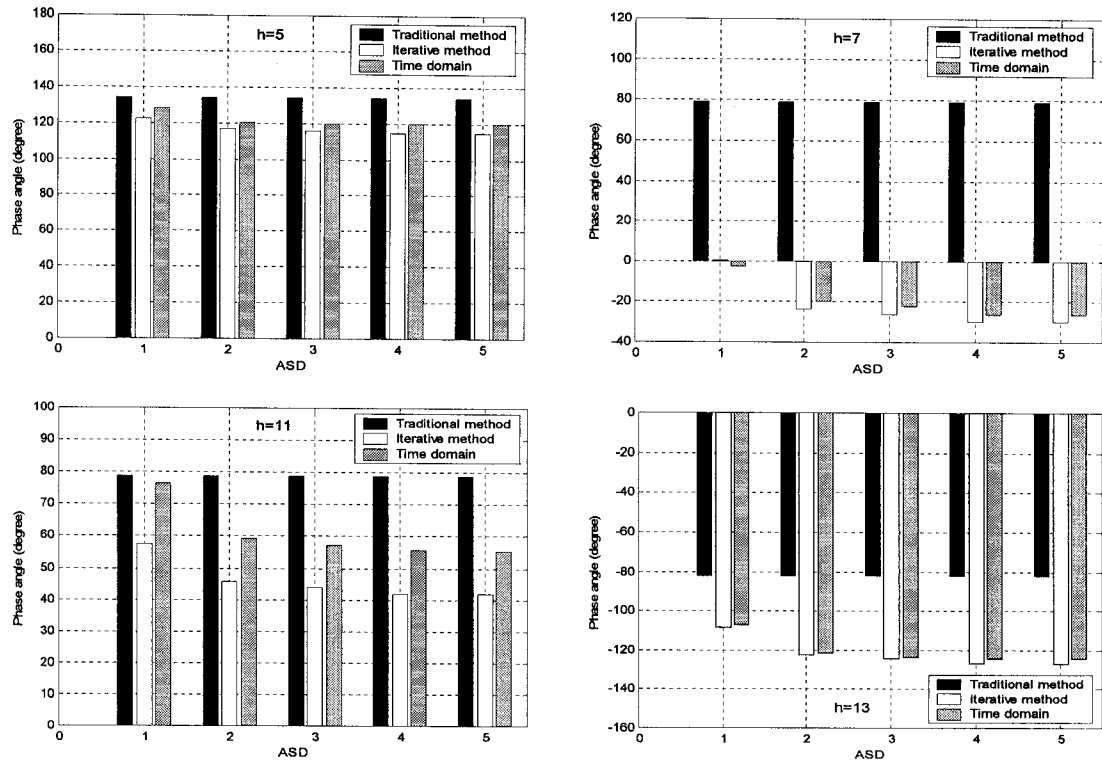


Figure 6.12: Individual harmonic current phase angles (same spectrum case).

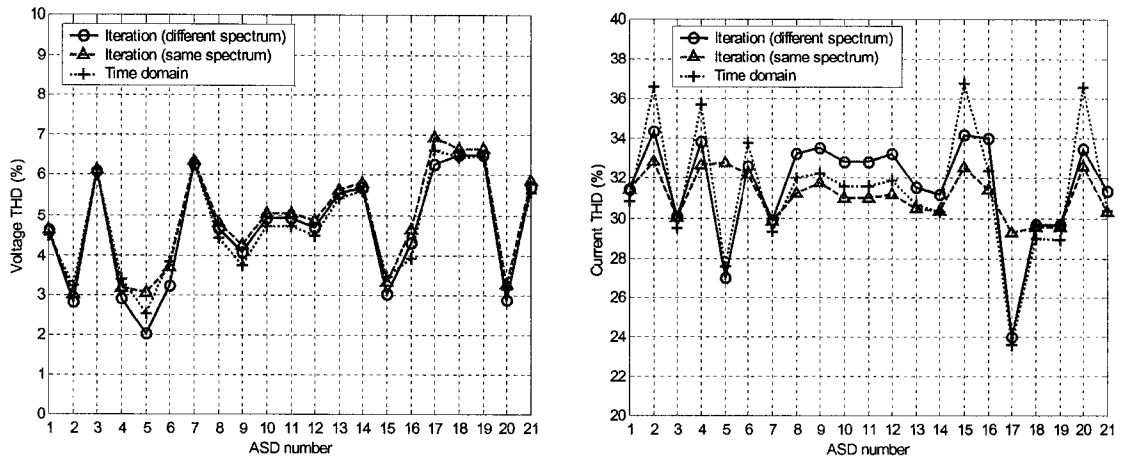


Figure 6.13: Comparison of the ASD supply voltage and current distortion levels when applying the same harmonic current spectrum characteristic to all drives.

### 6.2.2 Oil Field Systems F501 and F502

Systems F501 and F502 are typical oil field distribution systems in Alberta. They employ a large number of ASD loads, therefore, the distortion level is expected to be significant. Consequently, the attenuation and the diversity of harmonic currents will be more pronounced than those in the Goose River system. A 5% reactive impedance is assumed for all drive transformers. The transformer connections are either YY or DY randomly distributed across the feeders. The harmonic distortion is mainly due to the 11th and 13th harmonics since the 5th and 7th harmonics are partially cancelled out in the systems due to the mixed transformer connection scheme. Figure 6.14 shows the single-line diagram of the oil field systems. The main parameters of both system feeders are summarized in Table 6.1.

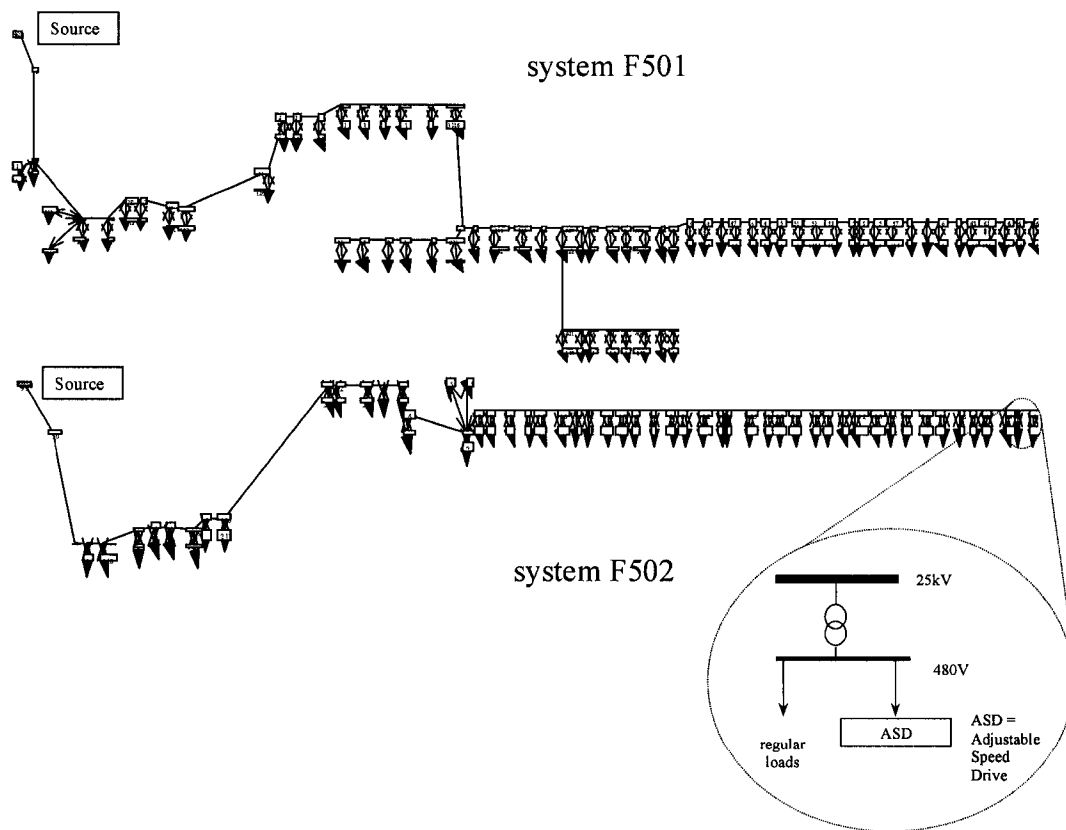


Figure 6.14: Single-line diagram of the oil field distribution systems F501 and F502.



Table 6.1: Technical information of the oil field feeders

Technical Information	F501	F502
Total real load (MW)	9.8	6.5
Total reactive load (MVAR)	4.2	2.1
Feeder length (mile)	28	25
Number of adjustable speed drives	67	51
Total size of harmonic-producing load (MW)	4.8	4.7

### 6.2.2.1 Damping Factor for Solution Convergence

When performing the iterative harmonic analysis method on these example systems, the solution is found oscillating between two values with no convergence. The reason is that the positive slope of system characteristic of voltage THD and current THD is approximately equal to the negative slope of the harmonic source characteristic. In order to overcome this problem, a modification should be performed on the iterative procedure. This is achieved by inserting a damping factor ( $DM$ ) to slow down the transition step in determining the voltage THD at harmonic source buses in each iteration. The obtained voltage THD in the  $i$ -th iteration is, therefore, modified according to the following equation:

$$VTHD_{mod_i} = VTHD_{mod_{i-1}} + DM \times (VTHD_i - VTHD_{mod_{i-1}}), \quad i \neq 1 \quad (6.1)$$

where  $VTHD_i$  is the voltage distortion calculated in the  $i$ -th iteration after getting the system harmonic voltages using the harmonic admittance matrices and the adjusted injected harmonic current spectra of the drives.  $VTHD_{mod_{i-1}}$  is the voltage distortion modified in the  $(i-1)$ -th iteration and then used in the  $i$ -th iteration to adjust the associated drive harmonic current spectrum. The modified voltage distortion for the first iteration is the initial value obtained using the typical current spectrum. The criterion of convergence in this case is applied to the maximum absolute difference between  $VTHD_i$  and  $VTHD_{mod_{i-1}}$  at all buses. It is clear that if the damping factor is equal unity, the method

reverts to the normal iterative one. In the concerned study, a damping factor of 0.55 is chosen and the convergence criterion is set at 0.1%.

Figure 6.15 shows the process of implementing the iterative method with and without using the damping factor. The system and harmonic source characteristics are obtained at one of ASDs distributed across system F502. The solution oscillation is clear when the damping factor is not used. On the other side, with using the damping factor, the iteration converges reaching to the solution point.

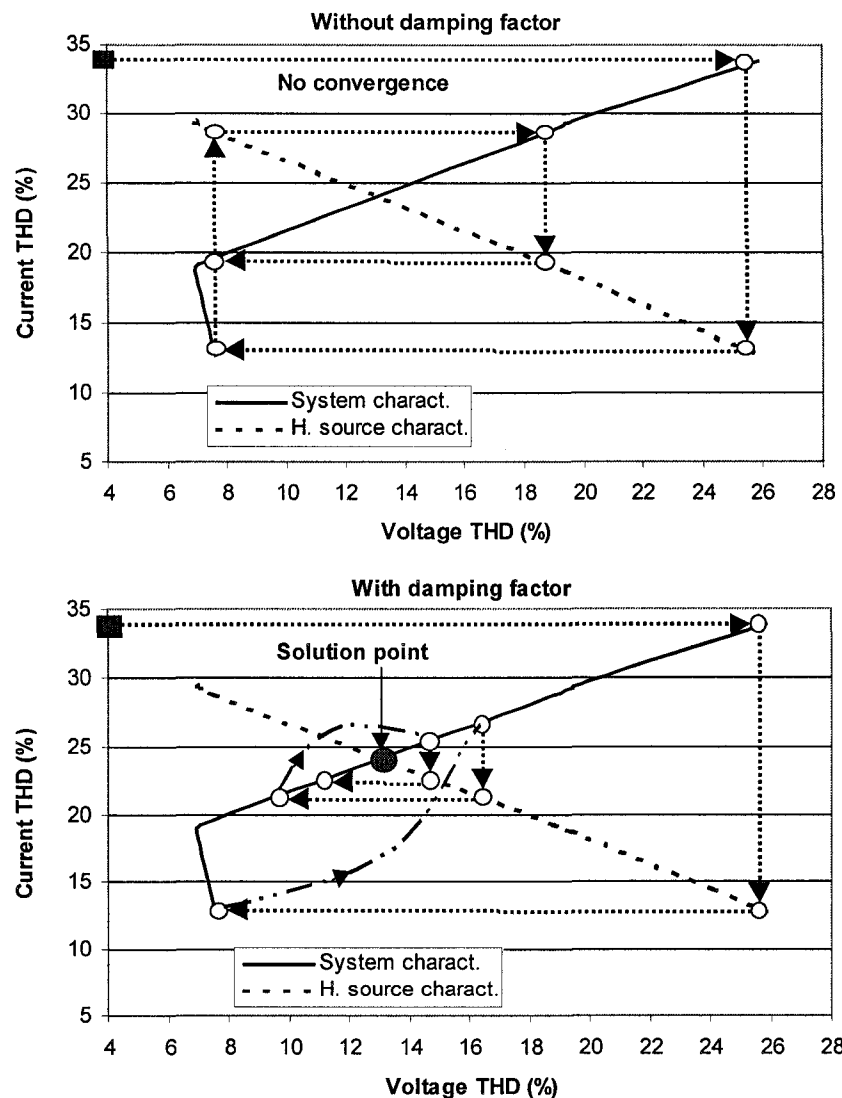


Figure 6.15: Iterative process with and without using the damping factor.

6.2.2.2 Calculation Results

The calculation results of the distortion of bus voltages and branch currents using the traditional method and the iterative method are shown in Figure 6.16 for both systems. Evidently, it can be inferred how the attenuation and diversity effects have substantial contribution to the reduction of the resultant distortion compared with the use of the typical spectrum. This reveals the importance of considering the voltage distortion influence on the injected harmonic currents. The impact can be significant with the increase in the number of distributed harmonic sources and the subsequent high distortion level across the system.

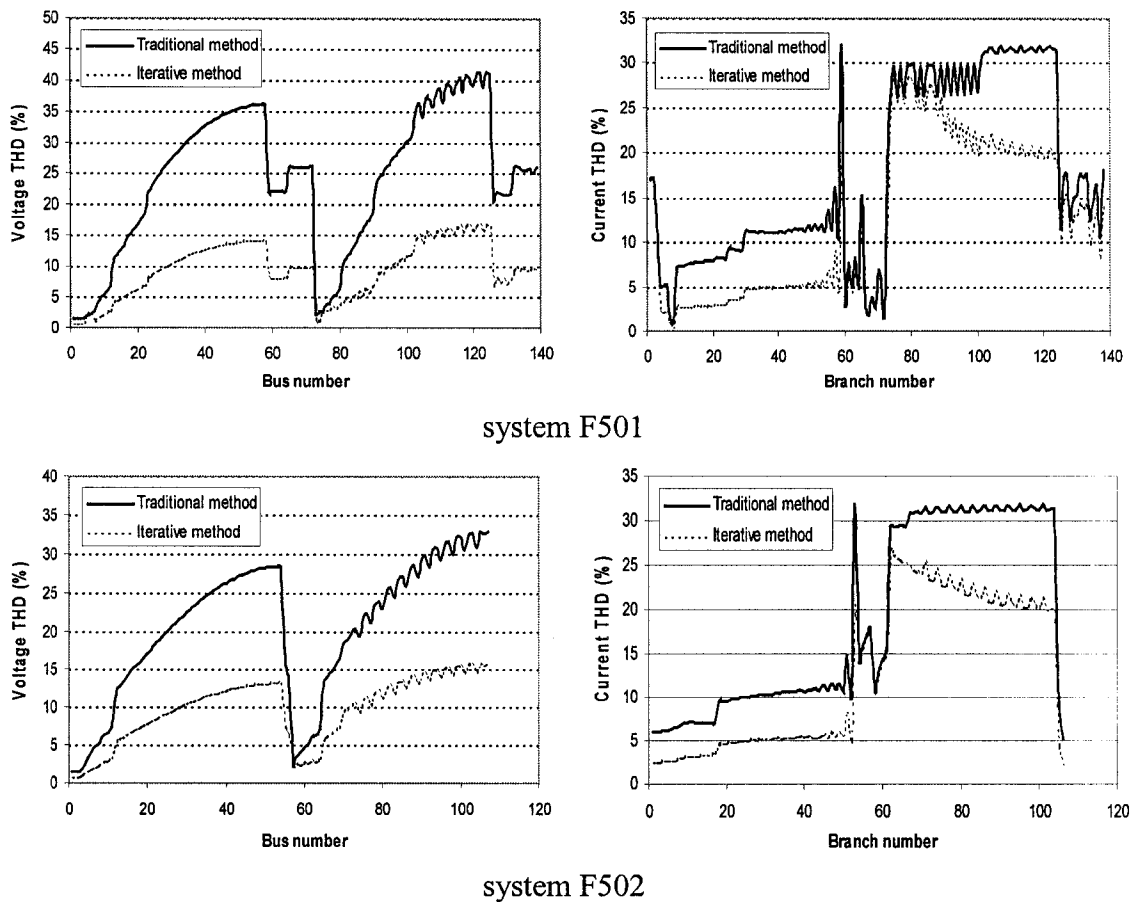


Figure 6.16: Results of voltage and current THD using the traditional method and the iterative method.

### 6.2.2.3 Sensitivity Studies

The same sensitivity studies considered for the Goose River system are performed on systems F501 and F502. In addition, the effect of applying different damping factors on the solution convergence speed is investigated in order to determine the most appropriate damping factor range.

#### Effect of Ignoring the Harmonic Currents Diversity

Figure 6.17 shows that implementing the iterative method without considering the diversity effect provides conservative voltage distortion results at most buses. The average of the absolute difference of voltage distortion with respect to the complete iterative method at all buses is 25.98% and 15.45% for systems F501 and F502 respectively. The conservative voltage distortion at the ASD buses causes the injected harmonic current distortion have more reduction due to the increase in harmonics attenuation, therefore, the distortion of most branch currents becomes lower. The average of the absolute difference of current distortion through all branches with respect to the complete iterative method is 11.7% and 6.18% for systems F501 and F502 respectively. The results of both systems in addition to the results of the Goose River system show how the attenuation effect is a substantial factor that should be considered to account for the reduction of the distortion level with distributed harmonic sources. The diversity provides an additional amount of harmonic cancellation. The significance of this amount depends on the resultant voltage distortion level.

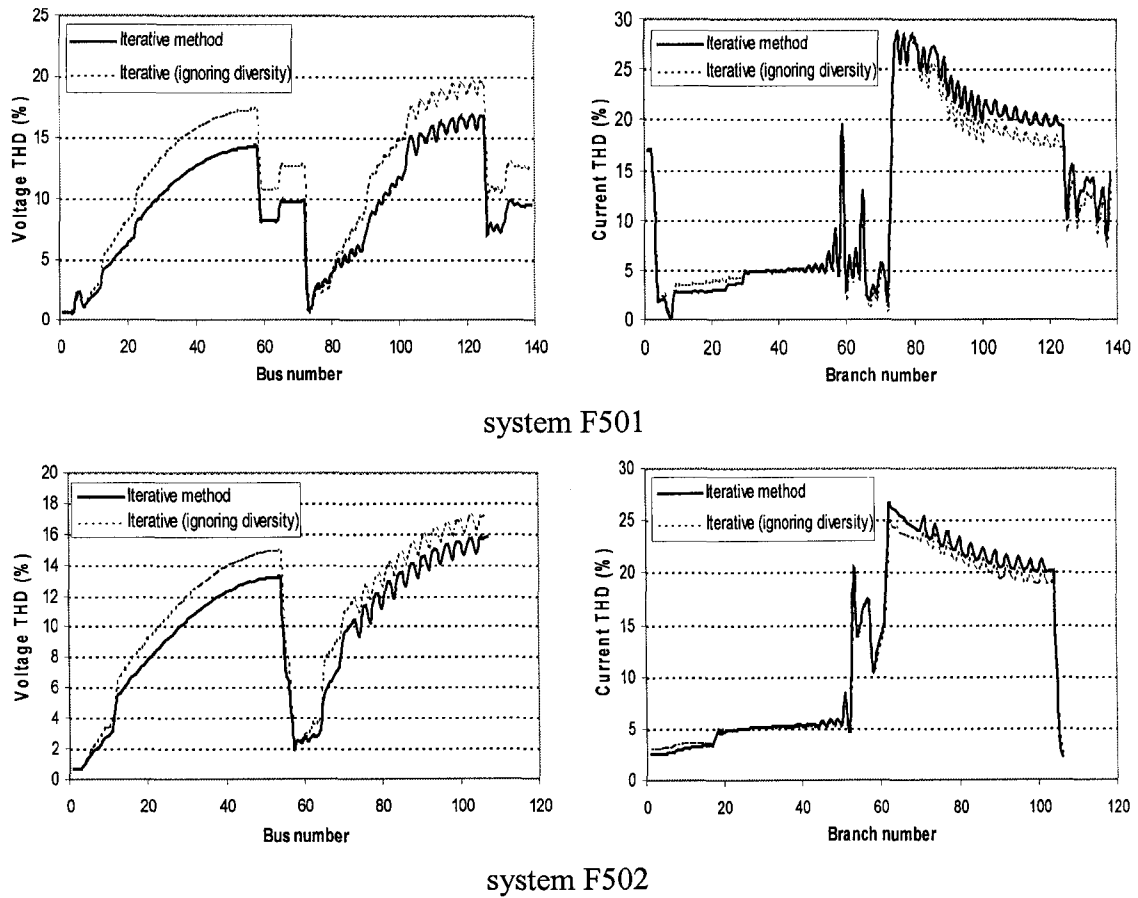


Figure 6.17: Results of voltage and current THD to show the impact of ignoring the harmonic currents diversity.

A Simplified Way to Estimate System Distortion Level

The typical current spectrum of the harmonic sources in the considered systems produces high voltage distortion level. This level exceeds the maximum limit in the harmonic source characteristic curves. Due to this reason combined with the implementation of the damping factor to perform the iterative method, the first iteration solution can not be determined directly from the typical one. Therefore, the  $MF_1$  defined in equation (4.10) is not considered for these two systems. Figure 6.18 shows the results of the  $MF_2$  obtained using equation (4.11). It can be seen that the  $MF_2$  values for voltage THD are concentrated in the range of 0.35 to 0.55 and in the range of 0.6 to 1 for harmonic source current THD. This highly depends on system characteristics where the results are

different from those obtained for the PC and Goose River systems. The obvious discrepancy among the multiplier factor results for current THD of the harmonic sources is due to the considerable difference between the individual supply voltage THD. This shows that the  $MF_2$  is not the proper factor to be considered to get approximate results. On the other side, the  $MF_1$  can be reasonably chosen for this purpose for systems with moderate distortion level as in the PC and Goose River systems or when the characteristic curves cover the voltage THD up to the typical results.

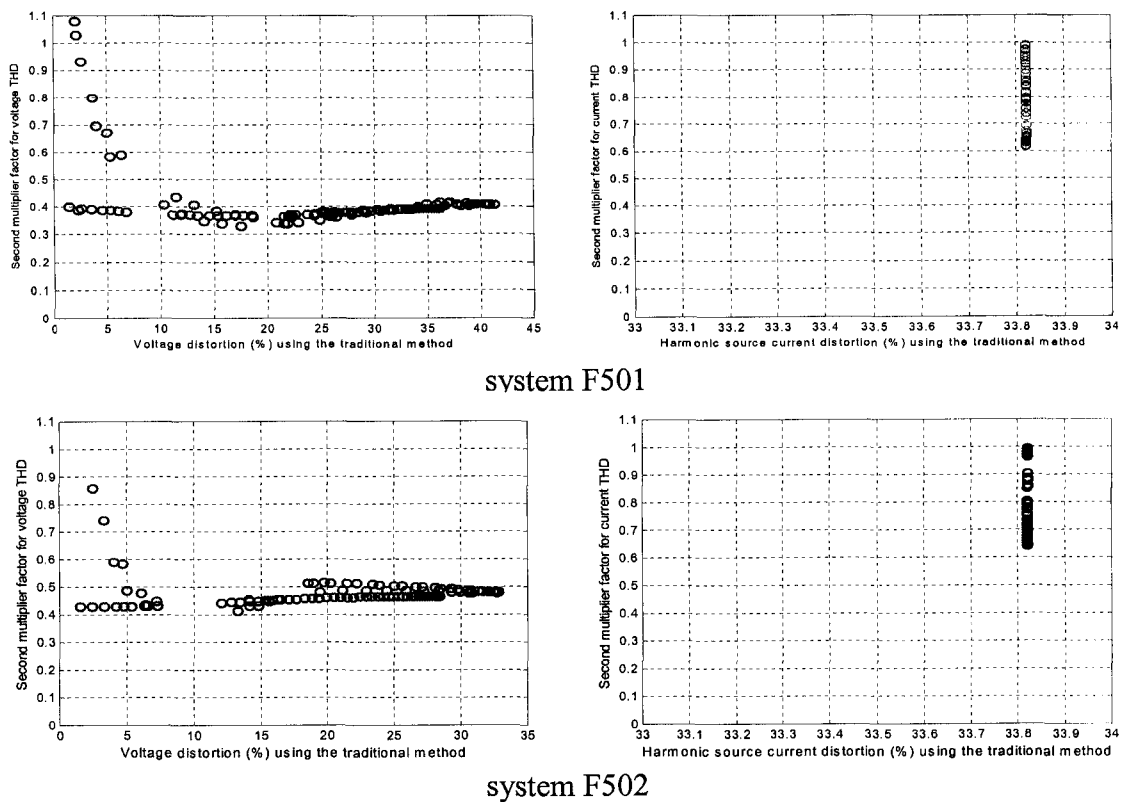


Figure 6.18: Different multiplier factors for voltage and current THD (systems F501 and F502).

Effect of Damping Factor on the Speed of Solution Convergence

The effect of the damping factor used in equation (6.1) during the iterative process is investigated to show the consequence on the convergence speed. This would provide the most effective range that gives faster converged solution for systems with high distortion level if solution oscillation or divergence occurs. Different damping factors are assumed

in the range of 0.2 to 0.7 with an increment of 0.05 and the harmonic analysis is performed using the complete iterative method and the approximate one that ignores the harmonics diversity. Figure 6.19 depicts that a damping factor range from 0.4 to 0.65 gives the lowest number of iterations for both systems. When the damping factor approaches unity or zero, the number of iterations required for convergence might increase significantly. A lower number of iterations is generally needed with ignoring the harmonics diversity. According to the obtained results, a damping factor of 0.55 was adopted in the harmonic analysis conducted for both systems.

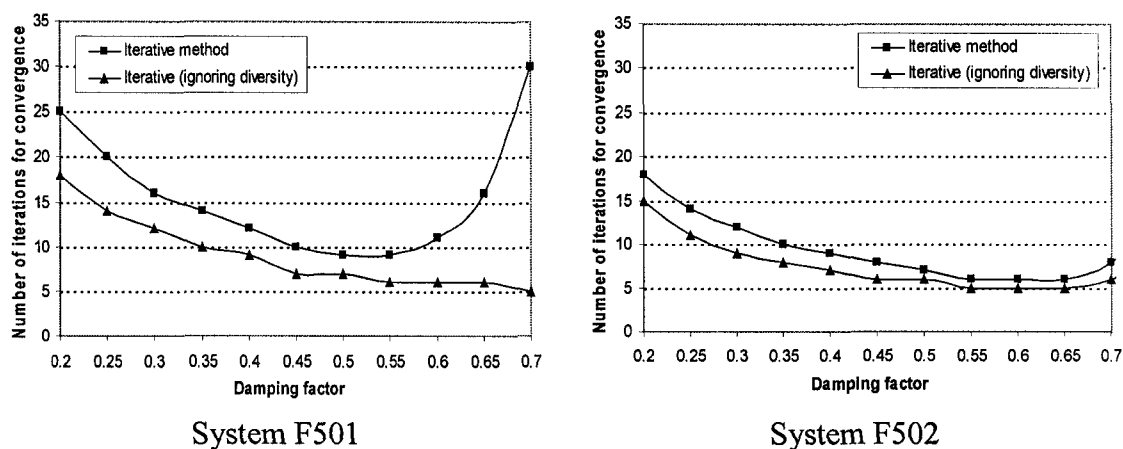


Figure 6.19: Effect of damping factor on the speed of solution convergence.

### Summary of the Results

The results are summarized and expressed in terms of the maximum and the average of the individual and total harmonic distortion of system bus voltages and branch currents as shown in Figure 6.20. It can be emphasized that using the traditional method that employs the typical harmonic current spectrum would significantly overestimate the distortion level compared with the iterative method. This clearly happens due to ignoring the harmonics attenuation and diversity that occur as a result of the system high voltage distortion associated with the operation of a considerable number of ASDs.

Ignoring the harmonics diversity when implementing the iterative method gives conservative voltage distortion results. This reflects the pronounced diversity among the harmonic source current phase angles for systems with high distortion level. In other

words, the adjustment of harmonic current phase angles without considering the voltage distortion effect includes only a limited diversity action and can not account for the whole diversity impact which is adopted by the complete iterative method. Considering the voltage distortion effect contributes to the harmonic current cancellation and consequently to the reduction in system voltage distortion level.

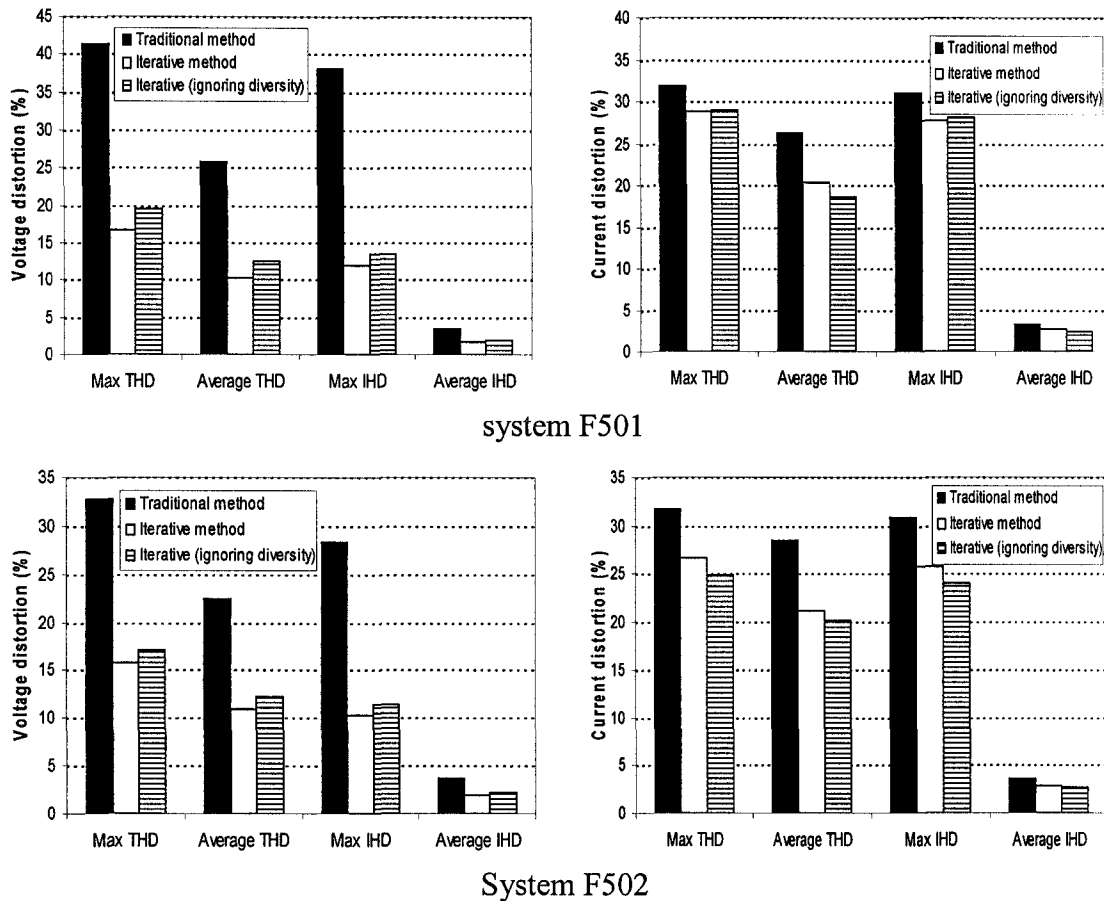


Figure 6.20: Summary of the system bus voltage and branch current distortion results.

### 6.3 Summary and Conclusions

The majority of industrial distribution systems in recent years is equipped with distributed harmonic sources and, therefore, yields considerable harmonic distortion levels. This entails applying harmonic analysis method that can consider the influence of the supply voltage waveform so that the harmonics attenuation and diversity can be taken



into account. The iterative harmonic analysis method proposed in Chapter 4 has been applied to different case studies with distributed ASD loads. With such systems, the distortion level provided by the iterative method was appreciably less than what obtained using the traditional method. The results were verified by time domain simulation to show the benefits gained by the iterative method on dealing with the attenuation and diversity of the harmonic currents.

It was found that the diversity effect for systems with considerable distortion levels could be significant to provide more reduction to the system distortion on top of the significant reduction amount that was already realized by the harmonics attenuation. As a result, ignoring any of the attenuation or the diversity effects can lead to conservative results. The multiplier factors defined in Chapter 4 were used with ASD loads to get an approximate range for system distortion level by implementing the traditional method with one iteration for the harmonic source current adjustment. A damping factor was introduced to narrow the variation of the voltage THD between successive iterations to overcome solution oscillation or divergence, which might occur while implementing the iterative method.

# Chapter 7

## Probabilistic Evaluation of Harmonics with Randomly Varying Nonlinear Loads

In this chapter, a probabilistic method is presented for the assessment of harmonic levels in distribution systems with distributed randomly varying nonlinear loads such as adjustable speed drives (ASDs). The drive loading impact on the produced harmonic current magnitudes and phase angles is illustrated. Accordingly, a probabilistic ASD model is developed to determine the statistical parameters of the injected harmonic current as a result of the randomness in the drive loading level. Then, the application of the bivariate normal distribution (BND) model using the Central Limit Theorem is discussed to get analytically the probability density functions (pdfs) of the magnitude of system harmonic voltages and currents. Monte Carlo simulation is performed to justify the analytical method.

### 7.1 Introduction

In practice, it has been recognized that power system harmonic voltages and currents can be randomly varying due to stochastic changes in operating mode of nonlinear loads such as electric arc furnaces and ASDs [35]. Consequently, deterministic harmonic analysis would lead to overdesign and excessive costs since it ignores the variability of the harmonic-producing load operating conditions that cause changes in the harmonic currents injected by these loads into the utility network [36]. Any random variations in

the harmonic injection are therefore not reflected in the harmonic current flows and resulting harmonic voltages which depend on the collective effect of harmonic sources. Depending on the degree of randomness, a large amount of vectorial cancellation is possible. The total harmonic current magnitude can be significantly less than the geometric sum of the random harmonic phasors [40]. Therefore, probabilistic techniques for harmonic analysis are more suitable to get realistic prediction of harmonic levels taking into account the random variation of harmonic current injection and propagation. Such an analysis would calculate harmonic voltages and currents based not simply on the expected average or maximum values, but would also obtain the complete spectrum of all probable values together with their respective probabilities [36].

This chapter presents a probabilistic analytical solution for predicting the resultant harmonic levels in a distribution system employing distributed ASDs of varying load. Such a system presents a potential problem in the form of excessive harmonic voltages and currents. The study deals with the harmonic currents generated due to the random variation of the loading level of the drives. Therefore, the drive loading level can be considered randomly varying to accommodate this variation.

The problem is stochastically formulated in order to reflect the randomness in the loading level of the individual ASDs. A probabilistic model for ASD load is used to account for the discrepancy in the injected harmonic current magnitudes and phase angles among different drives as a result of loading level variation. By utilizing the summation technique of randomly varying harmonic vectors presented in Chapter 2, in conjunction with harmonic power flow, an analytical expression of the pdfs of system bus harmonic voltages and branch harmonic currents can be obtained. The BND method is applied with the assumption of the presence of enough number of independent harmonic sources in a system. To assess the validity of the analytical method, a comparative study between the method and Monte Carlo simulation is carried out.

## 7.2 Variation of ASD Input Harmonic Currents with Loading Level

The problem of forecasting of harmonic levels in networks supplying many randomly varying ASD loads requires investigating the variation of the harmonic current injected from individual drives under different loading levels. PSCAD time domain simulation program is used for this purpose considering the drives employed in the Goose River distribution system described in Chapter 6. The input current of the individual drives has a typical normal distortion waveform type at full load condition.

Figure 7.1 shows the change of the input current waveform with loading level for 150 HP ASD. It can be inferred that as the drive loading increases the distortion of the current waveform becomes lower. Figure 7.2 illustrates how the associated current THD changes with the loading level. The considerable variation reveals the meaningful effect of ASD loading on the generated harmonic current distortion. Figure 7.3 depicts the corresponding variation of the individual harmonic current magnitudes and phase angles. It can be shown clearly how they are sensitive to the drive loading level.

As found in Chapter 6, the voltage distortion level for all drives in the Goose River system is less than 7%. Therefore, the effect of supply voltage distortion on the ASD harmonic currents can be considered of a secondary concern and the harmonic currents are assumed independent of the voltage waveform. Consequently, the harmonics attenuation and diversity are ignored and the loading level can be satisfactorily assumed as the main key factor upon which the ASD harmonic currents are determined in the proposed probabilistic study.

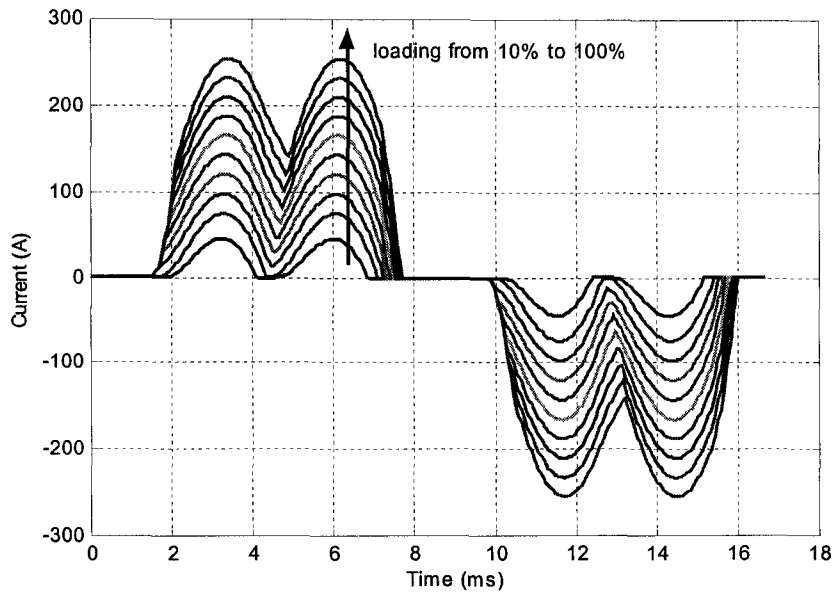


Figure 7.1: Variation of input current waveform with ASD loading level.

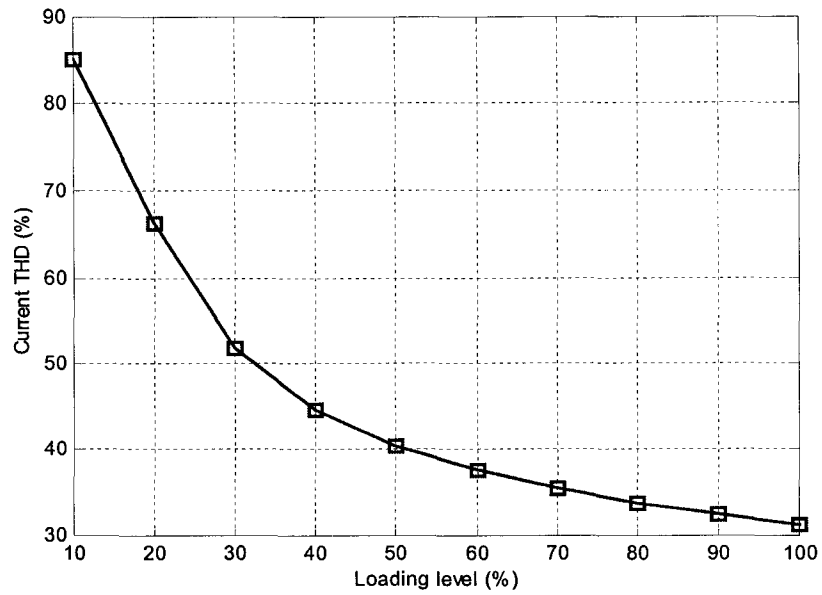


Figure 7.2: Variation of input current THD with ASD loading level.

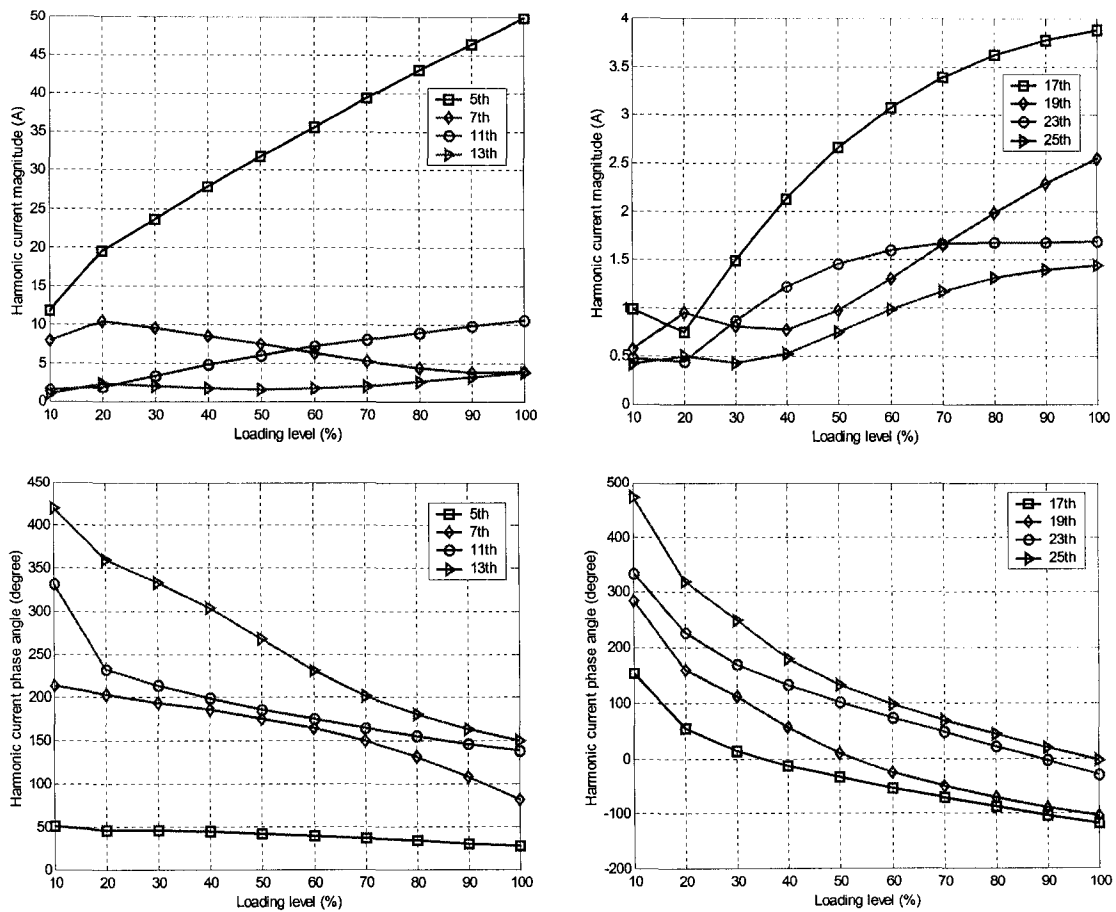


Figure 7.3: Variation of input harmonic current magnitudes and phase angles with ASD loading level.

### 7.3 Probabilistic ASD Model for Harmonics Assessment

The results of the change of ASD harmonic current magnitudes and phase angles with loading level constitute the basis to perform probabilistic harmonic analysis to account for the random loading variation of ASDs. The Goose River distribution system, with 21 ASDs distributed across the system feeder, is considered to apply the probabilistic study. The analysis begins by characterizing the harmonic currents for each individual drive with loading level. This would account for the discrepancy among the individual harmonic current magnitudes and phase angles of the drives when operating with random loading. Therefore, a more realistic collective effect of the harmonics can be obtained.

### 7.3.1 Determination of Statistical Parameters of ASD Harmonic Currents

By considering the ASD loading level as the concerned random variable, the injected harmonic currents at drive buses are also random and their statistical parameters can be obtained. The probabilistic harmonic analysis utilizes these parameters for the individual drives to provide the pdfs of the system bus harmonic voltages and branch harmonic currents. Accordingly, the non-exceeding probability of a specified value of harmonic voltage or current can be determined. The following assumptions will be made in conducting the probabilistic study:

- The ASD loads vary independently from each other. This implies that the harmonic current vectors injected from each individual drive are independent variables. This assumption eases the mathematical formulation of the sum of random vectors and can be reasonably applied with enough number of distributed harmonic sources [32,35,38,39,40,48]. Hence, it can be adopted in the case under study where 21 drives are considered.
- The variation of the harmonic current spectrum with the loading level for each drive is known where the loading is considered as the random variable with uniform distribution. The uniform distribution is reported as an acceptable approximation for most probabilistic studies [32,38,47]. Besides, with a considerable number of harmonic vectors, the resultant summation approaches normal pdf by virtue of the Central Limit Theorem irrespective of the pdf of the individual components.
- The configurations of the distribution lines as well as the linear loads are assumed to be non-varying.
- The distribution system is assumed balanced, consequently limiting the analysis to the equivalent single-phase case.

#### Extracting the Real and Imaginary Components of the Individual Harmonic Currents

- 1) The variation of the individual harmonic current magnitudes ( $I_h$ ) and phase angles ( $\phi_h$ ) for each ASD with loading level is determined.

- 2) The harmonic currents are decomposed into their real and imaginary components ( $I_{x-h}, I_{y-h}$ ) as follows:

$$I_{x-h} = I_h \cos \phi_h, \quad I_{y-h} = I_h \sin \phi_h \quad (7.1)$$

The following analysis applies to harmonics of any order  $h$ , consequently, the subscript  $h$  is left out in all symbols to simplify notation.

- 3) Mathematical relationships between the loading level and the rectangular harmonic current components can be obtained by interpolating their graphs by polynomial curves. Thus, the  $x$  and  $y$  current components for each harmonic order in Amps for the  $i$ -th ASD can be expressed as a function of the drive percentage loading level “ $p$ ” via the following equations:

$$I_{i-x} = g_{i-x}(p) = C_{5ix}p^5 + C_{4ix}p^4 + C_{3ix}p^3 + C_{2ix}p^2 + C_{1ix}p + C_{0ix} \quad (7.2)$$

$$I_{i-y} = g_{i-y}(p) = C_{5iy}p^5 + C_{4iy}p^4 + C_{3iy}p^3 + C_{2iy}p^2 + C_{1iy}p + C_{0iy} \quad (7.3)$$

The polynomial is chosen of the 5th order since the obtained least square error is minimum with this order and the corresponding values represent well the original curves without any need to increase the order to get improved values.

Harmonics above the 25th order are ignored in the study since their magnitudes are not considerable. Figures 7.4 and 7.5 show the relationships between the real and imaginary parts of the individual harmonic currents and the loading level for 150 HP ASD. The figures present the values obtained from the drive simulation and those obtained by curve fitting according to equations (7.2) and (7.3).

It can be shown that the resolved  $x$  and  $y$  harmonic current components are entirely determined by the loading level. This feature allows the deterministic ASD model to be easily extended to a probabilistic model by considering the loading level as a random variable. Therefore, the  $x$  and  $y$  harmonic current components become functions of the loading level and are also random variables.



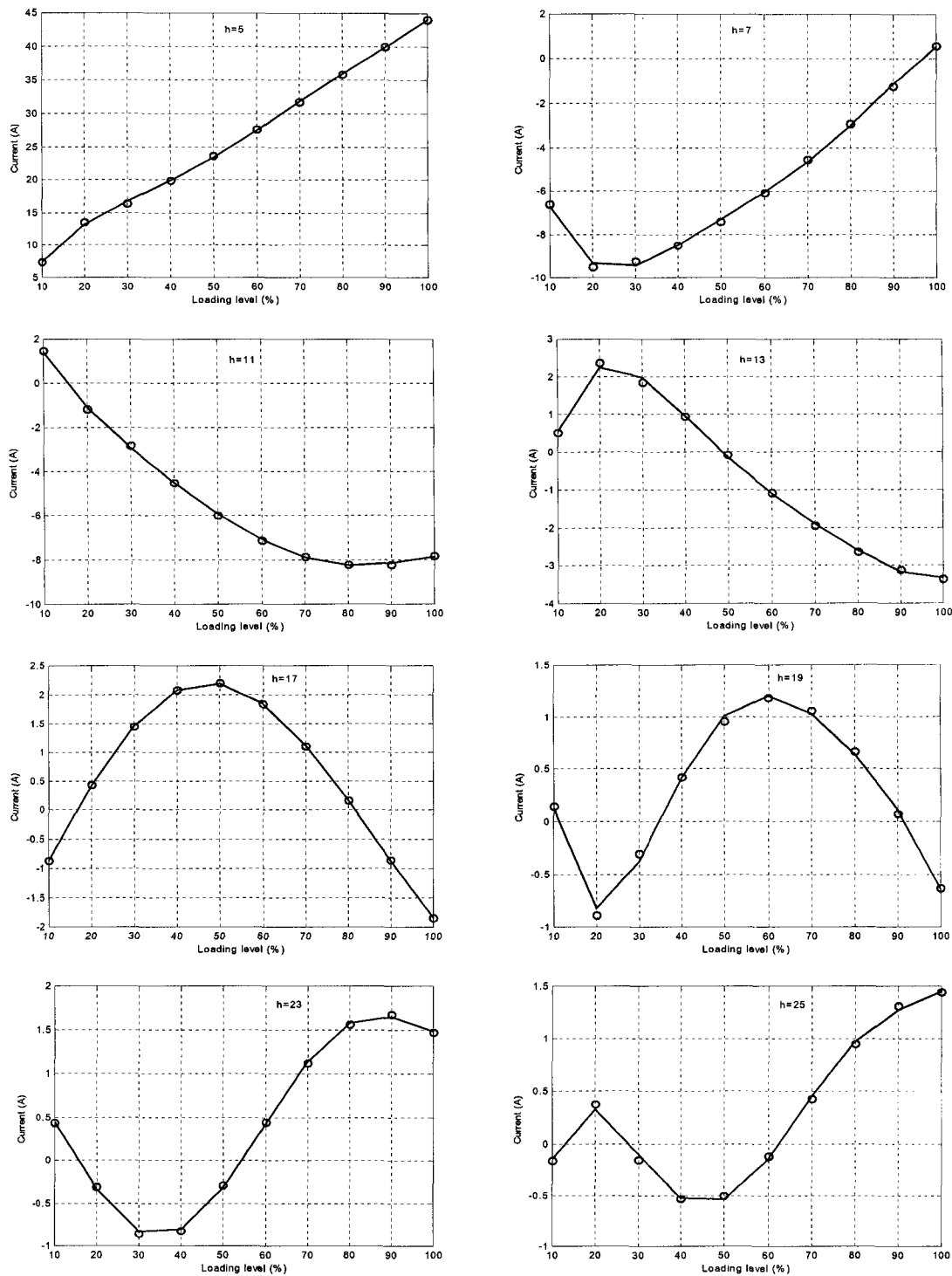


Figure 7.4: Variation of the real input harmonic current components with loading level for 150HP ASD.

Solid line represents the simulation results. Circles represent the points obtained by curve fitting.

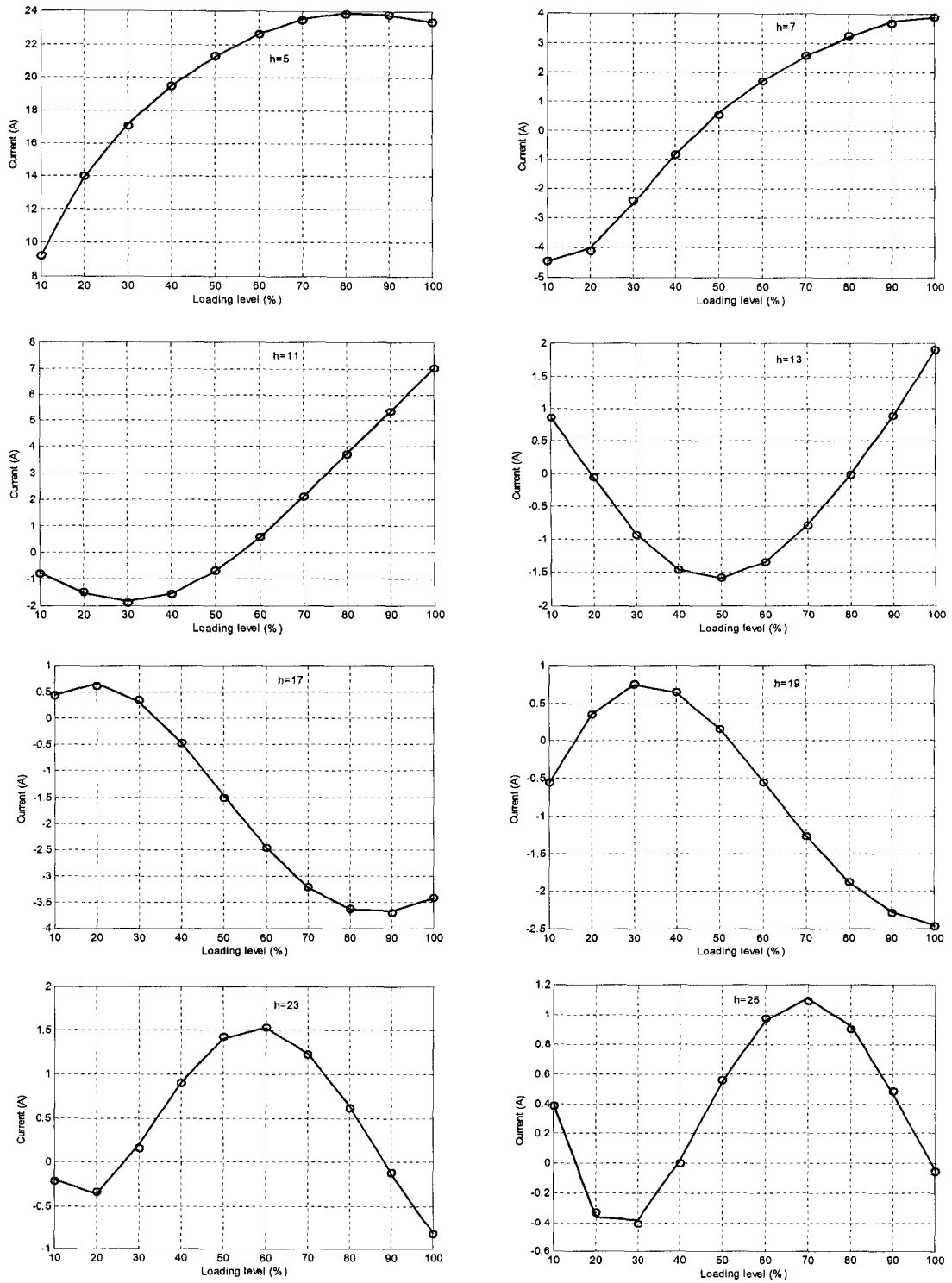


Figure 7.5: Variation of the imaginary input harmonic current components with loading level for 150HP ASD.

### Computing Harmonic Current Statistics of ASDs

With the assumption that the randomness of the loading variation of the  $i$ -th ASD is subjected to a uniform distribution between two limits  $p_{i-min}$  and  $p_{i-max}$ , the probability density function of the loading  $f_i(p)$  can be written as:

$$f_i(p) = \frac{1}{p_{i-max} - p_{i-min}} = \frac{1}{\Delta p_i} \quad (7.4)$$

The statistical parameters of the  $x$  and  $y$  harmonic components of the  $i$ -th ASD load current can be obtained as follows:

- Mean of  $I_{i-x}$  component:

$$E(I_{i-x}) = \mu_{I_{i-x}} = \int_{p_{i-min}}^{p_{i-max}} I_{i-x} f_i(p) dp = \frac{1}{\Delta p_i} \int_{p_{i-min}}^{p_{i-max}} g_{i-x}(p) dp \quad (7.5)$$

- Mean of  $I_{i-y}$  component:

$$E(I_{i-y}) = \mu_{I_{i-y}} = \int_{p_{i-min}}^{p_{i-max}} I_{i-y} f_i(p) dp = \frac{1}{\Delta p_i} \int_{p_{i-min}}^{p_{i-max}} g_{i-y}(p) dp \quad (7.6)$$

- Variance of  $I_{i-x}$  component:

$$\begin{aligned} \sigma_{i-x}^2 &= E(I_{i-x}^2) - E^2(I_{i-x}) = \int_{p_{i-min}}^{p_{i-max}} I_{i-x}^2 f_i(p) dp - E^2(I_{i-x}) = \\ &= \frac{1}{\Delta p_i} \int_{p_{i-min}}^{p_{i-max}} g_{i-x}^2(p) dp - \mu_{I_{i-x}}^2 \end{aligned} \quad (7.7)$$

- Variance of  $I_{i-y}$  component:

$$\begin{aligned} \sigma_{i-y}^2 &= E(I_{i-y}^2) - E^2(I_{i-y}) = \int_{p_{i-min}}^{p_{i-max}} I_{i-y}^2 f_i(p) dp - E^2(I_{i-y}) = \\ &= \frac{1}{\Delta p_i} \int_{p_{i-min}}^{p_{i-max}} g_{i-y}^2(p) dp - \mu_{I_{i-y}}^2 \end{aligned} \quad (7.8)$$

- Correlation coefficient of  $I_{i-x}$  and  $I_{i-y}$  components is given by:

$$\rho_{I_{i-x}I_{i-y}} = \frac{\text{cov}(I_{i-x}, I_{i-y})}{\sigma_{I_{i-x}} \sigma_{I_{i-y}}} = \frac{E(I_{i-x}I_{i-y}) - \mu_{I_{i-x}}\mu_{I_{i-y}}}{\sigma_{I_{i-x}} \sigma_{I_{i-y}}} \quad (7.9)$$

where

$$E(I_{i-x}I_{i-y}) = \int_{p_{i-\min}}^{p_{i-\max}} I_{i-x} I_{i-y} f_i(p) dp = \frac{1}{\Delta p_i} \int_{p_{i-\min}}^{p_{i-\max}} g_{i-x}(p) g_{i-y}(p) dp \quad (7.10)$$

Equations (7.5) to (7.10) give the mean values, variances, and correlation coefficient of the resolved harmonic current components,  $I_{i-x}$  and  $I_{i-y}$ , generated by each individual ASD.

### 7.3.2 Probabilistic Bus Harmonic Voltages

Most studies in the area of probabilistic modeling of harmonics primarily focused on the summation of harmonic currents at one point [38,46,47]. However, harmonic sources are virtually distributed across the entire system distribution feeder. Few publications dealt with such a situation where the statistical parameters of harmonic voltages can be handled in a way similar to that in which the harmonic sources are assumed to be concentrated at a point of summation [39,40].

Previous research work has shown that for a sufficiently large number of independent and random nonlinear loads connected to a bus, the resolved rectangular components of the total  $h$ -th harmonic current phasor injected into that bus would have a jointly normal probability density function (jpdf). This is irrespective of the random behavior of the individual loads. In addition, if enough nonlinear loads are distributed throughout a power network, the rectangular components of the system harmonic voltages approach jointly normal pdfs regardless the random characteristic of the loads. With knowledge of only the marginal means, marginal variances, and correlation coefficient of the rectangular components of each injected harmonic current phasor, the statistical parameters of the rectangular components, first and second order joint

moments, of the harmonic voltages can be analytically determined [40,45]. These moments define the random behavior of the system harmonic voltages in terms of the joint pdfs of the rectangular components. Therefore, the probabilistic harmonic voltage magnitude at system buses can be obtained irrespective of the joint pdfs of the rectangular components of each individual harmonic current.

Having harmonic sources distributed within the network, the system bus voltages for each harmonic order arising out of the harmonic current sources can be determined by the nodal equations in matrix form as follows:

$$[V] = [Z][I] \quad (7.11)$$

where  $[Z]$  is the system bus impedance matrix and  $[V]$  and  $[I]$  are vectors of random system bus harmonic voltage phasors and injected harmonic current phasors.

For a power network with  $m$  buses, expanding the above matrix equation yields:

$$\begin{bmatrix} V_1 \\ V_2 \\ \cdot \\ \cdot \\ V_k \\ \cdot \\ \cdot \\ V_m \end{bmatrix} = \begin{bmatrix} Z_{11} & Z_{12} & \cdot & \cdot & Z_{1k} & \cdot & \cdot & Z_{1m} \\ Z_{21} & Z_{22} & \cdot & \cdot & Z_{2k} & \cdot & \cdot & Z_{2m} \\ \cdot & \cdot & \cdot & \cdot & \cdot & \cdot & \cdot & \cdot \\ \cdot & \cdot & \cdot & \cdot & \cdot & \cdot & \cdot & \cdot \\ Z_{k1} & Z_{k2} & \cdot & \cdot & Z_{kk} & \cdot & \cdot & Z_{km} \\ \cdot & \cdot & \cdot & \cdot & \cdot & \cdot & \cdot & \cdot \\ \cdot & \cdot & \cdot & \cdot & \cdot & \cdot & \cdot & \cdot \\ Z_{m1} & Z_{m2} & \cdot & \cdot & Z_{mk} & \cdot & \cdot & Z_{mm} \end{bmatrix} \begin{bmatrix} I_1 \\ I_2 \\ \cdot \\ \cdot \\ I_k \\ \cdot \\ \cdot \\ I_m \end{bmatrix} \quad (7.12)$$

where  $I_k$  is the harmonic current injected at bus  $k$  and  $V_k$  is the harmonic voltage at that bus. The impedance  $Z_{ki}$  is the transfer impedance between buses  $k$  and  $i$  ( $k \neq i$ ) or the driving point impedance at bus  $k$  ( $k = i$ ). With the presence of  $N$  harmonic sources, there will only be  $N$  nonzero terms to form the harmonic voltage at each bus. The harmonic voltage at bus  $k$  due to  $N$  harmonic sources is expressed as:

$$V_k = Z_{k1}I_1 + Z_{k2}I_2 + \dots + Z_{kk}I_k + \dots + Z_{kN}I_N = V_{k1} + V_{k2} + \dots + V_{kk} + \dots + V_{kN} \quad (7.13)$$

With the assumption of independent harmonic sources, the harmonic voltage is a sum of weighted independent harmonic currents. The pdf of each voltage component is equal to the pdf of the corresponding current but scaled in magnitude and phase according to its transfer impedance. In this way, the probabilistic evaluation of the harmonic voltage  $V_k$  can be reduced to the study of the statistical properties of the resultant sum of many random vectors. Equation (7.13) can be rewritten in the following rectangular form:

$$V_k = V_{k-x} + jV_{k-y} = (V_{k1-x} + \dots + V_{kN-x}) + j(V_{k1-y} + \dots + V_{kN-y}) = \sum_{i=1}^N V_{ki-x} + j \sum_{i=1}^N V_{ki-y} \quad (7.14)$$

### Computing Harmonic Voltage Statistics

The contents of the  $x$  and  $y$  harmonic voltage components at bus  $k$  due to the harmonic current produced by the  $i$ -th ASD can be expressed as follows:

$$V_{ki-x} = R_{ki}I_{i-x} - X_{ki}I_{i-y} \quad (7.15)$$

$$V_{ki-y} = X_{ki}I_{i-x} + R_{ki}I_{i-y} \quad (7.16)$$

where  $R_{ki}$  and  $X_{ki}$  are the resistance and reactance of  $Z_{ki}$ .

With the random variation of the ASD loading level, the statistical parameters of the harmonic current rectangular components ( $I_{i-x}$ ,  $I_{i-y}$ ) can be determined as shown in the previous subsection. Accordingly, the means, variances, and correlation coefficient of the harmonic voltage components ( $V_{i-x}$ ,  $V_{i-y}$ ) can be calculated based on those of the corresponding current rectangular components using the following equations:

- Mean of  $V_{ki-x}$  component:

$$\mu_{V_{ki-x}} = R_{ki}\mu_{I_{i-x}} - X_{ki}\mu_{I_{i-y}} \quad (7.17)$$

- Mean of  $V_{ki-y}$  component:

$$\mu_{V_{ki-y}} = X_{ki}\mu_{I_{i-x}} + R_{ki}\mu_{I_{i-y}} \quad (7.18)$$

- Variance of  $V_{ki-x}$  component:

$$\begin{aligned}\sigma_{V_{ki-x}}^2 &= E(V_{ki-x}^2) - E^2(V_{ki-x}) = E(R_{ki}I_{i-x} - X_{ki}I_{i-y})^2 - (R_{ki}\mu_{i-x} - X_{ki}\mu_{i-y})^2 = \\ &R_{ki}^2 E(I_{i-x}^2) + X_{ki}^2 E(I_{i-y}^2) - 2R_{ki}X_{ki}E(I_{i-x}I_{i-y}) - (R_{ki}^2\mu_{i-x}^2 + X_{ki}^2\mu_{i-y}^2 - 2R_{ki}X_{ki}\mu_{i-x}\mu_{i-y}) = \\ &R_{ki}^2(E(I_{i-x}^2) - \mu_{i-x}^2) + X_{ki}^2(E(I_{i-y}^2) - \mu_{i-y}^2) - 2R_{ki}X_{ki}(E(I_{i-x}I_{i-y}) - \mu_{i-x}\mu_{i-y})\end{aligned}$$

Therefore, we can get the following:

$$\sigma_{V_{ki-x}}^2 = R_{ki}^2\sigma_{I_{i-x}}^2 + X_{ki}^2\sigma_{I_{i-y}}^2 - 2R_{ki}X_{ki}\rho_{I_{i-x}I_{i-y}}\sigma_{I_{i-x}}\sigma_{I_{i-y}} \quad (7.19)$$

- Variance of  $V_{ki-y}$  component:

$$\begin{aligned}\sigma_{V_{ki-y}}^2 &= E(V_{ki-y}^2) - E^2(V_{ki-y}) = E(X_{ki}I_{i-x} + R_{ki}I_{i-y})^2 - (X_{ki}\mu_{i-x} + R_{ki}\mu_{i-y})^2 = \\ &X_{ki}^2 E(I_{i-x}^2) + R_{ki}^2 E(I_{i-y}^2) + 2R_{ki}X_{ki}E(I_{i-x}I_{i-y}) - (X_{ki}^2\mu_{i-x}^2 + R_{ki}^2\mu_{i-y}^2 + 2R_{ki}X_{ki}\mu_{i-x}\mu_{i-y}) = \\ &X_{ki}^2(E(I_{i-x}^2) - \mu_{i-x}^2) + R_{ki}^2(E(I_{i-y}^2) - \mu_{i-y}^2) + 2R_{ki}X_{ki}(E(I_{i-x}I_{i-y}) - \mu_{i-x}\mu_{i-y})\end{aligned}$$

So, we obtain the following:

$$\sigma_{V_{ki-y}}^2 = X_{ki}^2\sigma_{I_{i-x}}^2 + R_{ki}^2\sigma_{I_{i-y}}^2 + 2R_{ki}X_{ki}\rho_{I_{i-x}I_{i-y}}\sigma_{I_{i-x}}\sigma_{I_{i-y}} \quad (7.20)$$

- Correlation coefficient of  $V_{ki-x}$  and  $V_{ki-y}$  components is calculated as follows:

$$\rho_{V_{ki-x}, V_{ki-y}} = \frac{\text{cov}(V_{ki-x}, V_{ki-y})}{\sigma_{V_{ki-x}}\sigma_{V_{ki-y}}} \quad (7.21)$$

where

$$\begin{aligned}\text{cov}(V_{ki-x}, V_{ki-y}) &= E(V_{ki-x}V_{ki-y}) - \mu_{V_{ki-x}}\mu_{V_{ki-y}} = \\ &E[(R_{ki}I_{i-x} - X_{ki}I_{i-y})(X_{ki}I_{i-x} + R_{ki}I_{i-y})] - (R_{ki}\mu_{i-x} - X_{ki}\mu_{i-y})(X_{ki}\mu_{i-x} + R_{ki}\mu_{i-y}) = \\ &E[R_{ki}X_{ki}(I_{i-x}^2 - I_{i-y}^2) + (R_{ki}^2 - X_{ki}^2)I_{i-x}I_{i-y}] - R_{ki}X_{ki}(\mu_{i-x}^2 - \mu_{i-y}^2) - (R_{ki}^2 - X_{ki}^2)\mu_{i-x}\mu_{i-y} = \\ &R_{ki}X_{ki}[E(I_{i-x}^2 - I_{i-y}^2) - (\mu_{i-x}^2 - \mu_{i-y}^2)] + (R_{ki}^2 - X_{ki}^2)[E(I_{i-x}I_{i-y}) - \mu_{i-x}\mu_{i-y}]\end{aligned}$$

Therefore, the covariance of  $V_{ki-x}$  and  $V_{ki-y}$  can be obtained by:

$$\text{cov}(V_{ki-x}, V_{ki-y}) = R_{ki}X_{ki}(\sigma_{I_{i-x}}^2 - \sigma_{I_{i-y}}^2) + (R_{ki}^2 - X_{ki}^2)\rho_{I_{i-x}I_{i-y}}\sigma_{I_{i-x}}\sigma_{I_{i-y}} \quad (7.22)$$

It can be shown from equation (7.14) that the resultant  $x$  and  $y$  harmonic voltage components are a sum of independent and random variables provided the harmonic currents are independent. Thus, the statistical parameters of the resultant rectangular components of the harmonic voltage at bus  $k$  ( $V_{k-x}$ ,  $V_{k-y}$ ) can be obtained using the following relationships:

$$\mu_{V_{k-x}} = \sum_{i=1}^N \mu_{V_{ki-x}}, \quad \mu_{V_{k-y}} = \sum_{i=1}^N \mu_{V_{ki-y}} \quad (7.23)$$

$$\sigma_{V_{k-x}}^2 = \sum_{i=1}^N \sigma_{V_{ki-x}}^2, \quad \sigma_{V_{k-y}}^2 = \sum_{i=1}^N \sigma_{V_{ki-y}}^2 \quad (7.24)$$

In addition, the covariance of the two sums  $V_{k-x}$  and  $V_{k-y}$  is equal to the sum of the covariances of the corresponding components  $V_{ki-x}$  and  $V_{ki-y}$  as follows:

$$\text{cov}(V_{k-x}, V_{k-y}) = \sum_{i=1}^N \text{cov}(V_{ki-x}, V_{ki-y}) \quad (7.25)$$

Hence, the correlation coefficient of  $V_{k-x}$  and  $V_{k-y}$  is given by:

$$\rho_{V_{k-x}, V_{k-y}} = \frac{\text{cov}(V_{k-x}, V_{k-y})}{\sigma_{V_{k-x}} \sigma_{V_{k-y}}} = \frac{\sum_{i=1}^N \rho_{V_{ki-x}, V_{ki-y}} \sigma_{V_{ki-x}} \sigma_{V_{ki-y}}}{\sigma_{V_{k-x}} \sigma_{V_{k-y}}} \quad (7.26)$$

In case when the number of independent random harmonic vectors  $N$  is sufficiently large, the bivariate normal distribution (BND) model can be applied. By virtue of the Central Limit Theorem, the sums of the rectangular components of the harmonic voltage will follow a normal distribution irrespective of the nature of the pdfs of the individual  $x$  and  $y$  components. Therefore, the pdfs of resultant rectangular components ( $V_{k-x}$ ,  $V_{k-y}$ ) can be given by:

$$f(V_{k-x}) = \frac{e^{-\frac{(V_{k-x} - \mu_{V_{k-x}})^2}{2\sigma_{V_{k-x}}^2}}}{\sigma_{V_{k-x}} \sqrt{2\pi}}, \quad f(V_{k-y}) = \frac{e^{-\frac{(V_{k-y} - \mu_{V_{k-y}})^2}{2\sigma_{V_{k-y}}^2}}}{\sigma_{V_{k-y}} \sqrt{2\pi}} \quad (7.27)$$



Moreover, the resultant rectangular components are approximately jointly normal with a joint normal pdf as follows:

$$f(V_{k-x}, V_{k-y}) = \frac{e^{-\frac{\eta}{2(1-\rho_{V_{k-x}V_{k-y}}^2)}}}{2\pi\sigma_{V_{k-x}}\sigma_{V_{k-y}}\sqrt{1-\rho_{V_{k-x}V_{k-y}}^2}} \quad (7.28)$$

where  $\eta$  can be defined as follows [18,40,41]:

$$\eta = \frac{(V_{k-x} - \mu_{V_{k-x}})^2}{\sigma_{V_{k-x}}^2} - \frac{2\rho_{V_{k-x}V_{k-y}}(V_{k-x} - \mu_{V_{k-x}})(V_{k-y} - \mu_{V_{k-y}})}{\sigma_{V_{k-x}}\sigma_{V_{k-y}}} + \frac{(V_{k-y} - \mu_{V_{k-y}})^2}{\sigma_{V_{k-y}}^2} \quad (7.29)$$

From the aforementioned, it can be inferred that the five statistical parameters that identify the joint pdf of the harmonic voltage rectangular components are determined by the corresponding parameters of the harmonic current rectangular components of each ASD load.

#### Calculation of the Probability Density Function of the Harmonic Voltage Magnitude

In order to assess the pdf of the harmonic voltage magnitude, the joint pdf is transformed into the polar form by expressing the harmonic voltage rectangular components through the corresponding magnitude “ $V$ ” and phase angle “ $\theta$ ”, where  $V_{k-x} = V \cos \theta$  and  $V_{k-y} = V \sin \theta$ . The pdf of the harmonic voltage phasor magnitude can be given by:

$$pdf(V) = \int_0^{2\pi} f(V \cos \theta, V \sin \theta) V d\theta \quad (7.30)$$

This integration can be solved numerically for the evaluation of the probability density function. The cumulative distribution function (cdf) can be obtained by integrating the voltage magnitude pdf as follows:

$$cdf(V) = \int pdf(V) dV \quad (7.31)$$

The cdf of a random variable indicates the probability that the variable is less than or equal to a given value such as the 50% or 95% non-exceeding probability.

### 7.3.3 Probabilistic Branch Harmonic Currents

Due to the random characteristic of the system bus harmonic voltages, the branch harmonic currents are also randomly varying. The harmonic current flowing from bus  $i$  to bus  $k$  is give by:

$$I_{(i-k)} = \frac{V_i - V_k}{Z_{i-k}} = \frac{V_{i-x} + jV_{i-y} - (V_{k-x} + jV_{k-y})}{r_{i-k} + jx_{i-k}} = \frac{V_{i-x} - V_{k-x} + j(V_{i-y} - V_{k-y})}{r_{i-k} + jx_{i-k}} =$$

$$\frac{1}{r_{i-k}^2 + x_{i-k}^2} [(V_{i-x} - V_{k-x} + j(V_{i-y} - V_{k-y}))(r_{i-k} - jx_{i-k})] = \quad (7.32)$$

$$\frac{1}{r_{i-k}^2 + x_{i-k}^2} [r_{i-k}(V_{i-x} - V_{k-x}) + x_{i-k}(V_{i-y} - V_{k-y}) + j(r_{i-k}(V_{i-y} - V_{k-y}) - x_{i-k}(V_{i-x} - V_{k-x}))]$$

where  $r_{i-k}$  and  $x_{i-k}$  are the resistance and reactance components of the harmonic impedance of link between buses  $i$  and  $k$ . The  $x$  and  $y$  components of the branch harmonic current can be obtained as follows:

$$I_{(i-k)-x} = \frac{1}{r_{i-k}^2 + x_{i-k}^2} [r_{i-k}(V_{i-x} - V_{k-x}) + x_{i-k}(V_{i-y} - V_{k-y})] \quad (7.33)$$

$$I_{(i-k)-y} = \frac{1}{r_{i-k}^2 + x_{i-k}^2} [r_{i-k}(V_{i-y} - V_{k-y}) - x_{i-k}(V_{i-x} - V_{k-x})] \quad (7.34)$$

- Mean of  $I_{(i-k)-x}$  component:

$$\mu_{I_{(i-k)-x}} = E(I_{(i-k)-x}) = \frac{1}{r_{i-k}^2 + x_{i-k}^2} [r_{i-k}(\mu_{V_{i-x}} - \mu_{V_{k-x}}) + x_{i-k}(\mu_{V_{i-y}} - \mu_{V_{k-y}})] \quad (7.35)$$

- Mean of  $I_{(i-k)-y}$  component:

$$\mu_{I_{(i-k)-y}} = E(I_{(i-k)-y}) = \frac{1}{r_{i-k}^2 + x_{i-k}^2} [r_{i-k}(\mu_{V_{i-y}} - \mu_{V_{k-y}}) - x_{i-k}(\mu_{V_{i-x}} - \mu_{V_{k-x}})] \quad (7.36)$$

The derivations to get the variances of the  $x$  and  $y$  harmonic current components and their correlation coefficient are included in Appendix B and the results are given as follows:

- Variance of  $I_{(i-k)-x}$  component:

$$\sigma_{I_{(i-k)-x}}^2 = \frac{1}{(r_{i-k}^2 + x_{i-k}^2)^2} \left[ \begin{array}{l} r_{i-k}^2 (\sigma_{V_{i-x}}^2 + \sigma_{V_{k-x}}^2) + x_{i-k}^2 (\sigma_{V_{i-y}}^2 + \sigma_{V_{k-y}}^2) - \\ 2r_{i-k}^2 \rho_{V_{i-x}V_{k-x}} \sigma_{V_{i-x}} \sigma_{V_{k-x}} - 2x_{i-k}^2 \rho_{V_{i-y}V_{k-y}} \sigma_{V_{i-y}} \sigma_{V_{k-y}} + \\ 2r_{i-k} x_{i-k} \left( \rho_{V_{i-x}V_{i-y}} \sigma_{V_{i-x}} \sigma_{V_{i-y}} + \rho_{V_{k-x}V_{k-y}} \sigma_{V_{k-x}} \sigma_{V_{k-y}} - \right. \\ \left. \rho_{V_{i-x}V_{k-y}} \sigma_{V_{i-x}} \sigma_{V_{k-y}} - \rho_{V_{k-x}V_{i-y}} \sigma_{V_{k-x}} \sigma_{V_{i-y}} \right) \end{array} \right] \quad (7.37)$$

- Variance of  $I_{(i-k)-y}$  component:

$$\sigma_{I_{(i-k)-y}}^2 = \frac{1}{(r_{i-k}^2 + x_{i-k}^2)^2} \left[ \begin{array}{l} r_{i-k}^2 (\sigma_{V_{i-y}}^2 + \sigma_{V_{k-y}}^2) + x_{i-k}^2 (\sigma_{V_{i-x}}^2 + \sigma_{V_{k-x}}^2) - \\ 2r_{i-k}^2 \rho_{V_{i-y}V_{k-y}} \sigma_{V_{i-y}} \sigma_{V_{k-y}} - 2x_{i-k}^2 \rho_{V_{i-x}V_{k-x}} \sigma_{V_{i-x}} \sigma_{V_{k-x}} - \\ 2r_{i-k} x_{i-k} \left( \rho_{V_{i-y}V_{i-x}} \sigma_{V_{i-y}} \sigma_{V_{i-x}} + \rho_{V_{k-y}V_{k-x}} \sigma_{V_{k-y}} \sigma_{V_{k-x}} - \right. \\ \left. \rho_{V_{i-y}V_{k-x}} \sigma_{V_{i-y}} \sigma_{V_{k-x}} - \rho_{V_{k-y}V_{i-x}} \sigma_{V_{k-y}} \sigma_{V_{i-x}} \right) \end{array} \right] \quad (7.38)$$

- Correlation coefficient of  $I_{(i-k)-x}$  and  $I_{(i-k)-y}$  components:

$$\rho_{I_{(i-k)-x}I_{(i-k)-y}} = \frac{\text{cov}(I_{(i-k)-x}, I_{(i-k)-y})}{\sigma_{I_{(i-k)-x}} \sigma_{I_{(i-k)-y}}} \quad (7.39)$$

where

$$\text{cov}(I_{(i-k)-x}, I_{(i-k)-y}) = \frac{1}{(r_{i-k}^2 + x_{i-k}^2)^2} \left[ \begin{array}{l} (r_{i-k}^2 - x_{i-k}^2) \left( \rho_{V_{i-x}V_{i-y}} \sigma_{V_{i-x}} \sigma_{V_{i-y}} + \rho_{V_{k-x}V_{k-y}} \sigma_{V_{k-x}} \sigma_{V_{k-y}} - \right. \\ \left. \rho_{V_{i-x}V_{k-y}} \sigma_{V_{i-x}} \sigma_{V_{k-y}} - \rho_{V_{k-x}V_{i-y}} \sigma_{V_{k-x}} \sigma_{V_{i-y}} \right) + \\ (r_{i-k} x_{i-k}) \left( (\sigma_{V_{i-y}}^2 + \sigma_{V_{k-y}}^2 - 2\rho_{V_{i-y}V_{k-y}} \sigma_{V_{i-y}} \sigma_{V_{k-y}}) - (\sigma_{V_{i-x}}^2 + \sigma_{V_{k-x}}^2 - 2\rho_{V_{i-x}V_{k-x}} \sigma_{V_{i-x}} \sigma_{V_{k-x}}) \right) \end{array} \right] \quad (7.40)$$

Calculating the variances and the correlation coefficient of the  $x$  and  $y$  branch harmonic current components implies the determination of the variances and a combination of correlation coefficients of the  $x$  and  $y$  harmonic voltage components. The correlation coefficient of the  $x$  and  $y$  harmonic voltage components at the same bus ( $i$  or  $k$ ) can be

determined via equation (7.26). The correlation coefficients of the other different harmonic voltage components can be obtained according to the derivations shown in Appendix B.

Since the  $x$  and  $y$  harmonic voltage components at system buses approach normal pdfs, the  $x$  and  $y$  components of branch harmonic currents also approach normal pdfs which are given by:

$$f(I_{(i-k)-x}) = \frac{e^{-\frac{(I_{(i-k)-x} - \mu_{I_{(i-k)-x}})^2}{2\sigma_{I_{(i-k)-x}}^2}}}{\sigma_{I_{(i-k)-x}} \sqrt{2\pi}}, \quad f(I_{(i-k)-y}) = \frac{e^{-\frac{(I_{(i-k)-y} - \mu_{I_{(i-k)-y}})^2}{2\sigma_{I_{(i-k)-y}}^2}}}{\sigma_{I_{(i-k)-y}} \sqrt{2\pi}} \quad (7.41)$$

The resultant rectangular components are approximately jointly normal with the following joint normal pdf:

$$f(I_{(i-k)-x}, I_{(i-k)-y}) = \frac{e^{-\frac{\lambda}{2(1-\rho_{I_{(i-k)-x}I_{(i-k)-y}}^2)}}}{2\pi\sigma_{I_{(i-k)-x}}\sigma_{I_{(i-k)-y}}\sqrt{1-\rho_{I_{(i-k)-x}I_{(i-k)-y}}^2}} \quad (7.42)$$

$$\text{where } \lambda = \frac{(I_{(i-k)-x} - \mu_{I_{(i-k)-x}})^2}{\sigma_{I_{(i-k)-x}}^2} + \frac{2\rho_{I_{(i-k)-x}I_{(i-k)-y}}(I_{(i-k)-x} - \mu_{I_{(i-k)-x}})(I_{(i-k)-y} - \mu_{I_{(i-k)-y}})}{\sigma_{I_{(i-k)-x}}\sigma_{I_{(i-k)-y}}} + \frac{(I_{(i-k)-y} - \mu_{I_{(i-k)-y}})^2}{\sigma_{I_{(i-k)-y}}^2} \quad (7.43)$$

By expressing the harmonic current rectangular components through the corresponding magnitude “ $I$ ” and phase angle “ $\phi$ ”, the pdf of the branch harmonic current magnitude can be given by:

$$pdf(I) = \int_0^{2\pi} f(I \cos \phi, I \sin \phi) I d\phi \quad (7.44)$$

where  $I_{(i-k)-x} = I \cos \phi$  and  $I_{(i-k)-y} = I \sin \phi$ .

The cumulative distribution function (cdf) can be obtained as follows:

$$cdf(I) = \int pdf(I) dI \quad (7.45)$$

Summary of the Main Procedure Required for Performing Probabilistic Harmonic Analysis

The main procedure for performing probabilistic harmonic analysis for systems with distributed random harmonic sources can be summarized as follows:

- 1) Determine the random variable that dominantly affects the harmonic source currents.
- 2) From the harmonic source deterministic model, the variation of harmonic current magnitudes and phase angle with the considered random variable should be obtained. Then, the relationships between the random variable and the real and imaginary harmonic current components can be developed.
- 3) Identify the pdf nature of the random variable. It is worth mentioning that uniform distribution is widely used as an acceptable approximation for most probabilistic studies.
- 4) Get the statistical parameters of the rectangular harmonic current components produced from different harmonic sources using steps 2 and 3.
- 5) Using the harmonic nodal equations, the corresponding statistical parameters of the rectangular components of system harmonic voltages can be calculated. Then, the probability density and cumulative distribution functions can be obtained to provide the probabilistic harmonic voltage magnitude.
- 6) The harmonic voltage statistical parameters and branch harmonic impedances are used to calculate the statistical parameters of the system branch harmonic current rectangular components to get the probabilistic harmonic current magnitude.

Some publications adopted the probabilistic approach considering different random variables that affect the generated harmonic currents. The main focus was on the summation of the injected currents at one point. Few publications extended this work to get the probabilistic system harmonic voltage magnitude when the harmonic sources are in different locations across the system. The supply voltage to the nonlinear load was assumed 1 per unit while obtaining the harmonic currents. Therefore, the harmonic nodal equations are directly implemented without scaling or shifting the harmonic currents

according to the actual supply voltage, which may be different from 1 per unit. In this research work, the analytical method is extended to get the probabilistic magnitude of branch harmonic currents. This implies deriving a combination of different correlation coefficients of the rectangular components of the system bus harmonic voltages. Besides, the analytical method is improved to have more accurate results. This is achieved by considering the system voltage profile and its impact on the injected harmonic currents.

#### 7.4 Results of Probabilistic Harmonic Voltage and Current Levels

The procedure in the previous section for calculating the probabilistic harmonic voltages and currents is applied to the Goose River system where 21 ASD loads are distributed across the system. A MATLAB program is written for this purpose. Four cases with different loading level limits are considered. The maximum loading limit for all cases is set at 100% for all drives. The minimum loading limit is set at 50, 60, 70, and 80% for all drives for the four cases respectively. However, the program is built such that it can handle the calculations with any specified loading limits for each drive. Considering the 100% as the maximum limit is logical to utilize the full capacity of the drives. Assuming the same minimum limit for all drives for each case would make it more obvious to observe the impact of the loading variation range on the pdfs of the harmonic levels.

Referring to the single-line diagram of the system in Chapter 6, the harmonic voltages at two buses, L1701 and L1711 are considered for the probabilistic study. The concerned harmonic currents are through two branches, L1700-L1701 and L1710-L1711. The means and standard deviations of the  $x$  and  $y$  components as well as their correlation coefficients are calculated. The statistical results of the 5th, 7th, 11th, and 13th harmonic voltages and currents are summarized in Tables 7.1 and 7.2 respectively. The mean values and standard deviations of the harmonic voltages are in percent of the base voltage and those of the harmonic currents are in Amps. These results are then used to derive the pdfs of the harmonic voltage and current magnitudes shown in Figures 7.6 and 7.7 respectively.

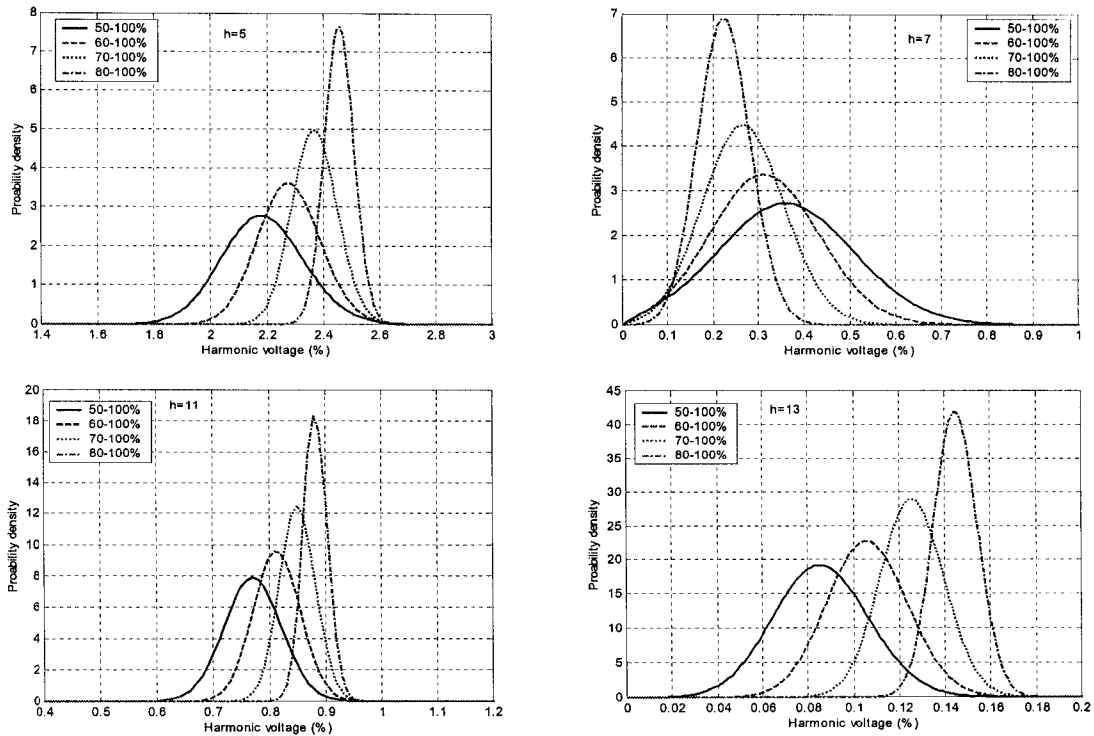
Table 7.1: Statistical parameters of harmonic voltage rectangular components

	Voltage at bus L1701 (%)					Voltage at bus L1711 (%)				
Case 1 (loading variation from 50-100%)										
h	$\mu_x$	$\mu_y$	$\sigma_x$	$\sigma_y$	$\rho_{xy}$	$\mu_x$	$\mu_y$	$\sigma_x$	$\sigma_y$	$\rho_{xy}$
5	0.517	-2.117	0.160	0.170	0.614	0.720	-2.852	0.217	0.229	0.616
7	0.296	0.196	0.130	0.101	0.628	0.387	0.272	0.174	0.136	0.639
11	0.716	-0.281	0.050	0.043	-0.083	0.961	-0.310	0.066	0.057	-0.025
13	0.081	0.021	0.020	0.020	0.282	0.110	0.038	0.025	0.030	0.241
Case 2 (loading variation from 60-100%)										
h	$\mu_x$	$\mu_y$	$\sigma_x$	$\sigma_y$	$\rho_{xy}$	$\mu_x$	$\mu_y$	$\sigma_x$	$\sigma_y$	$\rho_{xy}$
5	0.499	-2.220	0.133	0.130	0.603	0.697	-2.991	0.180	0.175	0.606
7	0.278	0.135	0.109	0.076	0.582	0.365	0.190	0.146	0.103	0.595
11	0.737	-0.342	0.041	0.035	-0.148	0.993	-0.388	0.054	0.045	-0.083
13	0.104	0.014	0.017	0.015	0.326	0.142	0.032	0.022	0.023	0.332
Case 3 (loading variation from 70-100%)										
h	$\mu_x$	$\mu_y$	$\sigma_x$	$\sigma_y$	$\rho_{xy}$	$\mu_x$	$\mu_y$	$\sigma_x$	$\sigma_y$	$\rho_{xy}$
5	0.475	-2.320	0.102	0.092	0.587	0.666	-3.126	0.139	0.125	0.589
7	0.253	0.074	0.085	0.055	0.520	0.333	0.108	0.113	0.074	0.536
11	0.748	-0.405	0.030	0.026	-0.216	1.012	-0.470	0.040	0.034	-0.151
13	0.125	0.004	0.014	0.011	0.323	0.172	0.021	0.018	0.016	0.380
Case 4 (loading variation from 80-100%)										
h	$\mu_x$	$\mu_y$	$\sigma_x$	$\sigma_y$	$\rho_{xy}$	$\mu_x$	$\mu_y$	$\sigma_x$	$\sigma_y$	$\rho_{xy}$
5	0.444	-2.416	0.070	0.059	0.564	0.625	-3.256	0.095	0.080	0.566
7	0.222	0.013	0.058	0.035	0.443	0.293	0.026	0.077	0.047	0.461
11	0.749	-0.466	0.020	0.018	-0.277	1.018	-0.550	0.027	0.023	-0.222
13	0.144	-0.008	0.010	0.006	0.263	0.199	0.006	0.013	0.010	0.376

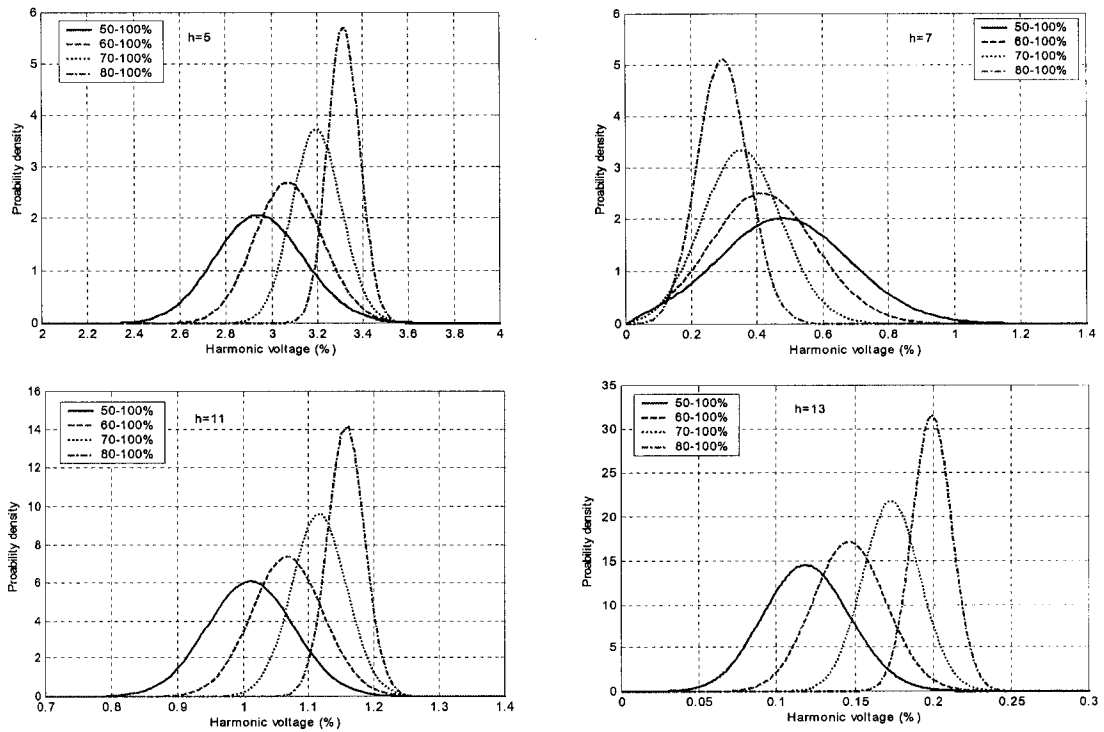
Table 7.2: Statistical parameters of harmonic current rectangular components

	Current through branch L1700-L1701 (A)					Current through branch L1710-L1711 (A)				
Case 1 (loading variation from 50-100%)										
h	$\mu_x$	$\mu_y$	$\sigma_x$	$\sigma_y$	$\rho_{xy}$	$\mu_x$	$\mu_y$	$\sigma_x$	$\sigma_y$	$\rho_{xy}$
5	5.962	2.172	0.525	0.432	-0.596	3.943	2.821	0.434	0.301	-0.547
7	-0.454	0.581	0.223	0.260	-0.647	-0.514	0.106	0.199	0.135	-0.615
11	0.319	0.953	0.056	0.066	0.068	-0.812	0.591	0.099	0.080	-0.105
13	-0.026	0.088	0.022	0.021	-0.279	-0.150	0.091	0.064	0.054	0.306
Case 2 (loading variation from 60-100%)										
h	$\mu_x$	$\mu_y$	$\sigma_x$	$\sigma_y$	$\rho_{xy}$	$\mu_x$	$\mu_y$	$\sigma_x$	$\sigma_y$	$\rho_{xy}$
5	6.265	2.154	0.402	0.361	-0.597	4.162	2.874	0.335	0.253	-0.569
7	-0.324	0.553	0.169	0.219	-0.613	-0.432	0.130	0.154	0.118	-0.639
11	0.398	0.984	0.045	0.054	0.131	-0.812	0.671	0.080	0.065	-0.193
13	-0.020	0.113	0.017	0.018	-0.333	-0.179	0.127	0.055	0.039	0.245
Case 3 (loading variation from 70-100%)										
h	$\mu_x$	$\mu_y$	$\sigma_x$	$\sigma_y$	$\rho_{xy}$	$\mu_x$	$\mu_y$	$\sigma_x$	$\sigma_y$	$\rho_{xy}$
5	6.563	2.114	0.288	0.280	-0.593	4.383	2.912	0.241	0.199	-0.582
7	-0.194	0.512	0.122	0.171	-0.564	-0.347	0.147	0.112	0.096	-0.640
11	0.479	1.002	0.034	0.040	0.201	-0.799	0.748	0.059	0.050	-0.276
13	-0.010	0.137	0.012	0.015	-0.342	-0.200	0.165	0.043	0.027	0.111
Case 4 (loading variation from 80-100%)										
h	$\mu_x$	$\mu_y$	$\sigma_x$	$\sigma_y$	$\rho_{xy}$	$\mu_x$	$\mu_y$	$\sigma_x$	$\sigma_y$	$\rho_{xy}$
5	6.851	2.056	0.185	0.192	-0.579	4.602	2.935	0.155	0.138	-0.582
7	-0.063	0.458	0.077	0.117	-0.502	-0.258	0.157	0.071	0.068	-0.639
11	0.559	1.008	0.023	0.026	0.268	-0.776	0.819	0.038	0.035	-0.343
13	0.002	0.158	0.007	0.010	-0.295	-0.214	0.203	0.030	0.017	-0.066



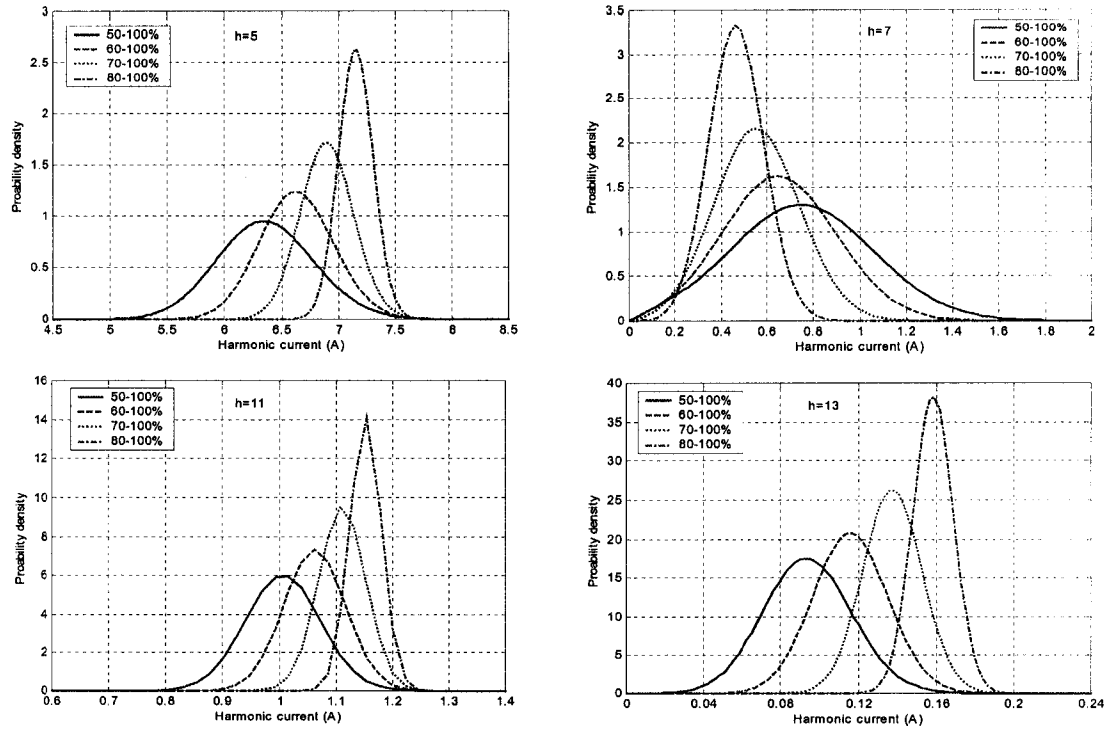


(a) Voltage at bus L1701

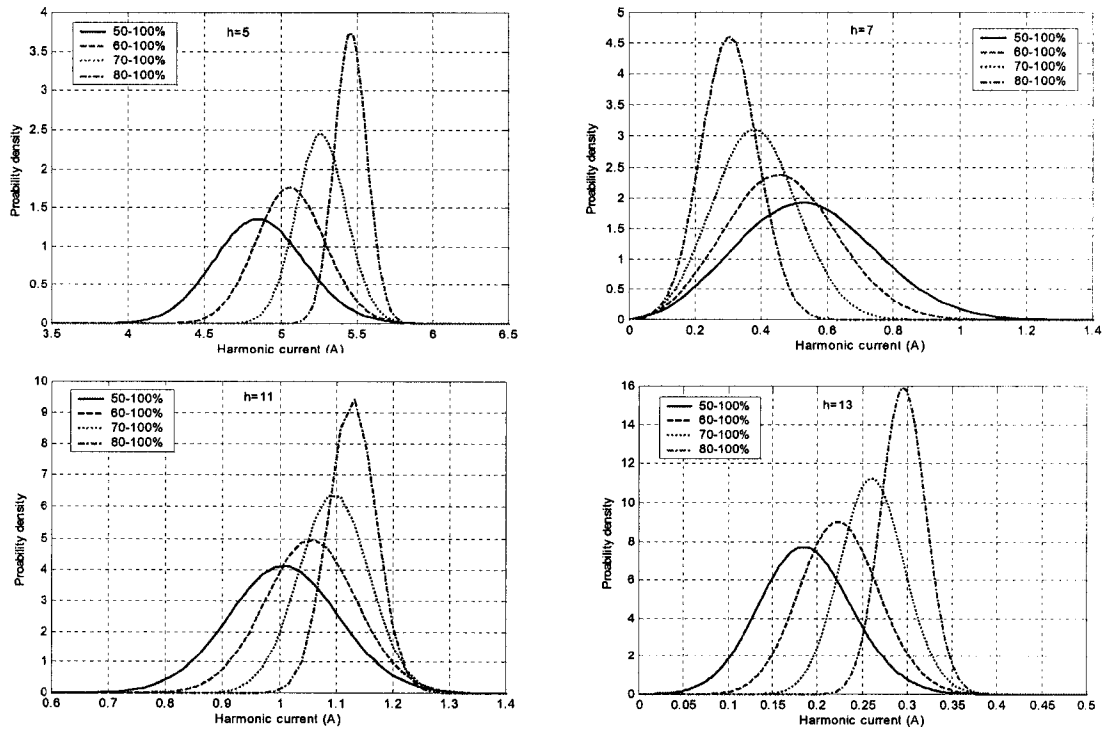


(b) Voltage at bus L1711

Figure 7.6: Probability density function curves of the harmonic voltage magnitudes.



(a) Current through branch L1700-L1701



(b) Current through branch L1710-L1711

Figure 7.7: Probability density function curves of the harmonic current magnitudes.

The figures reveal that the harmonic magnitudes are highly affected by the loading variation range. When the minimum loading limit increases, the harmonic voltages and currents increase except for the 7th harmonic order whose values decrease. Thus, reflecting the influence of the drive loading level on the input harmonic current magnitudes illustrated in Figure 7.3. Also, with the increase in the minimum loading limit, the spread of the results around the mean values becomes less as can be inferred from the standard deviations in Tables 7.1 and 7.2. This shows that in order to get accurate pdfs of the resultant harmonic voltage and current magnitudes produced by distributed varying load harmonic sources, care must be taken while identifying the interval of loading variation.

Accurate prediction of power system harmonic levels will provide important information to electric utility engineers and equipment designers. With random harmonic currents, assuming worst case situations when designing equipment may be too conservative and more costly. One of the potential applications of the probabilistic model of harmonic current injection and propagation is to set limitations of harmonic levels [35]. With the widespread use of distributed harmonic sources, harmonic levels are expected to increase to intolerable levels. Existing regulations generally do not reflect harmonic variations and their randomness in power systems. For example, the recommended IEEE Std. 519-1992 harmonic voltage and current limits are static and do not take into account the random behavior. Universal limits will be accepted after harmonic effects on equipment are quantified and well documented [36]. Further work on this subject is recommended.

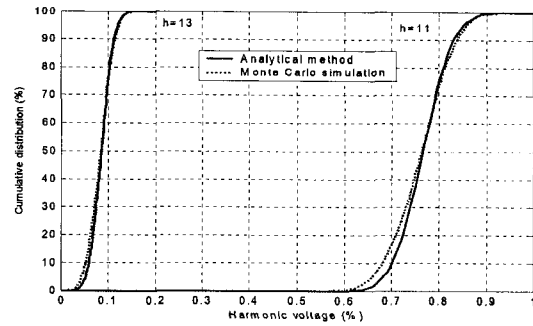
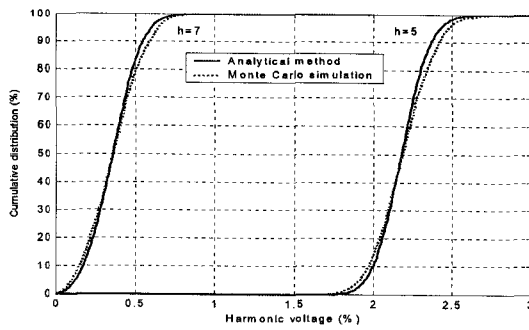
## 7.5 Comparison with Monte Carlo Simulation

In order to assess the reliability of the presented analytical method using the BND model, the results are compared with the Monte Carlo simulation. The Monte Carlo simulation is simply a repeated process of generating deterministic solutions to the problem, with each solution corresponding to a set of deterministic values of the random variables. It can

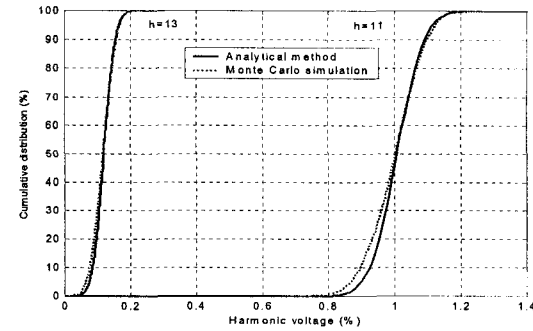
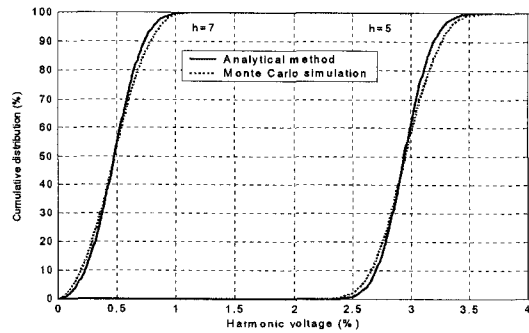
handle practically any statistical problem. A MATLAB computer program using the Monte Carlo simulation technique has been written to simulate the considered four cases of the drives loading variation for the Goose River system. All simulation runs have been made using 3,000 trials. The cumulative distribution functions (cdfs) of the harmonic voltage and current magnitudes calculated analytically by the BND model are shown in Figures 7.8 and 7.9 for cases 1 and 4 where the minimum loading limit is 50% and 80% respectively. In these figures, the cdfs obtained by the Monte Carlo simulation are also shown for comparison. It can be inferred that the two methods yield results that agree closely. This makes the analytical method a feasible approach to evaluate the probabilistic harmonic levels with randomly varying injected harmonic currents.

It is worth mentioning that the analytical results are obtained by employing the nodal equation (7.12) to calculate the harmonic voltages. The harmonic currents used in this equation are those obtained directly from the simulation for each individual drive at the nominal supply voltage, i.e., 1 per unit. Based on this voltage the statistical parameters of the drive harmonic currents are determined when performing the analytical method. Therefore, the Monte Carlo simulation is carried out using equation (7.12) in order to be able to compare the results with those obtained from the analytical method for verification, which is the main goal of the conducted analysis.

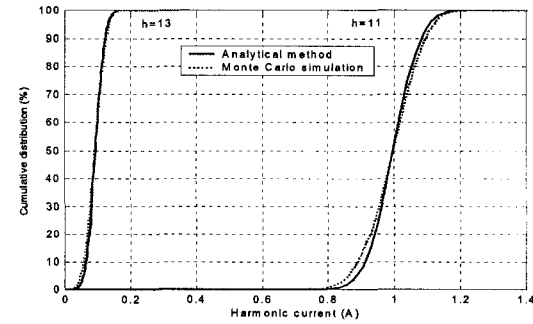
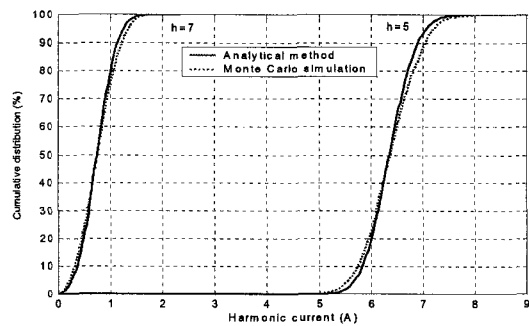
However, the obtained harmonic levels in this case can be considered approximated ones since it does not reflect the actual fundamental voltage level at each bus, which might be slightly different from 1 per unit when solving for the power flow. Figure 7.10 shows a comparison for case 1 when the Monte Carlo simulation is performed including the fundamental frequency power flow that provides the system fundamental voltages upon which the drive load fundamental current is determined. Consequently the harmonic currents are adjusted (rescaled and shifted) using equations (4.1) and (4.2). The difference in the results for some harmonics is clear. This is mainly due to the implementation of the analytical method assuming 1 per unit supply voltage. Therefore, for more accurate results, the analytical method should be improved by trying to include the system voltage profile effect into the probabilistic calculations.



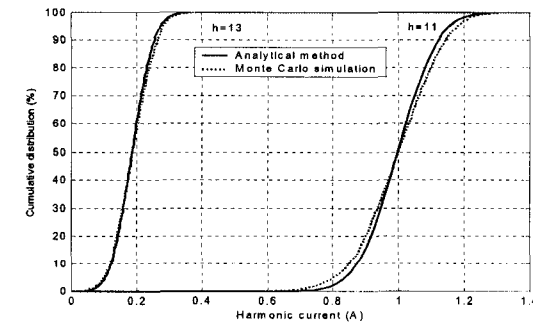
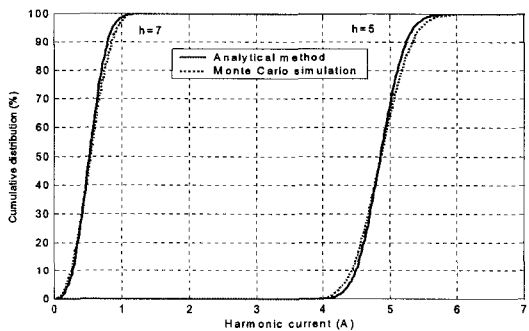
(a) Voltage at bus L1701



(b) Voltage at bus L1711

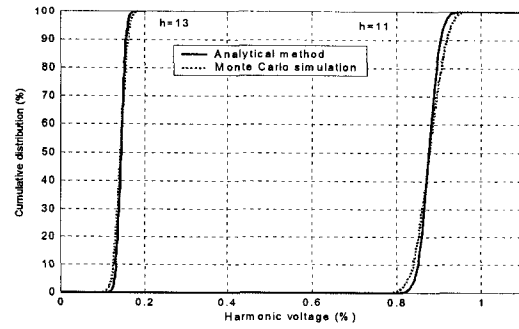
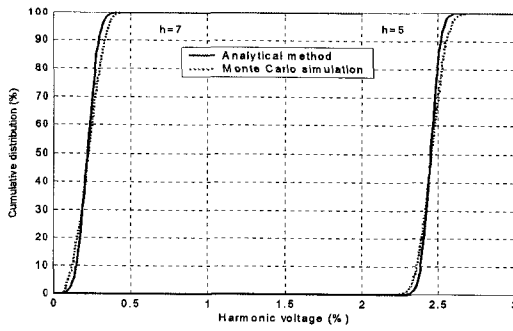


(c) Current through branch L1700-L1701

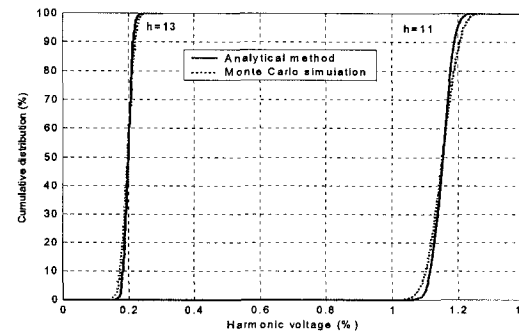
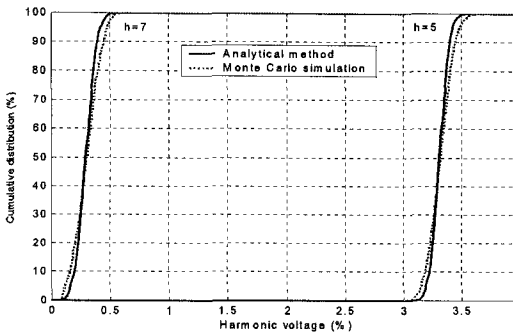


(d) Current through branch L1710-L1711

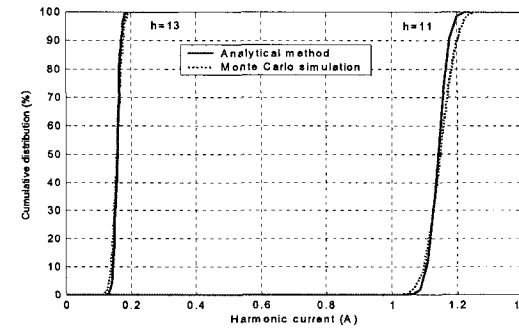
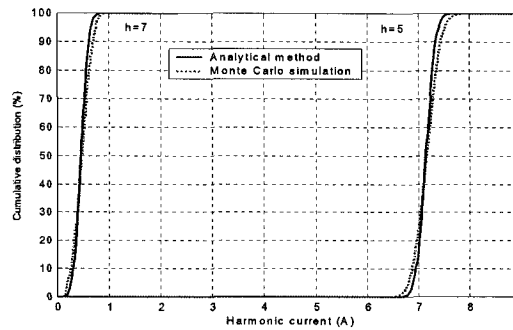
Figure 7.8: The cdfs of harmonic magnitudes obtained from the analytical method and Monte Carlo simulation using the nodal equation with loading variation from 50-100%.



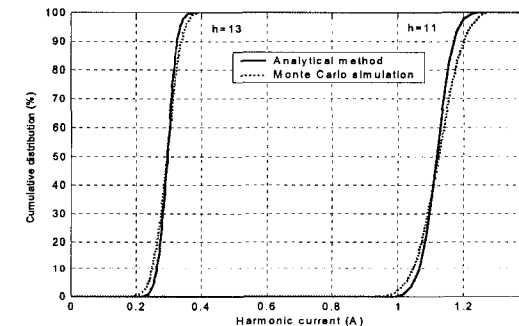
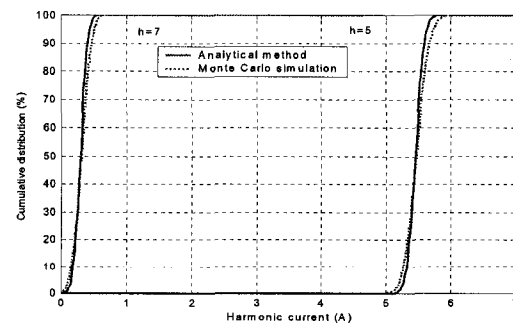
(a) Voltage at bus L1701



(b) Voltage at bus L1711

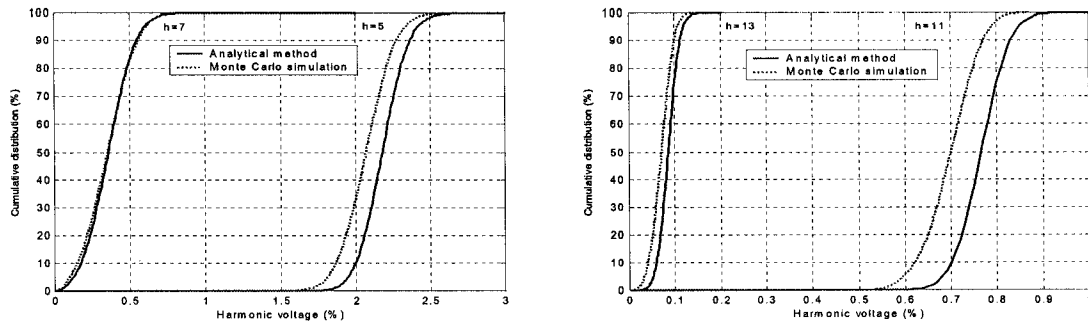


(c) Current through branch L1700-L1701

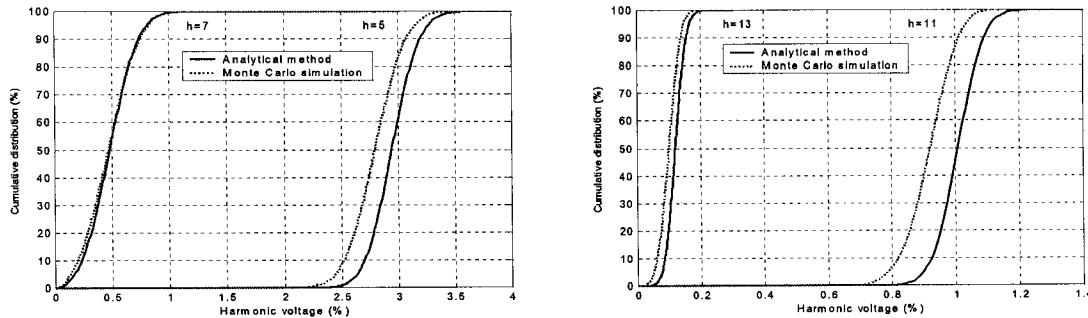


(d) Current through branch L1710-L1711

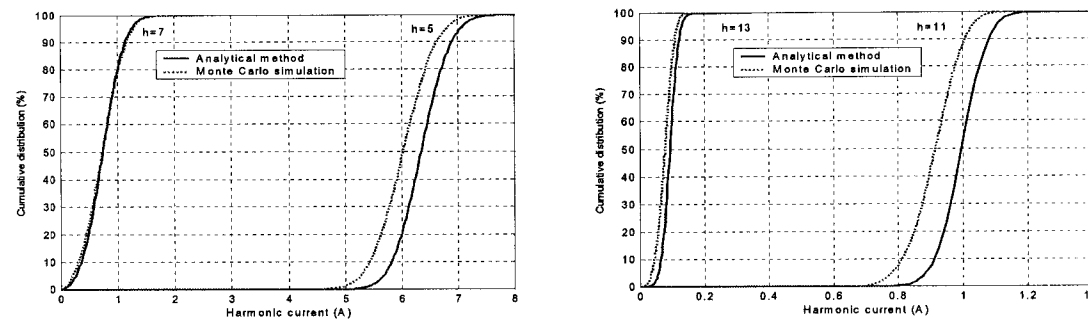
Figure 7.9: The cdfs of harmonic magnitudes obtained from the analytical method and Monte Carlo simulation using the nodal equation with loading variation from 80-100%.



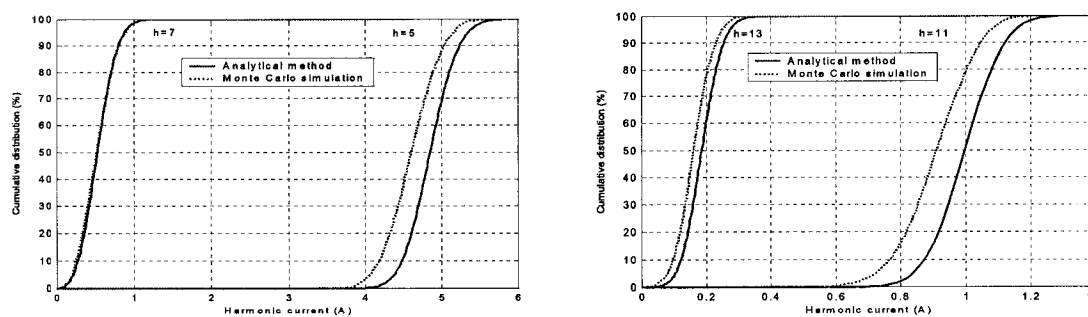
(a) Voltage at bus L1701



(b) Voltage at bus L1711



(c) Current through branch L1700-L1701



(d) Current through branch L1710-L1711

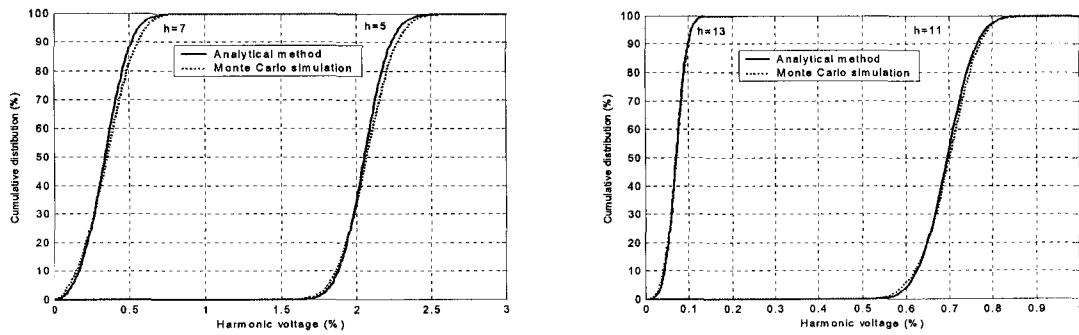
Figure 7.10: The cdfs of harmonic magnitudes obtained from the analytical method using the nodal equation and from the Monte Carlo simulation including the power flow analysis with loading variation from 50-100%.

### Improving the Analytical Method

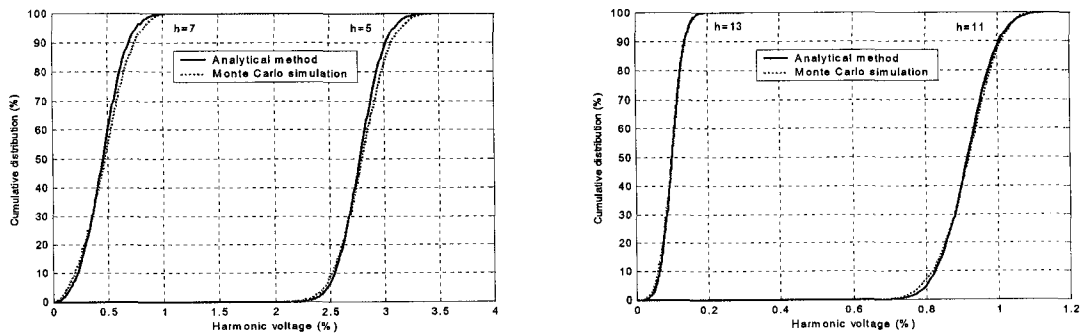
In order to improve the implementation of the analytical method to provide more accurate results, the harmonic current characteristics should be determined with the use of the power flow analysis to reflect the impact of the system voltage profile. This can be reasonably achieved by performing the fundamental and harmonic power flow assuming all drives are operating at the same loading level. This is repeated for different loading levels. The obtained harmonic currents are adjusted (rescaled and shifted) according to the results of the fundamental current of each individual drive using the harmonic current spectrum. This would constitute the modified harmonic currents at each loading level. It means the supply voltage of each drive at different loading is considered, so that more accurate ASD harmonic currents can be obtained, upon which the statistical parameters of the analytical method are calculated. In this way, the probabilistic program operates in conjunction with the power flow program. Therefore, the probabilistic harmonics calculated by the analytical method can be comparable to the results obtained by the Monte Carlo simulation including the power flow analysis.

This process involves some dependency among the harmonic currents for different drives since they are adjusted according to the respective fundamental current that is affected by the corresponding fundamental voltage. However, the assumption of independent harmonic currents that permits the application of the Central Limit Theorem is acceptable with the presence of enough number of harmonic sources and also because the dependency is of a minor effect on the harmonic current characteristics for each drive. The cdf curves of the harmonic voltage and current magnitudes for cases 1 and 4 are shown in Figures 7.11 and 7.12 respectively. It can be seen how the results obtained by the improved analytical method are close to those obtained by the Monte Carlo simulation. This affirms the validity of the analytical method. Besides, it shows how its improvement could lead to more accurate results. A comparison of simulated values and those calculated by the improved analytical method for the important points such as the 50% and 95% non-exceeding probability levels of the harmonic voltage and current magnitudes is given in Tables 7.3 and 7.4 respectively.

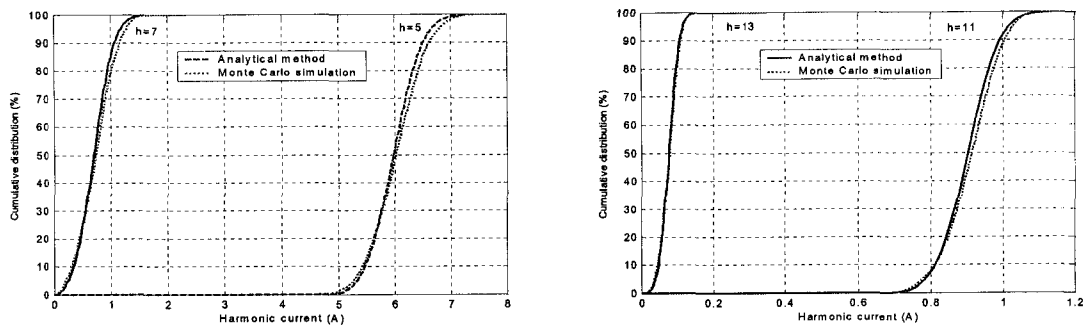




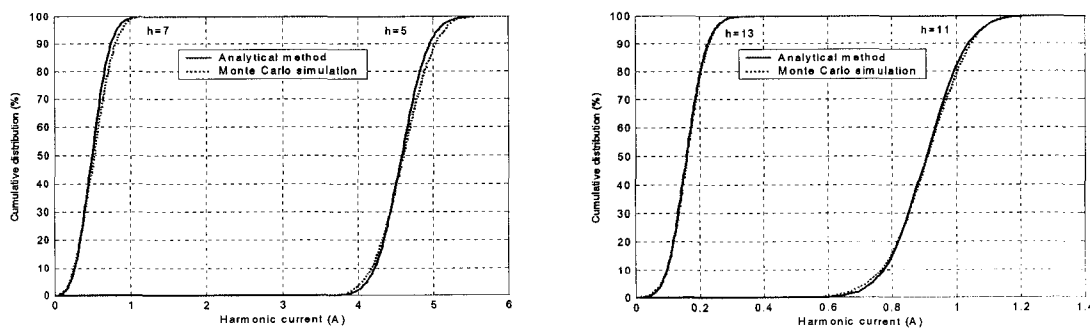
(a) Voltage at bus L1701



(b) Voltage at bus L1711

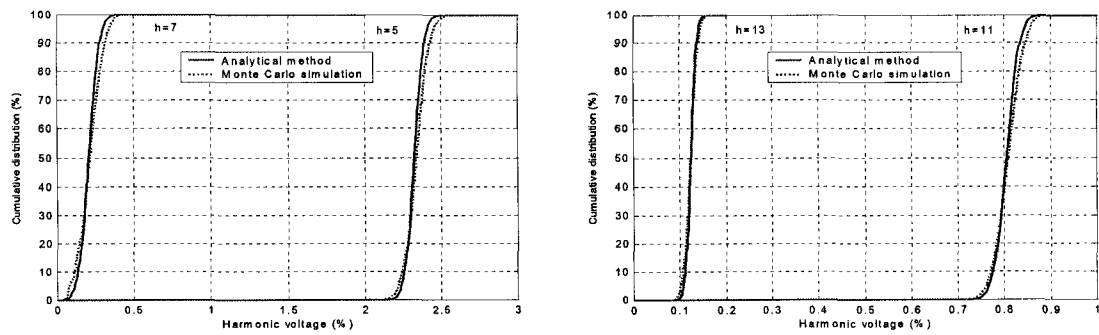


(c) Current through branch L1700-L1701

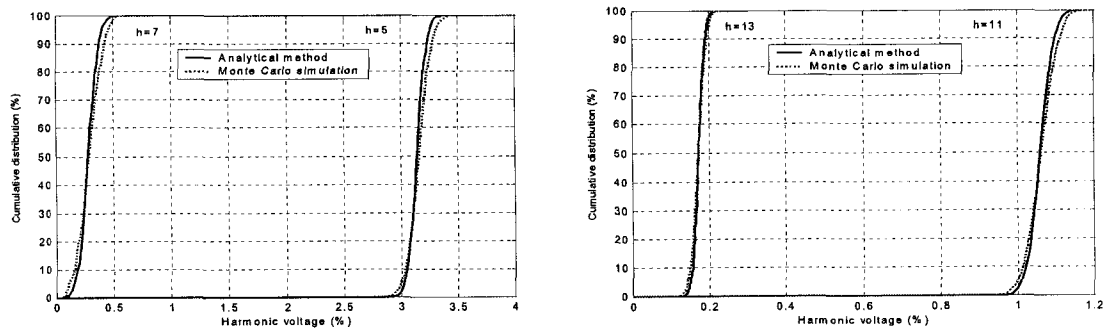


(d) Current through branch L1710-L1711

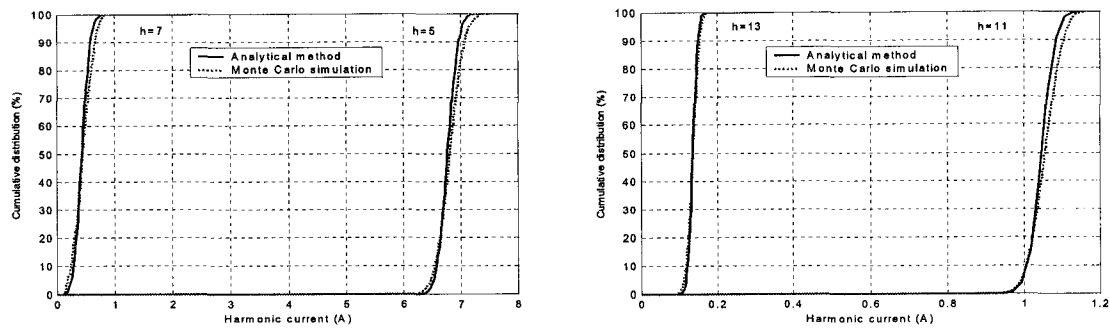
Figure 7.11: The cdfs of harmonic magnitudes obtained from the improved analytical method and Monte Carlo simulation including the power flow (loading 50-100%).



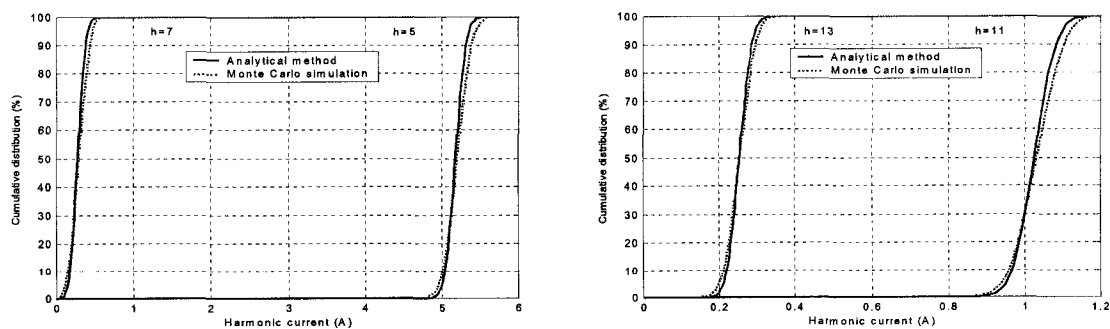
(a) Voltage at bus L1701



(b) Voltage at bus L1711



(c) Current through branch L1700-L1701



(d) Current through branch L1710-L1711

Figure 7.12: The cdfs of harmonic magnitudes obtained from the improved analytical method and Monte Carlo simulation including the power flow (loading 80-100%).

Table 7.3: Comparison of the 50% and 95% non-exceeding probability of the harmonic voltage magnitudes obtained by the Monte Carlo simulation and the improved analytical solution including the power flow analysis

	Voltage at bus L1701 (%)				Voltage at bus L1711 (%)			
	Monte Carlo		Analytical		Monte Carlo		Analytical	
	50%	95%	50%	95%	50%	95%	50%	95%
h	Case 1 (loading variation from 50-100%)							
5	2.068	2.337	2.055	2.291	2.793	3.152	2.776	3.093
7	0.352	0.614	0.336	0.566	0.469	0.821	0.450	0.758
11	0.700	0.788	0.695	0.784	0.919	1.033	0.916	1.030
13	0.070	0.107	0.070	0.107	0.098	0.146	0.099	0.147
h	Case 2 (loading variation from 60-100%)							
5	2.162	2.376	2.147	2.330	2.918	3.204	2.901	3.145
7	0.299	0.518	0.292	0.478	0.398	0.693	0.391	0.641
11	0.739	0.816	0.736	0.810	0.971	1.069	0.970	1.065
13	0.088	0.121	0.089	0.120	0.123	0.166	0.124	0.165
h	Case 3 (loading variation from 70-100%)							
5	2.252	2.412	2.238	2.370	3.041	3.255	3.023	3.200
7	0.253	0.430	0.249	0.390	0.335	0.574	0.332	0.522
11	0.774	0.838	0.773	0.829	1.018	1.100	1.018	1.091
13	0.105	0.132	0.107	0.131	0.147	0.182	0.148	0.181
h	Case 4 (loading variation from 80-100%)							
5	2.339	2.453	2.325	2.412	3.157	3.310	3.141	3.257
7	0.214	0.342	0.209	0.303	0.284	0.455	0.278	0.404
11	0.808	0.856	0.805	0.843	1.062	1.124	1.059	1.109
13	0.124	0.144	0.124	0.141	0.171	0.199	0.172	0.194

Table 7.4: Comparison of the 50% and 95% non-exceeding probability of the harmonic current magnitudes obtained by the Monte Carlo simulation and the improved analytical solution including the power flow analysis

	Current through branch L1700-L1701 (A)				Current through branch L1710-L1711 (A)			
	Monte Carlo		Analytical		Monte Carlo		Analytical	
	50%	95%	50%	95%	50%	95%	50%	95%
h	Case 1 (loading variation from 50-100%)							
5	6.022	6.806	5.987	6.674	4.604	5.154	4.583	5.068
7	0.731	1.274	0.697	1.174	0.517	0.884	0.492	0.818
11	0.914	1.030	0.903	1.018	0.909	1.079	0.905	1.076
13	0.077	0.117	0.076	0.116	0.159	0.248	0.159	0.247
h	Case 2 (loading variation from 60-100%)							
5	6.296	6.920	6.256	6.787	4.808	5.247	4.785	5.159
7	0.622	1.077	0.606	0.992	0.438	0.734	0.421	0.686
11	0.965	1.066	0.957	1.054	0.957	1.110	0.952	1.094
13	0.096	0.132	0.096	0.130	0.190	0.275	0.190	0.268
h	Case 3 (loading variation from 70-100%)							
5	6.557	7.025	6.520	6.904	5.000	5.333	4.984	5.256
7	0.525	0.893	0.515	0.808	0.358	0.610	0.349	0.550
11	1.011	1.094	1.005	1.079	0.996	1.118	0.992	1.102
13	0.115	0.145	0.116	0.143	0.222	0.293	0.222	0.285
h	Case 4 (loading variation from 80-100%)							
5	6.810	7.143	6.774	7.027	5.197	5.442	5.177	5.356
7	0.445	0.710	0.433	0.627	0.288	0.471	0.276	0.412
11	1.055	1.119	1.046	1.098	1.031	1.122	1.025	1.101
13	0.135	0.158	0.135	0.154	0.253	0.307	0.252	0.297

## 7.6 Summary and Conclusions

In this chapter, an analytical method was presented for predicting the probabilistic harmonic voltage and current magnitudes for systems with randomly varying harmonic source loads. The method was applied for a typical distribution system in the presence of distributed ASDs. The BND model was employed to obtain analytically the system probabilistic harmonic levels. This utilized one of the most important theorems in probability theory, which pertains to the limiting distribution of the sum of independent random variables. This is known as the Central Limit Theorem, which states that the probability density function of the sum approaches a normal distribution regardless of the distributions of the individual variables as long as the number of variables is sufficiently large. This could be applied to the sums of the rectangular harmonic components. Hence, the probability density function of the system harmonic levels could be obtained.

Different cases of loading level variation range were conducted. A comparison of the cumulative distribution functions of the harmonic voltage and current magnitudes obtained analytically from the BND model and those obtained from the Monte Carlo simulation was made to verify the analytical method. It was found that the two methods yield close results. However, the analytical method can give more explanation and understanding to the probabilistic solution by knowing the statistical parameters of the individual harmonic voltage and current components that lead to and affect the final result. An improvement of the analytical method was made to reflect the system voltage profile. The presented formulation procedure to conduct the probabilistic analysis can also be applied to other types of nonlinear loads with any concerned random variable provided that the relationships between this variable and the injected harmonic currents can be obtained using the load deterministic harmonic model.

# Chapter 8

## Conclusions

Harmonic analysis methods have been focused on systems with one or several harmonic sources. They use typical harmonic current source model determined with nondistorted supply voltage. However, the situation is different with distributed harmonic sources and this deterministic traditional technique is not the best candidate for harmonic analysis for two reasons. The first one is that the voltage supplied to each harmonic source can have significant distortion, therefore, the current spectrum would be different from the typical one. The second reason is that the randomness of harmonic currents produced from randomly varying loads can not be handled by the deterministic technique, which would give overestimated harmonic levels. In view of the importance of the mentioned concerns, there was a need to have more advanced harmonic analysis methods to provide reliable prediction of harmonic levels in the presence of distributed harmonic sources.

### 8.1 Thesis Contributions

This thesis dealt with the limitations of the traditional harmonic analysis methods. The objective of the conducted work was to develop a reliable frequency domain based harmonic analysis method for the assessment of harmonic levels in distribution systems with distributed PC and ASD loads. The main contributions of this thesis are summarized as follows:

- Two experiments with extensive measurements were conducted on a personal computer (PC) load as one of the most common single-phase harmonic sources to determine the interaction with system voltage. The variation of harmonic current spectrum with the supply voltage distortion was realized. It was found that the total harmonic distortion of the supply voltage is the best index that can be used for harmonic analysis to account for the harmonics attenuation and diversity.
- Extensive simulations were conducted for an adjustable speed drive (ASD) load, which is widely used in industrial distribution systems. The characterization of the harmonic source current spectrum with the voltage distortion was developed. It was confirmed that the voltage total harmonic distortion could also be considered for predicting harmonic currents of such three-phase harmonic source considering the attenuation and diversity effects.
- Based on the harmonic source and the system characteristics, an iterative frequency domain based harmonic analysis method was developed for the assessment of harmonic distortion levels for systems with distributed harmonic sources. The major emphasis was given to the fact that the proposed iterative method could consider the interaction between the system and the harmonic sources by taking into account the harmonics attenuation and diversity.
- A MATLAB program was written to implement the developed method and conduct case studies for different systems with distributed PC and ASD loads. Measurements and time domain simulation were carried out to verify the proposed method and show its reliability. The proposed method has many advantages over the time domain based harmonic analysis methods as follows:
  - It can be implemented using the common frequency domain harmonic analysis tools where the adjustment of the harmonic source current spectrum is based on the associated voltage THD.
  - It can adequately model the harmonic source for harmonic analysis considering the attenuation and diversity effects. For time domain, the device

model can be detailed as necessary, however, the solution time and engineering effort increase significantly. Moreover, time domain simulation is practically limited to the study of small systems and few number of case studies.

- It is time efficient where it can easily handle a large number of harmonic sources and is computationally efficient. On the other hand, using time domain simulations is not an easy task and is computationally demanding, time consuming and an exhaustive process for large size network.
- It was revealed that that the attenuation effect of harmonic currents is the main factor responsible for harmonics reduction in distribution systems. The harmonics diversity might have an additional effect depending on the severity of the system distortion level.
- An analytical technique was proposed to deal with the generation of random harmonic currents. The method was implemented in a program written for MATLAB considering a typical distribution system with distributed ASD loads working randomly between different loading levels, thus producing random harmonic currents.
- An improvement for implementing the analytical technique is made by considering the impact of system voltage profile. Monte Carlo simulation of probabilistic harmonic power flow was conducted. There was a close agreement between the results obtained by the two methods. However, the analytical method had the advantage of being useful to the interpretation of the obtained results and to the understanding of the variation of the statistical parameters of the individual harmonic source currents due to the loading variation, yet could provide accurate results.

## 8.2 Suggestions for Future Work

As with any work of research, there is always more that can be done. Based on what was achieved in this thesis, several extensions and modifications can be explored as follows:



- In this thesis, the developed methods for harmonic analysis considered separately two main issues; 1) harmonics attenuation and diversity; and 2) random variation of harmonic currents. So, future work is suggested to consider simultaneously the two problems to solve a general case; systems with distributed random loads while the attenuation and diversity effects are included.
- Most harmonic standards are deterministic and, therefore, they can not be applied directly to harmonics of random nature or their implementation would be conservative. Future work is recommended on the development of the existing standards and setting new limitations for randomly varying harmonics.
- In the presence of distributed harmonic sources there is no specific rule can be followed to provide cost-effective filtering scheme. It means determining the best locations, types, and number of harmonic filters to get the required filtering performance with minimum cost. This challenging task is recommended for future research work investigating the impact of the attenuation and diversity of harmonic currents.

# Bibliography

- [1] Robert G. Ellis, "Harmonic Analysis of Industrial Power Systems", IEEE Transactions on Industry Applications, Vol. 32, No. 2, March/April 1996, pp. 417-421.
- [2] IEEE Std 1100-1999, "IEEE recommended practice for powering and grounding electronic equipment," March 1999.
- [3] W. Edward Reid, "Power Quality Issues-Standards and Guidelines", IEEE Transactions on Industry Applications, Vol. 32, No. 3, May/June 1996, pp. 625-632.
- [4] Wael R. Anis and Medhat M. Morcos, "Artificial Intelligence and Advanced Mathematical Tools for Power Quality Applications: A Survey", IEEE Transactions on Power Delivery, Vol. 17, No. 2, April 2002, pp. 668-673.
- [5] R. S. Thallam, W. M. Grady, and M. J. Samotyj, "Estimating Future Harmonic Distortion Levels in Distribution Systems Due to Single-Phase Adjustable Speed Drive Air Conditioners: A Case Study", Proceedings of IEEE-ICHPS 1992, Atlanta, CA, September 23-25, 1992, pp. 65-69.
- [6] James K. Phipps, John P. Nelson, and Pankaj K. Sen, "Power Quality and Harmonic Distortion on Distribution Systems", IEEE Transactions on Industry Applications, Vol. 30, No. 2, Marc/April 1994, pp. 476-484.
- [7] M. F. McGranaghan, R. C. Dugan, J. A. King, and W. T. Jewel, "Distribution Feeder Harmonic Study Methodology", IEEE Transactions on Power Apparatus and Systems, Vol. PAS-103, No. 12, December 1984, pp. 3663-3671.
- [8] Alvin L. Day and Aly A. Mahmoud, "Methods of Evaluation of Harmonic Levels in Industrial Plant Distribution Systems", IEEE Transactions on Industry Applications, Vol. IA-23, No. 3, May/June 1987, pp. 498-503.

- [9] T. E. Grebe, "Application of Distribution System Capacitor Banks and Their Impact on Power Quality", *IEEE Transactions on Industry Applications*, Vol. 32, No. 3, May/June 1996, pp. 714-719.
- [10] Task Force on Harmonics Modeling and Simulation, S. Ranade, W. Xu, and J. Mahseredjian (Editors), "Modeling and Simulation of the Propagation of Harmonics in Electric Power Networks, Part II: Sample Systems and Examples", *IEEE Transactions on Power Delivery*, Vol. 11, No. 1, January 1996, pp. 466-474.
- [11] IEEE Std. 519-1992, "IEEE Recommended Practices and Requirements for Harmonic Control in Electrical Power Systems," April 1993.
- [12] T. C. Shuter, H. T. Vollkommer, and T. L. Kirkpatrick, "Survey of Harmonic Levels on the American Electric Power Distribution System", *IEEE Transactions on Power Delivery*, Vol. 4, No. 4, Oct. 1989, pp. 2204-2213.
- [13] A. Domijan, G. T. Heydt, A. P. S. Meliopoulos, S. S. Venkata, and S. West, "Directions of Research on Electric Power Quality", *IEEE Transactions on Power Delivery*, Vol. 8, No. 1, January 1993, pp. 429-436.
- [14] W. Xu, J. R. Marti, and H. W. Dommel, "A Multiphase Harmonic Load Flow Solution Technique", *IEEE Transactions on Power Systems*, Vol. 6, No. 1, Feb. 1991, pp. 174-182.
- [15] S. M. Williams, G. T. Brownfield, and J. W. Duffus, "Harmonic Propagation on an Electric Distribution System: Field Measurements Compared with Computer Simulation", *IEEE Transactions on Power Delivery*, Vol. 8, No. 2, Jan. 1993, pp. 547-552.
- [16] S. N. Govindarajan, M. D. Cox, and F. C. Berry, "Survey of Harmonic Levels on the Southwestern Electric Power Company System", *IEEE Transactions on Power Delivery*, Vol. 6, No. 4, October 1991, pp. 1869-1875.
- [17] A. Mansoor, W. M. Grady, A. H. Chowdhury, and M. J. Samotyj, "An Investigation of Harmonics Attenuation and Diversity Among Distributed Single-Phase Power Electronic Loads", *IEEE Transactions on Power Delivery*, Vol. 10, No. 1, Jan. 1995, pp. 467-473.

- [18] Y. J. Wang, L. Pierrat, and L. Wang, "Summation of Harmonic Currents Produced by AC/DC Static Power Converters with Randomly Fluctuating Loads", *IEEE Transactions on Power Delivery*, Vol. 9, No. 2, April 1994, pp. 1129-1135.
- [19] T. Hiyama, M. S. A. A. Hammam, and T. H. Ortmeier, "Distribution System Modeling with Distributed Harmonic Sources", *IEEE Transactions on Power Delivery*, Vol. 4, No. 2, April 1989, pp. 1297-1304.
- [20] Task Force on Harmonics Modeling and Simulation, S. Ranade, W. Xu, and J. Mahseredjian (Editors), "Modeling and Simulation of the Propagation of Harmonics in Electric Power Networks, Part I: Concepts, Models, and Simulation Techniques", *IEEE Transactions on Power Delivery*, Vol. 11, No. 1, January 1996, pp. 452-465.
- [21] Task Force on Harmonics Modeling and Simulation, IEEE PES Harmonic Working Group, "Characteristics and Modeling of Harmonic Sources—Power Electronic Devices", *IEEE Transactions on Power Delivery*, Vol. 16, No. 4, October 2001, pp. 791-800.
- [22] Task Force on Harmonics Modeling and Simulation, "Test Systems for Harmonics Modeling and Simulation", *IEEE Transactions on Power Delivery*, Vol. 14, No. 2, April 1999, pp. 579-587.
- [23] Jos Arrillaga, Bruce C. Smith, N. R. Watson, and Alan R. Wood, "Power System Harmonic Analysis", John Wiley & Sons, 1997.
- [24] Christopher K. Duffry and Ray P. Stratford, "Update of Harmonic Standard IEEE-519: IEEE Recommended Practices and Requirements for Harmonic Control in Electric Power Systems", *IEEE Transactions on Industry Applications*, Vol. 25, No. 6, November/December 1989, pp. 1025-1034.
- [25] N. R. Watson and J. Arrillaga, "Frequency-Dependence AC System Equivalents for Harmonic Studies and Transient Converter Simulation", *IEEE Transactions on Power Delivery*, Vol. 3, No. 3, July 1988, pp. 1196-1203.
- [26] James W. Gray and Frank J. Haydock, "Industrial Power Quality Considerations When Installing Adjustable Speed Drives", *IEEE Transactions on Industry Applications*, Vol. 32, No. 3, May/June 1996, pp. 646-652.

- [27] B. C. Smith, N. R. Watson, A. R. Wood, and J. Arrillaga, "A Newton Solution for the Harmonic Phasor Analysis of AC/DC Converters", *IEEE Transactions on Power Delivery*, Vol. 11, No. 2, April 1996, pp. 965-971.
- [28] H. W. Dommel, "Electromagnetic Transients Program Reference Manual (EMTP Theory Book)", Prepared for Bonneville Power Administration, Department of Electrical Engineering, University of British Columbia, Aug. 1986.
- [29] Vinay Sharma, R. J. Fleming, and Leo Niekamp, "An Iterative Approach for Analysis of Harmonic Penetration in the Power Transmission Networks", *IEEE Transactions on Power Delivery*, Vol. 6, No. 4, October 1991, pp. 1698-1706.
- [30] G. P. Christoforidis and A. P. Sakis Meliopoulos, "Effects of Modeling on the Accuracy of Harmonic Analysis", *IEEE Transactions on Power Delivery*, Vol. 5, No. 3, July 1990, pp. 1598-1607.
- [31] D. Xia and G. T. Heydt, "Harmonic Power Flow Studies, Part I- Formulation and Solution, Part II-Implementation and Practical Application", *IEEE Transactions on Power Apparatus and Systems*, Vol. PAS-101, No. 6, June 1982, pp. 1257-1270.
- [32] T. H. Ortmeier, N. Kakimoto, T. Hiyama, and M. S. A. A. Hammam, "Harmonic Performance of Individual and Grouped Loads", *Proceedings of the 3rd International Conference on Harmonics in Power Systems*, Nashville, Indiana, September 28- October 1, 1988, pp. 277-283.
- [33] A. Mansoor, W. M. Grady, R. S. Thallam, M. T. Doyle, S. D. Krein, and M. J. Samotyj, "Effect of Supply Voltage Harmonics on the Input Current of Single-Phase Diode Bridge Rectifier Loads", *IEEE Transactions on Power Delivery*, Vol. 10, No. 3, July 1995, pp. 1416-1422.
- [34] J. M. Crucq and A. Robert, "Statistical Approach for Harmonics Measurements and Calculations", *10th International Conference On Electricity Distribution*, Brighton, UK, 8-12 May 1989, IEE Conference Publication No. 305, pp. 91-96.
- [35] A. Mansoor, W. M. Grady, P. T. Staats, R. S. Thallam, M. T. Doyle, and M. J. Samotyj, "Predicting the Net Harmonic Currents Produced by Large Numbers of Distributed Single-Phase Computer Loads", *IEEE Transactions on Power Delivery*, Vol. 10, No. 4, Oct. 1995, pp. 2001-2006.

- [36] E. Duggan and R. E. Morrison, "Prediction of Harmonic Voltage Distortion when a Nonlinear Load is Connected to an Already Distorted Supply", IEE Proceedings, Part C, Vol. 140, No. 3, May 1993, pp. 161-166.
- [37] Yahia Baghzouz and Owen T. Tan, "Probabilistic Modeling of Power System Harmonics", IEEE Transactions on Industry Applications, Vol. IA-23, No. 1, Jan./Feb. 1987, pp. 173-180.
- [38] Probabilistic Aspects Task Force of the Harmonics Working Group Subcommittee of the Transmission and Distribution Committee, "Time-Varying Harmonics: Part II- Harmonic Summation and Propagation", IEEE Transactions on Power Delivery, Vol. 17, No. 1, January 2002, pp. 279-285.
- [39] Probabilistic Aspects Task Force of the Harmonics Working Group Subcommittee of the Transmission and Distribution Committee, "Time-Varying Harmonics: Part I – Characterizing Measured Data", IEEE Transactions on Power Delivery, Vol. 13, No. 3, July 1998, pp. 938-944.
- [40] W. E. Kazibwe, T. H. Ortmeier, and M. S. A. A. Hammam, "Summation of Probabilistic Harmonic Vectors", IEEE Transactions on Power Delivery, Vol. 4, No. 1, Jan. 1989, pp. 621-628.
- [41] S. R. Kaprielian, A. E. Emanuel, R. V. Dwyer, and H. Mehta, "Predicting Voltage Distortion in a System with Multiple Random Harmonic Sources", IEEE Transactions on Power Delivery, Vol. 9, No. 3, July 1994, pp. 1632-1638.
- [42] R. E. Morrison, "Probabilistic Representation of Harmonic Currents in AC Traction Systems", IEE Proceedings, Vol. 131, Part B, No. 5, September 1984, pp. 181-189.
- [43] P. T. Staats, W. M. Grady, A. Arapostathis, and R. S. Thallam, "A Statistical Method for Predicting the Net Harmonic Currents Generated by a Concentration of Electric Vehicle Battery Chargers", IEEE Transactions on Power Delivery, Vol. 12, No. 3, July 1997, pp. 1258-1266.
- [44] P. T. Staats, W. M. Grady, A. Arapostathis, and R. S. Thallam, "A Statistical Analysis of the effect of Electric Vehicle Battery Charging on Distribution System Harmonic Voltages", IEEE Transactions on Power Delivery, Vol. 13, No. 2, April 1998, pp. 640-646.

- [45] J. A. Orr, A. E. Emanuel, and K. W. Oberg, "Current Harmonics Generated by a Cluster of Electric Vehicle Battery Chargers", *IEEE Transactions on Power Apparatus and Systems*, Vol. PAS-101, No. 3, March 1982, pp. 691-700.
- [46] S. R. Kaprielian and A. Rabbani, "Determining the Joint Moments of a Motor Drive's Harmonic Current Phasors", *IEEE Transactions on Power Delivery*, Vol. 11, No. 1, January 1996, pp. 444-451.
- [47] N. B. Rowe, "The Summation of Randomly-Varying Phasors or Vectors with Particular Reference to Harmonic Levels", *IEE Conference Publications*, No. 110, 1974, pp. 177-181.
- [48] W. G. Sherman, "Summation of Harmonics with Random Phase Angles", *IEE Proceedings*, Vol. 119, No. 11, November 1972, pp. 1643-1648.
- [49] M. Lehtonen, "A General Solution to the Harmonics Summation Problem", *European Transaction on Electrical Power Engineering ETEP*, Vol. 3, No. 4, July/Aug. 1993, pp. 293-297.
- [50] A. Cavallini, M. Cacciari, M. Loggini, and G. C. Montanari, "Evaluation of Harmonic Levels in Electrical Networks by Statistical Indexes", *IEEE Transactions on Industry Applications*, Vol. 30, No. 4, July/August 1994, pp. 1116-1125.
- [51] Duk-Gyoo Kim, Tatsuhito Nakajima, and Eisuke Masada, "Harmonic Analysis of a Capacitor-Filtered Rectifier with Line Impedance", *Electronics and Communications in Japan, Part 1*, Vol. 72, No. 4, 1989.
- [52] Wenyuan Xu, "A Multiphase Harmonic Load Flow Solution Technique", Department of Electrical Engineering, University of British Columbia, Ph.D. Thesis, November 1999.
- [53] Richard S. Wallace, "The Harmonic Impact of Variable Speed Air Conditioners on Residential Power Distribution", *Proceedings of 7th Annual Applied Power Electronics Conference and Exposition*, Boston, Massachusetts, February 23-27, 1992, pp. 293-298.
- [54] Y. Y. Hong, T. Y. Chen, and Y. Z. Hsu, "Experiences in the Investigation of Harmonic penetrations: Case Studies", *Electric Power System Research*, Vol. 39, 1996, pp. 187-193.

- [55] I. M. Nejdawi, A. E. Emanuel, D. J. Pileggi, M. J. Corridori, and R. D. Archambeault, "Harmonics Trend in NE USA: A Preliminary Survey", *IEEE Transactions on Power Delivery*, Vol. 14, No. 4, October 1999, pp. 1488-1494.
- [56] Mark F. McGranaghan and Davide R. Mueller, "Designing Harmonic Filters for Adjustable-Speed Drives to Comply with IEEE-519 Harmonic Limits", *IEEE Transactions on Industry Applications*, Vol. 35, No. 2, March/April 1999, pp. 312-318.
- [57] Wilsun Xu, Hermann W. Dommel, M. B. Hughes, Gary W. K. Chang, and Le Tan, "Modelling of Adjustable Speed Drives for Power System Harmonic Analysis", *IEEE Transactions on Power Delivery*, Vol. 14, No. 2, April 1999, pp. 595-601.
- [58] Thomas S. Key and Jih-Sheng Lai, "Comparison of Standards and Power Supply Design Options for Limiting Harmonic Distortion in Power Systems", *IEEE Transactions on Industry Applications*, Vol. 29, No. 4, July/August 1993, pp. 688-695.
- [59] David E. Rice, "A Detailed Analysis of Six-Pulse Converter Harmonic Currents", *IEEE Transactions on Industry Applications*, Vol. 30, No. 2, March/April 1999, pp. 294-304.
- [60] G. T. Heydt and W. M. Grady, "Distributed Rectifier Loads in Electric Power Systems", *IEEE Transactions on Power Apparatus and Systems*, Vol. PAS-103, No. 9, Sept. 1984, pp. 2452-2459.
- [61] S. M. Peeran and C. W. P. Cascadden, "Application, Design, and Specification of Harmonic Filters for Variable Frequency Drives", *IEEE Transactions on Industry Applications*, Vol. 31, No. 4, July/August 1995, pp. 841-847.



# Appendix A

## Experiments Set Up

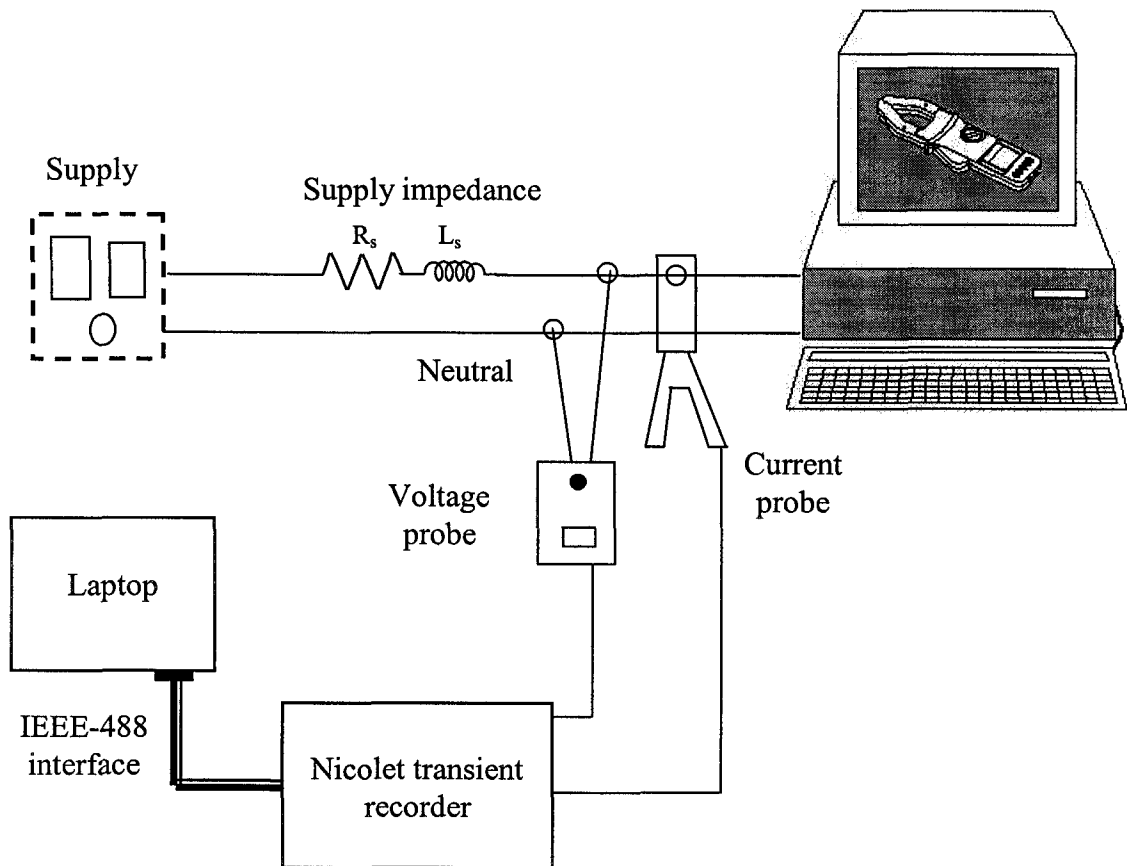


Figure A.1 Main set up of the conducted experiments for the PC load harmonic measurements.

➤ **Nicolet Transient Recorder for Data Acquisition: Model “BE256-LE”**

1) 4-Channel Single Ended Input Card

- Model: 672
- 16 bit resolution (0.015%)
- Sampling rate:  
Maximum sampling rate: 100Ksamples/second  
Minimum sampling rate: 1 sample/second
- Ranges (Full Scale): Four programmable ranges:  $\pm 1.25$  V,  $\pm 2.5$  V,  $\pm 5$  V,  $\pm 10$  V
- DC Inaccuracy: 0.01 % of Full Scale
- Bandwidth:  $\geq 50$  kHz @  $-3$  dB

2) 4-Channel Differential Input Card

- Model: 672 CB
- 16 bit resolution
- Sampling rate:  
Maximum sampling rate: 100Ksamples/second  
Minimum sampling rate: 1 sample/second
- Ranges (Full Scale):  $\pm 100$  mV to  $\pm 100$  V in 28 steps
- DC Inaccuracy: 0.02 % of Full Scale
- Bandwidth:  $\geq 50$  kHz @  $-3$  dB

➤ **Fluke AC/DC Current Probe: Model 80i-110s**

- **Current Ranges:**  
0 to 10A DC or AC peak  
0 to 100A DC or AC peak
- **Output Signals:**  
10A range: 100 mV/A  
100A range: 10 mV/A

- **Accuracy (DC to 1kHz):**  
3% of reading + 50 mA for 10 A range.  
3, 4, 12, and 15% of reading + 50 mA for 100 A range with input current ranges of 10, 40, 80, and 100 A respectively.
- **Useful Bandwidth (-3 dB):** 0 to 100 kHz

➤ **SI-9000 Differential Voltage Probe**

- **Attenuation ratio:** 1/50 and 1/500
- **Voltage Ranges:**  
1/50 attenuation, ranges are 70 V DC, 50 V RMS  
1/500 attenuation, ranges are 700 V DC, 500 V RMS
- **Accuracy:** 2%
- **Bandwidth:** DC to 25 MHz

Table A.1: List of chosen supply impedance parameters with different X/R ratios for the case of impedance change

Step	X/R = 0.2		X/R = 0.5		X/R = 1		X/R = 2		X/R = 5	
	$X_s$	$R_s$	$X_s$	$R_s$	$X_s$	$R_s$	$X_s$	$R_s$	$X_s$	$R_s$
1	0.377	1.885	0.377	0.754	0.377	0.377	0.377	0.188	0.377	0.075
2	0.565	2.827	0.942	1.885	0.942	0.942	0.942	0.471	0.942	0.188
3	0.754	3.77	1.32	2.639	1.319	1.319	1.32	0.66	1.32	0.264
4	0.942	4.712	1.508	3.016	1.508	1.508	1.885	0.942	1.885	0.377
5	1.131	5.655	1.885	3.77	1.885	1.885	2.262	1.131	2.262	0.452
6	1.32	6.597	2.262	4.524	2.261	2.261	2.827	1.414	2.827	0.566
7	1.508	7.54	2.827	5.655	2.827	2.827	3.204	1.602	3.204	0.64
8	1.696	8.482	3.204	6.409	3.204	3.204	3.77	1.885	3.77	0.754
9	1.885	9.425	3.393	6.786	3.392	3.392	4.147	2.073	4.147	0.83
10	2.073	10.36	3.77	7.54	3.77	3.77	4.712	2.356	4.712	0.94

\* X and R values are in ohm.

Table A.2: Chosen supply impedances for different X/R ratios for the case of background voltage distortion change

X/R = 0.2		X/R = 0.5		X/R = 1		X/R = 2	
$X_s$	$R_s$	$X_s$	$R_s$	$X_s$	$R_s$	$X_s$	$R_s$
0.377	1.885	0.754	1.508	0.754	0.754	0.754	0.377
0.754	3.77	1.508	3.016	1.508	1.508	1.508	0.754
1.131	5.655	2.262	4.524	2.262	2.262	2.262	1.131
1.508	7.54	3	6	3	3	3	1.508

\* X and R values are in ohm.

# Appendix B

## Branch Current Statistical Parameters

### Derivation of the statistical parameters of branch harmonic currents:

- Variance of  $I_{(i-k)-x}$  component:

$$\begin{aligned}
 \sigma_{I_{(i-k)-x}}^2 &= E(I_{(i-k)-x}^2) - E^2(I_{(i-k)-x}) = \\
 &= \frac{1}{(r_{i-k}^2 + x_{i-k}^2)^2} \left[ E(r_{i-k}(V_{i-x} - V_{k-x}) + x_{i-k}(V_{i-y} - V_{k-y}))^2 - (r_{i-k}(\mu_{V_{i-x}} - \mu_{V_{k-x}}) + x_{i-k}(\mu_{V_{i-y}} - \mu_{V_{k-y}}))^2 \right] = \\
 &= \frac{1}{(r_{i-k}^2 + x_{i-k}^2)^2} \left[ \begin{aligned} & \left( r_{i-k}^2 E(V_{i-x}^2 + V_{k-x}^2 - 2V_{i-x}V_{k-x}) + x_{i-k}^2 E(V_{i-y}^2 + V_{k-y}^2 - 2V_{i-y}V_{k-y}) + \right. \\ & \left. 2r_{i-k}x_{i-k} E(V_{i-x}V_{i-y} + V_{k-x}V_{k-y} - V_{i-x}V_{k-y} - V_{k-x}V_{i-y}) \right) - \\ & \left( r_{i-k}^2 (\mu_{V_{i-x}}^2 + \mu_{V_{k-x}}^2 - 2\mu_{V_{i-x}}\mu_{V_{k-x}}) + x_{i-k}^2 (\mu_{V_{i-y}}^2 + \mu_{V_{k-y}}^2 - 2\mu_{V_{i-y}}\mu_{V_{k-y}}) + \right. \\ & \left. 2r_{i-k}x_{i-k} (\mu_{V_{i-x}}\mu_{V_{i-y}} + \mu_{V_{k-x}}\mu_{V_{k-y}} - \mu_{V_{i-x}}\mu_{V_{k-y}} - \mu_{V_{k-x}}\mu_{V_{i-y}}) \right) \end{aligned} \right] = \\
 &= \frac{1}{(r_{i-k}^2 + x_{i-k}^2)^2} \left[ \begin{aligned} & r_{i-k}^2 (\sigma_{V_{i-x}}^2 + \sigma_{V_{k-x}}^2) + x_{i-k}^2 (\sigma_{V_{i-y}}^2 + \sigma_{V_{k-y}}^2) - 2r_{i-k} (E(V_{i-x}V_{k-x}) - \mu_{V_{i-x}}\mu_{V_{k-x}}) - \\ & 2x_{i-k} (E(V_{i-y}V_{k-y}) - \mu_{V_{i-y}}\mu_{V_{k-y}}) + \\ & 2r_{i-k}x_{i-k} \left( E(V_{i-x}V_{i-y}) - \mu_{V_{i-x}}\mu_{V_{i-y}} + E(V_{k-x}V_{k-y}) - \mu_{V_{k-x}}\mu_{V_{k-y}} - \right. \\ & \left. (E(V_{i-x}V_{k-y}) - \mu_{V_{i-x}}\mu_{V_{k-y}}) - (E(V_{k-x}V_{i-y}) - \mu_{V_{k-x}}\mu_{V_{i-y}}) \right) \end{aligned} \right] \\
 &= \frac{1}{(r_{i-k}^2 + x_{i-k}^2)^2} \left[ \begin{aligned} & r_{i-k}^2 (\sigma_{V_{i-x}}^2 + \sigma_{V_{k-x}}^2) + x_{i-k}^2 (\sigma_{V_{i-y}}^2 + \sigma_{V_{k-y}}^2) - \\ & 2r_{i-k}^2 \rho_{V_{i-x}V_{k-x}} \sigma_{V_{i-x}} \sigma_{V_{k-x}} - 2x_{i-k}^2 \rho_{V_{i-y}V_{k-y}} \sigma_{V_{i-y}} \sigma_{V_{k-y}} + \\ & 2r_{i-k}x_{i-k} \left( \rho_{V_{i-x}V_{i-y}} \sigma_{V_{i-x}} \sigma_{V_{i-y}} + \rho_{V_{k-x}V_{k-y}} \sigma_{V_{k-x}} \sigma_{V_{k-y}} - \right. \\ & \left. \rho_{V_{i-x}V_{k-y}} \sigma_{V_{i-x}} \sigma_{V_{k-y}} - \rho_{V_{k-x}V_{i-y}} \sigma_{V_{k-x}} \sigma_{V_{i-y}} \right) \end{aligned} \right] \tag{B.1}
 \end{aligned}$$

- Variance of  $I_{(i-k)-y}$  component:

$$\begin{aligned}
\sigma_{I_{(i-k)-y}}^2 &= E(I_{(i-k)-y}^2) - E^2(I_{(i-k)-y}) = \\
&= \frac{1}{(r_{i-k}^2 + x_{i-k}^2)^2} \left[ E(r_{i-k}(V_{i-y} - V_{k-y}) - x_{i-k}(V_{i-x} - V_{k-x}))^2 - (r_{i-k}(\mu_{V_{i-y}} - \mu_{V_{k-y}}) - x_{i-k}(\mu_{V_{i-x}} - \mu_{V_{k-x}}))^2 \right] = \\
&= \frac{1}{(r_{i-k}^2 + x_{i-k}^2)^2} \left[ \begin{aligned} & \left( r_{i-k}^2 E(V_{i-y}^2 + V_{k-y}^2 - 2V_{i-y}V_{k-y}) + x_{i-k}^2 E(V_{i-x}^2 + V_{k-x}^2 - 2V_{i-x}V_{k-x}) - \right. \\ & \left. 2r_{i-k}x_{i-k} E(V_{i-y}V_{i-x} + V_{k-y}V_{k-x} - V_{i-y}V_{k-x} - V_{k-y}V_{i-x}) \right) - \\ & \left( r_{i-k}^2 (\mu_{V_{i-y}}^2 + \mu_{V_{k-y}}^2 - 2\mu_{V_{i-y}}\mu_{V_{k-y}}) + x_{i-k}^2 (\mu_{V_{i-x}}^2 + \mu_{V_{k-x}}^2 - 2\mu_{V_{i-x}}\mu_{V_{k-x}}) - \right. \\ & \left. 2r_{i-k}x_{i-k} (\mu_{V_{i-y}}\mu_{V_{i-x}} + \mu_{V_{k-y}}\mu_{V_{k-x}} - \mu_{V_{i-y}}\mu_{V_{k-x}} - \mu_{V_{k-y}}\mu_{V_{i-x}}) \right) \end{aligned} \right] = \\
&= \frac{1}{(r_{i-k}^2 + x_{i-k}^2)^2} \left[ \begin{aligned} & r_{i-k}^2 (\sigma_{V_{i-y}}^2 + \sigma_{V_{k-y}}^2) + x_{i-k}^2 (\sigma_{V_{i-x}}^2 + \sigma_{V_{k-x}}^2) - 2r_{i-k} (E(V_{i-y}V_{k-y}) - \mu_{V_{i-y}}\mu_{V_{k-y}}) - \\ & 2x_{i-k}^2 (E(V_{i-x}V_{k-x}) - \mu_{V_{i-x}}\mu_{V_{k-x}}) - \\ & 2r_{i-k}x_{i-k} \left( \begin{aligned} & E(V_{i-y}V_{i-x}) - \mu_{V_{i-y}}\mu_{V_{i-x}} + E(V_{k-y}V_{k-x}) - \mu_{V_{k-y}}\mu_{V_{k-x}} - \\ & (E(V_{i-y}V_{k-x}) - \mu_{V_{i-y}}\mu_{V_{k-x}}) - (E(V_{k-y}V_{i-x}) - \mu_{V_{k-y}}\mu_{V_{i-x}}) \end{aligned} \right) \end{aligned} \right] \\
&= \frac{1}{(r_{i-k}^2 + x_{i-k}^2)^2} \left[ \begin{aligned} & r_{i-k}^2 (\sigma_{V_{i-y}}^2 + \sigma_{V_{k-y}}^2) + x_{i-k}^2 (\sigma_{V_{i-x}}^2 + \sigma_{V_{k-x}}^2) - \\ & 2r_{i-k}^2 \rho_{V_{i-y}V_{k-y}} \sigma_{V_{i-y}} \sigma_{V_{k-y}} - 2x_{i-k}^2 \rho_{V_{i-x}V_{k-x}} \sigma_{V_{i-x}} \sigma_{V_{k-x}} - \\ & 2r_{i-k}x_{i-k} \left( \begin{aligned} & \rho_{V_{i-y}V_{i-x}} \sigma_{V_{i-y}} \sigma_{V_{i-x}} + \rho_{V_{k-y}V_{k-x}} \sigma_{V_{k-y}} \sigma_{V_{k-x}} - \\ & \rho_{V_{i-y}V_{k-x}} \sigma_{V_{i-y}} \sigma_{V_{k-x}} - \rho_{V_{k-y}V_{i-x}} \sigma_{V_{k-y}} \sigma_{V_{i-x}} \end{aligned} \right) \end{aligned} \right] \tag{B.2}
\end{aligned}$$

- Correlation coefficient of  $I_{(i-k)-x}$  and  $I_{(i-k)-y}$  components:

$$\rho_{I_{(i-k)-x}I_{(i-k)-y}} = \frac{\text{cov}(I_{(i-k)-x}, I_{(i-k)-y})}{\sigma_{I_{(i-k)-x}} \sigma_{I_{(i-k)-y}}} \tag{B.3}$$

$$\begin{aligned}
\text{cov}(I_{(i-k)-x}, I_{(i-k)-y}) &= E(I_{(i-k)-x} I_{(i-k)-y}) - \mu_{I_{(i-k)-x}} \mu_{I_{(i-k)-y}} = \\
&= \frac{1}{(r_{i-k}^2 + x_{i-k}^2)^2} \left[ E \left( (r_{i-k}(V_{i-x} - V_{k-x}) + x_{i-k}(V_{i-y} - V_{k-y})) (r_{i-k}(V_{i-y} - V_{k-y}) - x_{i-k}(V_{i-x} - V_{k-x})) \right) - \right. \\
&= \frac{1}{(r_{i-k}^2 + x_{i-k}^2)^2} \left[ (r_{i-k}(\mu_{V_{i-x}} - \mu_{V_{k-x}}) + x_{i-k}(\mu_{V_{i-y}} - \mu_{V_{k-y}})) (r_{i-k}(\mu_{V_{i-y}} - \mu_{V_{k-y}}) - x_{i-k}(\mu_{V_{i-x}} - \mu_{V_{k-x}})) \right] = \\
&= \frac{1}{(r_{i-k}^2 + x_{i-k}^2)^2} \left[ (r_{i-k}^2 - x_{i-k}^2) E((V_{i-x} - V_{k-x})(V_{i-y} - V_{k-y})) + r_{i-k} x_{i-k} E((V_{i-y} - V_{k-y})^2 - (V_{i-x} - V_{k-x})^2) - \right. \\
&= \frac{1}{(r_{i-k}^2 + x_{i-k}^2)^2} \left[ (r_{i-k}^2 - x_{i-k}^2) (\mu_{V_{i-x}} - \mu_{V_{k-x}}) (\mu_{V_{i-y}} - \mu_{V_{k-y}}) - r_{i-k} x_{i-k} ((\mu_{V_{i-y}} - \mu_{V_{k-y}})^2 - (\mu_{V_{i-x}} - \mu_{V_{k-x}})^2) \right] = \\
&= \frac{1}{(r_{i-k}^2 + x_{i-k}^2)^2} \left[ (r_{i-k}^2 - x_{i-k}^2) (E(V_{i-x} V_{i-y}) + E(V_{k-x} V_{k-y}) - E(V_{i-x} V_{k-y}) - E(V_{k-x} V_{i-y})) + \right. \\
&= \frac{1}{(r_{i-k}^2 + x_{i-k}^2)^2} \left[ (r_{i-k} x_{i-k}) (E(V_{i-y}^2) + E(V_{k-y}^2) - 2E(V_{i-y} V_{k-y})) - (E(V_{i-x}^2) + E(V_{k-x}^2) - 2E(V_{i-x} V_{k-x})) \right] - \\
&= \frac{1}{(r_{i-k}^2 + x_{i-k}^2)^2} \left[ (r_{i-k}^2 - x_{i-k}^2) (\mu_{V_{i-x}} \mu_{V_{i-y}} + \mu_{V_{k-x}} \mu_{V_{k-y}} - \mu_{V_{i-x}} \mu_{V_{k-y}} - \mu_{V_{k-x}} \mu_{V_{i-y}}) - \right. \\
&= \frac{1}{(r_{i-k}^2 + x_{i-k}^2)^2} \left[ (r_{i-k} x_{i-k}) (\mu_{V_{i-y}}^2 + \mu_{V_{k-y}}^2 - 2\mu_{V_{i-y}} \mu_{V_{k-y}}) - (\mu_{V_{i-x}}^2 + \mu_{V_{k-x}}^2 - 2\mu_{V_{i-x}} \mu_{V_{k-x}}) \right] = \\
&= \frac{1}{(r_{i-k}^2 + x_{i-k}^2)^2} \left[ (r_{i-k}^2 - x_{i-k}^2) \left( \begin{array}{l} \rho_{V_{i-x} V_{i-y}} \sigma_{V_{i-x}} \sigma_{V_{i-y}} + \rho_{V_{k-x} V_{k-y}} \sigma_{V_{k-x}} \sigma_{V_{k-y}} \\ \rho_{V_{i-x} V_{k-y}} \sigma_{V_{i-x}} \sigma_{V_{k-y}} - \rho_{V_{k-x} V_{i-y}} \sigma_{V_{k-x}} \sigma_{V_{i-y}} \end{array} \right) + \right. \\
&= \frac{1}{(r_{i-k}^2 + x_{i-k}^2)^2} \left[ (r_{i-k} x_{i-k}) (\sigma_{V_{i-y}}^2 + \sigma_{V_{k-y}}^2 - 2\rho_{V_{i-y} V_{k-y}} \sigma_{V_{i-y}} \sigma_{V_{k-y}}) - (\sigma_{V_{i-x}}^2 + \sigma_{V_{k-x}}^2 - 2\rho_{V_{i-x} V_{k-x}} \sigma_{V_{i-x}} \sigma_{V_{k-x}}) \right] \tag{B.4}
\end{aligned}$$

### Correlation coefficients of the harmonic voltage components:

- Correlation coefficient of  $V_{i-x}$  and  $V_{k-y}$  components:

$$\rho_{V_{i-x} V_{k-y}} = \frac{\text{cov}(V_{i-x}, V_{k-y})}{\sigma_{V_{i-x}} \sigma_{V_{k-y}}} = \frac{\sum_{j=1}^N \rho_{V_{ij-x} V_{kj-y}} \sigma_{V_{ij-x}} \sigma_{V_{kj-y}}}{\sigma_{V_{i-x}} \sigma_{V_{k-y}}} \tag{B.5}$$

$$\rho_{V_{ij-x} V_{kj-y}} = \frac{\text{cov}(V_{ij-x}, V_{kj-y})}{\sigma_{V_{ij-x}} \sigma_{V_{kj-y}}} \tag{B.6}$$

where

$$\begin{aligned}
\text{cov}(V_{ij-x}, V_{kj-y}) &= E(V_{ij-x} V_{kj-y}) - \mu_{V_{ij-x}} \mu_{V_{kj-y}} = \\
&= E[(R_{ij} I_{j-x} - X_{ij} I_{j-y})(X_{kj} I_{j-x} + R_{kj} I_{j-y})] - (R_{ij} \mu_{I_{j-x}} - X_{ij} \mu_{I_{j-y}})(X_{kj} \mu_{I_{j-x}} + R_{kj} \mu_{I_{j-y}}) = \\
&= R_{ij} X_{kj} [E(I_{j-x}^2) - \mu_{I_{j-x}}^2] - R_{kj} X_{ij} [E(I_{j-y}^2) - \mu_{I_{j-y}}^2] + \\
&= R_{ij} R_{kj} [E(I_{j-x} I_{j-y}) - \mu_{I_{j-x}} \mu_{I_{j-y}}] - X_{ij} X_{kj} [E(I_{j-x} I_{j-y}) - \mu_{I_{j-x}} \mu_{I_{j-y}}] = \\
&= R_{ij} X_{kj} (\sigma_{I_{j-x}}^2) - R_{kj} X_{ij} (\sigma_{I_{j-y}}^2) + (R_{ij} R_{kj} - X_{ij} X_{kj}) (\rho_{I_{j-x} I_{j-y}} \sigma_{I_{j-x}} \sigma_{I_{j-y}}) \tag{B.7}
\end{aligned}$$

The correlation coefficient of  $V_{k-x}$  and  $V_{i-y}$  components can be obtained similarly to the correlation coefficient of  $V_{i-x}$  and  $V_{k-y}$  components by exchanging the subscripts  $i$  and  $k$ .

- Correlation coefficient of  $V_{i-x}$  and  $V_{k-x}$  components:

$$\rho_{V_{i-x}V_{k-x}} = \frac{\text{cov}(V_{i-x}, V_{k-x})}{\sigma_{V_{i-x}} \sigma_{V_{k-x}}} = \frac{\sum_{j=1}^N \rho_{V_{ij-x}V_{kj-x}} \sigma_{V_{ij-x}} \sigma_{V_{kj-x}}}{\sigma_{V_{i-x}} \sigma_{V_{k-x}}} \quad (\text{B.8})$$

$$\rho_{V_{ij-x}V_{kj-x}} = \frac{\text{cov}(V_{ij-x}, V_{kj-x})}{\sigma_{V_{ij-x}} \sigma_{V_{kj-x}}} \quad (\text{B.9})$$

where

$$\begin{aligned} \text{cov}(V_{ij-x}, V_{kj-x}) &= E(V_{ij-x}V_{kj-x}) - \mu_{V_{ij-x}}\mu_{V_{kj-x}} = \\ &E[(R_{ij}I_{j-x} - X_{ij}I_{j-y})(R_{kj}I_{j-x} - X_{kj}I_{j-y})] - (R_{ij}\mu_{I_{j-x}} - X_{ij}\mu_{I_{j-y}})(R_{kj}\mu_{I_{j-x}} - X_{kj}\mu_{I_{j-y}}) = \\ &R_{ij}R_{kj}[E(I_{j-x}^2) - \mu_{I_{j-x}}^2] + X_{ij}X_{kj}[E(I_{j-y}^2) - \mu_{I_{j-y}}^2] - \\ &R_{ij}X_{kj}[E(I_{j-x}I_{j-y}) - \mu_{I_{j-x}}\mu_{I_{j-y}}] - R_{kj}X_{ij}[E(I_{j-x}I_{j-y}) - \mu_{I_{j-x}}\mu_{I_{j-y}}] = \\ &R_{ij}R_{kj}(\sigma_{I_{j-x}}^2) + X_{ij}X_{kj}(\sigma_{I_{j-y}}^2) - (R_{ij}X_{kj} + R_{kj}X_{ij})(\rho_{I_{j-x}I_{j-y}}\sigma_{I_{j-x}}\sigma_{I_{j-y}}) \end{aligned} \quad (\text{B.10})$$

- Correlation coefficient of  $V_{i-y}$  and  $V_{k-y}$  components:

$$\rho_{V_{i-y}V_{k-y}} = \frac{\text{cov}(V_{i-y}, V_{k-y})}{\sigma_{V_{i-y}} \sigma_{V_{k-y}}} = \frac{\sum_{j=1}^N \rho_{V_{ij-y}V_{kj-y}} \sigma_{V_{ij-y}} \sigma_{V_{kj-y}}}{\sigma_{V_{i-y}} \sigma_{V_{k-y}}} \quad (\text{B.11})$$

$$\rho_{V_{ij-y}V_{kj-y}} = \frac{\text{cov}(V_{ij-y}, V_{kj-y})}{\sigma_{V_{ij-y}} \sigma_{V_{kj-y}}} \quad (\text{B.12})$$

where

$$\begin{aligned} \text{cov}(V_{ij-y}, V_{kj-y}) &= E(V_{ij-y}V_{kj-y}) - \mu_{V_{ij-y}}\mu_{V_{kj-y}} = \\ &E[(X_{ij}I_{j-x} + R_{ij}I_{j-y})(X_{kj}I_{j-x} + R_{kj}I_{j-y})] - (X_{ij}\mu_{I_{j-x}} + R_{ij}\mu_{I_{j-y}})(X_{kj}\mu_{I_{j-x}} + R_{kj}\mu_{I_{j-y}}) = \\ &X_{ij}X_{kj}[E(I_{j-x}^2) - \mu_{I_{j-x}}^2] + R_{ij}R_{kj}[E(I_{j-y}^2) - \mu_{I_{j-y}}^2] + \\ &R_{ij}X_{kj}[E(I_{j-x}I_{j-y}) - \mu_{I_{j-x}}\mu_{I_{j-y}}] + R_{kj}X_{ij}[E(I_{j-x}I_{j-y}) - \mu_{I_{j-x}}\mu_{I_{j-y}}] = \\ &X_{ij}X_{kj}(\sigma_{I_{j-x}}^2) + R_{ij}R_{kj}(\sigma_{I_{j-y}}^2) + (R_{ij}X_{kj} + R_{kj}X_{ij})(\rho_{I_{j-x}I_{j-y}}\sigma_{I_{j-x}}\sigma_{I_{j-y}}) \end{aligned} \quad (\text{B.13})$$



# Appendix C

## Data for Study Systems

There are many case studies presented in this dissertation. The extensively tested systems are PC systems 1 and 2 for single-phase loads and Goose River system for three-phase loads. The data of these systems are listed in this appendix.

- PC system 2

PC system 2 is an extension of PC system 1, therefore, the data of PC system 2 will only be presented as it includes implicitly the data of PC system 1.

\* Source Data (Bus #1)

Voltage Setting (pu) = 1.0411

Base Voltage (V) = 120

Table C.1: Bus Load Data

Bus #	Nominal voltage (V)	P (W)	Q (VAR)
2	120	31.34	-0.91
3	120	32.93	-1.87
4	120	33.17	-0.59
5	120	31.20	-2.64
6	120	38.83	-4.77
7	120	27.25	-1.74
8	120	45.45	-3.35
9	120	31.50	-0.95

Table C.2: Branch System Data

Impedance	From Bus	To Bus	R (ohm)	L (mH)
$Z_s$	1	2	0.5	1
$Z_{2-3}$	2	3	1	1
$Z_{3-4}$	3	4	1	1
$Z_{4-5}$	4	5	1	1
$Z_{5-6}$	5	6	1	1
$Z_{4-7}$	4	7	1	2.5
$Z_{7-8}$	7	8	1	2.5
$Z_{8-9}$	8	9	1	2.5

- Goose River System

Table C.3: Equivalent Source Data

Bus #	Voltage Setting (pu)	R <sub>1</sub> (pu)	X <sub>1</sub> (pu)	R <sub>0</sub> (pu)	X <sub>0</sub> (pu)
1	1.00	0.1309	0.77399	0.02633	0.34151

Base MVA = 100

Base voltage (kV) = 25

Table C.4: System Bus Load Data

Bus name	Bus #	Nominal voltage (kV)	P (kW)	Q (kVAR)	Bus name	Bus #	Nominal voltage (kV)	P (kW)	Q (kVAR)
GRSRC	1	25	0	0	L211X*	45	0.48	394.7	104.66
25KKVB	2	25	0	0	L112X*	46	0.48	136	23.34
174-10	3	25	0	0	L212X*	47	0.48	134.78	26.66
L1700	4	25	0	0	L113X*	49	0.48	74.85	9.58
L1701	5	25	0	0	L114X*	50	0.48	82.21	9.64
L1702	6	25	0	0	L214X*	51	0.48	81.9	11.33
L1703	7	25	0	0	L414X*	53	0.48	81.9	11.33
L1704	8	25	0	0	L514X*	54	0.48	74.74	9.6
L1705	9	25	0	0	L116X*	55	0.48	103.91	17.11
L1707	10	25	0	0	L117X*	57	0.48	108.2	18.44
L1708	11	25	0	0	L118X*	58	0.48	90.87	11.88
L1709	12	25	0	0	L218X*	59	0.48	59.07	6.11
L1710	13	25	0	0	L318X*	60	0.48	385	117.15
L1711	14	25	0	0	L119X*	61	0.48	133.44	26.37
L1713	15	25	0	0	L120X*	62	0.48	133.3	26.36
L1714	16	25	0	0	L121X*	63	0.48	117.68	16.2
L1712	17	25	0	0	L122X*	64	0.48	103.05	16.89
L1716	18	25	0	0	L103X	33	0.48	153.75	76.87
L1717	19	25	0	0	L105X	35	0.48	300	150
L1718	20	25	0	0	L205X	36	0.48	300	150
L1719	21	25	0	0	L305X	37	0.48	300	150
L1720	22	25	0	0	L308X	40	0.48	153.75	76.875
L1721	23	25	0	0	L209X	42	0.48	153.75	76.875
L1722	24	25	0	0	L110X	43	0.48	153.75	76.875
L104X*	34	0.48	137.63	23.51	L111X	44	4.16	675	337.5
L108X*	38	0.48	92.22	12	L312X	48	0.48	153.75	76.875
L208X*	39	0.48	135.82	26.5	L314X	52	0.48	153.75	76.875
L109X*	41	0.48	105.63	15.26	L216X	56	0.48	153.75	76.875

\* ASD load

Table C.5: System Branch Data

From Bus	To Bus	Length	$R_1$ (pu/length)	$X_1$ (pu/length)	$B_1$ (pu/length) $10^6$	$R_0$ (pu/length)	$X_0$ (pu/length)	$B_0$ (pu/length) $10^6$
2	3	3	0.142080	0.116960	38.6	0.187840	0.500800	17.388
3	4	1.2	0.142080	0.116960	38.6	0.187840	0.500800	17.388
4	5	2.24	0.056000	0.100480	42.317	0.101760	0.484320	18.284
6	7	0.5	0.056000	0.100480	42.317	0.101760	0.484320	18.284
7	8	2	0.056000	0.100480	42.317	0.101760	0.484320	18.284
8	9	0.2	0.142080	0.116960	38.6	0.187840	0.500800	17.388
8	10	0.5	0.142080	0.116960	38.6	0.187840	0.500800	17.388
10	11	0.5	0.569600	0.128960	34.047	0.615360	0.512800	16.376
11	12	0.74	0.569600	0.128960	34.047	0.615360	0.512800	16.376
10	13	0.5	0.142080	0.116960	38.6	0.187840	0.500800	17.388
13	14	0.5	0.142080	0.116960	38.6	0.187840	0.500800	17.388
14	15	0.5	0.569600	0.128960	34.047	0.615360	0.512800	16.376
15	16	0.5	0.569600	0.128960	34.047	0.615360	0.512800	16.376
14	17	1.1	0.358400	0.123840	41.5	0.404100	0.507600	17.460
14	18	0.5	0.569600	0.128960	34.047	0.615360	0.512800	16.376
18	19	1	0.569600	0.128960	34.047	0.615360	0.512800	16.376
18	20	0.7	0.569600	0.128960	34.047	0.615360	0.512800	16.376
20	21	0.675	0.569600	0.128960	34.047	0.615360	0.512800	16.376
21	22	0.5	0.569600	0.128960	34.047	0.615360	0.512800	16.376
22	23	0.375	0.569600	0.128960	34.047	0.615360	0.512800	16.376
22	24	0.313	0.569600	0.128960	34.047	0.615360	0.512800	16.376

Table C.6: Capacitor and Load Impedance Data

Bus	R (pu)	X (pu)	B (pu)
35			0.0005
36			0.0005
37			0.0005
40			0.0004
42			0.0003
43			0.0004
48			0.0004
52			0.0004
56			0.0004
45	2244.7900		
45		4634.5033	
45	320.74650	155.44324	
60	4357.2000		
60		8996.4086	
60	622.82986	301.72371	

For a specific bus, elements in the same row are in series and elements in different rows are in parallel.

Table C.7: Transformer Data

From Bus	To Bus	Rated kVA	Tap (pu)	R (%)	X (%)
1	2	5001	0.9639	0	0.1
5	6	8661	0.909	0	0.29
8	34	500	1	0	5
11	38	300	1	0	5
11	39	300	1	0	5
12	41	300	1	0	5
14	45	1000	1	0	5
17	46	300	1	0	5
17	47	300	1	0	5
15	49	300	1	0	5
16	50	500	1	0	5
16	51	300	1	0	5
16	53	300	1	0	5
16	54	300	1	0	5
18	55	300	1	0	5
19	57	300	1	0	5
20	58	300	1	0	5
20	59	300	1	0	5
20	60	750	1	0	5
21	61	300	1	0	5
22	62	300	1	0	5
23	63	500	1	0	5
24	64	300	1	0	5
7	33	300	1	0	5
9	35	500	1	0	5
9	36	500	1	0	5
9	37	500	1	0	5
11	40	300	1	0	5
12	42	300	1	0	5
13	43	300	1	0	5
14	44	1500	1	0	5
17	48	300	1	0	5
16	52	300	1	0	5
18	56	300	1	0	5

Transformer tap (pu):  $V_{\text{from bus}}/V_{\text{to bus}}$